Semiannual Report for

NUMERICAL METHODS FOR ANALYZING ELECTROMAGNETIC SCATTERING

March 25, 1985 to September 24, 1985

Submitted to

Mr. Edward J. Rice

National Aeronautics and Space Administration
Lewis Research Center (MS 54-3)
Cleveland, OH 44113

(NASA-CR-176141) NUMERICAL METHODS FOR ANALYZING ELECTROMAGNETIC SCATTERING Seimannual Report, 25 Mar. - 24 Sep. 1985 (Illinois Univ.) 176 p HC A09/MF A01 CSCL 20N G3/32

N86-10377

Unclas 22286

Grant No. NAG-3-475

Prepared by

S. W. Lee, Y. T. Lo, S. L. Chuang, and C. S. Lee

Electromagnetics Laboratory
Department of Electrical and Computer Engineering
University of Illinois
Urbana, IL 61801

September 24, 1985

Semiannual Report for

NUMERICAL METHODS FOR ANALYZING ELECTROMAGNETIC SCATTERING

March 25, 1985 to September 24, 1985

Submitted to

Mr. Edward J. Rice

National Aeronautics and Space Administration
Lewis Research Center (MS 54-3)
Cleveland, OH 44113

Grant No. NAG-3-475

Prepared by

S. W. Lee, Y. T. Lo, S. L. Chuang, and C. S. Lee

Electromagnetics Laboratory
Department of Electrical and Computer Engineering
University of Illinois
Urbana, IL 61801

September 24, 1985

TABLE OF CONTENTS

LIST OF FIGURES

I. INTRODUCTION

The research grant NAG 3-475 entitled "Numerical Methods for Analyzing Electromagnetic Scattering" was awarded to the University of Illinois by NASA-Lewis Research Center on September 28, 1983. Mr. Edward M. Rice of NASA's Lewis Research Center is the Technical Officer, and Mr. Boyd M. Bane is the contracting officer. The total amount of funds received by the University is

$$\$74,985 + \$80,009 = \$154,994$$

to cover the period from

September 25, 1983 to November 25, 1985 (26 months).

This report is the fourth semiannual report which covers the period March 25, 1985 to September 24, 1985.

II. TECHNICAL PERSONNEL

S. W. Lee	Professor of Electrical and Computer Engineering
Y. T. Lo	Professor of Electrical and Computer Engineering
S. L. Chuang	Assistant Professor of Electrical and Computer Engineering
C. S. Lee	Research Assistant of the Department of Electrical and Computer Engineering

III. PRESENTATION AND PUBLICATIONS

1. Professor S. W. Lee traveled to NASA Lewis on August 16, 1985 to present a talk entitled "Lecture Notes on RCS: Volume I." Viewgraphs of the presentation are attached here as Appendix B.

2. C. S. Lee, S. L. Chuang, and S. W. Lee, "A Simple Version of Corrugated Waveguide: Smooth-Walled Circular Waveguide Coated with Lossy Magnetic Material," AP-S International Symposium Digest, Vol. 1, pp. 303-306, June 1985; also presented at Seventh Annual Electromagnetics Propagation and Communication Affiliates Workshop, Urbana, IL, April 1985. Viewgraphs of the presentation at the AP meeting in Vancouver, B.C., are attached as Appendix C.

3. C. S. Lee, S. W. Lee, and S. L. Chuang, "Normal Modes in an Overmoded Circular Waveguide Coated with Lossy Material," submitted for publication to IEEE Trans. Microwave Theory Tech. (See Appendix A.)

4. C. S. Lee, S. W. Lee, and S. L. Chuang, "Scattering from an Open-Ended Circular Guide Using the Equivalent-Current Method," in preparation, to be submitted for publication.

5. C. S. Lee, "Scattering from a Circular Waveguide Coated with Lossy Material," in preparation, for Ph.D. thesis, Department of Electrical and Computer Engineering, University of Illinois, Urbana, IL, January 1986.

IV. TECHNICAL PROGRESS

Abstract

Major items accomplished in this reporting period are:

1. The attenuation properties of the normal modes in an overmoded waveguide coated with a lossy material are analyzed and submitted for publication. The preprint of the paper is attached in Appendix A. It is found that the low-order modes (which contribute the most to the radar cross section (RCS) from a circular waveguide terminated by a perfect electric conductor (PEC)) can be significantly attenuated even with a thin layer of coating if the coating material is not too lossy. A thinner layer of coating is required for large attenuation of the low-order modes if the coating material is magnetic rather than dielectic.
2. The RCS from an uncoated circular guide terminated by a PEC has been calculated and compared with available experimental data. It is confirmed that the interior irradation contributes to the RCS much more than the rim diffraction. Thus suppressing the interior irradiation by coating the interior waveguide wall or by other means will be very effective in reducing the RCS from the PEC-terminated guide, especially for a large value of a/λ (>1) at a small incident angle.
3. For the calculation of the contribution from the rim diffraction, we have chosen the equivalent-current method based on the geometrical theory of diffraction (GTD), and the RCS's with the inclusion of the rim-diffraction contribution are compared with the

experimental data of the RCS from an uncoated guide terminated by a PEC. The agreement improves significantly with the inclusion of the rim-diffraction contribution. Especially, the term from the rim-diffraction contribution accounts well for the fine features of the RCS.

4. We are planning for experiments on the RCS reduction from a coated circular guide terminated by a PEC and the detailed schemes for the experiments are included in this report.

5. As shown in the previous report [1], the waveguide coated with a lossy magnetic material has been suggested as a substitute for the corrugated waveguide. The experiments to verify the theory are in progress and the details of the experiment are included.

Details are explained below.

(1) Normal modes in an overmoded circular waveguide coated with lossy material

The normal modes in an overmoded waveguide coated with a lossy material are analyzed, particularly for their attenuation properties as a function of coating material, layer thickness, and frequency. When the coating material is not too lossy, the low-order modes are highly attenuated even with a thin layer of coating. This coated guide serves as a mode suppressor of the low-order modes, which can be particularly useful for reducing the radar cross section (RCS) of a cavity structure such as a jet engine inlet. When the coating material is very lossy, low-order modes fall into two distinct groups: highly and lowly attenuated modes. However, as a/λ (a = radius of the cylinder; λ = the free-space wavelength) increases, the separation between these two groups becomes less distinctive. The attenuation constants of most of the low-order modes become small, and decrease as a function of λ^2/a^3. See Appendix A for details.

(2) Scattering from an uncoated circular guide terminated by a PEC

Previous investigation has shown that the jet intake contributes significantly to the RCS from a modern military aircraft, and coating the interior wall of the jet intake with a lossy material has been proposed to reduce the RCS [2]. The first step in this research is to investigate the RCS from an uncoated structure. For the theoretical model, the jet intake is approximated by a circular waveguide terminated by a PEC as shown in Figure 1.

The RCS from the PEC-terminated guide comes mainly from the rim diffraction and interior irradiation. The transmitted normal modes due to the outside illumination are responsible for the interior irradiation, which can be reduced by coating the interior waveguide wall. On the other hand, the scattered wave from the edges and the evanescent modes is not affected by the coating.

The theoretical study at the Universiy of Illnois has shown that when a/λ is not too small, the contribution to the RCS from the interior irradiation is much larger than that from the rim diffraction [1]. The purpose of this section is to illustrate this point with available experimental data and suggest that if the interior irradiation is

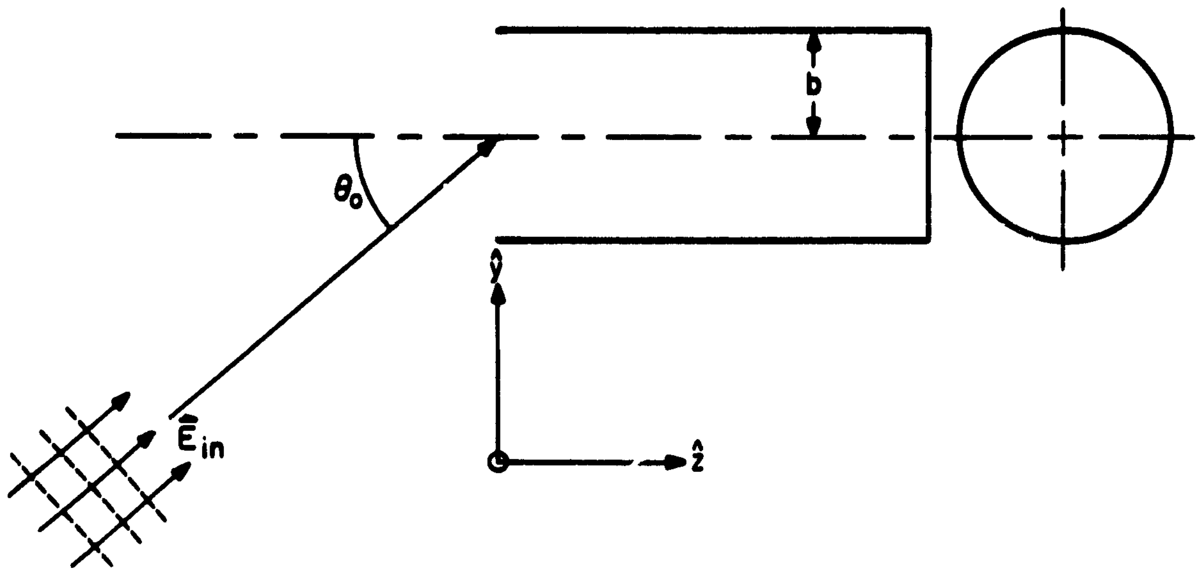

Figure 1. A circular waveguide terminated by a perfect electric conductor (PEC) is illuminated by an incident plane wave.

suppressed by coating the waveguide wall, the RCS from the PEC-terminated guide can be significantly reduced.

There are three steps in calculating the RCS from the waveguide:

i) Find the excited normal modes at the waveguide opening due to the incident plane wave.

ii) Find the phase shifts after the normal modes are reflected from the PEC termination and calculate the field distribution at the waveguide opening.

iii) Evaluate the radiated energy in the direction of the incident plane wave from the field distribution at the waveguide opening in step (ii) above.

In step (i), the tangential field at the waveguide opening is expanded as a sum of the tangential fields of the normal modes. The unknown field at the opening is assumed to be that of the incident field. In this approximation, the choice between the matchings of the tangential electric field and magnetic field is arbitrary. The magnetic-field matching is used in this calculation [1], [3].

Since the evanescent modes can not be attenuated by the coating, only the transmitted modes are accounted for in order to illustrate the effectiveness of the coating in the RCS reduction.

The transmitted normal modes interfere with one another within the waveguide because their propagation constants are different, and the radiation pattern is largely dependent on the waveguide length. The Stratton-Chu formula is used along with the Kirchhoff approximation to evaluate the radiation pattern.

The RCS measurements from the PEC-terminated circular guide for 7 different frequencies ranging from $a/\lambda = 0.636$ to 1.882 were reported by Brooks and Crispin, Jr. [4]. Their report also contains the RCS measurements from a circular guide when the PEC termination is removed and the guide is open-ended. These values would be approximately equal to those from the PEC-terminated guide if all the transmitted normal modes could be eliminated before being reemitted to the outside.

Those experimental values are compared with the theoretical calculations for which the contribution only from the interior irradiation is taken into account in order to emphasize the importance of the interior irradiation (Table 1 and Figures 2-8). We have made the following observations:

1. As a/λ becomes larger, the RCS from the rim diffraction becomes less significant, and the agreement between the experimental and theoretical values (from interior irradiation only) of RCS from the PEC-terminated circular guide becomes better. This observation confirms our previous claim [1] that the interior irradiation from a PEC-terminated circular guide contributes to the RCS much more than the rim diffraction, especially at high frequency (more than 10 dB for $a/\lambda > 1$). These features are more clearly seen in Figure 9, where the RCS's at a normal incidence are plotted as a function of a/λ. Note that the RCS from a PEC-terminated guide at a normal incidence is approximately equal to that from a circular plate, which is proportional to $(a^2/\lambda)^2$ [5]. On the other hand, the RCS in terms of the cross sectional area from the rim diffraction does not change much with a variation of a/λ. Thus as a/λ

TABLE 1.

PARAMETERS FOR THE RCS MEASUREMENTS FROM
A CIRCULAR WAVEGUIDE

Figure	Polarization	Frequency (GHz)	a/λ
2 a b	HH VV	6.08	0.636
3 a b	HH VV	9.13	0.955
4 a b	HH VV	10.63	1.112
5 a b	HH VV	12.17	1.237
6 a b	HH VV	13.68	1.430
7 a b	HH VV	15.20	1.589
8 a b	HH VV	18.0	1.88

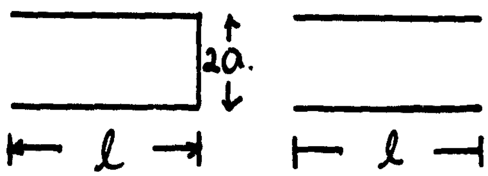

$a = 3.137$ cm $\quad l = 21.59$ cm

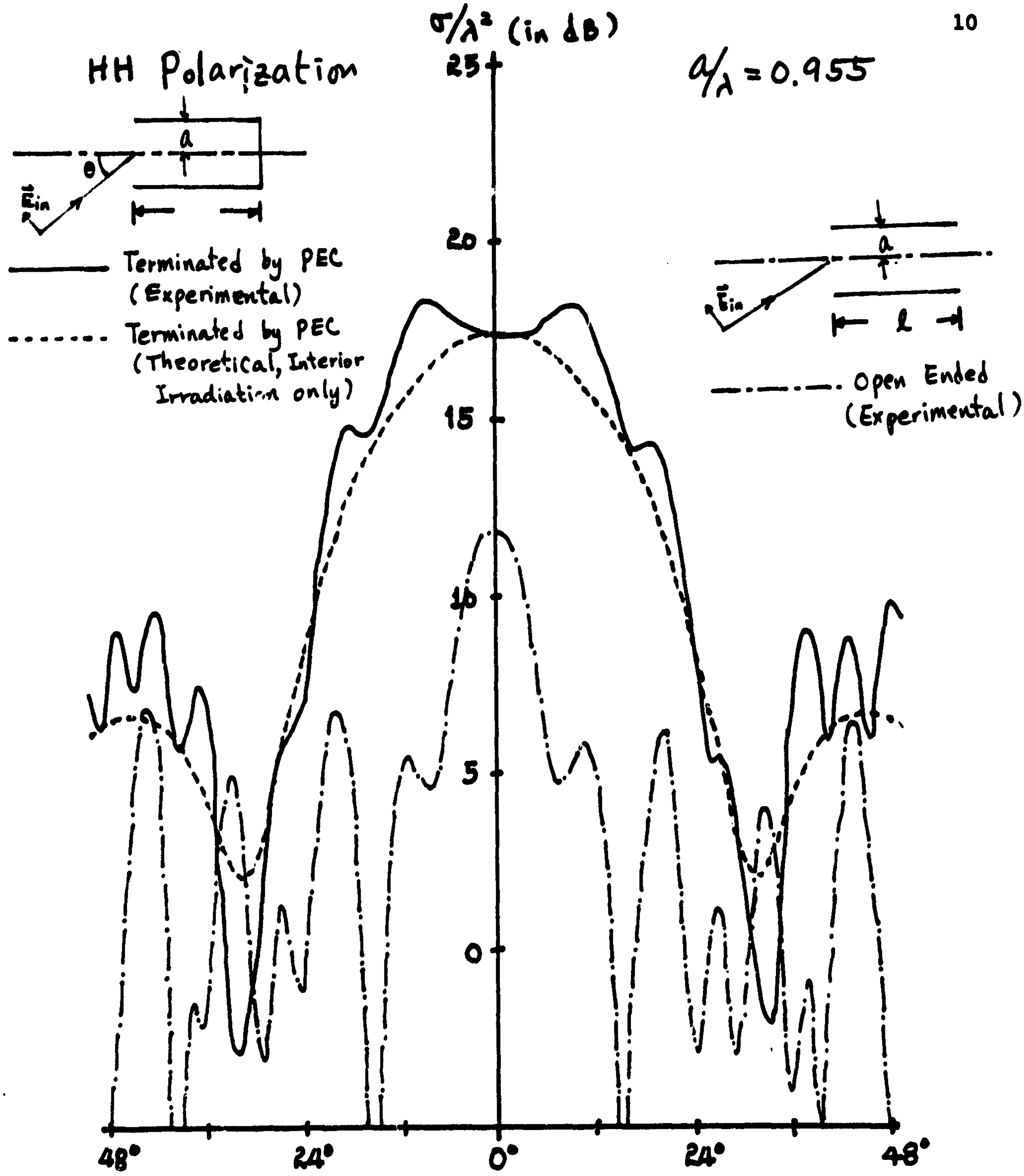

Figure 2a. The RCS's from a PEC-terminated waveguide (——— experimental, - - - - - theoretical, interior irradiation only) and from an open-ended waveguide (—·—— experimental) as a function of the incident angle (HH polarization, a = 3.137 cm, f = 6.08 GHz, a/λ = 0.636, length = 21.59 cm).

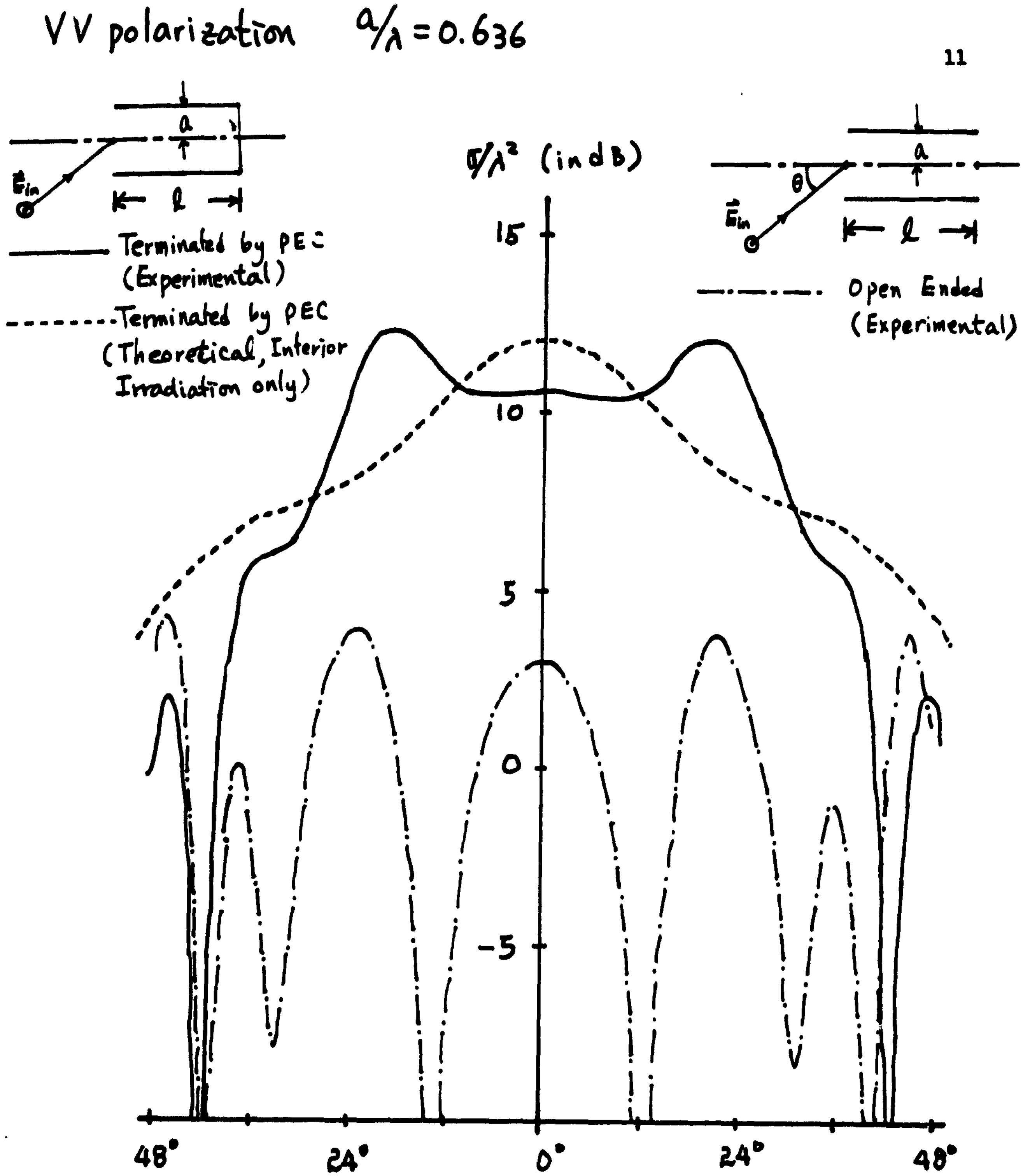

Figure 2b. The RCS's from a PEC-terminated waveguide (——— experimental, - - - - - theoretical, interior irradiation only) and from an open-ended waveguide (—·—·— experimental) as a function of the incident angle (VV polarization, a = 3.137 cm, f = 6.08 GHz, a/λ = 0.636, length = 21.59 cm).

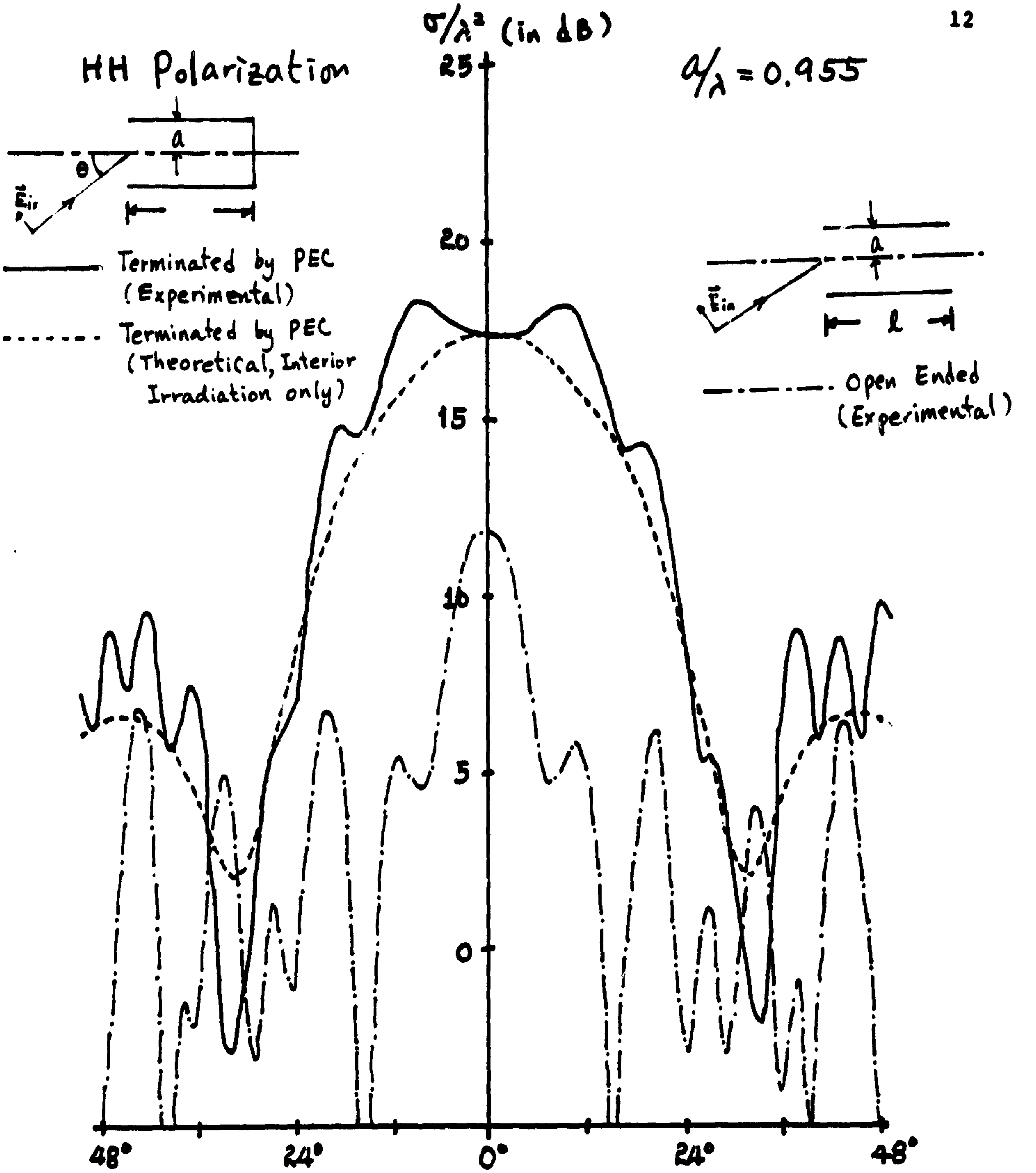

Figure 3a. The RCS's from a PEC-terminated waveguide (——— experimental, - - - - - theoretical, interior irradiation only) and from an open-ended waveguide (—·— experimental) as a function of the incident angle (HH polarization, a = 3.137 cm, f = 9.13 GHz, a/λ = 0.955, length = 21.59 cm).

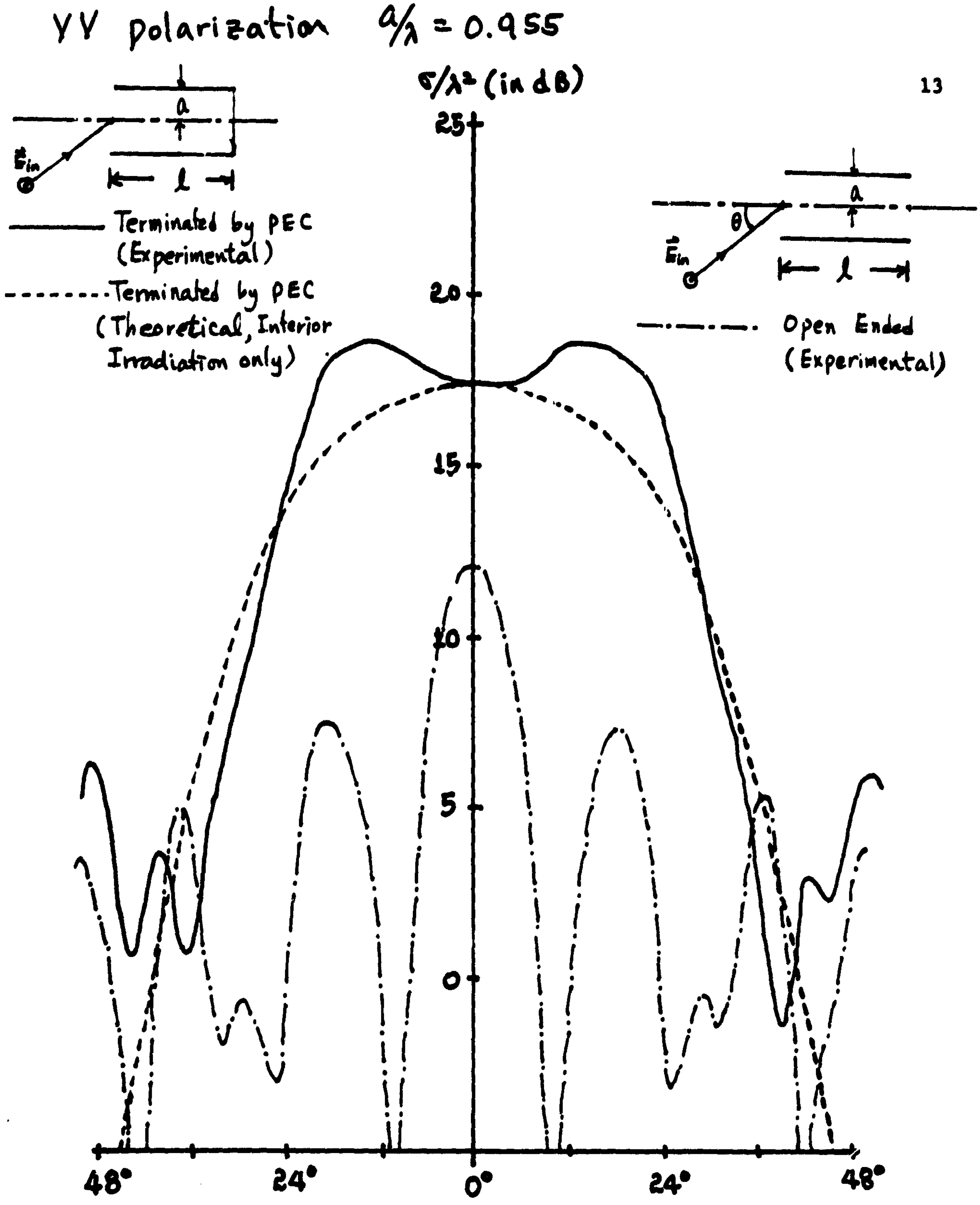

Figure 3b. The RCS's from a PEC-terminated waveguide (——— experimental,- - - - -theoretical, interior irradiation only) and from an open-ended waveguide (—·—experimental) as a function of the incident angle (VV polarization, a = 3.137 cm, f = 9.13 GHz, a/λ = 0.955, length = 21.59 cm).

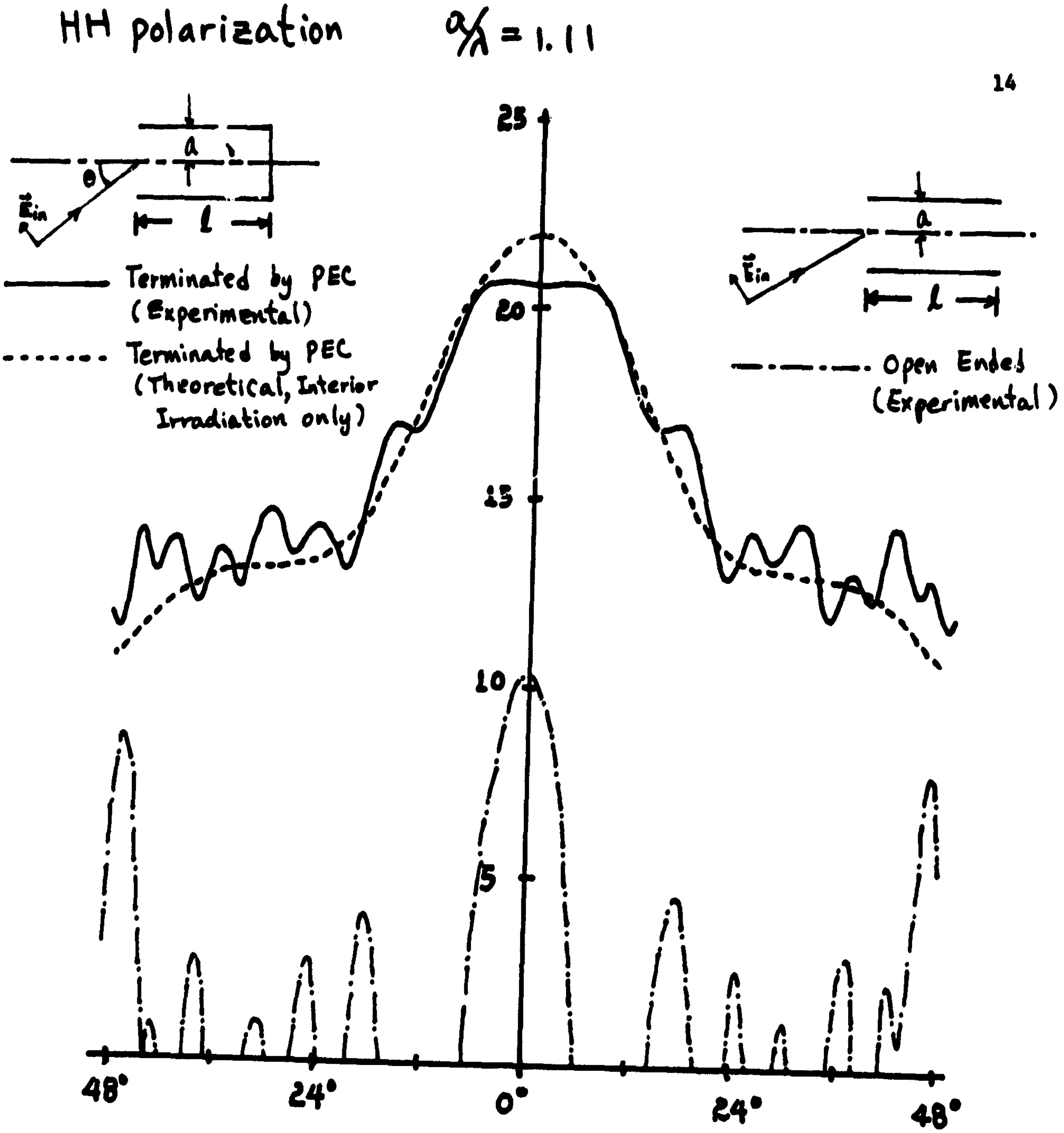

Figure 4a. The RCS's from a PEC-terminated waveguide (——— experimental, - - - - - theoretical, interior irradiation only) and from an open-ended waveguide (—·—·— experimental) as a function of the ncident angle (HH polarization, a = 3.137 cm, f = 10.63 GHz, a/λ = 1.112, length = 21.59 cm).

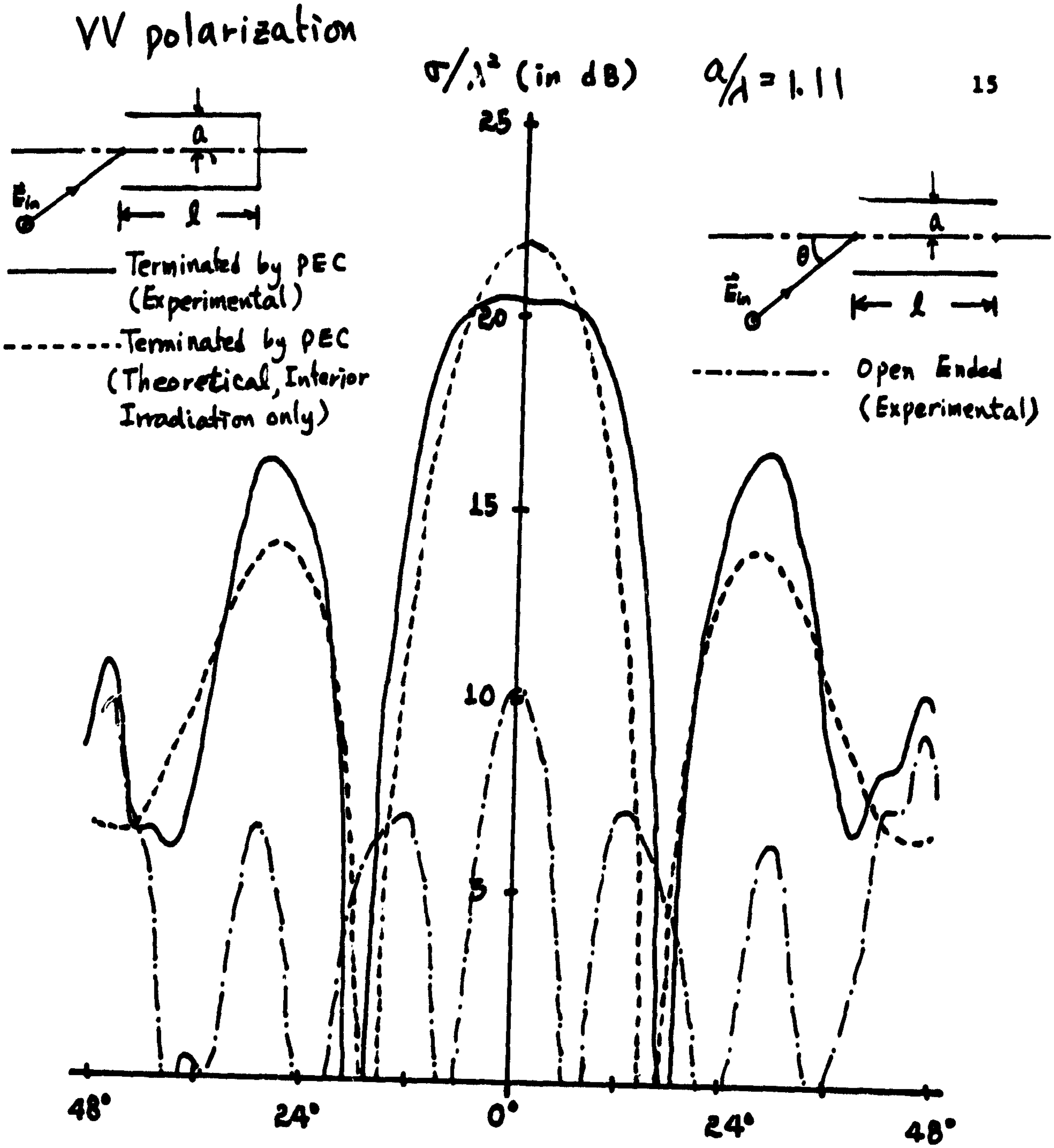

Figure 4b. The RCS's from a PEC-terminated waveguide (——— experimental, – – – – theoretical, interior irradiation only) and from an open-ended waveguide (—·—·— experimental) as a function of the incident angle (VV polarization, a = 3.137 cm, f = 10.63 GHz, a/λ = 1.112, length = 21.59 cm).

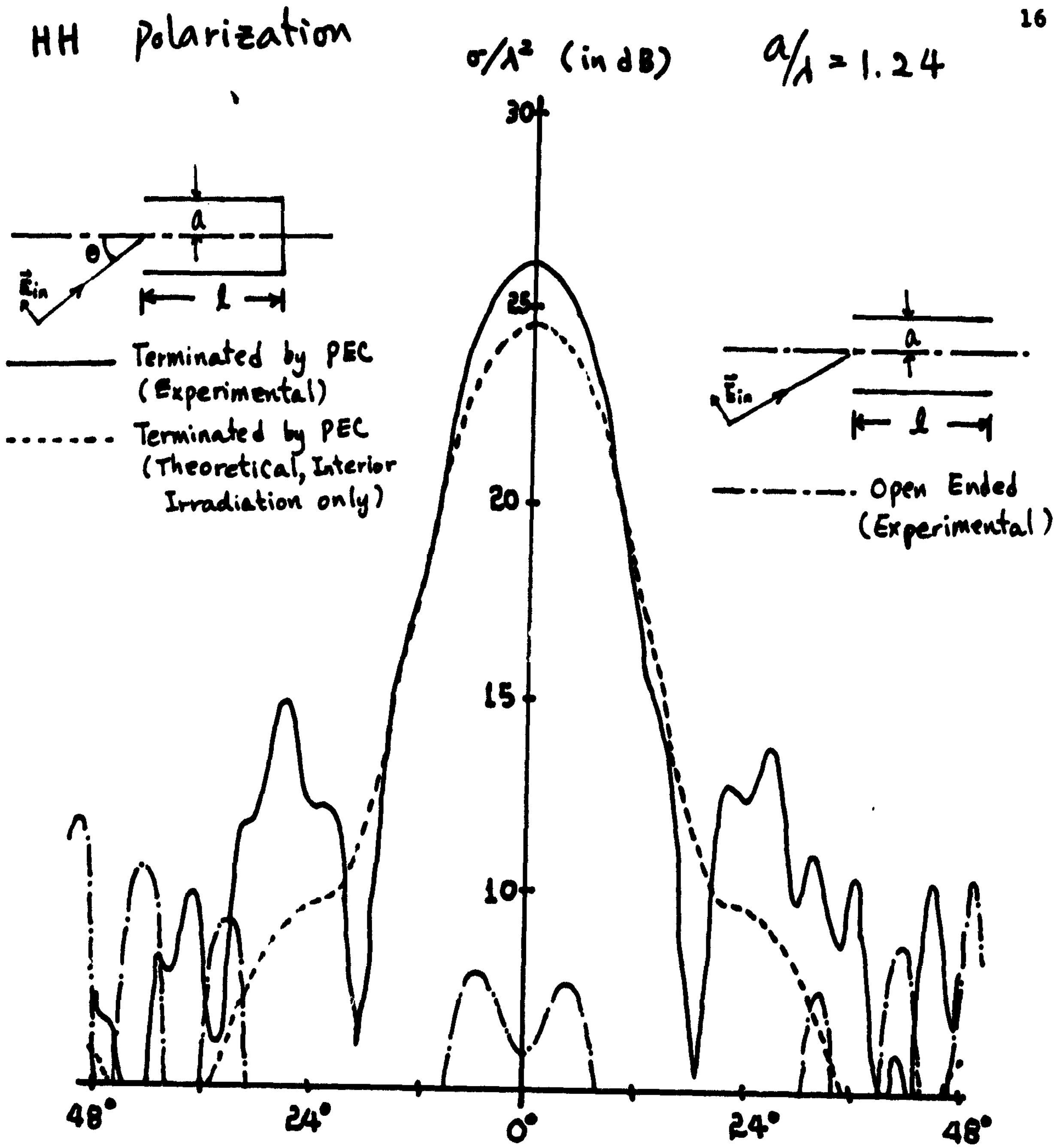

Figure 5a. The RCS's from a PEC-terminated waveguide (———experimental,- - - - -theoretical, interior irradiation only) and from an open-ended waveguide (—·—experimental) as a function of the incident angle (HH polarization, a = 3.137 cm, f = 12.17 GHz, a/λ = 1.237, length = 21.59 cm).

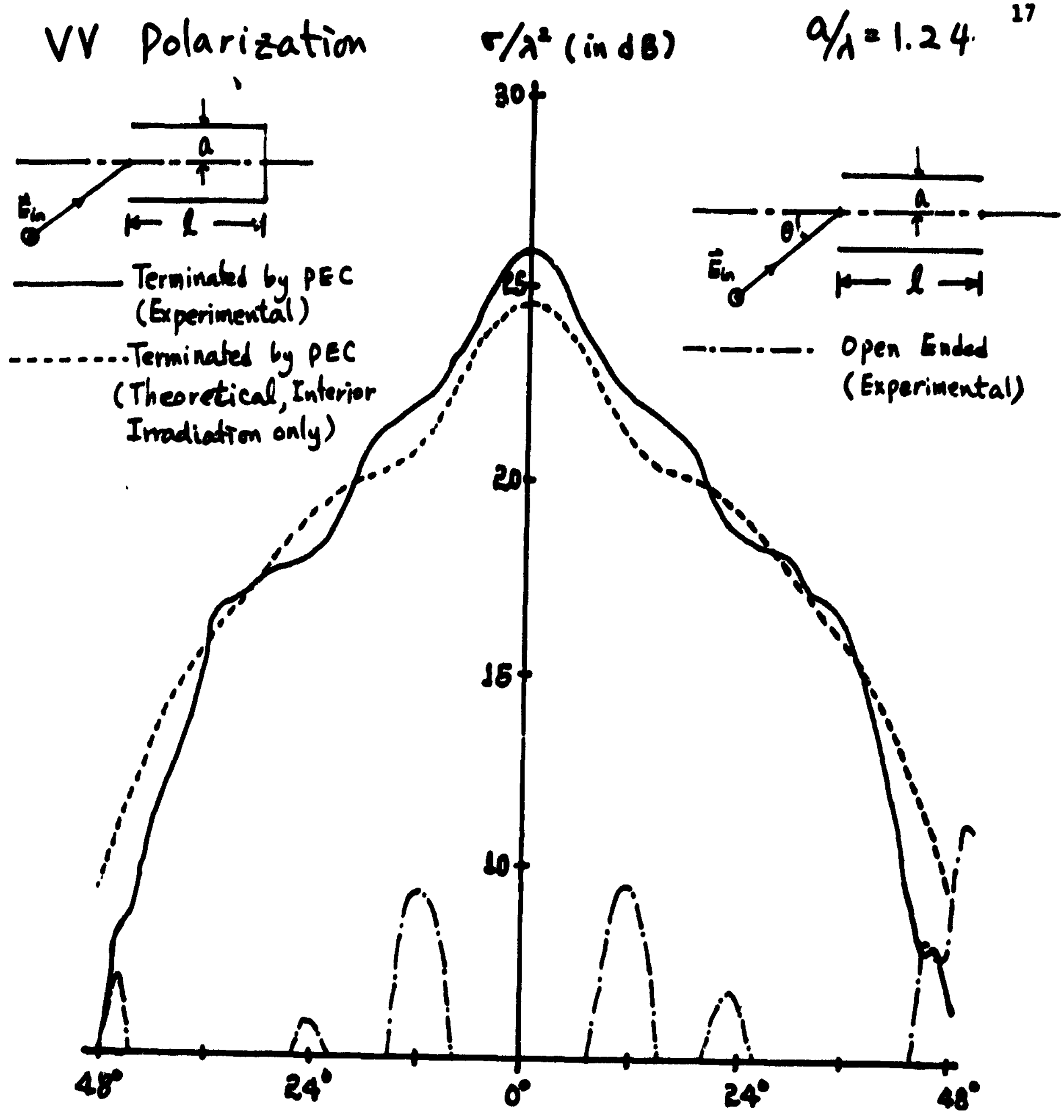

Figure 5b. The RCS's from a PEC-terminated waveguide (——— experimental, - - - - - theoretical, interior irradiation only) and from an open-ended waveguide (—·-·— experimental) as a function of the incident angle (VV polarization, a = 3.137 cm, f = 12.17 GHz, a/λ = 1.237, length = 21.59 cm).

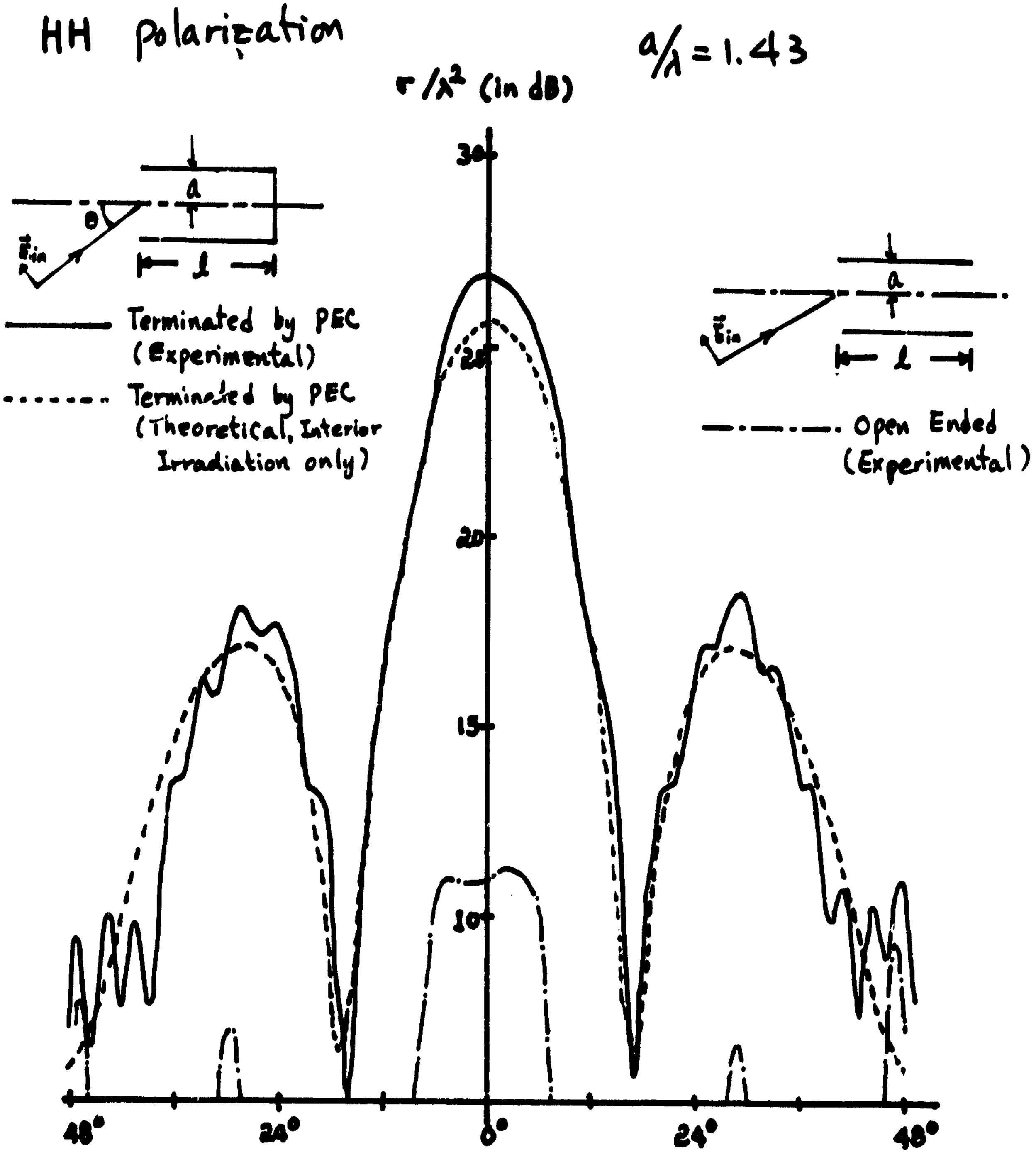

Figure 6a. The RCS's from a PEC-terminated waveguide (——— experimental, - - - - - theoretical, interior irradiation only) and from an open-ended waveguide (—·— experimental) as a function of the incident angle (HH polarization, a = 3.137 cm, f = 13.68 GHz, a/λ = 1.430, length = 21.59 cm).

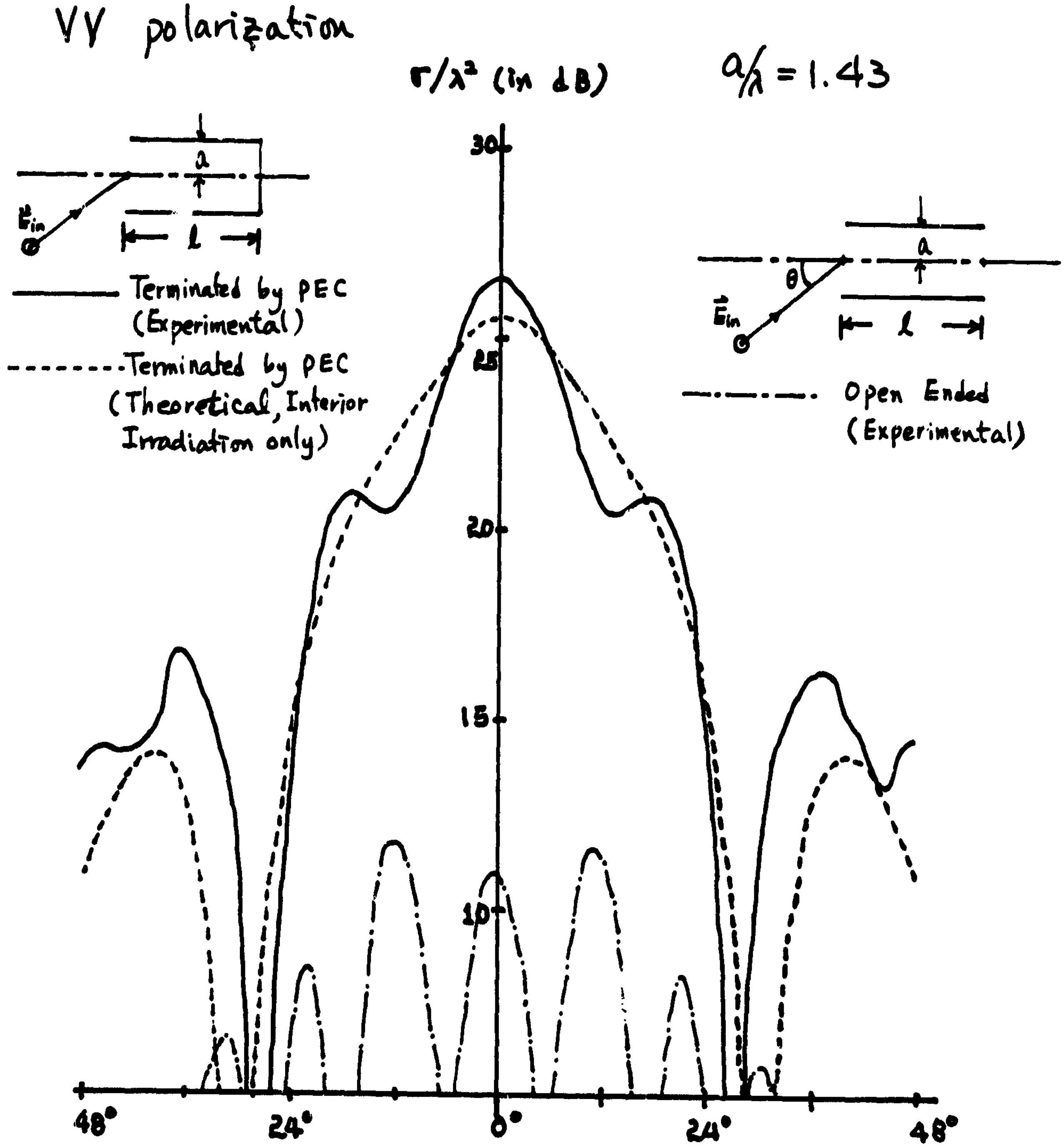

Figure 6b. The RCS's from a PEC-terminated waveguide (——— experimental, - - - - - theoretical, interior irradiation only) and from an open-ended waveguide (—·— experimental) as a function of the incident angle (VV polarization, a = 3.137 cm, f = 13.68 GHz, a/λ = 1.430, length = 21.59 cm).

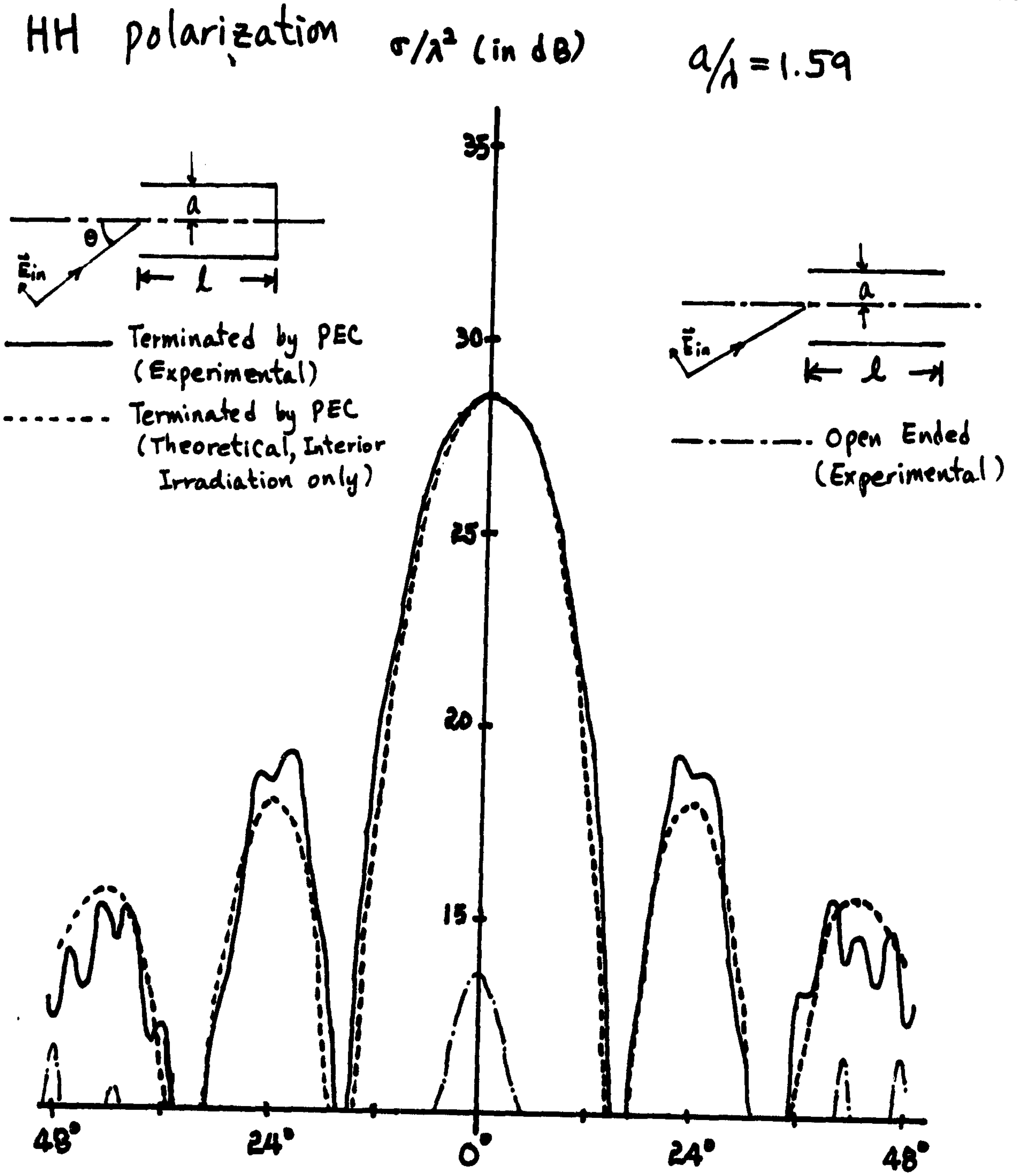

Figure 7a. The RCS's from a PEC-terminated waveguide (——— experimental, - - - - - theoretical, interior irradiation only) and from an open-ended waveguide (—·—·— experimental) as a function of the incident angle (HH polarization, a = 3.137 cm, f = 15.20 GHz, a/λ = 1.589, length = 21.59 cm).

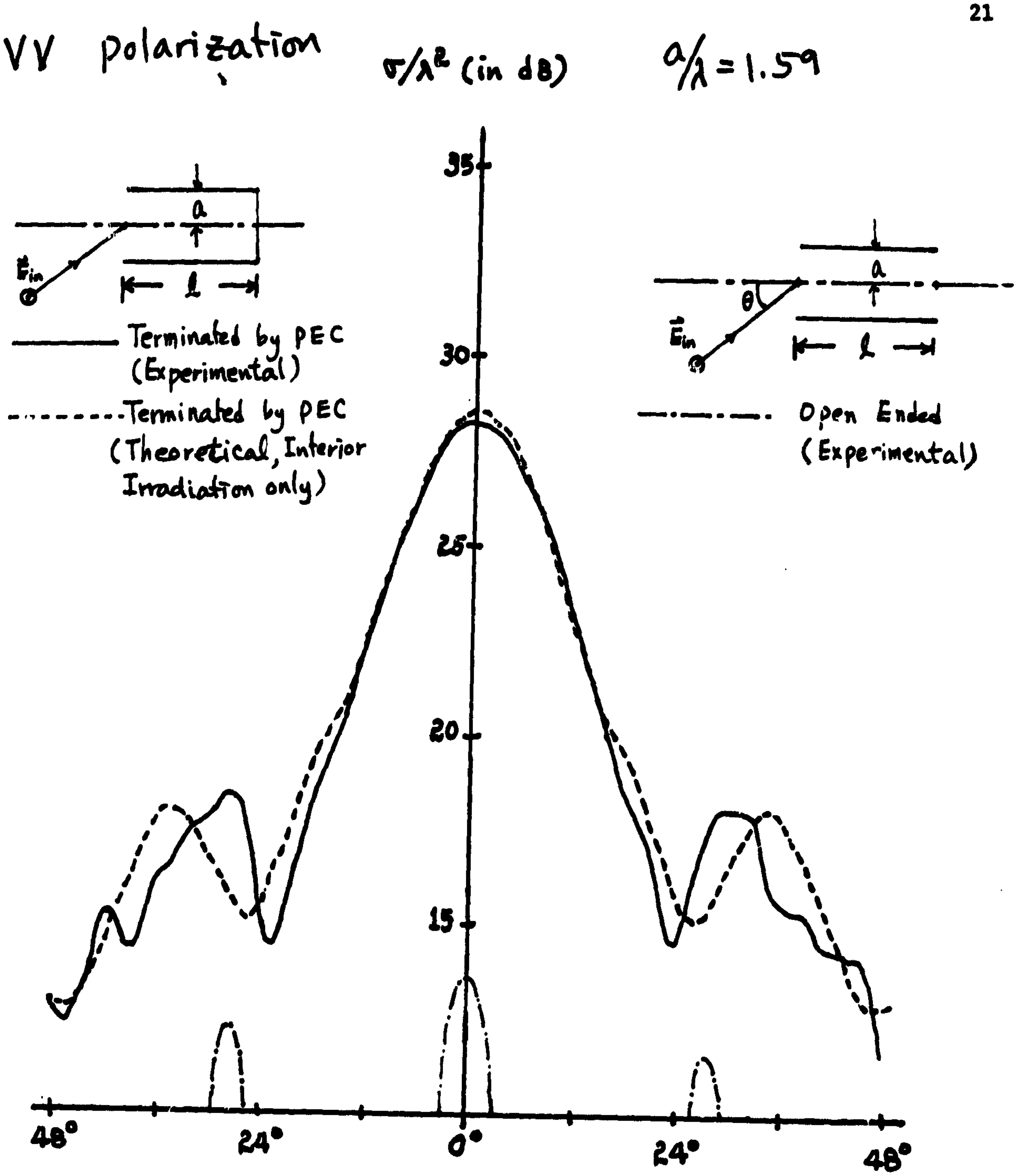

Figure 7b. The RCS's from a PEC-terminated waveguide (——— experimental, - - - - - theoretical, interior irradiation only) and from an open-ended waveguide (—·—·— experimental) as a function of the incident angle (VV polarization, a = 3.137 cm, f = 15.20 GHz, a/λ = 1.589, length = 21.59 cm).

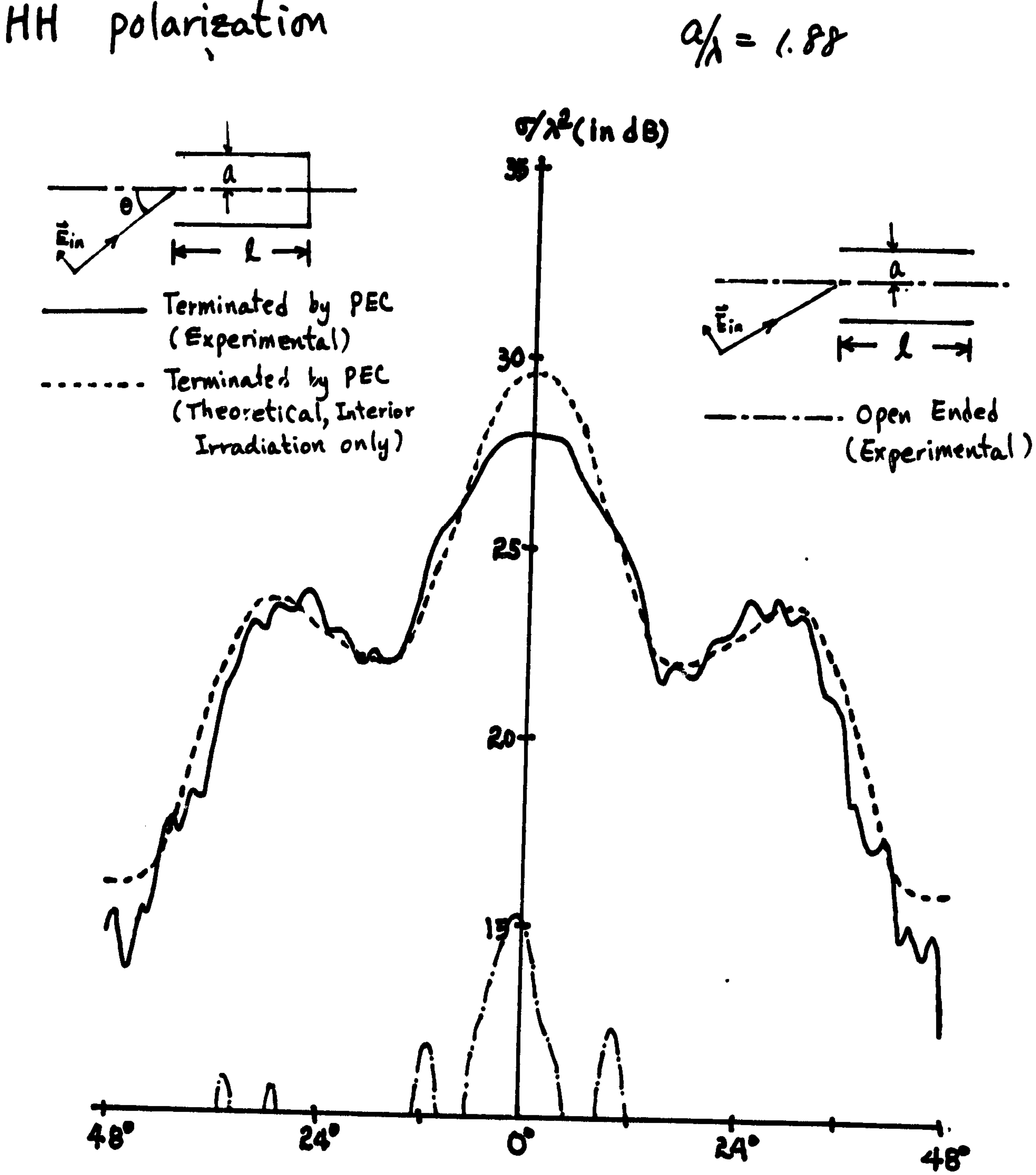

Figure 8a. The RCS's from a PEC-terminated waveguide (—— experimental,-----theoretical, interior irradiation only) and from an open-ended waveguide (——--experimental) as a function of the incident angle (HH polarization, a = 3.137 cm, f = 18.0 GHz, a/λ = 1.88, length = 21.59 cm).

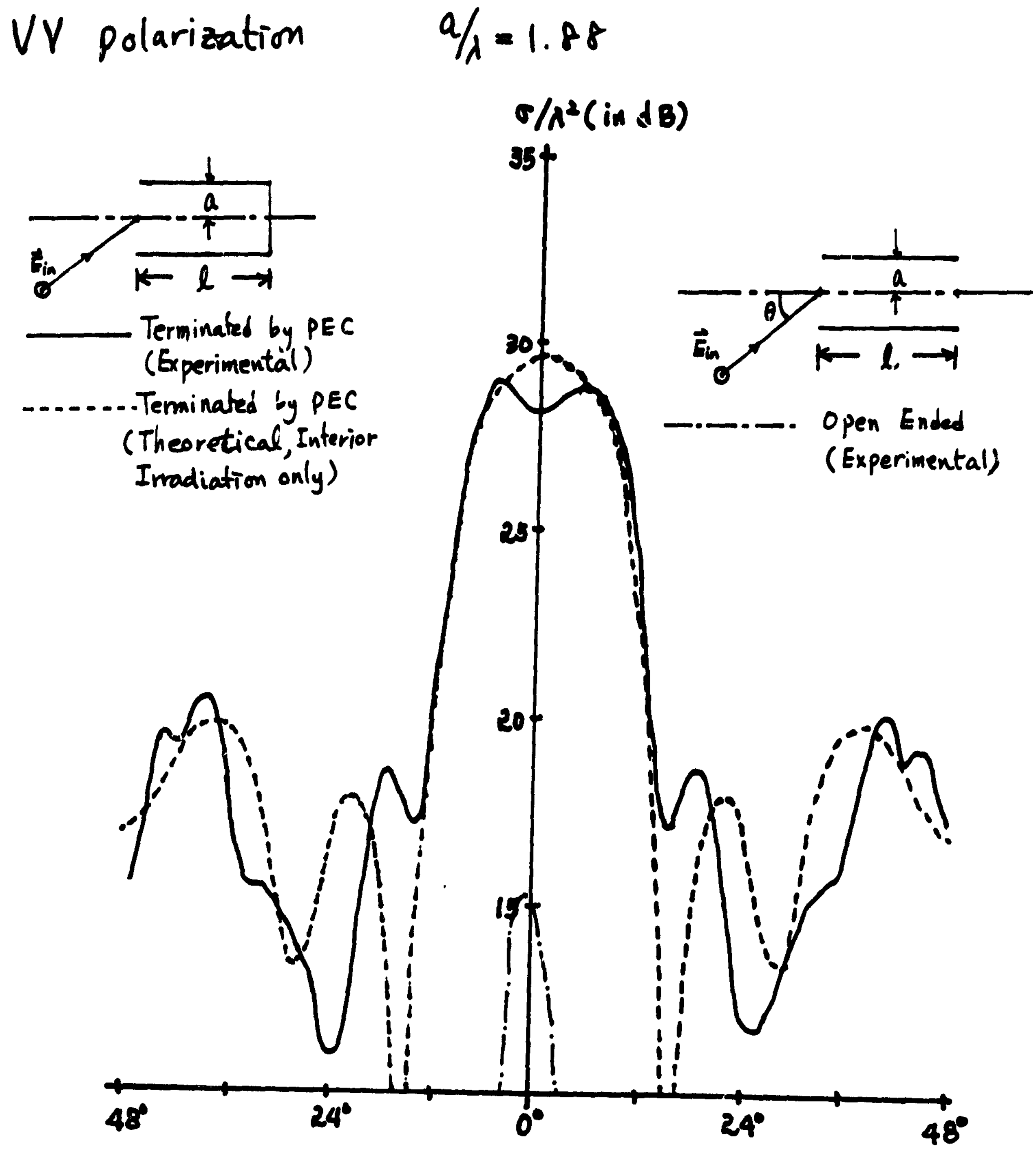

Figure 8b. The RCS's from a PEC-terminated waveguide (——— experimental, ------ theoretical, interior irradiation only) and from an open-ended waveguide (—·— experimental) as a function of the incident angle (VV polarization, a = 3.137 cm, f = 18.0 GHz, a/λ = 1.88, length = 21.59 cm).

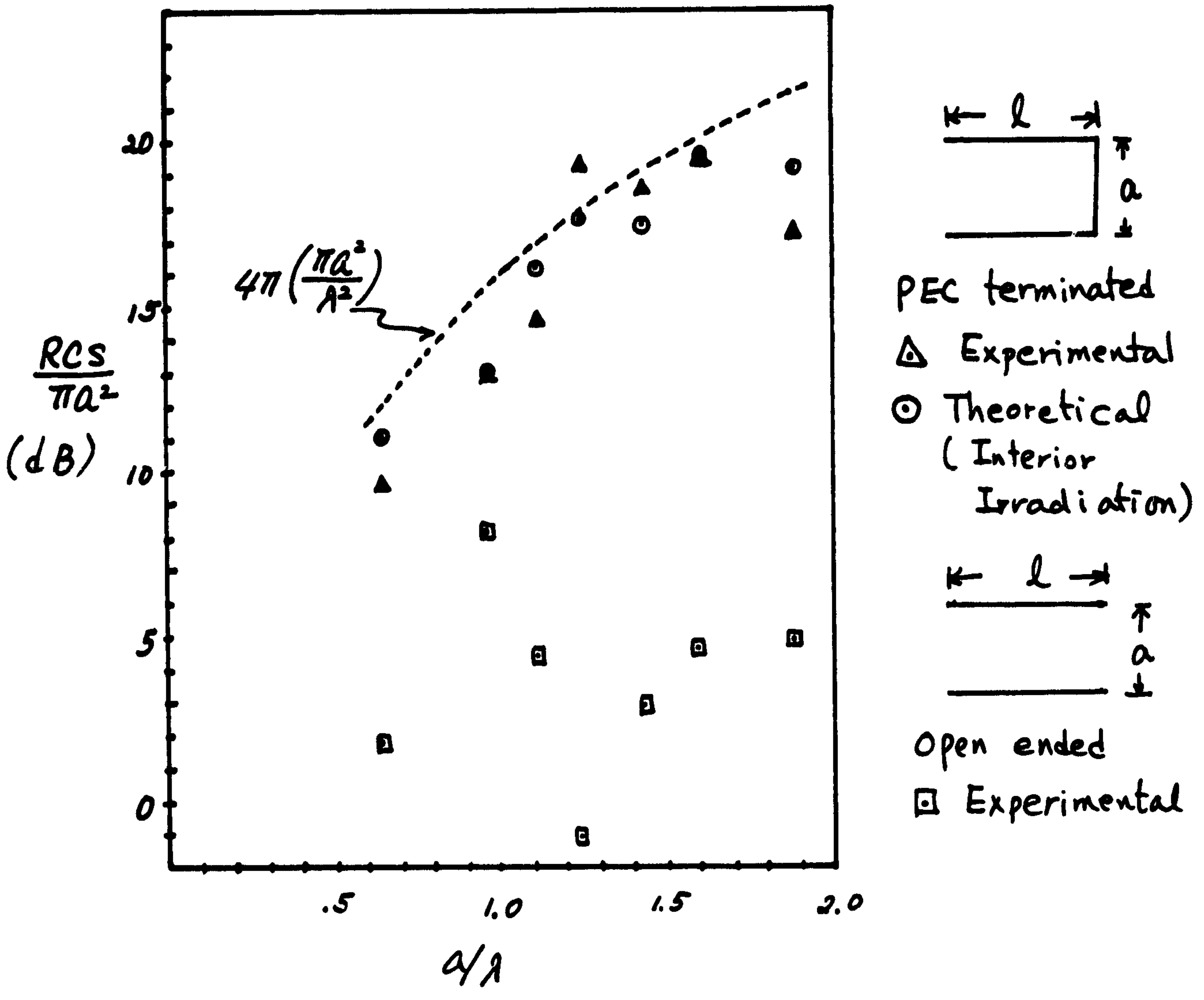

Figure 9. The RCS's from circular guides (PEC-terminated, open-ended) at a normal incidence as a function of a/λ. (----- approximate RCS from a circular plate [5].)

increases, the difference between the RCS's from the interior irradiation and the rim diffraction becomes large.

2. At a large incident angle, the rim diffraction contributes significantly to the total RCS, and the coating may not be as effective as in the case at a small incident angle, especially for a small value of a/λ.

From above results, we conclude that suppressing the interior irradiation by coating the interior waveguide wall or by other means will be very effective in reducing the RCS from the PEC-terminated guide, especially for the case with a large value of a/λ (>1) at a small incident angle.

(3) The RCS from an uncoated guide terminated by a PEC including the effect of the rim diffraction

Scattering from the rim of an open-ended waveguide has been studied by many authors [6]. The simplest method would be the standard geometrical theory of diffraction (GTD). However, the theory fails near the caustic and the shadow boundary [7]. More extensive calculations using the Wiener-Hopf technique [6] provide a better solution, but this method can be applied only to a limited number of geometrical cases. To improve the solution of the GTD near the caustic and the shadow boundary, the equivalent-current (EC) method based on the GTD was suggested [8-9]. It has been reported that the EC method is valid only near the caustic [10-11] or near the normal incidence to the edge [12].

The purpose of this section is to illustrate that the EC method is valid not only near the caustic but also over a wide range of the incident angle, using a simple example of the scattering from an open-ended circular guide. One noticeable advantage of this method is that this technique can be extended to problems of arbitrary shape with relatively simple mathematical manipulations.

First, we evaluated the RCS from an open-ended circular guide using the EC method, and compared the results with available experimental data and another known method (Wiener-Hopf) [13] (Figures 10 and 11). The agreement is good except for the cases of HH polarization at a large incident angle. We speculate that the discrepancy in this case is due to the second-order diffraction. This possibility is now under investigation. In fact the EC solution is almost identical to the simple version of the Wiener-Hopf solution [14], which also shows such a discrepancy.

Fortunately, in our problem the contribution to the RCS from the rear edge of the cylinder becomes large and the error due to the second-order term from the front edge would not be too critical for the case of HH-polarization at a large incident angle (Figure 12a). On the other hand, the contribution from the back edge is much smaller than that from the front edge for VV polarization (Figure 12b).

Using the first-order EC method [8], we have added the contribution from the rim diffraction to the RCS from the interior irradiation (Section (2)). The agreement of the theory with the experimental data is improved significantly. Especially, the fine wiggling features of the RCS can be mostly accounted for (Figures 13-19).

As demonstrated in Section (2), the rim diffraction does not contribute much to the total RCS compared to the interior irradiation.

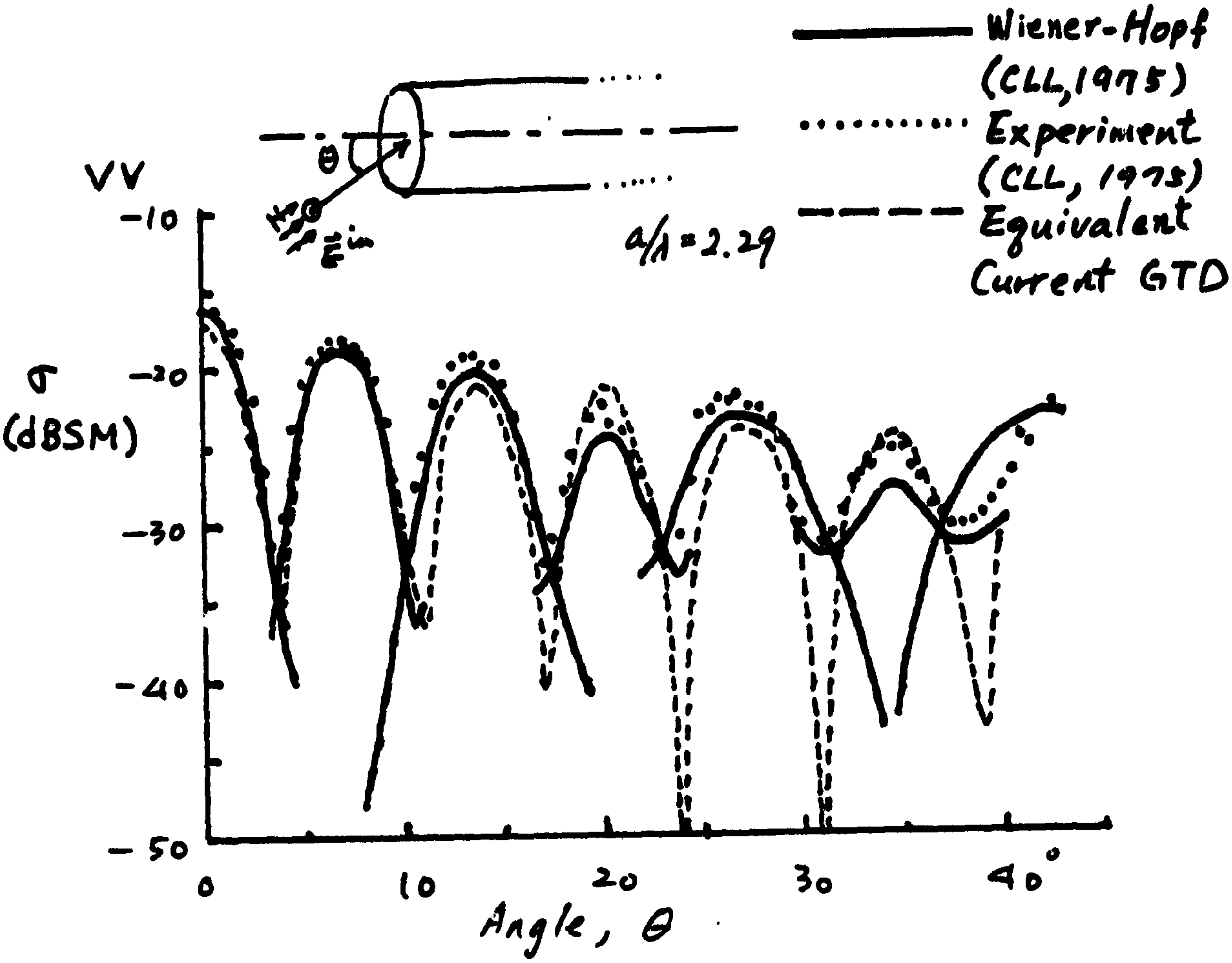

Figure 10a. The RCS's from an open-ended semi-infinite circular waveguide using the equivalent-current (EC) method (– – – – –) in comparison with the results using the Wiener-Hopf technique (————) and the experimental data (••••••) [13] (VV polarization, a = 7.56 cm, f = 9.1 GHz, a/λ = 2.29).

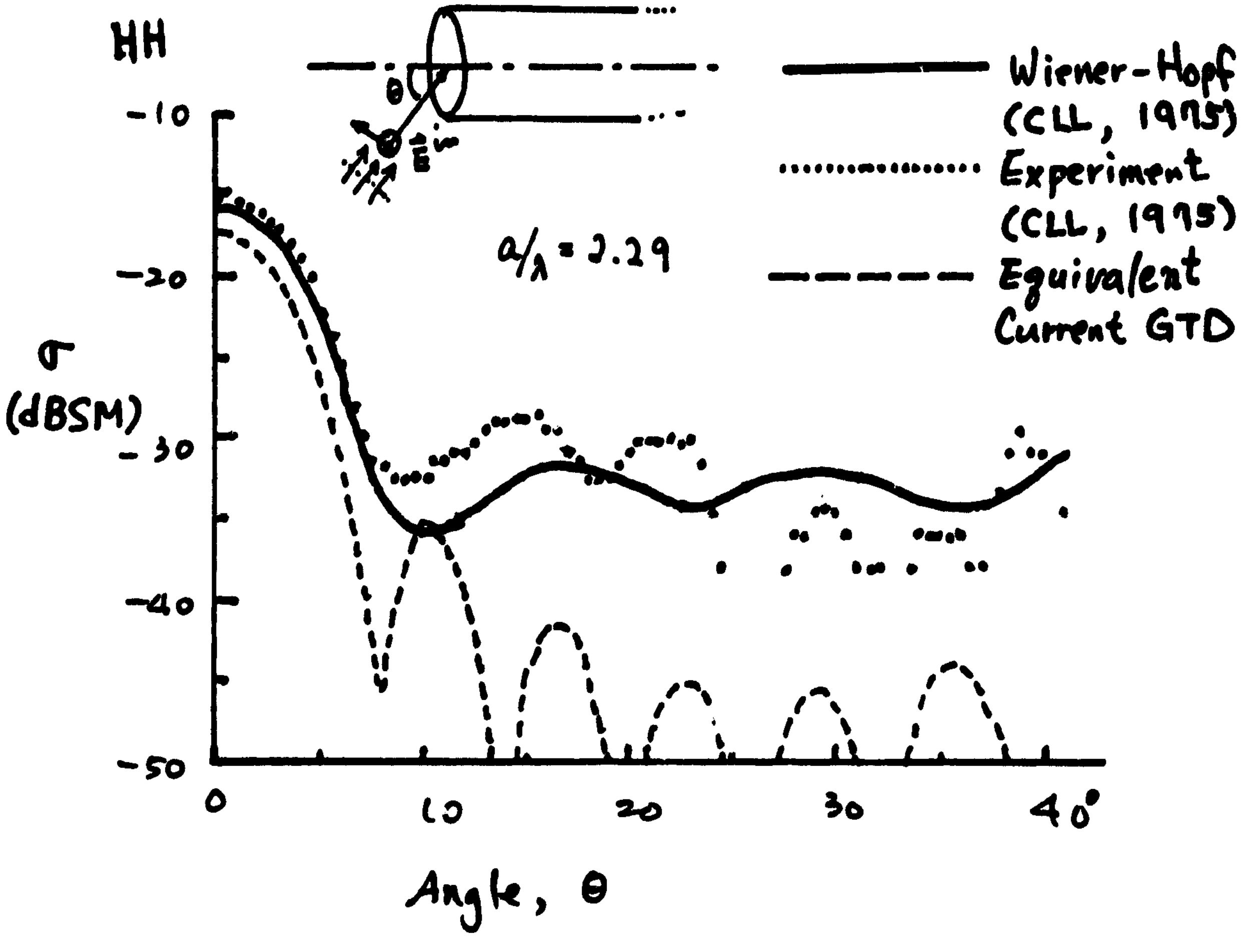

Figure 10b. The RCS's from an open-ended semi-infinite circular waveguide using the equivalent-current (EC) method (—-—-—) in comparison with the results using the Wiener-Hopf technique (————) and the experimental data (•••••••) [13] (HH polarization, a = 7.56 cm, f = 9.1 GHz, a/λ = 2.29).

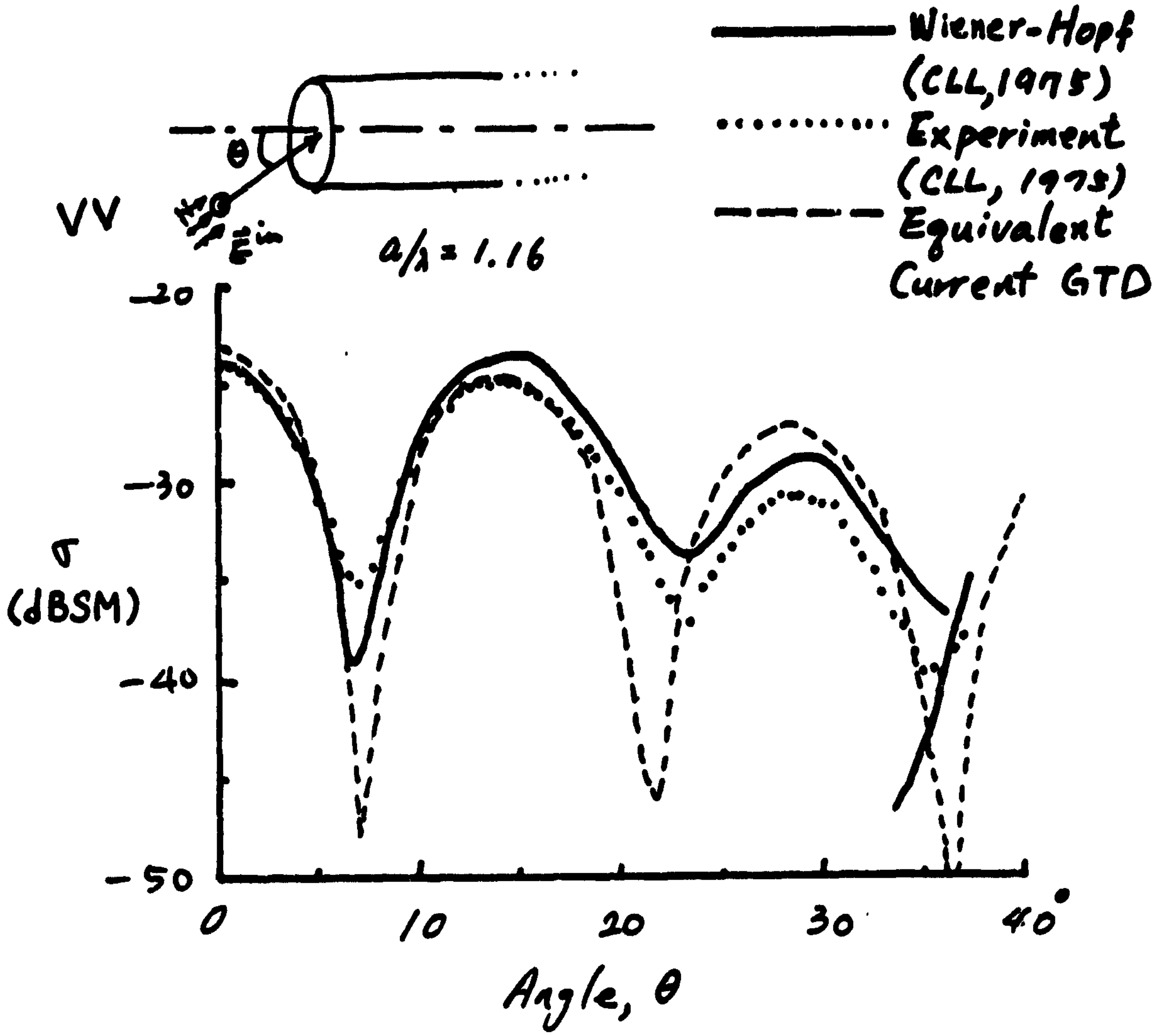

Figure 11a. The RCS's from an open-ended semi-infinite circular waveguide using the equivalent-current (EC) method (– – – – –) in comparison with the results using the Wiener-Hopf technique (————) and the experimental data (•••••••) [13] (VV polarization, a = 3.81 cm, f = 9.1 GHz, a/λ = 1.16).

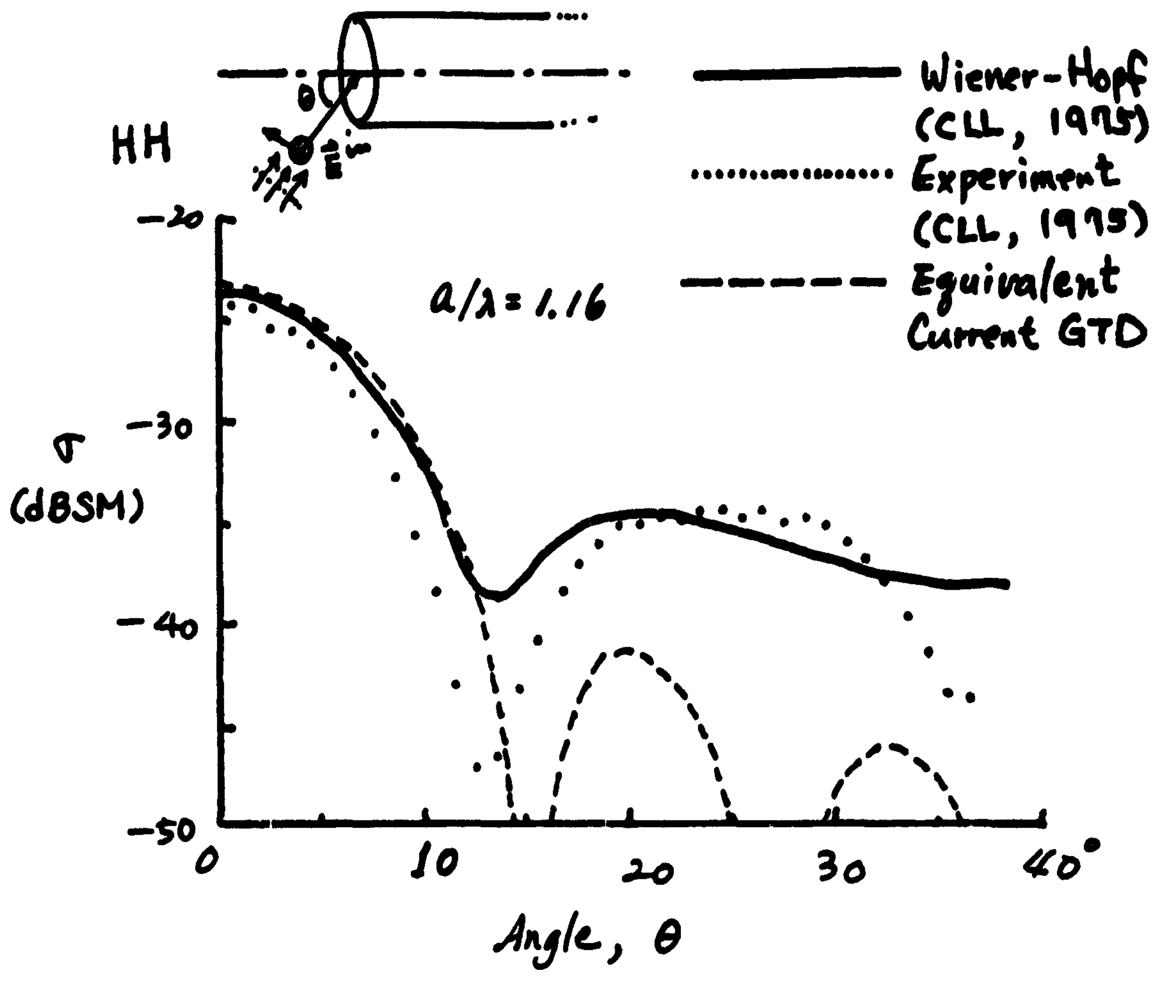

Figure 11b. The RCS's from an open-ended semi-infinite circular waveguide using the equivalent-current (EC) method (– – – – –) in comparison with the results using the Wiener-Hopf technique (———) and the experimental data (•••••••) [13] (HH polarization, a = 3.81 cm, f = 9.1 GHz, a/λ = 1.16).

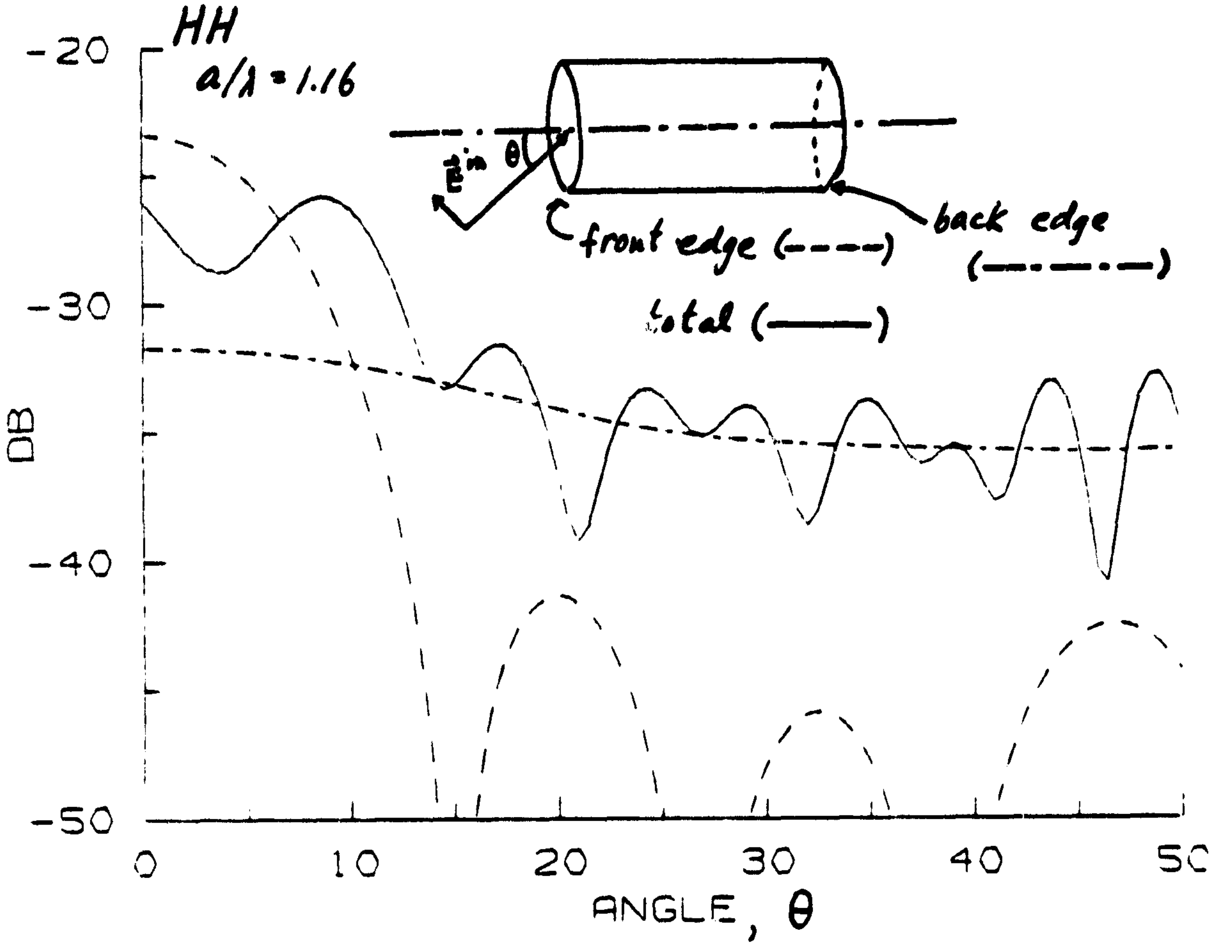

Figure 12a. The RCS from the rim diffraction of a PEC-terminated circular waveguide assuming the interior irradiation is completely suppressed (——— total, — — — —from front edge only, —·—·from back edge only, HH polarization, a = 3.81 cm, f = 9.1 GHz, a/λ = 1.16)

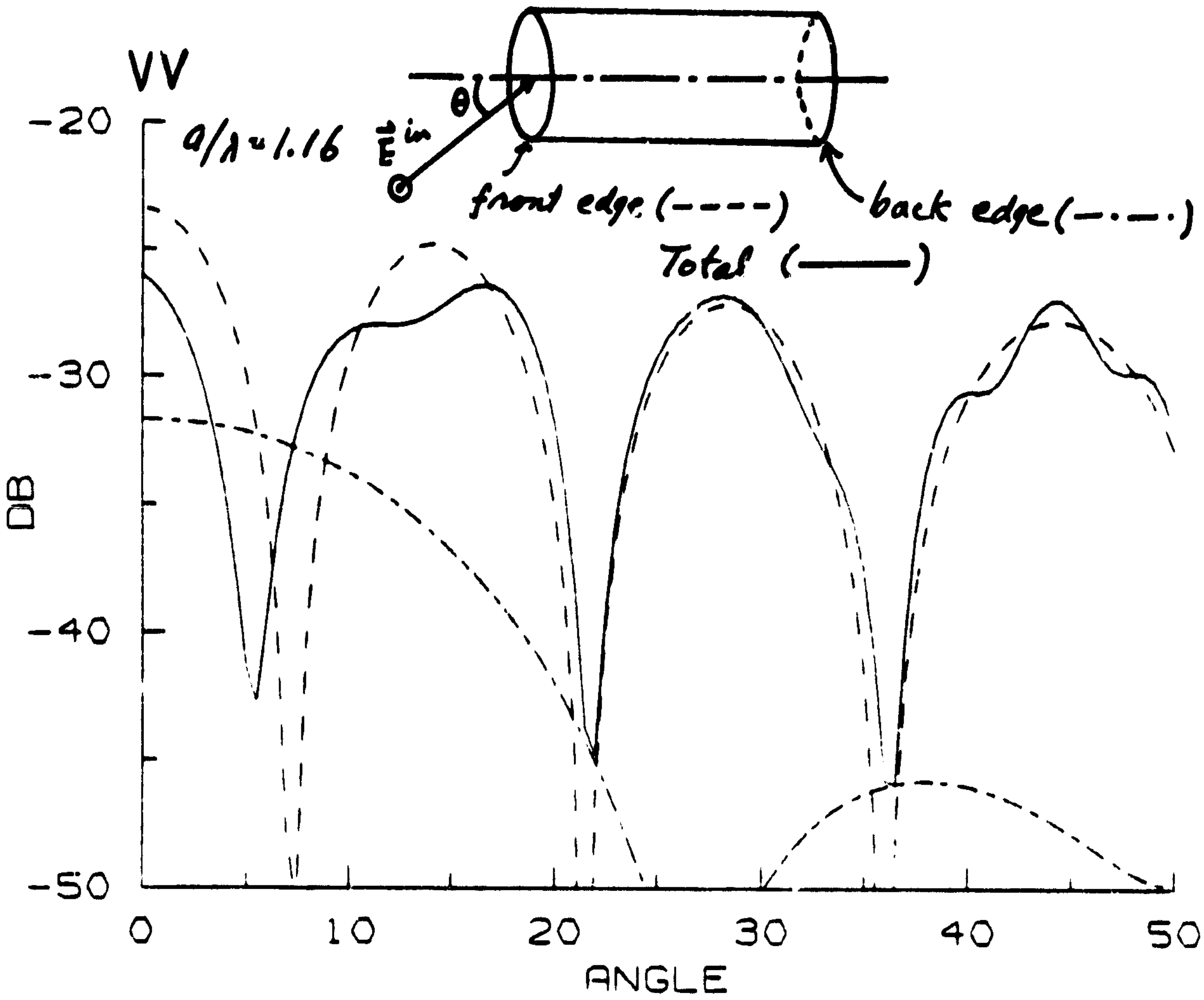

Figure 12b. The RCS from the rim diffraction of a PEC-terminated circular waveguide assuming the interior irradiation is completely suppressed (——— total, – – – – from front edge only, —·—· from back edge only, VV polarization, a = 3.81 cm, f = 9.1 GHz, a/λ = 1.16

ORIGINAL PAGE IS
OF POOR QUALITY

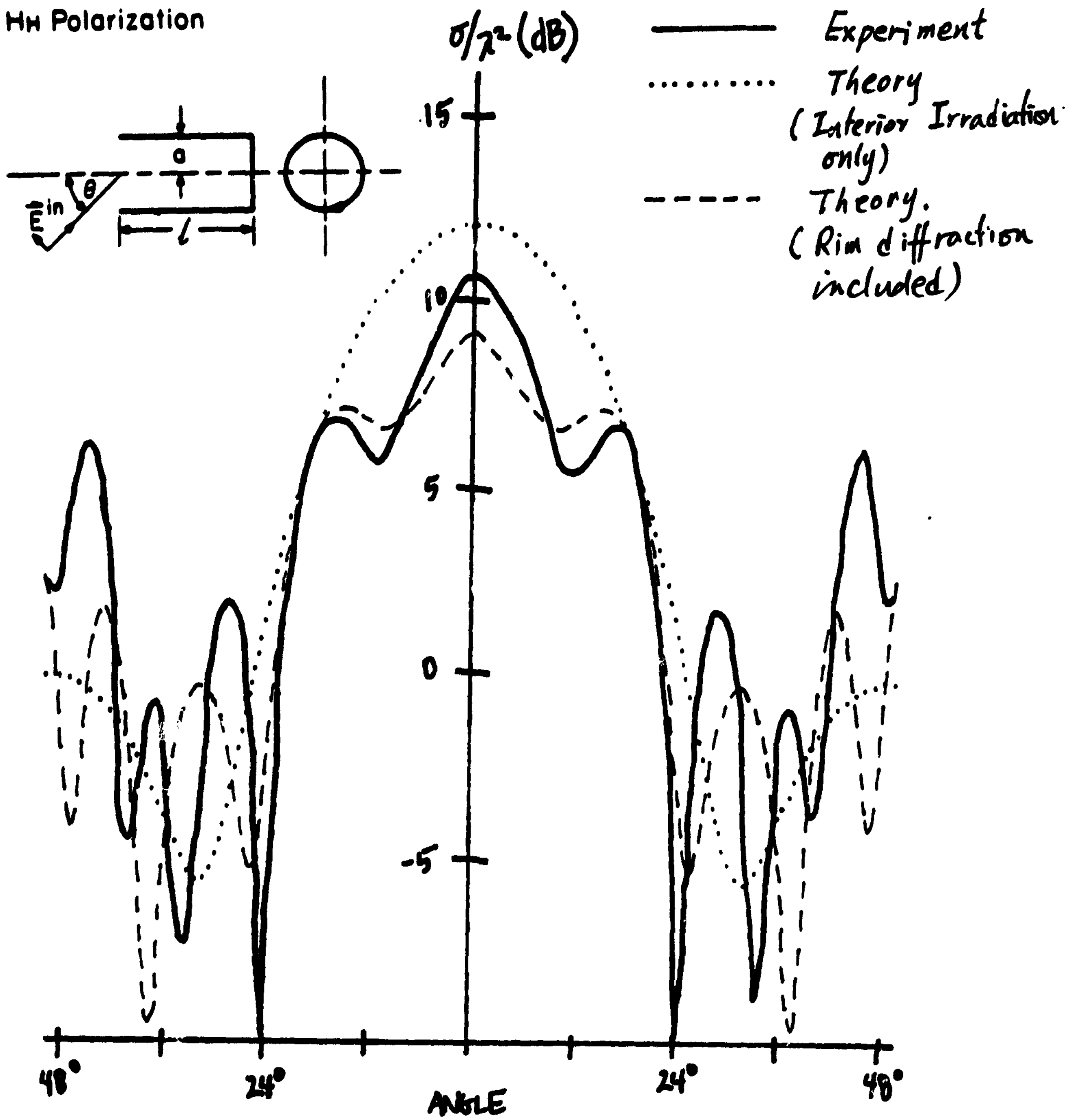

Figure 13a. The RCS's from a PEC-terminated waveguide (———experimental;·······theoretical, interior irradiation only;- - - - theoretical, rim diffraction included) as a function of the incident angle (HH polarization, a = 3.137 cm, f = 6.08 GHz, a/λ = 0.636, length = 21.59 cm).

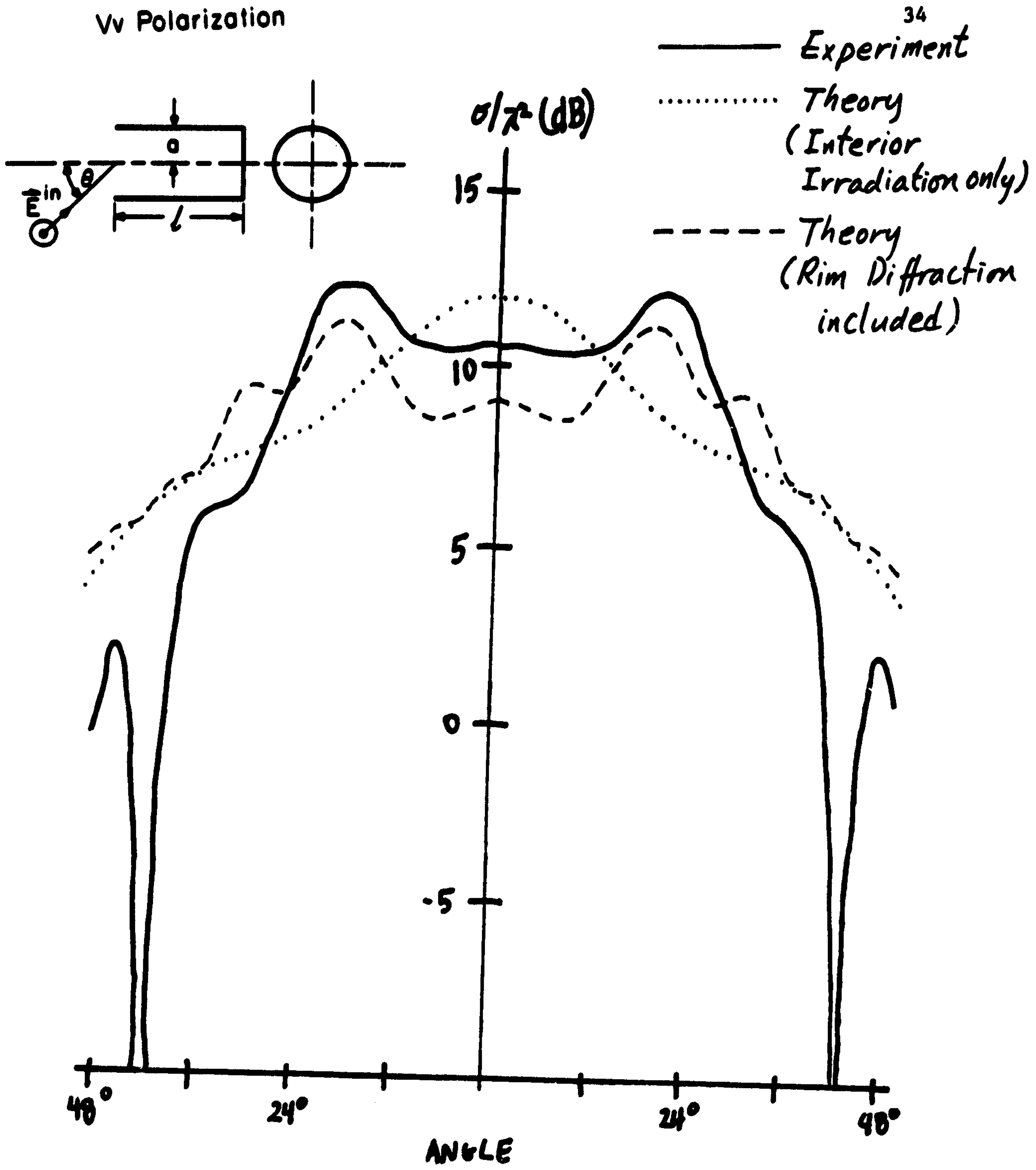

Figure 13b. The RCS's from a PEC-terminated waveguide (——— experimental, ······ theoretical, interior irradiation only; – – – – theoretical, rim diffraction included) as a function of the incident angle (VV polarization, a = 3.137 cm, f = 6.08 GHz, a/λ = 0.636, length = 21.59 cm).

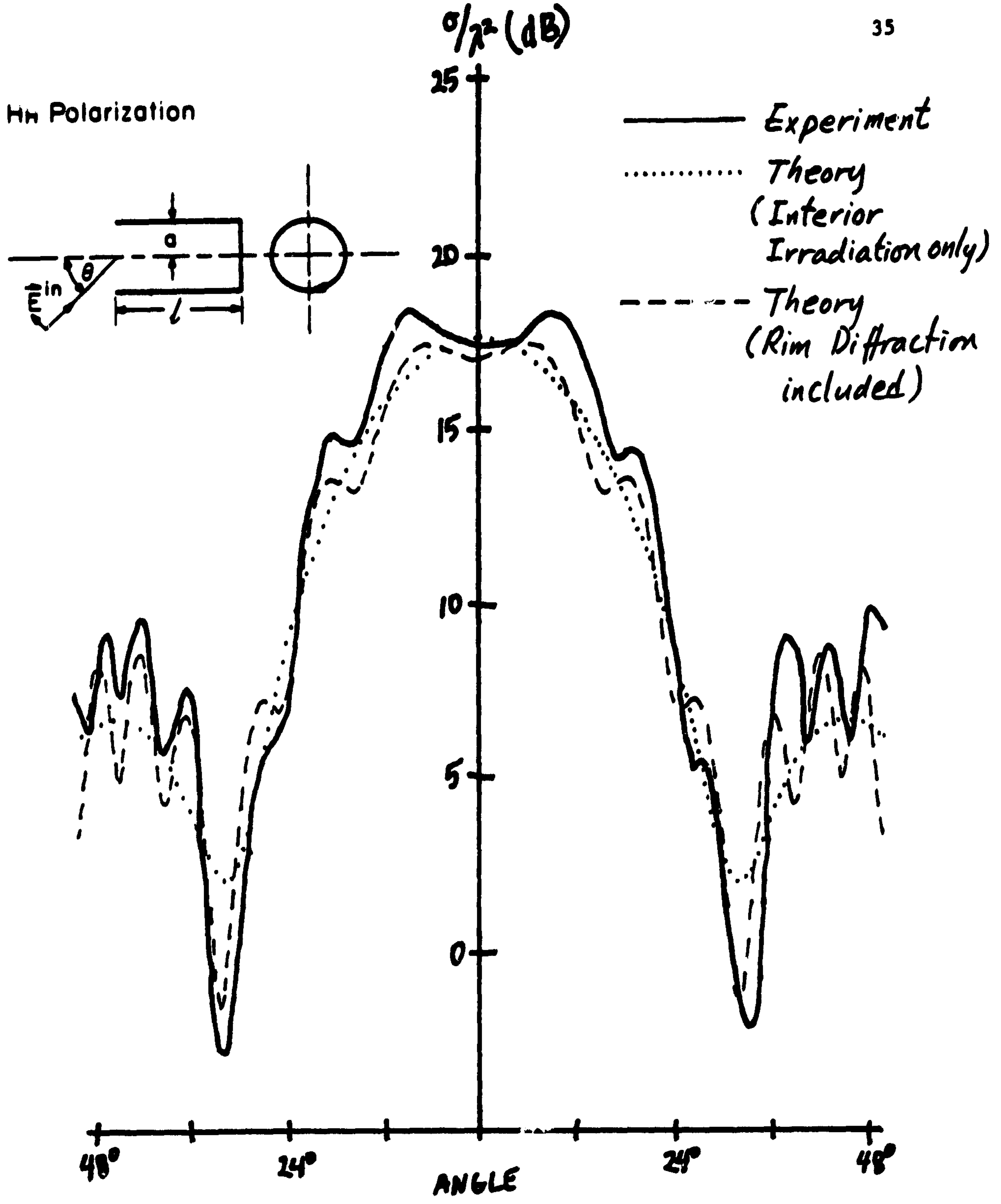

Figure 14a. The RCS's from a PEC-terminated waveguide (——— experimental, ······· theoretical, interior irradiation only; – – – – theoretical, rim diffraction included) as a function of the incident angle (HH polarization, a = 3.137 cm, f = 9.13 GHz, a/λ = 0.955, length = 21.59 cm).

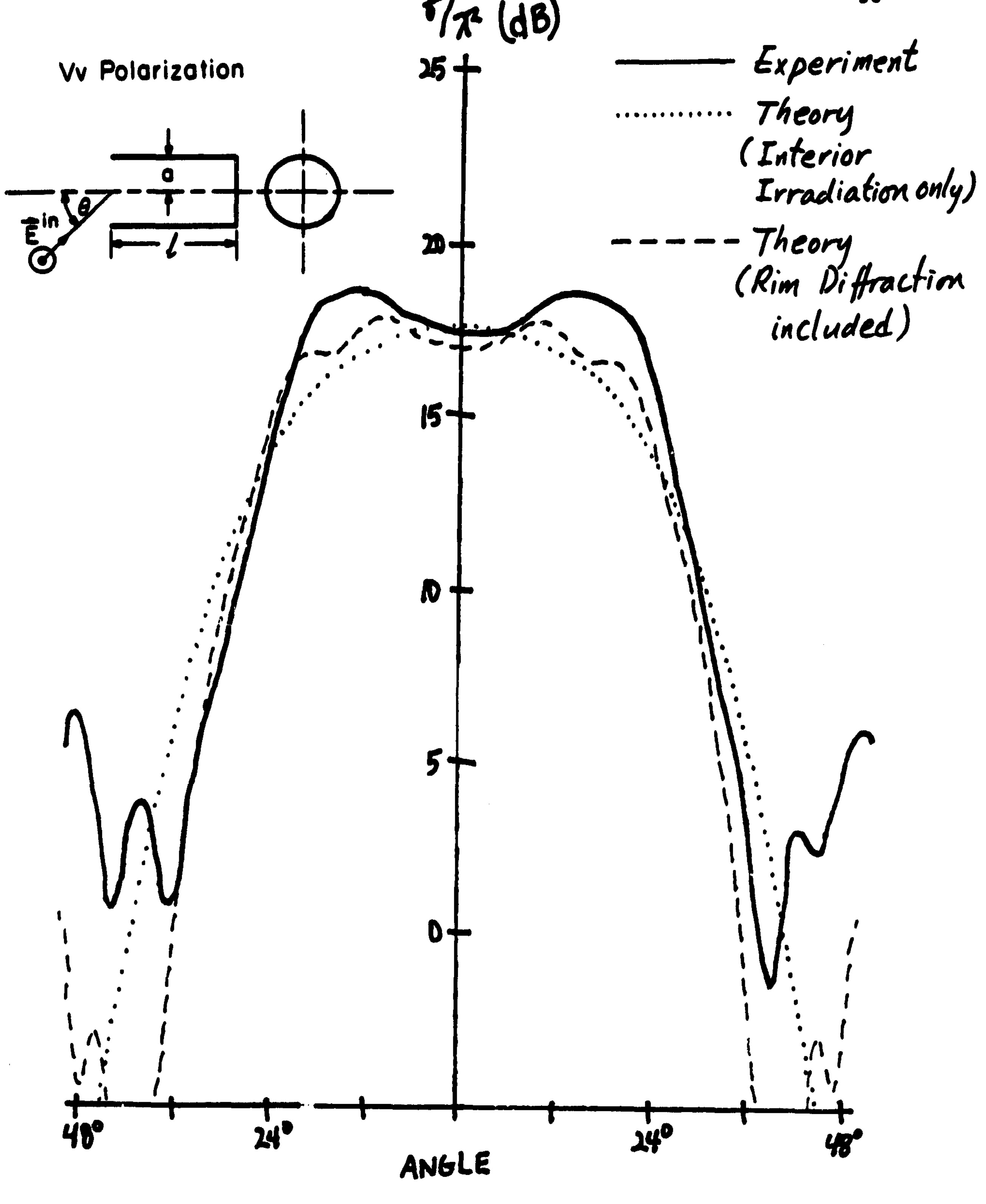

Figure 14b. The RCS's from a PEC-terminated waveguide (——— experimental, ······ theoretical, interior irradiation only; – – – – theoretical, rim diffraction included) as a function of the incident angle (VV polarization, a = 3.137 cm, f = 9.13 GHz, a/λ = 0.955, length = 21.59 cm).

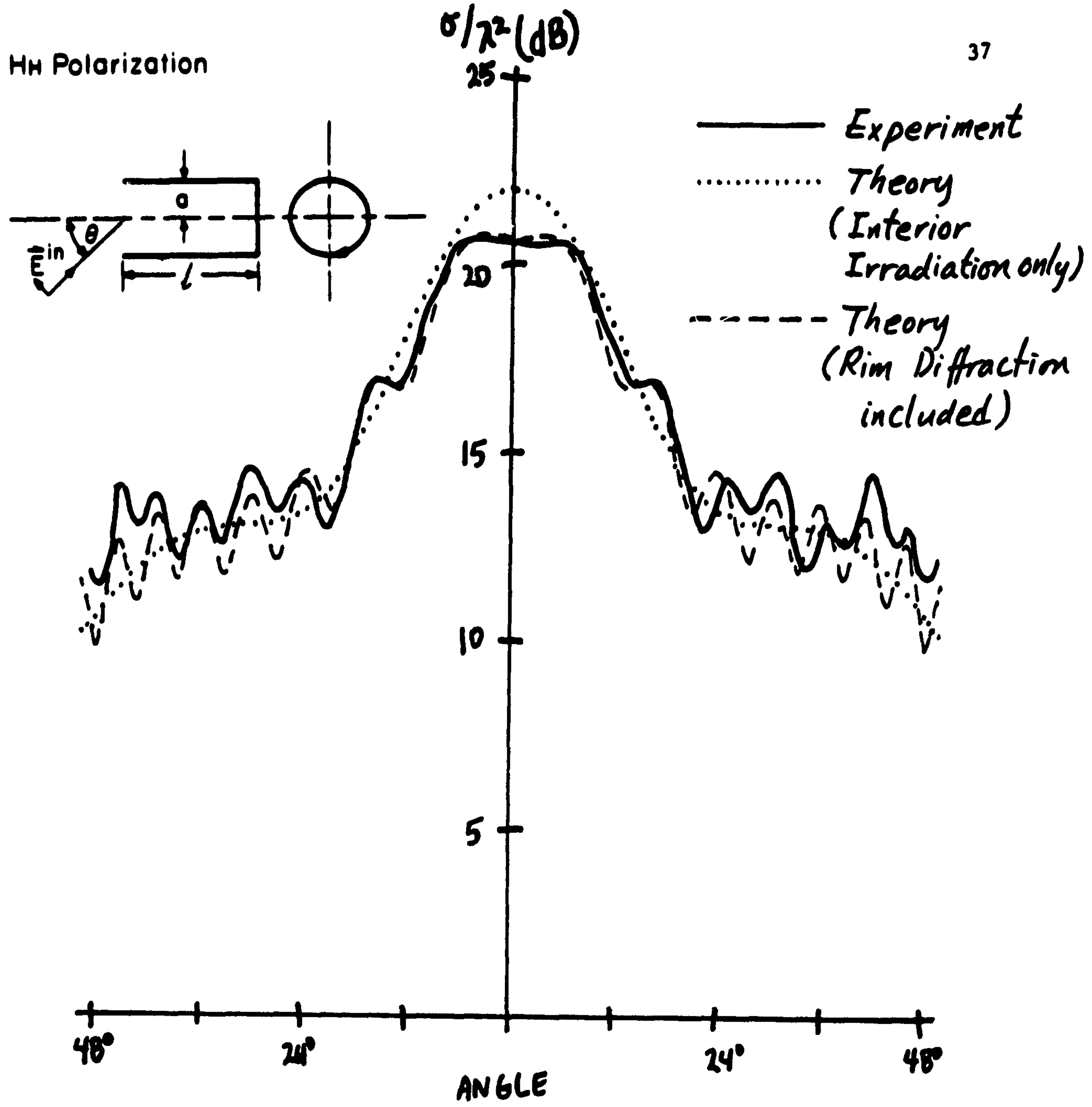

Figure 15a. The RCS's from a PEC-terminated waveguide (——— experimental, ········ theoretical, interior irradiation only; – – – – theoretical, rim diffraction included) as a function of the incident angle (HH polarization, a = 3.137 cm, f = 10.63 GHz, a/λ = 1.112, length = 21.59 cm).

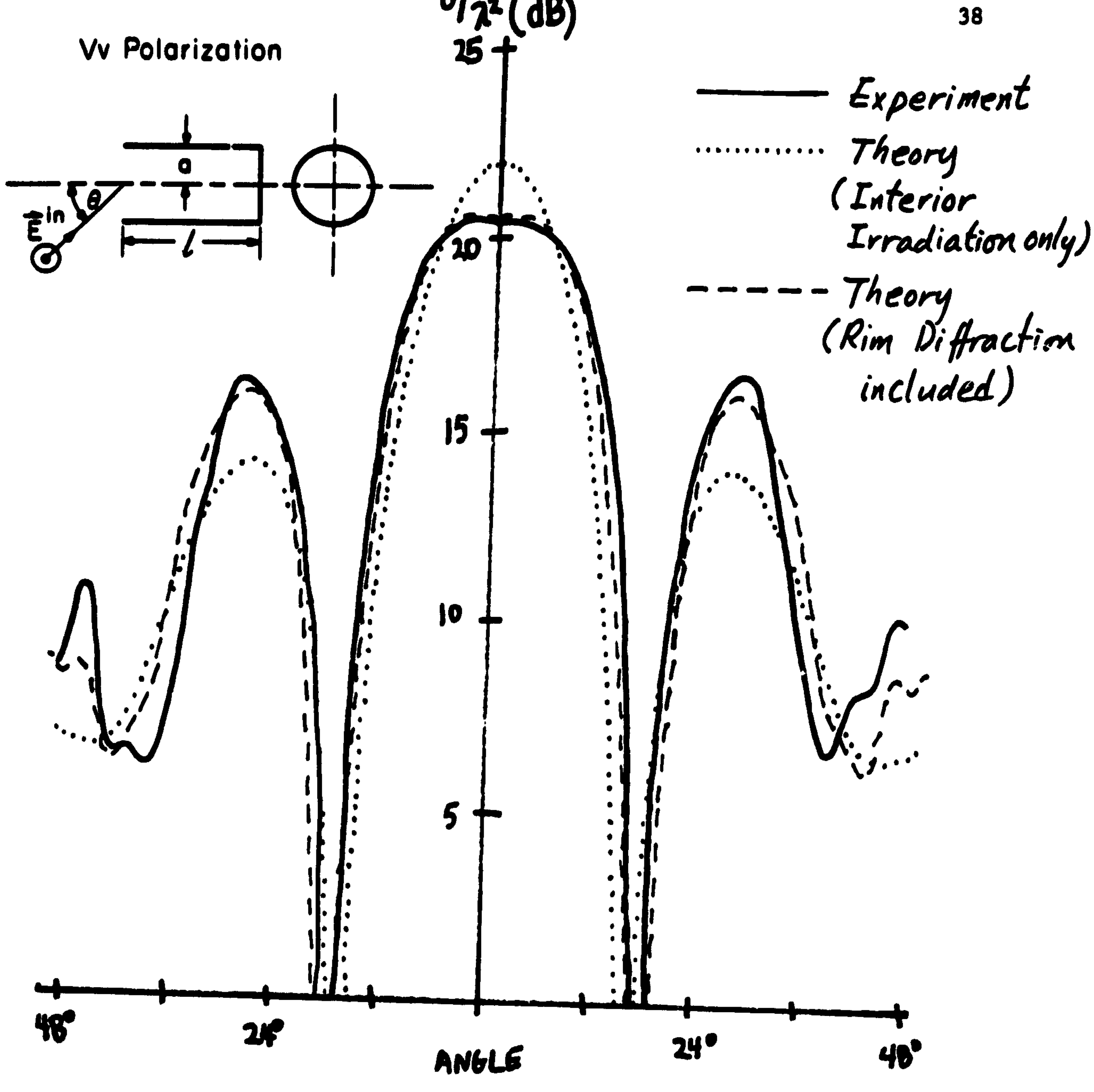

Figure 15b. The RCS's from a PEC-terminated waveguide (——— experimental, ······ theoretical, interior irradiation only; - - - - theoretical, rim diffraction included) as a function of the incident angle (VV polarization, a = 3.137 cm, f = 10.63 GHz, a/λ = 1.112, length = 21.59 cm).

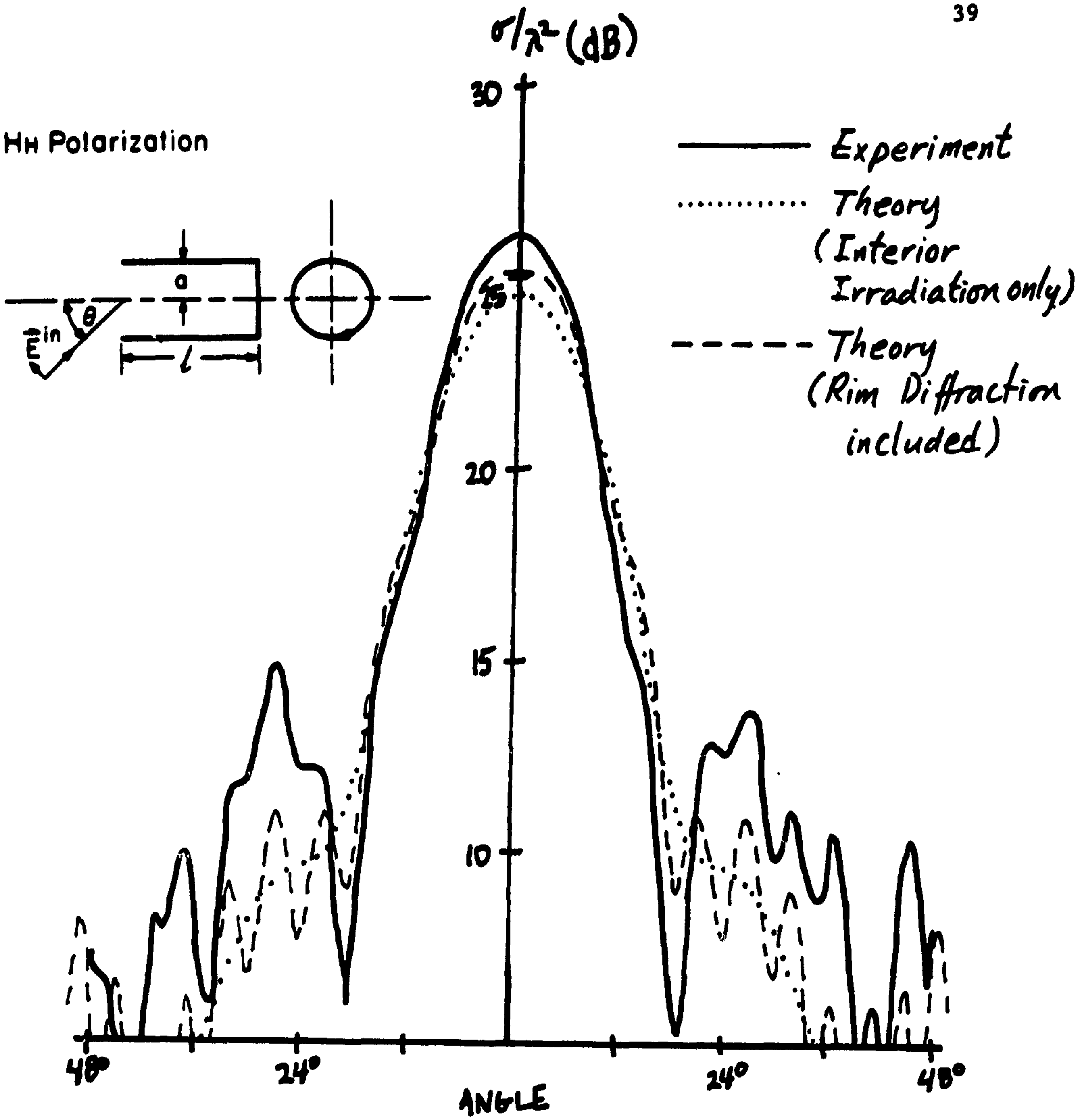

Figure 16a. The RCS's from a PEC-terminated waveguide (——— experimental, ······ theoretical, interior irradiation only; – – – – theoretical, rim diffraction included) as a function of the incident angle (HH polarization, a = 3.137 cm, f = 12.17 GHz, a/λ = 1.237, length = 21.59 cm).

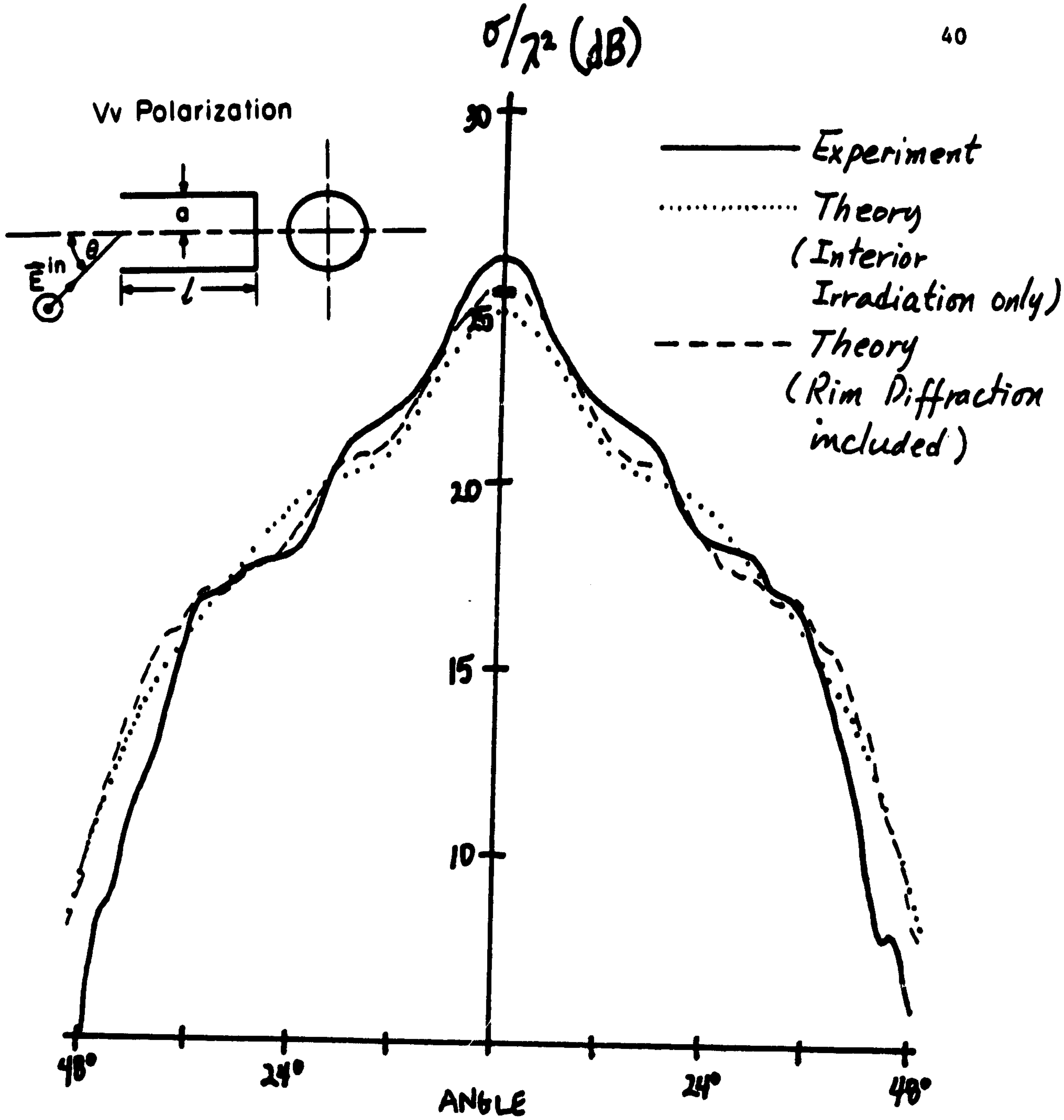

Figure 16b. The RCS's from a PEC-terminated waveguide (——— experimental, ······· theoretical, interior irradiation only; – – – –theoretical, rim diffraction included) as a function of the incident angle (VV polarization, a = 3.137 cm, f = 12.17 GHz, a/λ = 1.237, length = 21.59 cm).

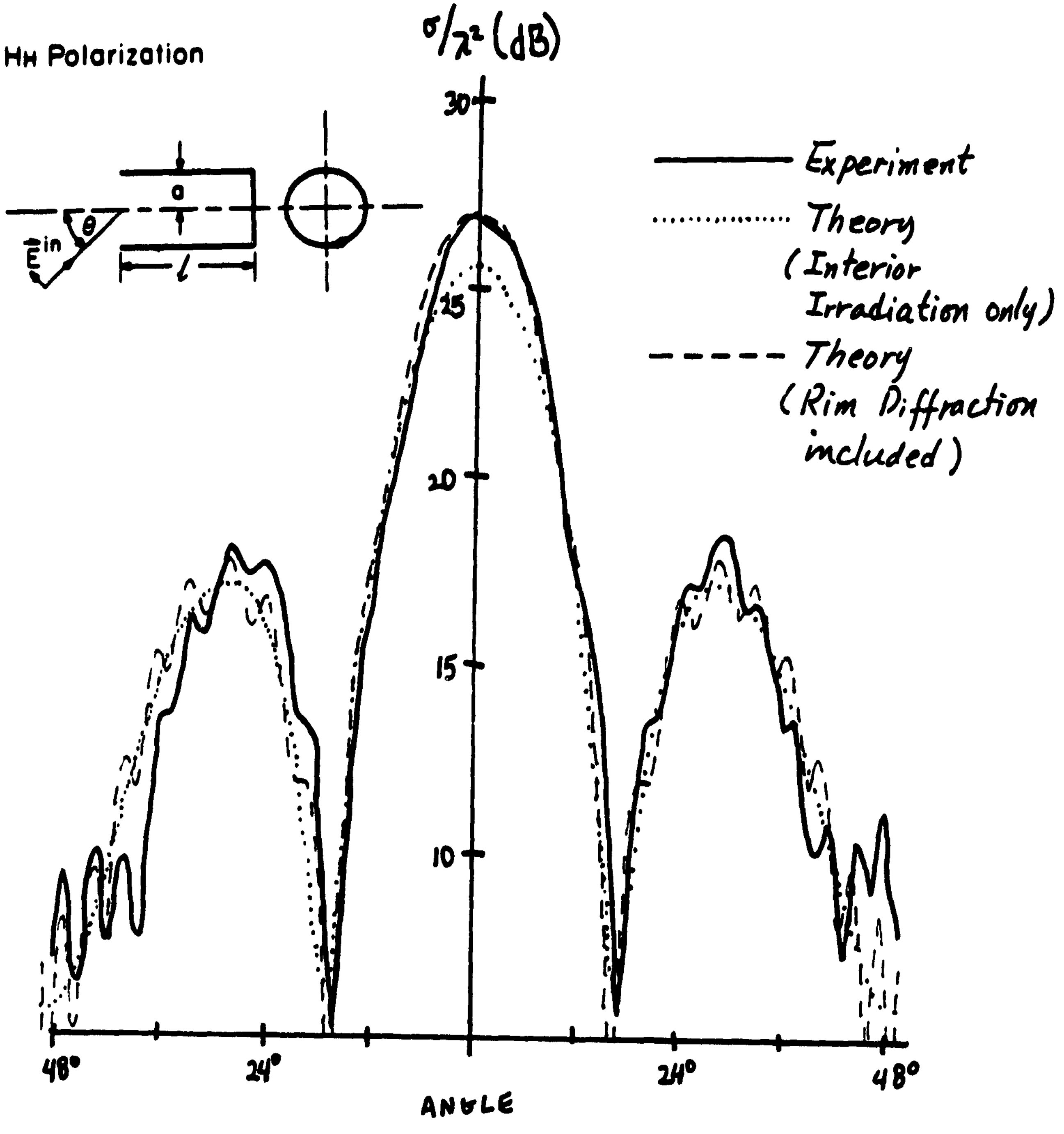

Figure 17a. The RCS's from a PEC-terminated waveguide (——— experimental,······ theoretical, interior irradiation only;– – – –theoretical, rim diffraction included) as a function of the incident angle (HH polarization, a = 3.137 cm, f = 13.68 GHz, a/λ = 1.430, length = 21.59 cm).

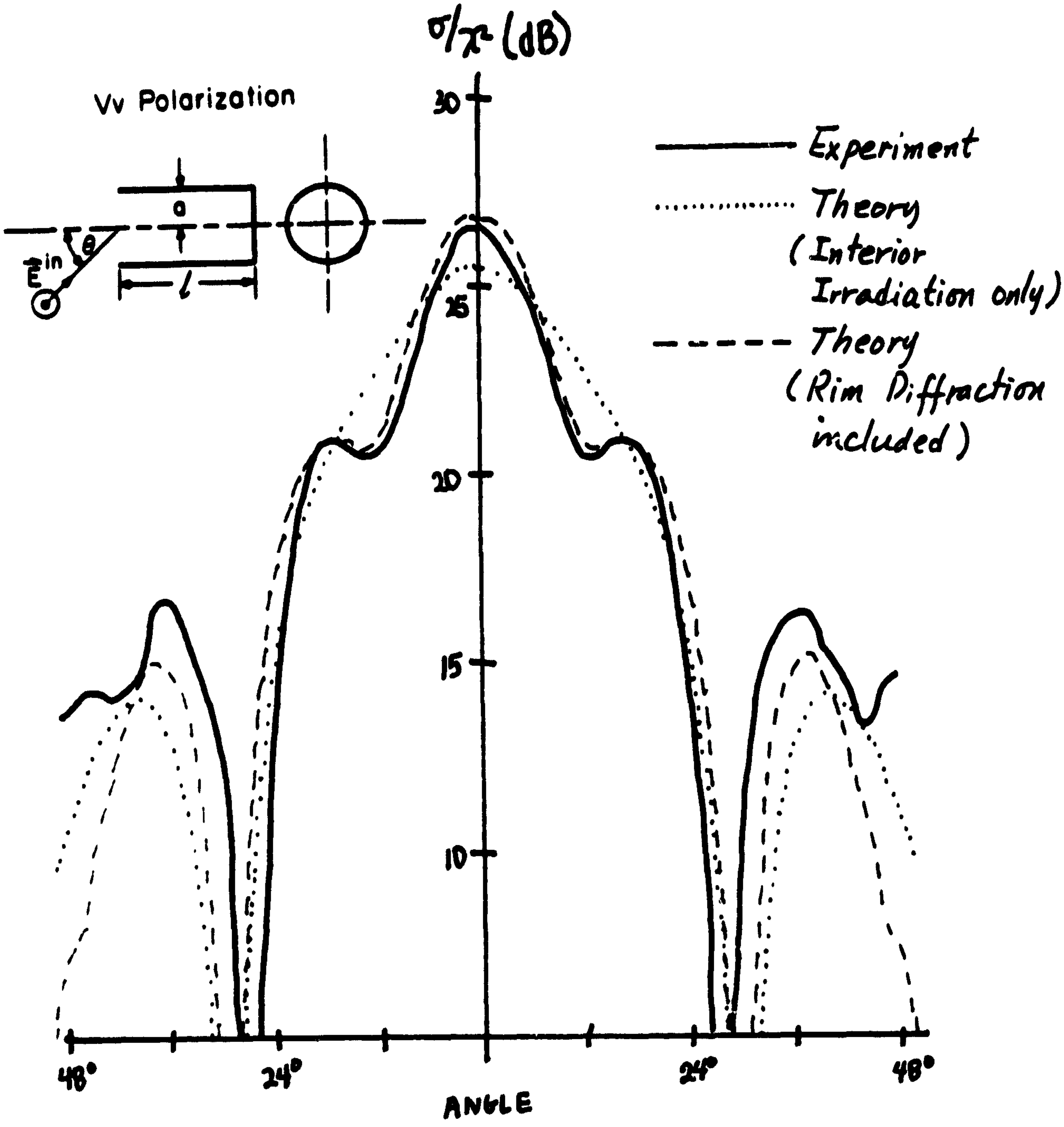

Figure 17b. The RCS's from a PEC-terminated waveguide (——— experimental, ······· theoretical, interior irradiation only; – – – – theoretical, rim diffraction included) as a function of the incident angle (VV polarization, a = 3.137 cm, f = 13.68 GHz, a/λ = 1.430, length = 21.59 cm).

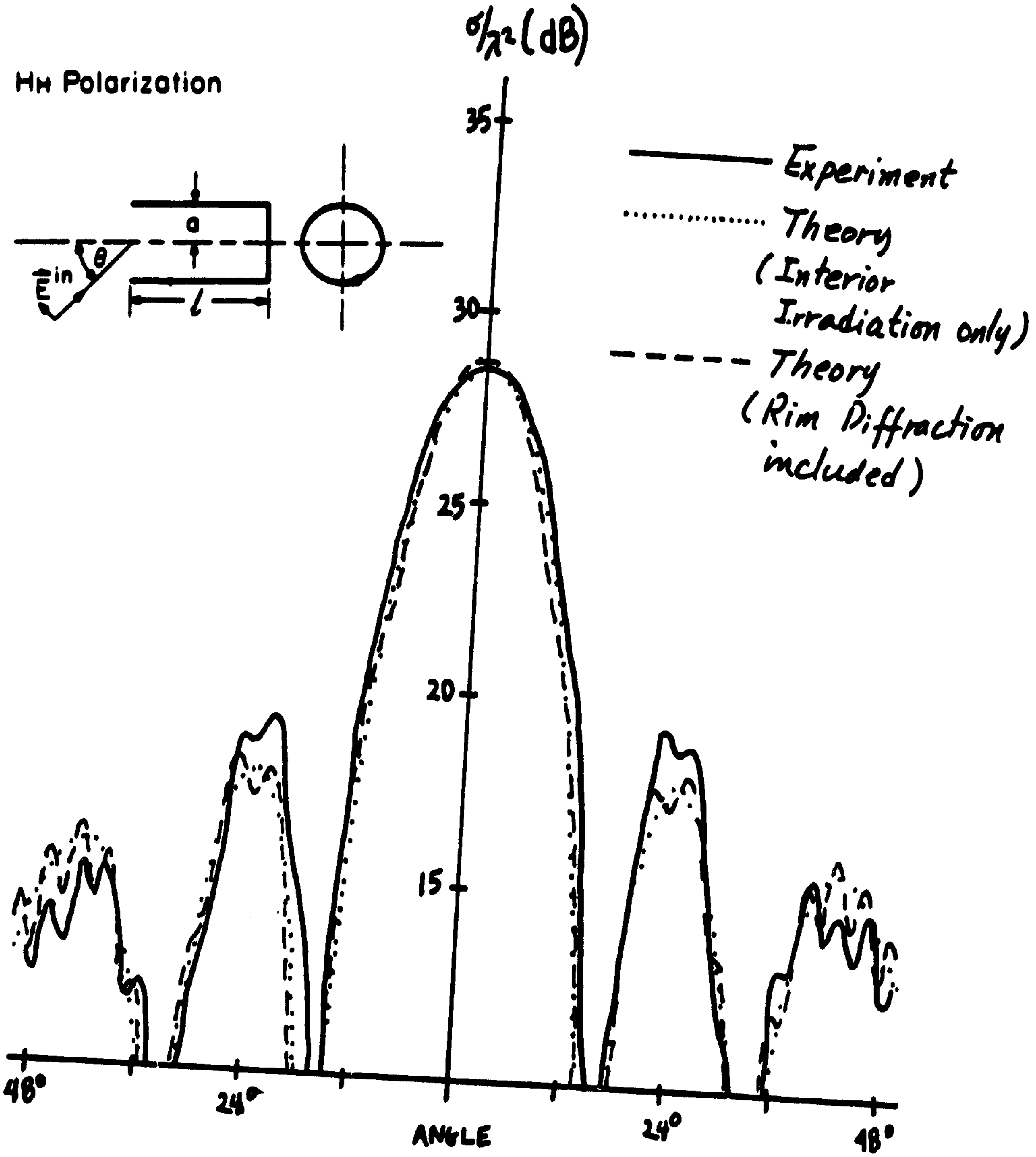

Figure 18a. The RCS's from a PEC-terminated waveguide (——— experimental, ······· theoretical, interior irradiation only; – – – – theoretical, rim diffraction included) as a function of the incident angle (HH polarization, a = 3.137 cm, f = 15.20 GHz, a/λ = 1.589, length = 21.59 cm).

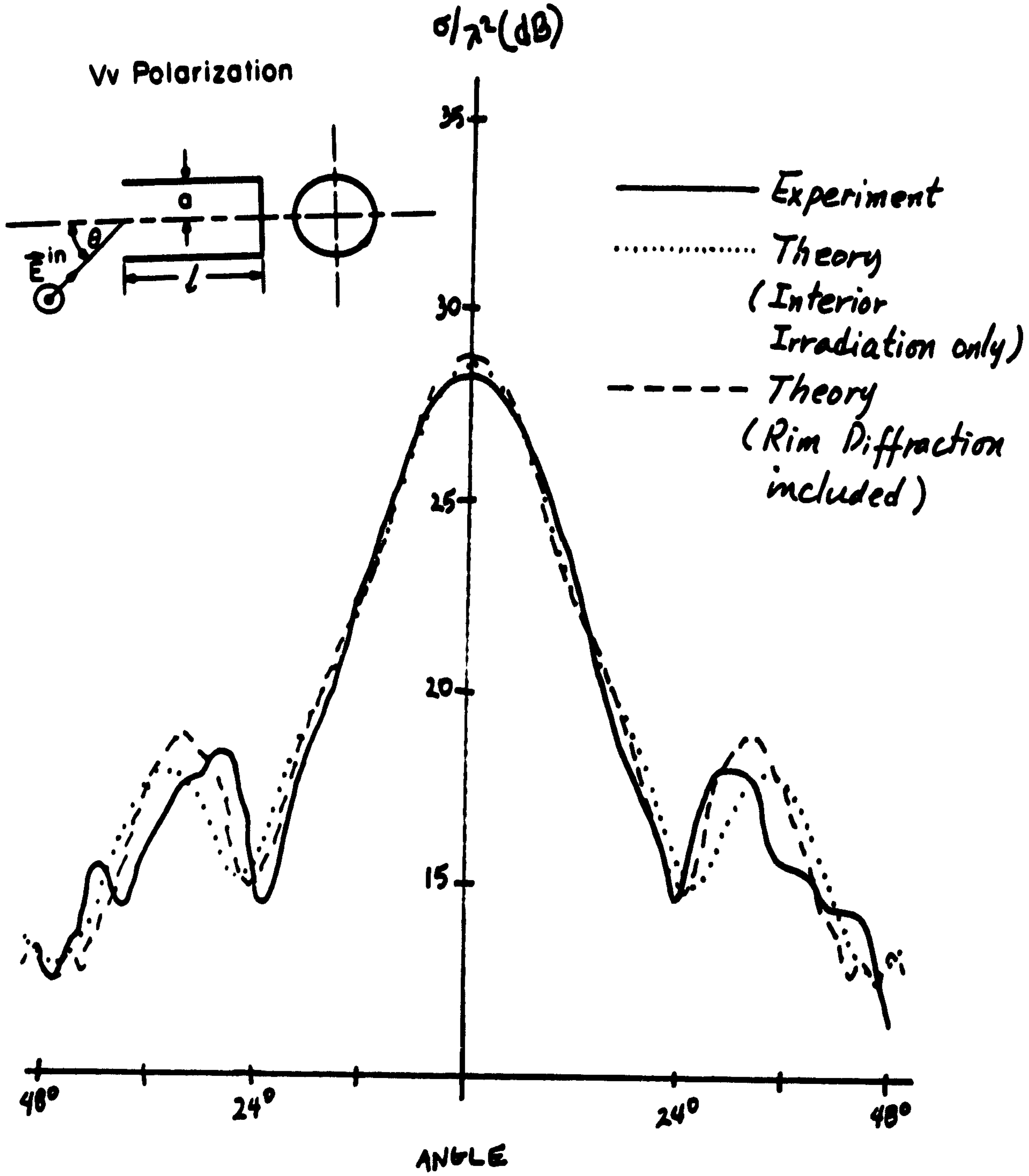

Figure 18b. The RCS's from a PEC-terminated waveguide (——— experimental, ······ theoretical, interior irradiation only; – – – – theoretical, rim diffraction included) as a function of the incident angle (VV polarization, a = 3.137 cm, f = 15.20 GHz, a/λ = 1.589, length = 21.59 cm).

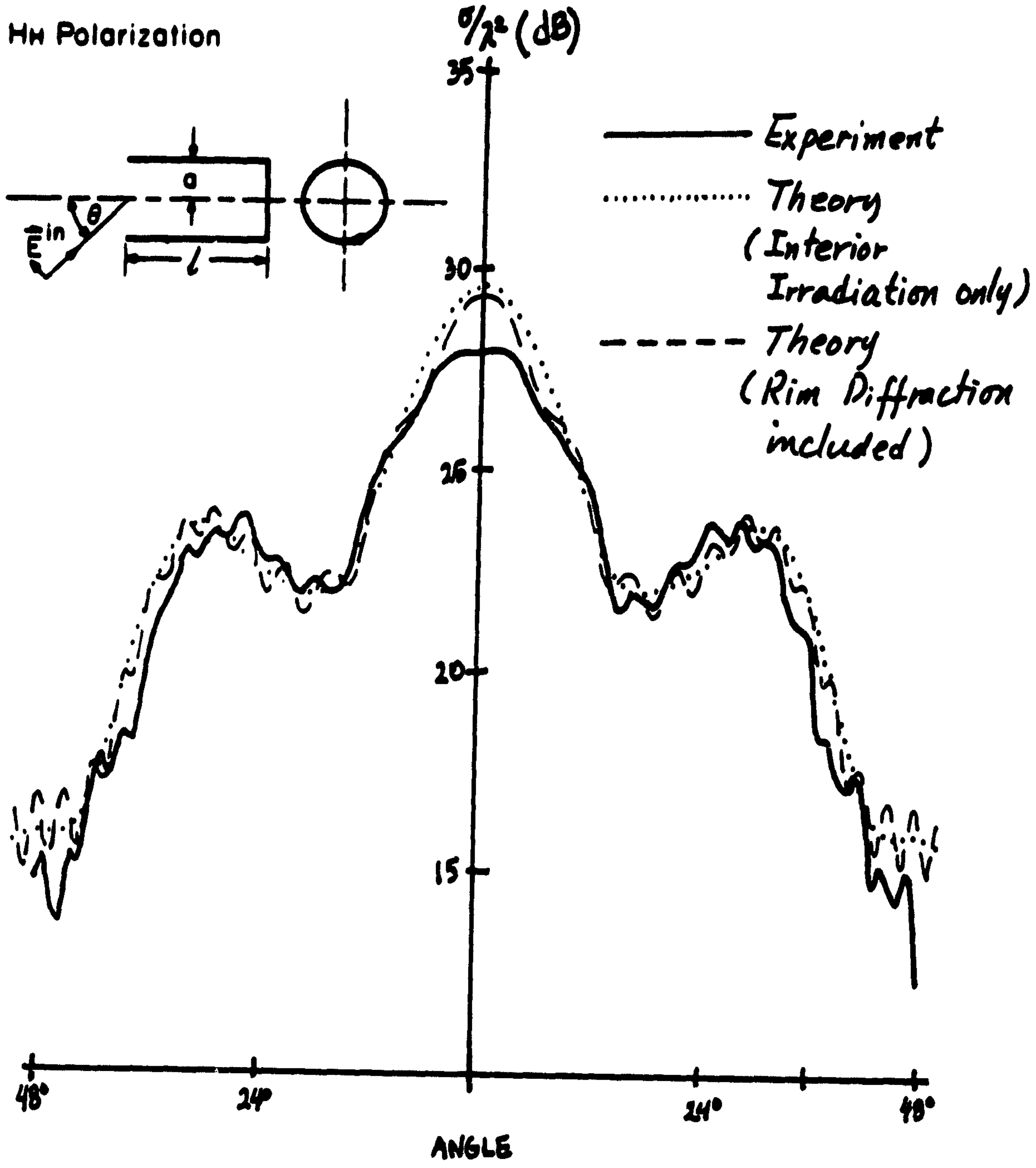

Figure 19a. The RCS's from a PEC-terminated waveguide (———experimental,······theoretical, interior irradiation only; – – – –theoretical, rim diffraction included) as a function of the incident angle (HH polarization, a = 3.137 cm, f = 18.0 GHz, a/λ = 1.88, length = 21.59 cm).

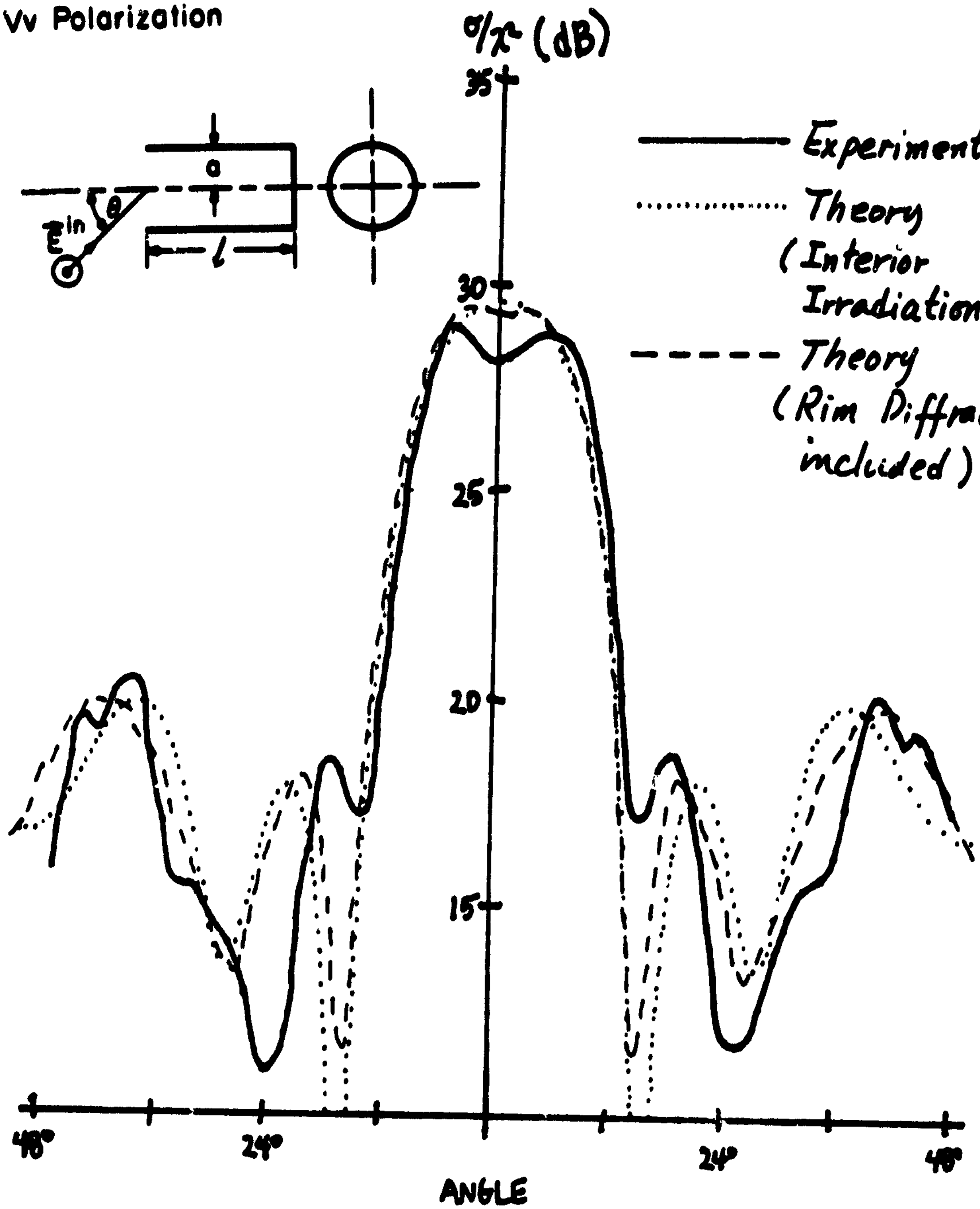

Figure 19b. The RC s from a PEC-terminated waveguide (——— experimental, ······· theoretical, interior irradiation only; – – – – theoretical, rim diffraction included) as a function of the incident angle (VV polarization, a = 3.137 cm, f = 18.0 GHz, a/λ = 1.88, length = 21.59 cm).

However, if the transmitted modes due to the outside illumination can be attenuated by the coating, we expect the contributions from other than the interior irradiation, e.g., the rim diffraction, will be significant enough to affect the overall RCS. Thus, we have to include the effect of the rim diffraction in our calculation when comparing our analysis with future experimental data of the RCS from a coated guide. Further details are given in Section (4) below.

(4) <u>The outlines of the proposed experiments for the RCS reduction from a circular waveguide coated with lossy material</u>

The RCS from the jet intake is mainly due to the rim diffraction and interior irradiation. The main goal of our research is to reduce, as much as possible, the interior irradiation from the jet intake. One way to achieve this goal is to coat the interior wall of the jet intake with a lossy material. Once the wave is transmitted from the outside illumination, the wave will attenuate as it propagates through the interior of the jet intake before it scatters back to the outside.

For our theoretical model, we approximate the jet intake by a cylindrical waveguide terminated by a PEC. From the theoretical study at the University of Illinois, the following results are obtained:

1. The interior irradiation from a circular waveguide terminated by a PEC contributes to the RCS much more than the rim diffraction (more than 10 dB for $a/\lambda > 1$).
2. A very lossy magnetic material is suggested for coating at low frequency ($a/\lambda > 1$). With a layer thickness less than 1% of the radius, the RCS from a 7-radius-long circular waveguide ($a/\lambda = 1.2$)

terminated by a PEC can be reduced by more than 10 dB over a broad incident angle, using the best coating material reported in the literature.

3. At high frequency ($a/\lambda > 3$), the modal separation between the highly attenuated and the lowly attenuated modes occurs if the coating material is too lossy. This is not desirable in the application of the RCS reduction because the unattenuated normal modes will cause a large RCS in a certain incident angle. With the modal separation, increasing the coating thickness would not help much to reduce the RCS because the attenuation constants of the normal modes do not change much with the coating thickness in this limit. Therefore, at the high frequency, the coating material must be less lossy than that at the low frequency. Using the less lossy material for the coating, some high-order modes do not attenuate much and a much thicker layer is required for those modes to attenuate considerably. However, the RCS for a small incident angle is mainly due to the low-order modes. Since in most practical applications, the RCS reduction is required only for a small incident angle, the coating layer does not have to be thick to get a desired RCS reduction.

The purpose of the proposed experiment is to verify our theoretical predictions of the RCS reduction from a circular waveguide coated with a lossy material. Since the behavior of the normal modes in the lossy waveguide depends strongly on the value of a/λ, the low- and high-frequency cases should be treated separately.

Low-Frequency Case

1. The low-frequency case is defined when the field distributions of the normal modes do not change much due to the coating inside the waveguide. The suggested value of a/λ is 1.2, e.g., $a = 3.95$ cm and $f = 9.2$ GHz. Any combinations of a and λ will be acceptable as far as a/λ is close to 1.2.
2. The coating near the opening of the waveguide must be gradual to prevent any mode conversions from highly attenuated modes to lowly attenuated modes. The detailed geometries of the waveguides are shown in Figure 20. Two different coating thicknesses for each waveguide with a tapered coating are suggested. Thus we need five cylinders, one empty guide and four coated waveguides. The coating thickness τ is approximately given by $\tau/a = 1 \sim 2$ % depending on the available coating material.
3. The coating material must be very lossy and magnetic, e.g., Crowloy BX113 ($\epsilon_r = 12-j0.144$, $\mu_r = 1.74-j3.306$) [15].
4. The scanning angle should be from $\theta = 0°$ (normal incidence) up to $\theta = 45°$ at least.
5. The anticipated results of the RCS reduction from our theoretical calculation are shown in Figure 21. Using the best material (Crowloy BX113) that we can find in the literature, more than 10 dB RCS reduction is achieved over a broad incident angle for both VV and HH polarizations with a coating thickness of $\tau/a = 1$ %. Note that as the interior irradiation is reduced by the coating, the rim diffraction becomes significant enough to affect the overall shape of the RCS.

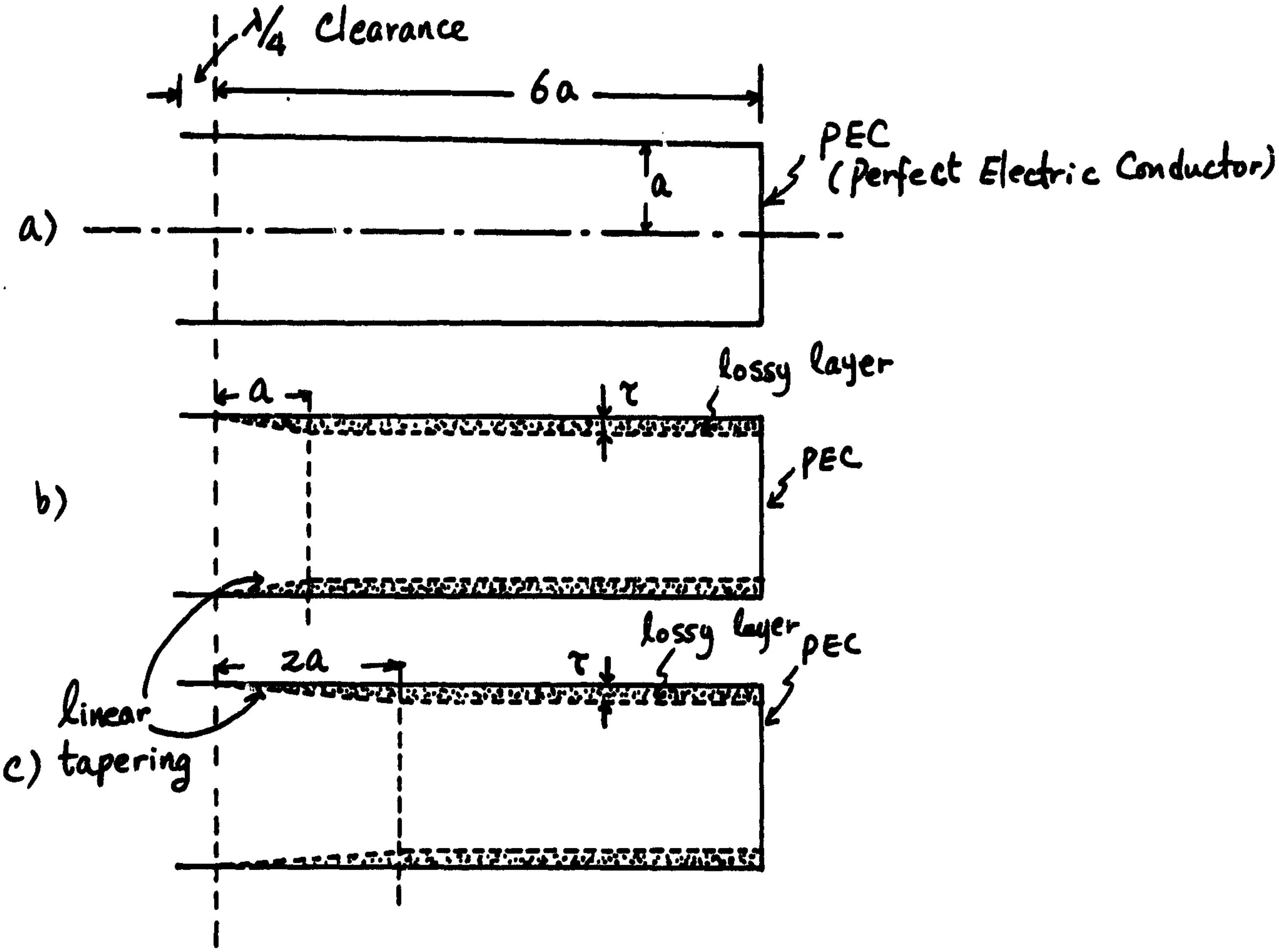

Figure 20. The geometries of the waveguides for the proposed experiments: a) empty guide, b) coated guide with a tapering distance of a, and c) coated guide with a tapering distance of 2a.

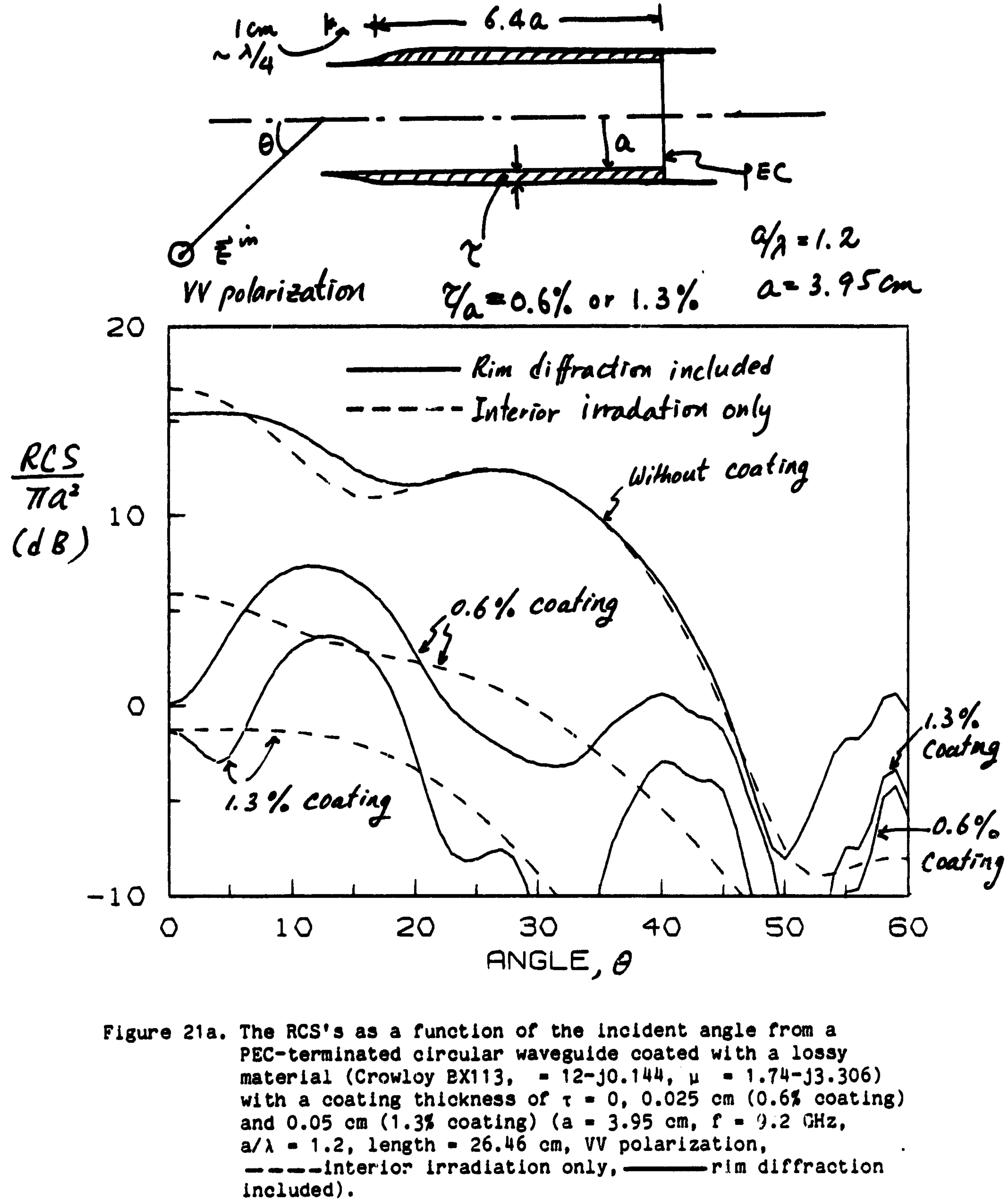

Figure 21a. The RCS's as a function of the incident angle from a PEC-terminated circular waveguide coated with a lossy material (Crowloy BX113, = 12-j0.144, μ = 1.74-j3.306) with a coating thickness of τ = 0, 0.025 cm (0.6% coating) and 0.05 cm (1.3% coating) (a = 3.95 cm, f = 9.2 GHz, a/λ = 1.2, length = 26.46 cm, VV polarization, ----interior irradiation only, ——— rim diffraction included).

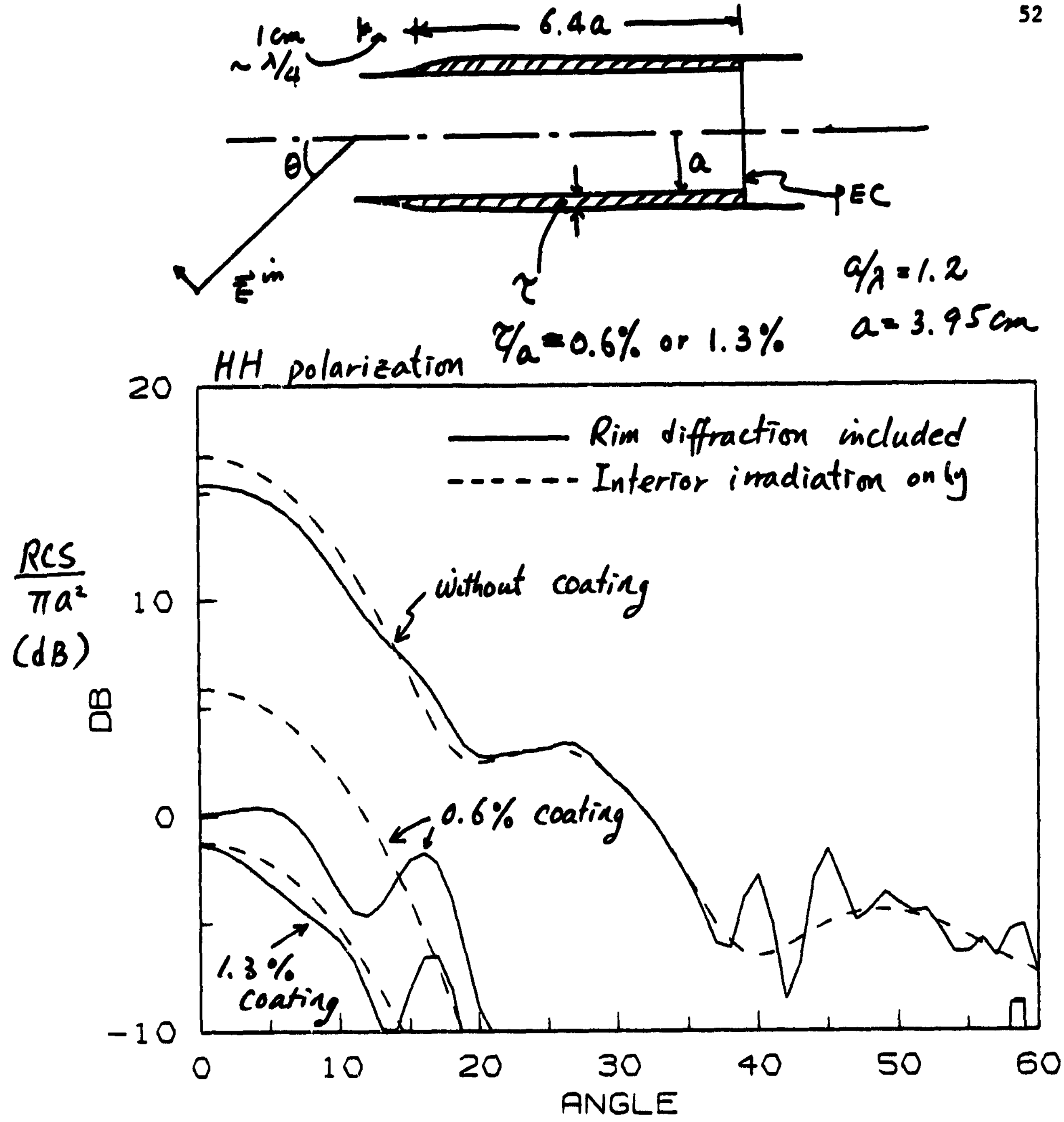

Figure 21b. The RCS's as a function of the incident angle from a PEC-terminated circular waveguide coated with a lossy material (Crowloy BX113, = 12-j0.144, μ = 1.74-j3.306) with a coating thickness of τ = 0, 0.025 cm (0.6% coating) and 0.05 cm (1.3% coating) (a = 3.95 cm, f = 9.2 GHz, a/λ = 1.2, length = 26.46 cm, HH polarization, ----interior irradiation only, ——— rim diffraction included).

High-Frequency Case

1. At this frequency, the change of the modal fields due to the coating is significant. The suggested value of a/λ is 3.3, e.g., a = 10 cm and f = 10 GHz. Any combinations of a and λ will be acceptable as far as a/λ is close to 3.3.

2. The geometries of the waveguides for the proposed experiment are the same as those of the low-frequency case as shown Figure 20. As in the low-frequency case, we need five cylinders, one empty guide and four coated guides. $\tau/a = 1 \sim 3$ % depending on the available coating material.

3. The coating material should be magnetic and less lossy than that of the low-frequency case, e.g., Poly-2,5-dichlorostyrene ($\epsilon_r = 7.3$, $\mu_r = 0.91 - j0.32$) [15].

4. The scanning angle is $\theta = 0 \sim 45°$.

5. The anticipated results of the RCS reduction from our theoretical calculation are shown in Figure 22. The RCS for the small incident angle (< 10°) is reduced significantly even with a thin layer of coating. However, increasing the coating thickness does not help to reduce the RCS as much as in the low-frequency case. This indicates the sign of the mode separation between the lowly and highly attenuated modes. For the RCS reduction over a larger incident angle, a thick layer of coating with a less lossy coating material is suggested. Note that the rim diffraction does not affect the overall RCS as much as in the low-frequency case. This confirms our previous statement (Sections (2) and (3)) that the rim diffraction becomes less significant for a larger value of a/λ.

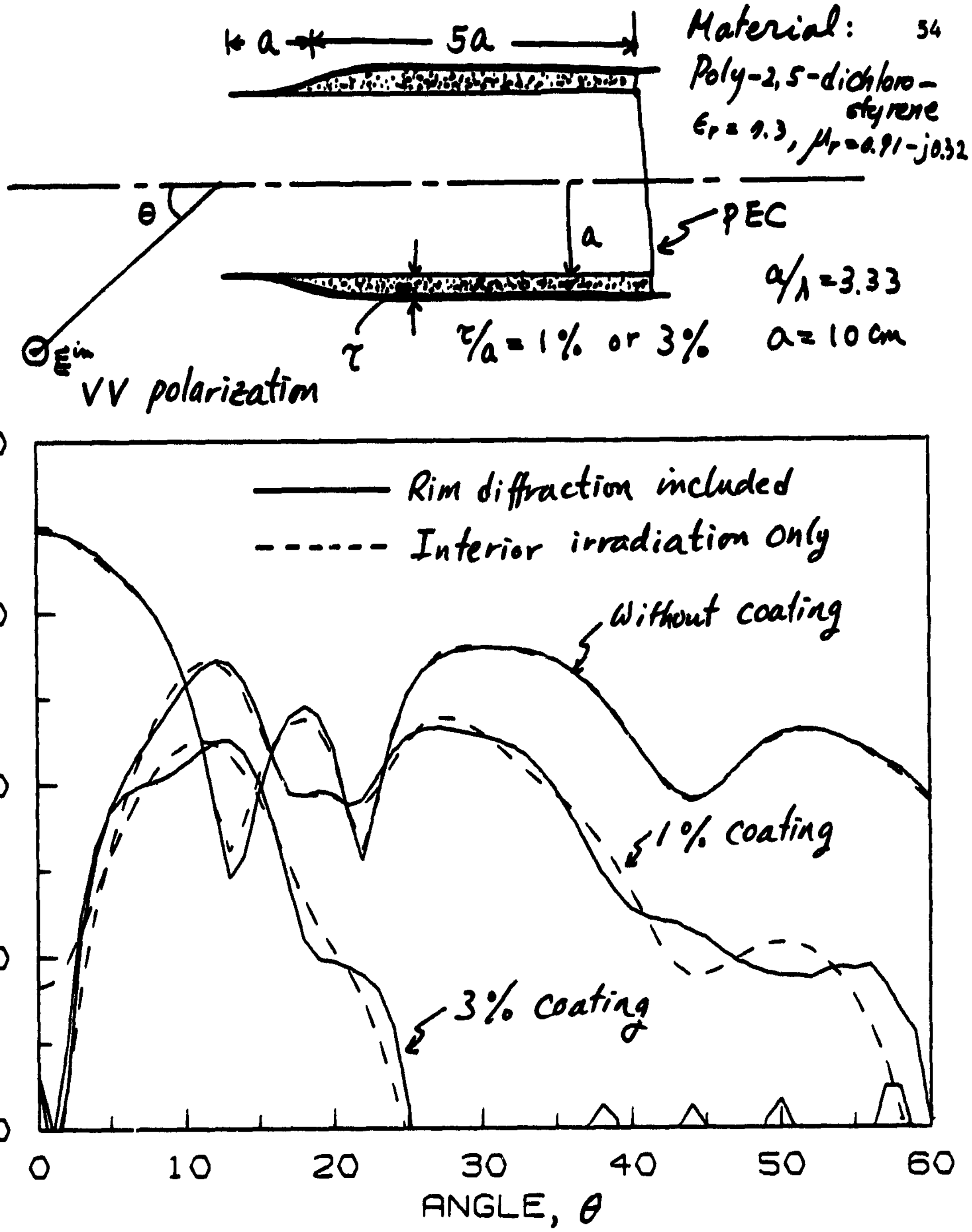

Figure 22a. The RCS's as a function of the incident angle from a PEC-terminated circular waveguide coated with a lossy material (poly-2,5-dichlorostyrene, = 7.3, μ = 0.91-j0.32) with a coating thickness of τ = 0, 0.1 cm (1% coating) and 0.3 cm (3% coating) (a = 10 cm, f = 10 GHz, a/λ = 3.33, length = 60 cm, VV polarization, ----interior irradiation only, ———rim diffraction included).

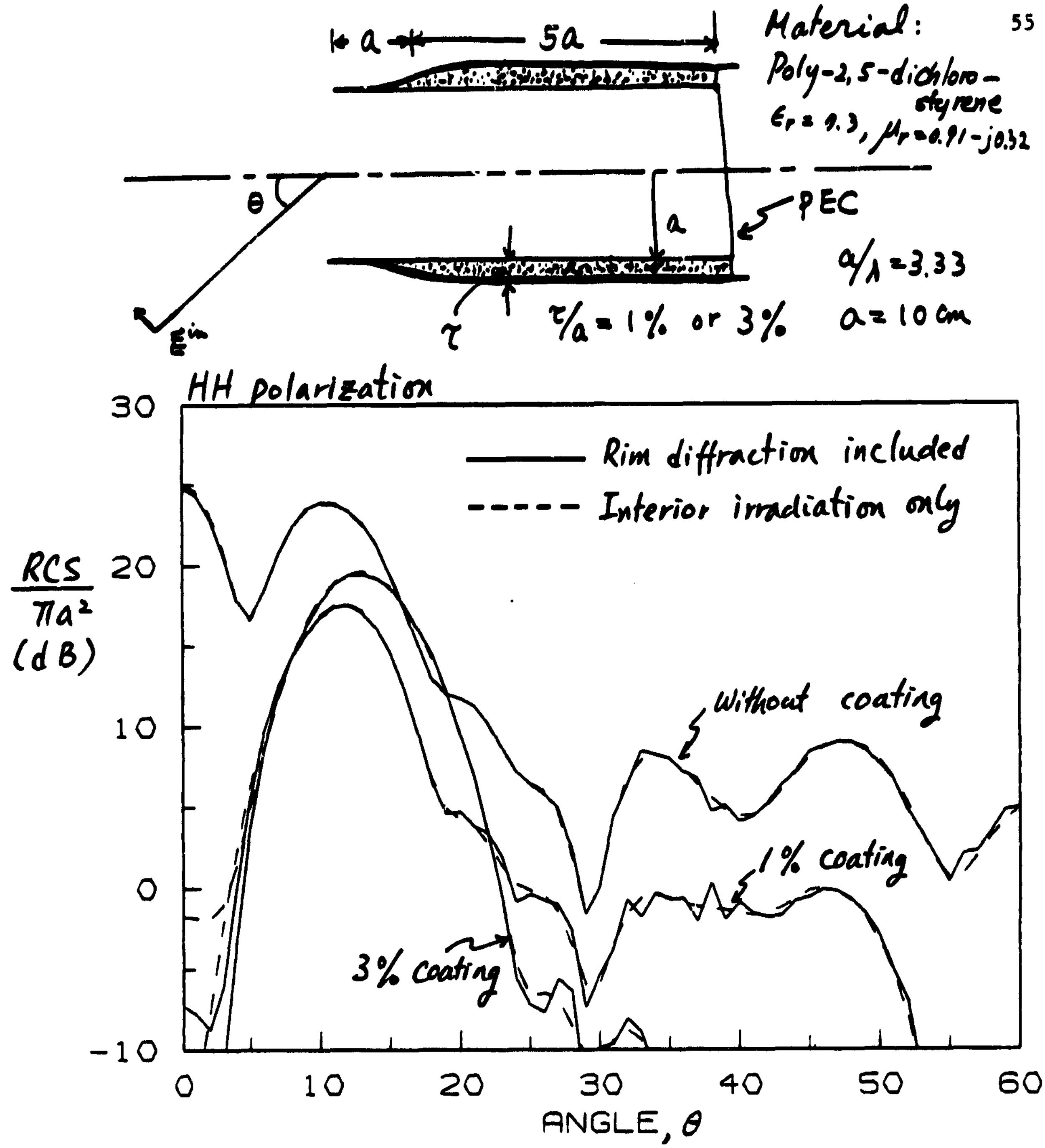

Figure 22b. The RCS's as a function of the incident angle from a PEC-terminated circular waveguide coated with a lossy material (poly-2,5-dichlorostyrene, = 7.3, μ = 0.91-j0.32) with a coating thickness of τ = 0, 0.1 cm (1% coating) and 0.3 cm (3% coating) (a = 10 cm, f = 10 GHz, a/λ = 3.33, length = 60 cm, HH polarization, ----interior irradiation only, ——— rim diffraction included).

(5) Experiments on a waveguide coated with very lossy magnetic material as a substitute for a corrugated waveguide

To produce circularly polarized (CP) radiation, an open-ended corrugated waveguide is commonly used. Since the corrugated waveguide is expensive and heavy, it has been suggested that the waveguide coated with a lossy magnetic material be used as a substitute for the corrugated waveguide (See Appendix C). In this reporting period, we have proceeded to perform experiments to verify our theory.

There are two requirements for a coated guide to be a successful CP antenna: The coating material must be magnetic and lossy, and a/λ must be sufficiently large.

The first step in these experiments is to produce a relatively pure TE_{11} mode in an overmoded waveguide. Since it is easy to generate a pure TE_{11} in a waveguide with a small radius, we made a waveguide as shown in Figure 23, which has a smooth transition between the regions of small and large radii. The waveguide consists of a few pieces so that four different sets of waveguide can be assembled without repeating the difficulty in making the pieces at the transition region.

We are in the process of testing those sets of waveguide, and eventually we are going to measure the effect of the waveguide size on the radiation polarization.

(6) Conclusions and future prospects

In this reporting period, the previous theoretical results are refined and confirmed with available experimental data, and the

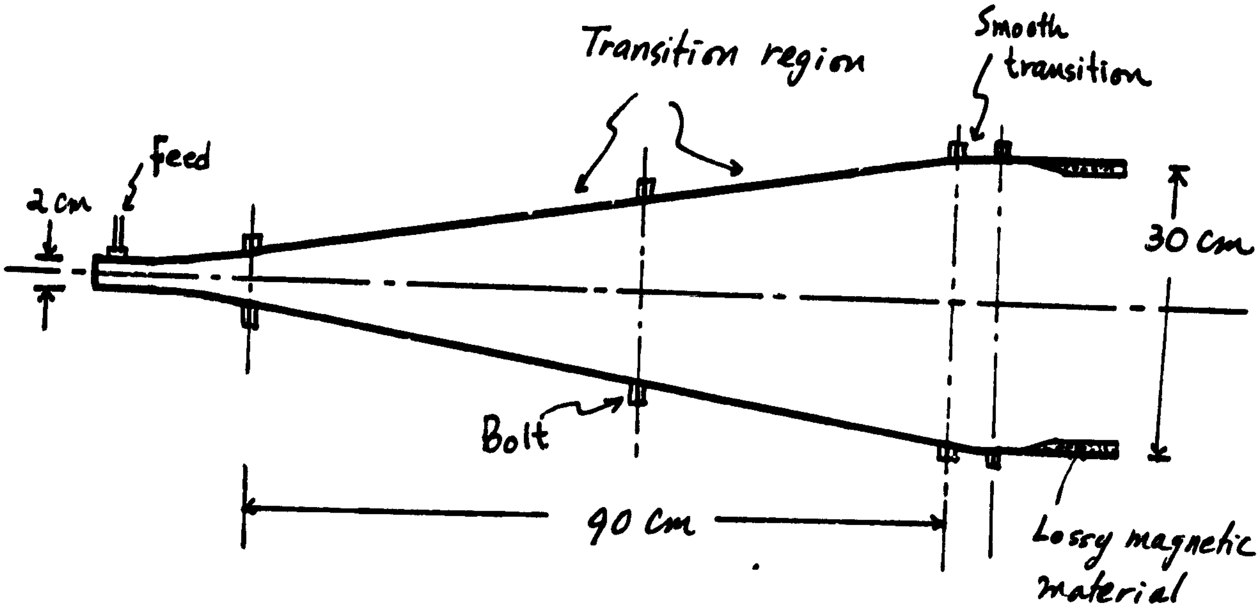

Figure 23. The waveguide structure for the experiments on a CP antenna (not to scale).

experiments to verify our theoretical predictions have been proposed. We summarize our progress as follows:

1. The analysis of the normal modes in an overmoded waveguide is complete. These findings are very useful for the further research on the RCS reduction from a waveguide with a large value of a/λ.
2. It has been confirmed with available experimental data that the interior irradiation contributes to the total RCS much more than the rim diffraction, especially for the case at a small incident angle with a large value of a/λ.
3. The theory for the rim diffraction is formulated and the theoretical calculations with this theory are in good agreement with available experimental data.
4. It has been theoretically predicted that the interior irradiation can be reduced significantly by coating the waveguide with a lossy magnetic material. The coating material must be less lossy for a larger value of a/λ. Experiments to verify these findings are proposed.
5. A waveguide coated with a very lossy magnetic material has been suggested as a substitute for a corrugated waveguide. Experiments for this possibility are in progress.

Our objective in this research is to achieve a large RCS reduction from a cavity structure with the following conditions: (1) The structure does not have to be long, and (2) the thin layer of coating is effective over a wide range of frequency.

As indicated in the previous report, the coating thickness must increase gradually from the opening to the inside of the waveguide to prevent any undesirable mode conversions from highly to lowly attenuating modes. The properties of the wave propagation at the transition region are to be investigated in the near future to make the transition length as short as possible.

We have found that the coating with a single layer is effective for the RCS reduction over a certain range of frequency. Double layers of coating are suggested so that the thin coated layer is effective over a wide range of frequency.

Eventually, we will expand our research to more realistic cases where the structure does not have to be a circular waveguide.

The details of the further studies are in the proposal attached in Appendix D of this report.

REFERENCES

[1] S. W. Lee, Y. T. Lo, S. L. Chuang, and C. S. Lee, "Numerical methods for analyzing electromagnetic scattering," Semiannual Report to NASA Lewis Research Center, Cleveland, Ohio, March 1985.

[2] S. W. Lee and Y. T. Lo, "Electromagnetic scattering by cylinder and sphere," Electromagnetic Laboratory Report No. 83-1, University of Illinois, Urbana, Illinois, 1983.

[3] H. R. Witt and E. L. Price, "Scattering from hollow conducting cylinders," Proc. IEE, Vol. 115, pp. 94-99, January 1968.

[4] H. A. Brooks and J. W. Crispin, Jr., "Comments on the RCS characteristics of cylinders, hollow pipes, and cylindrical cavities," Conductor Corporation Report No. 1801-2-T(0043-147), Ann Arbor, Michigan, August 1966.

[5] J. W. Crispin, Jr. and A. L. Maffett, "Radar cross-section estimation for simple shapes," Proc. IEEE, Vol. 53, pp. 833-848, August 1965.

[6] T. W. Johnson and D. L. Moffatt, "Electromagnetic scattering by open circular waveguide," The Ohio State Univ. ElectroScience Laboratory, Columbus, Ohio, Technical Report 710816-9, December 1980, and references therein.

[7] S. W. Lee, Geometrical theory of diffraction. Champaign: EM Publishing Co., 1983, Vol. I.

[8] C. E. Ryan, Jr. and L. Peters, Jr., "Evaluation of edge-diffracted fields including equivalent currents for the caustic regions," IEEE Trans. Antennas Propagat., Vol. AP-17, pp. 292-299, May 1969; see also correction in Vol. AP-18, p. 275, March 1970.

[9] W. D. Burnside and L. Peters, Jr., "Axial-radar cross section of finite cones by the equivalent-current concept with higher-order diffraction," Radio Science, Vol. 7, pp. 943-948, October 1972.

[10] W. D. Burnside and L. Peters, Jr., "Edge diffracted caustic fields," IEEE Trans. Antennas Propagat., Vol. AP-22, pp. 620-623, July 1974.

[11] E. F. Knott and T. B. A. Senior, "Equivalent Currents for a ring discontinuity," IEEE Trans. Antennas Propagat., Vol. AP-21, pp. 693-695, September 1973.

[12] G. L. James and V. Kerdemelidis, "Reflector antenna radiation pattern analysis by equivalent edge currents," IEEE Trans. Antennas Propagat., Vol. AP-21, pp. 19-24, January 1973; see also correction in Vol. AP-21, p. 756, September 1973.

[13] C. A. Chuang, C. S. Liang, and S. W. Lee, "High frequency scattering from an open-ended semi-infinite cylinder," IEEE Trans. antennas Propagat., Vol. AP-23, pp. 770-776, November 1975.

[14] J. J. Bowman, S. W. Lee, and C. Liang, "High-frequency backscattering from a semi-infinite hollow cylinder," Proc. IEEE, Vol. 61, pp. 681-682, May 1968.

[15] A. R. Von Hippel, Ed., Dielectric Material and Applications. Cambridge, Massachusetts: Technolgy Press, M.I.T., 1954.

APPENDIX A

NORMAL MODES IN AN OVERMODED CIRCULAR WAVEGUIDE COATED WITH LOSSY MATERIAL

The preprint of this paper was submitted for publication to IEEE Trans. Microwave Theory Tech.

NORMAL MODES IN AN OVERMODED CIRCULAR WAVEGUIDE COATED WITH LOSSY MATERIAL*

C. S. Lee, Student Member IEEE, S. W. Lee, Fellow IEEE,
and S. L. Chuang, Member IEEE

ABSTRACT

The normal modes in an overmoded waveguide coated with a lossy material are analyzed, particularly for their attenuation properties as a function of coating material, layer thickness, and frequency. When the coating material is not too lossy, the low-order modes are highly attenuated even with a thin layer of coating. This coated guide serves as a mode suppressor of the low-order modes, which can be particularly useful for reducing the radar cross section (RCS) of a cavity structure such as a jet engine inlet. When the coating material is very lossy, low-order modes fall into two distinct groups: highly and lowly attenuated modes. However, as a/λ (a = radius of the cylinder; λ = the free-space wavelength) increases, the separation between these two groups becomes less distinctive. The attenuation constants of most of the low-order modes become small, and decrease as a function of λ^2/a^3.

*This work was supported by NASA contract NAG3-475.

I. INTRODUCTION

In many applications, it is desirable to line the wall of a conventional circular waveguide by a layer of dielectric or magnetic material. With proper design, the lining can significantly alter the modal fields in the waveguide, so as to achieve either less attenuation or more attenuation for certain modes. The past studies of this problem are mostly connected with microwave/infrared transmission over a long distance [1] - [5]. Two assumptions are usually made:

(1) The waveguide diameter is very large in terms of wavelength (overmoded waveguide); and

(2) The coating material is either nearly lossless [2] - [4] or very lossy [5].

These assumptions simplify the theoretical analysis and oftentimes bring out a clearer physical picture. Nevertheless, in many practical situations, these assumptions are too restrictive. A more general analysis of the coated circular waveguide is needed.

It is the purpose of this paper to fill in this need. Instead of using the perturbation theory [2], [3], [5], transmission-line model [1] - [4] or asymptotic theory [6], we solve the modal characteristic equation of a coated circular waveguide exactly by a numerical method. This is feasible because of today's fast computers and efficient subroutines for calculating Bessel functions with a complex argument.

The organization of the paper is as follows: First, an overview of the normal modes in a coated circular waveguide in comparison with those in an uncoated waveguide is presented. In Section III, the exact characteristic equation for the normal modes in a circular waveguide coated with a lossy material is given. Three types of normal modes, i.e., the inner mode, the surface mode and the interface mode, are discussed, along with their approximate solutions. Numerical results and potential applications are discussed in Section IV.

II. OVERVIEW OF MODAL FIELDS IN A COATED CIRCULAR WAVEGUIDE

Before presenting detailed numerical results, it is beneficial to explain some unique features of the coated waveguide, which are absent in the conventional uncoated waveguide. Figure 1 shows a circular waveguide with a perfectly conducting wall, uniformly coated with a material of permittivity $\epsilon_2\epsilon_0$ and permeability $\mu_2\mu_0$. Both ϵ_2 and μ_2 can be complex, with their negative imaginary parts representing material losses for the present exp($j\omega t$) time convention. The medium in Region I is assumed to be air, i.e., permittivity ϵ_0 and permeability μ_0. Our problem at hand is to study the normal modes in such a waveguide.

A. Mode Classification

In an uncoated waveguide, the normal modes are either TE or TM with respect to z. Here index m describes the azimuthal variation in the form of sin $m\phi$ or cos $m\phi$, whereas index n describes the radial distribution in the form of $J_m(k_{\rho n}\rho)$ or $J_m'(k_{\rho n}\rho)$. In the ascending order of their cutoff frequencies, the dominant modes are

$$TE_{11},\ TM_{01},\ TE_{21},\ TM_{11}/TE_{01},\ \cdots$$

When the waveguide is coated with a dielectric layer, there are no longer pure TE or TM modes. The modes are commonly classified into HE_{mn} and EH_{mn} modes in such a way that, in the limiting case of a vanishingly thin coating [7],

$$HE_{mn} \rightarrow TE_{mn}\ , \quad \text{and} \quad EH_{mn} \rightarrow TM_{mn}$$

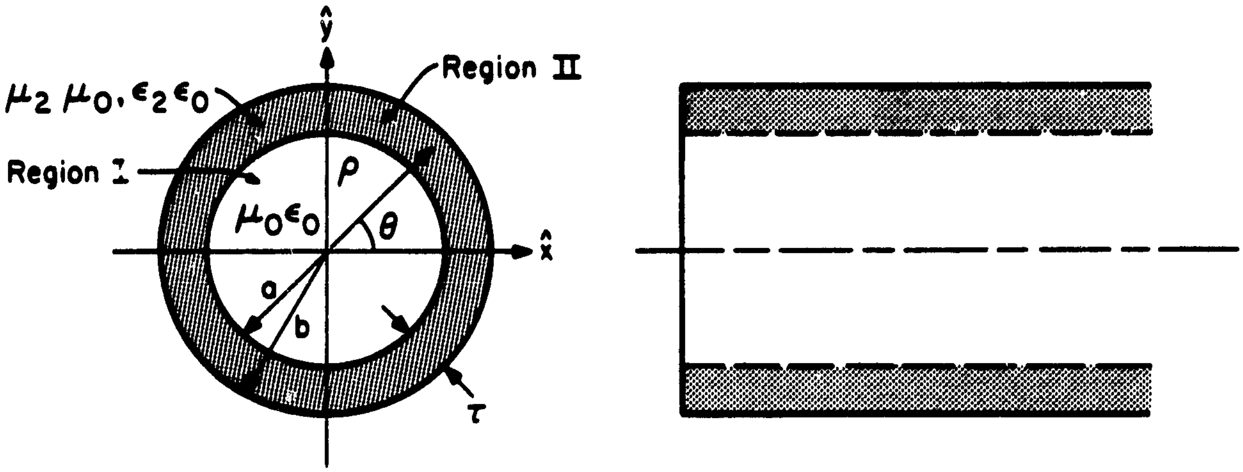

Figure 1. A coated circular waveguide.

There exist three special cases where HE_{mn}(EH_{mn}) becomes identically or approximately TE_{mn}(TM_{mn}), namely,

(i) circularly symmetrical modes (m = 0) such as TE_{0n} and TM_{0n},

(ii) all modes at frequencies near their cutoff frequencies [8], [9], and

(iii) the low-order modes in an overmoded waveguide coated with a lossless material, (in this limit $HE_{mn} \to TM_{mn}$, and $EH_{mn} \to TE_{mn}$).

B. Cutoff Frequencies

Near the cutoff frequency, the normal mode is either quasi TE or TM. In Figures 2 and 3, we plot the cutoff frequencies f_c's of the normal modes in a coated circular guide as a function of layer thickness τ. f_c is normalized with respect to f_{co}, which is the cutoff frequency of the dominant TE_{11} mode in an empty guide of radius a, and is given by

$$f_{co} = \frac{1.84118\ c}{2\pi a}$$

where c is the speed of light in free space. Figure 2 shows the modal inversion between the TM_{01} and TE_{21}, which has been previously reported [8], [9]. However, the modal inversion between those two modes is not evident if the coating is of a magnetic material ($\mu_2 \neq 1$) instead of a dielectric material (Figure 3). Coating reduces the cutoff frequencies of the normal modes, especially for the magnetic-coated waveguide. This is due to the fact that, with coating, the modal field distribution tends to concentrate near the air-material interface. Note also that the degeneracy between the TM_{11} and TE_{01} modes near their cutoff frequencies is not removed by the dielectric coating (see Appendix 1), but the degeneracy can be removed by the magnetic coating. The near degeneracy of the TE_{01} mode with the TM_{11} mode in a dielectric-coated guide can

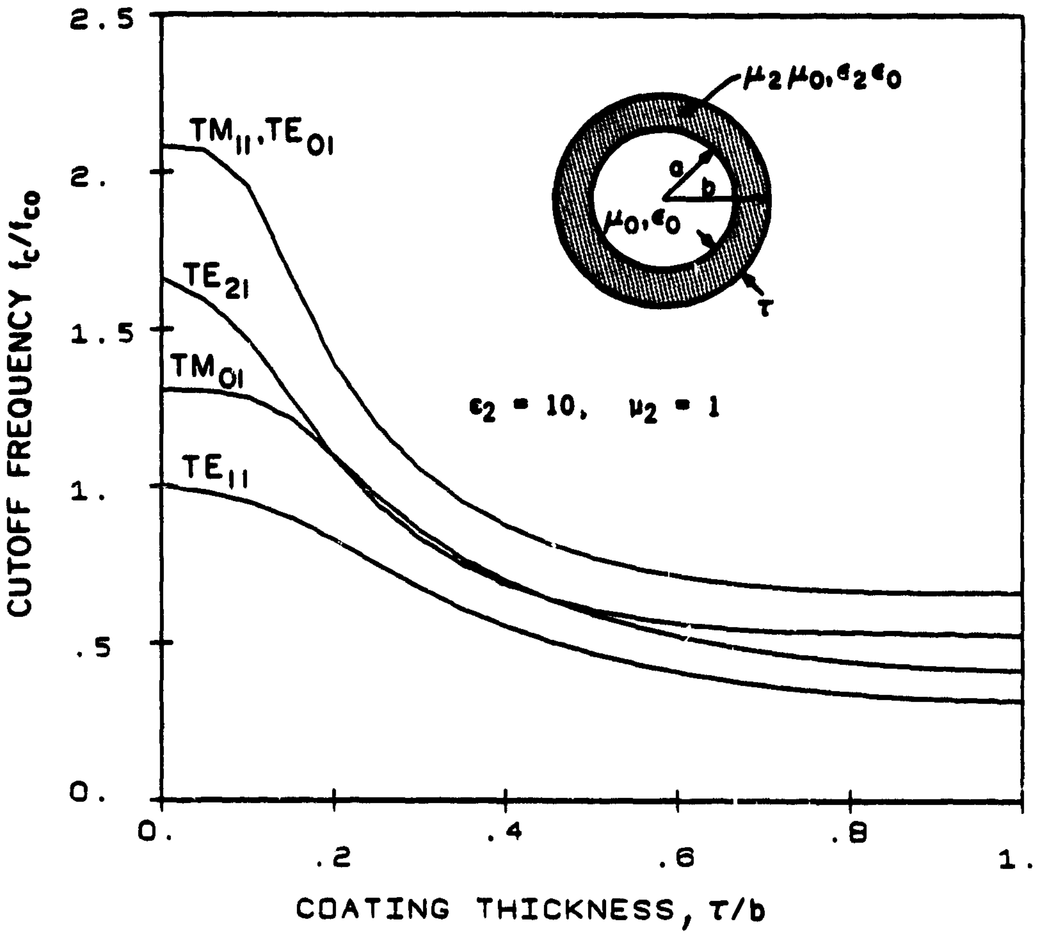

Figure 2. The cutoff frequencies in a dielectric-coated waveguide ($\epsilon_2 = 10$, $\mu_2 = 1$) normalized to that of the TE_{11} mode in an empty guide (f_{co}) as a function of coating thickness.

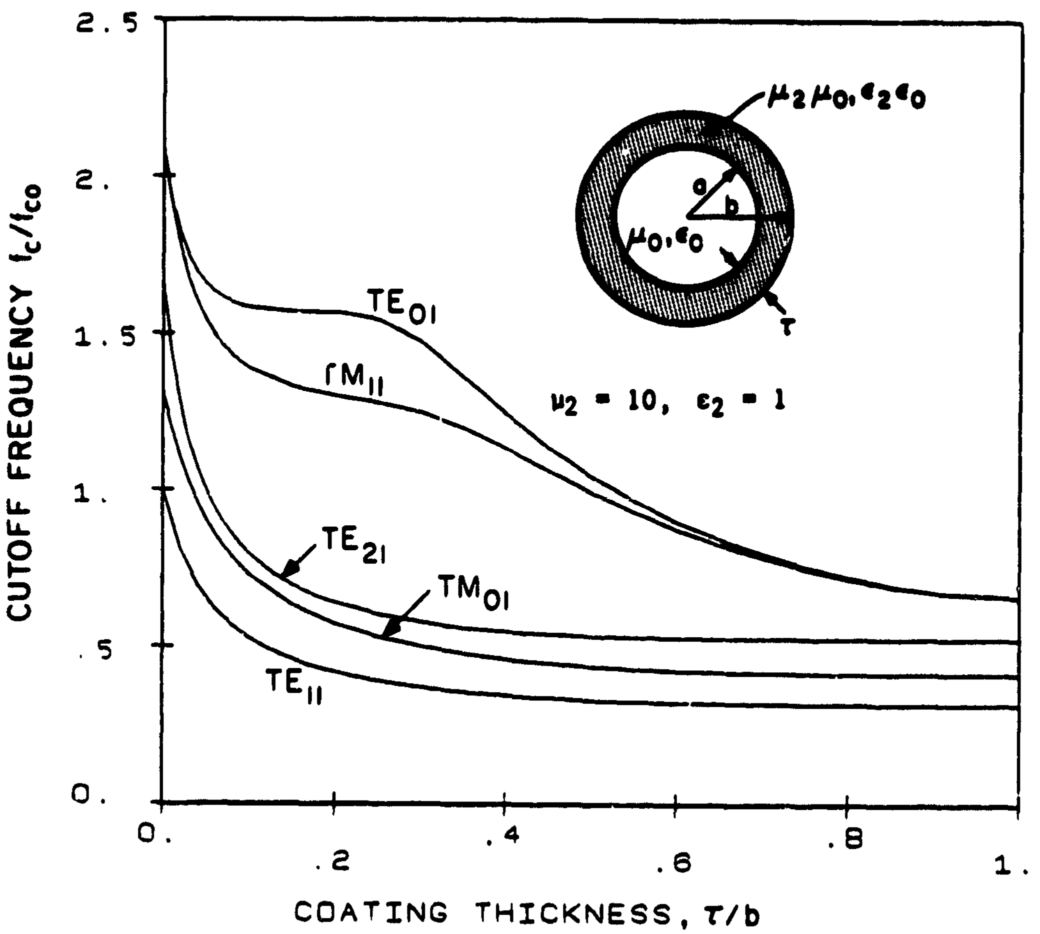

Figure 3. The cutoff frequencies in a magnetic-coated waveguide ($\mu_2 = 10$, $\epsilon_2 = 1$) normalized to that of the TE_{11} mode in an empty guide (f_{co}) as a function of coating thickness.

cause a serious problem for a long-distance communication utilizing the lowly attenuating TE_{01} mode because there may be a large mode conversion due to a strong coupling between these two modes [2] - [4]. The magnetic coating can be very useful in this application.

C. Modal Propagation Constant and Power Distribution

When the coating thickness is small in terms of the free-space wavelength ($\tau/\lambda << 1$), the modal field distribution in the air region and the propagation constant are not much perturbed. As the coating thickness is increased in the manner

$$\tau/\lambda \to \infty, \text{ for a fixed value of } a$$

the low-order modes approach, one by one, their counterparts in the parallel-plate waveguide. More precisely, the HE_{mn} modes in a coated circular waveguide approach those modes in a parallel-plate waveguide formed by a perfect magnetic conductor (PMC) and perfect electric conductor (PEC) as sketched in Figure 4a. The EH_{mn} modes approach those modes in a parallel-plate waveguide formed by two PEC's as shown in Figure 4b.

The propagation constant k_z and modal power distribution of the dominant HE_{11} mode in a guide coated with a lossless dielectric material ($\epsilon_2 = 10$, $\mu_2 = 1$) are shown in Figures 5 and 6. When the coating thickness is small ($\tau'/\lambda = \tau/\lambda_2 < 0.05$, where $\lambda_2 = \lambda/\sqrt{\epsilon_2\mu_2}$ = wavelength in Region II), the transverse wave number $k_{\rho 1}$ in Region I defined by

$$k_{\rho 1} = \sqrt{k_0^2 - k_z^2}$$

is real, where $k_0 = 2\pi/\lambda$, and both propagation constant and its power-intensity distribution are very similar to those of an empty guide. When the coating thickness τ is much larger than $0.05\ \lambda_2$, $k_{\rho 1}$ is imaginary and its magnitude

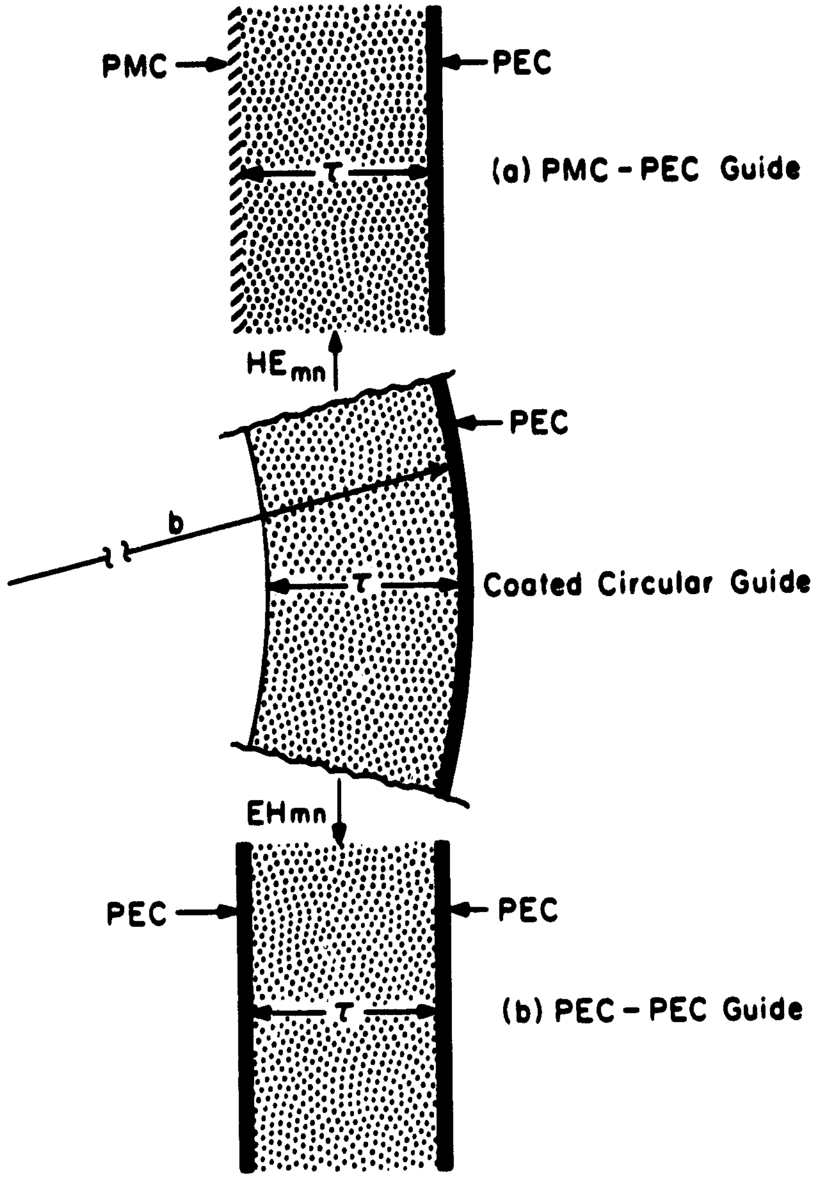

Figure 4. Mode transition in a coated circular guide at the high-frequency limit. The HE_{mn} modes approach modes in a PMC-PEC guide, and the EH_{mn} approach modes in PEC-PEC guide.

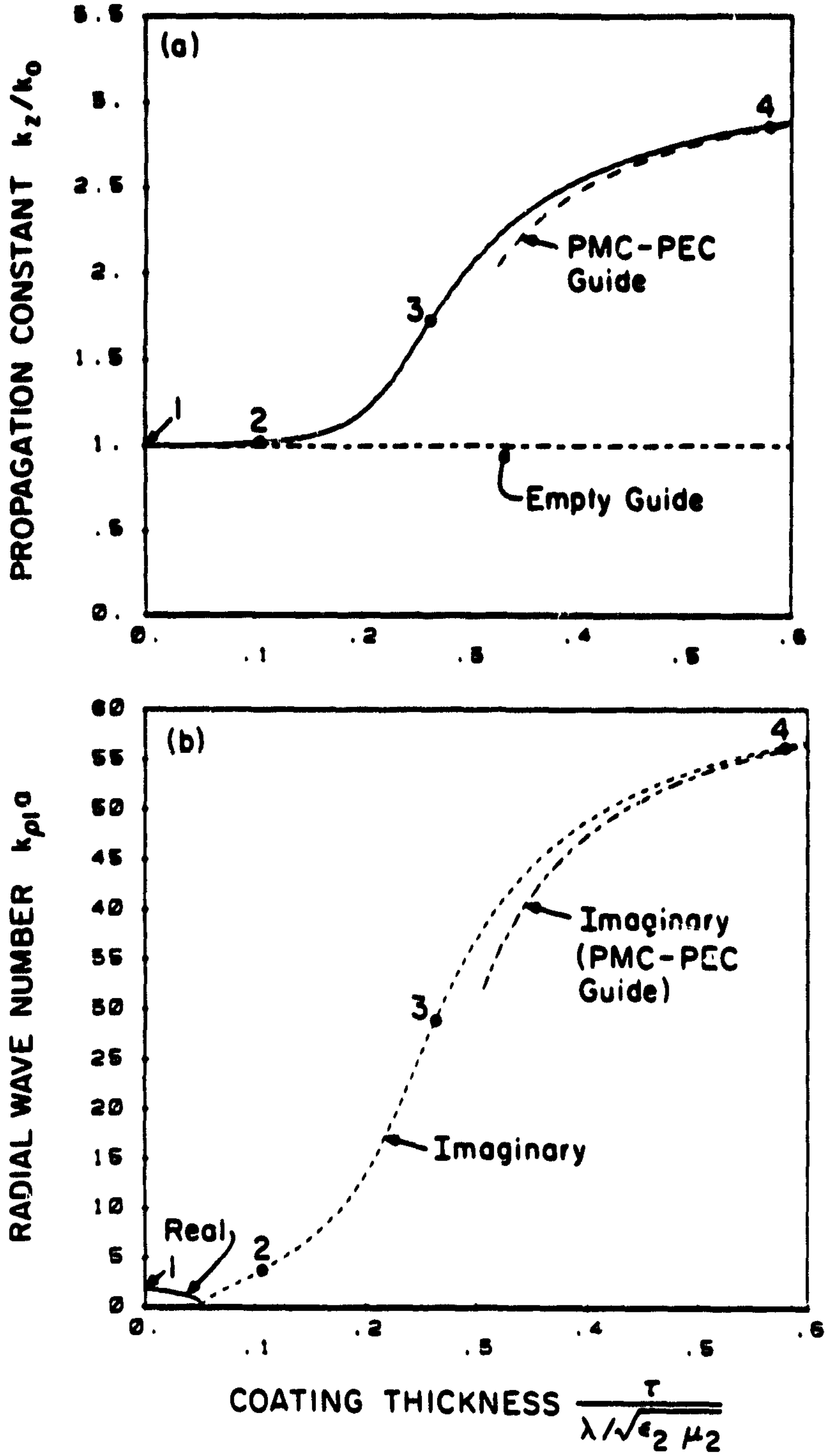

Figure 5. a) Normalized propagation constant and b) radial wave number ($k_{\rho 1}a$) of the HE_{11} mode in a dielectric-coated waveguide ($\epsilon_2 = 10, \mu_2 = 1$) as a function of the coating thickness in "effective" wavelength ($\tau' = \tau\sqrt{\epsilon_2 \mu_2}/\lambda$). The power distributions for the four marked points are shown in Figure 6. The approximate solution of the surface mode using the two-slab model is also shown (see Section III).

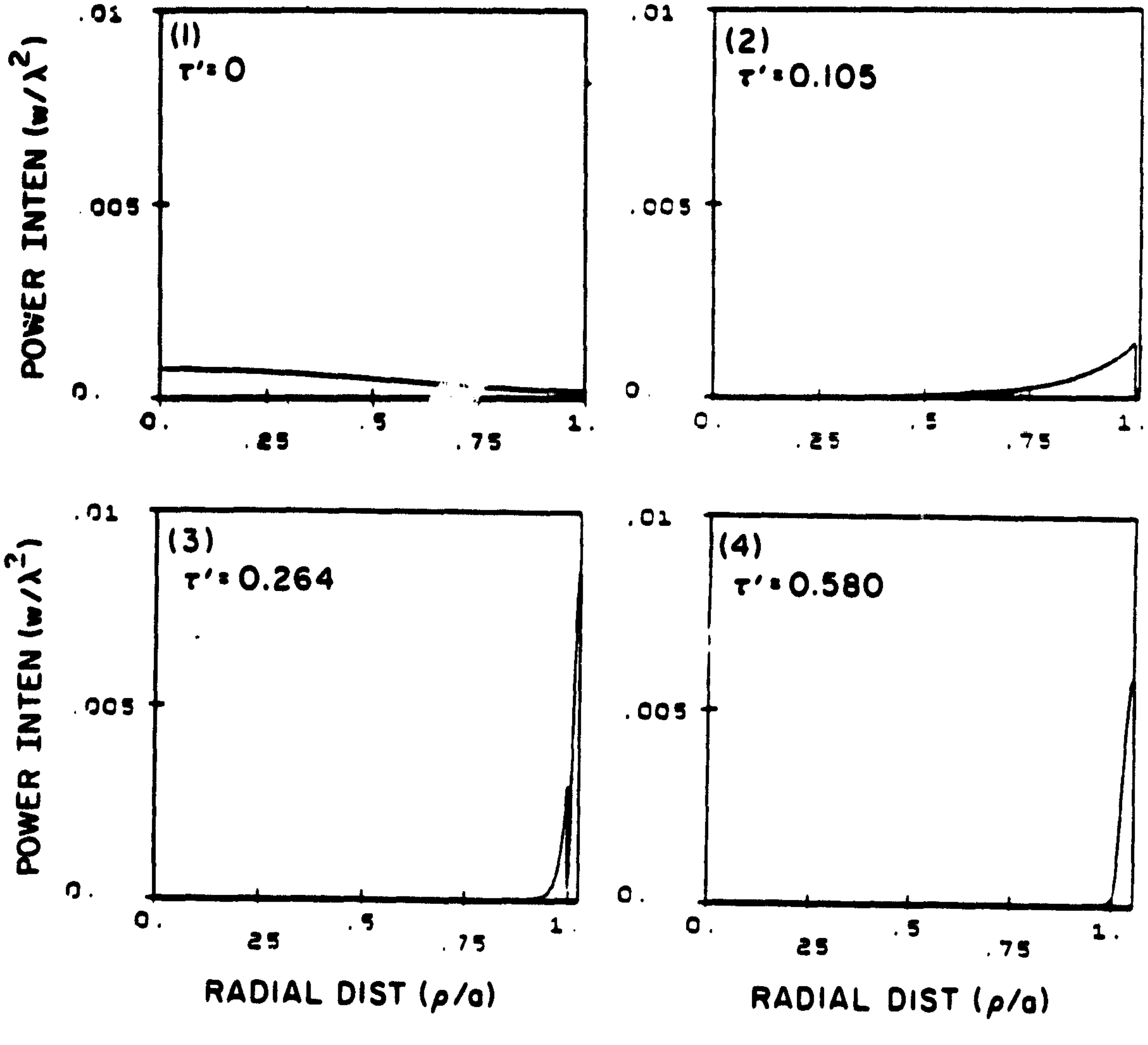

Figure 6. Normalized angle-averaged power distribution in watts/λ^2 as a function of radial distance in a dielectric-coated waveguide ($\varepsilon_2 = 10$, $\mu_2 = 1$) with four different coating thicknesses. The corresponding points for these diagrams are marked in Figure 5 ($\tau' = \tau\sqrt{\varepsilon_2\mu_2}/\lambda$).

approaches $k_0\sqrt{\epsilon_2\mu_2 - 1}$. Consequently, the modal power distribution is largely concentrated in the dielectric layer (Region II). In Figure 6, the total power carried by the HE_{11} mode is normalized to 1 watt. In case (4) of Figure 6, more than 99% of the power is confined in the dielectric layer, despite the fact that the dielectric layer ($1.06 < \rho/a < 1$) covers only 12% of the waveguide cross section.

Figures 7 and 8 are similar to Figures 5 and 6 except that the coating material is magnetic ($\mu_2 = 10$ and $\epsilon_2 = 1$). It is most interesting to observe that the transition point where k_z becomes imaginary occurs at a much smaller coating thickness ($\tau = 0.05\ \lambda_2$ in Figure 5 and $\tau = 0.005\ \lambda_2$ in Figure 7). Thus, in applications where large field concentration in the material layer is desired, the magnetic coating is more effective (more discussion is given in Section IV).

It is worthwhile to note that the normal mode at the transition point is not TEM even though the radial wave number vanishes (see Appendix 2). Thus, both the hybrid-mode method and the techniques for TEM modes fail to provide the modal fields at the transition point. Only the direct method as discussed in Appendix 2 is applicable in this case.

D. Transverse-field Distribution

The transverse fields of the five lowest-order modes in an uncoated circular guide and in a coated (dielectric and magnetic) circular guide at the cutoff frequencies and the high-frequency limits are shown in Figure 9. The TE (TM) modes in a circular guide at the cutoff frequencies do not have transverse magnetic (electric) fields, which are not shown in the diagrams. We notice that the nonvanishing fields at the cutoff frequencies are similar to those in an uncoated guide. At high frequency, the fields are confined within the coated

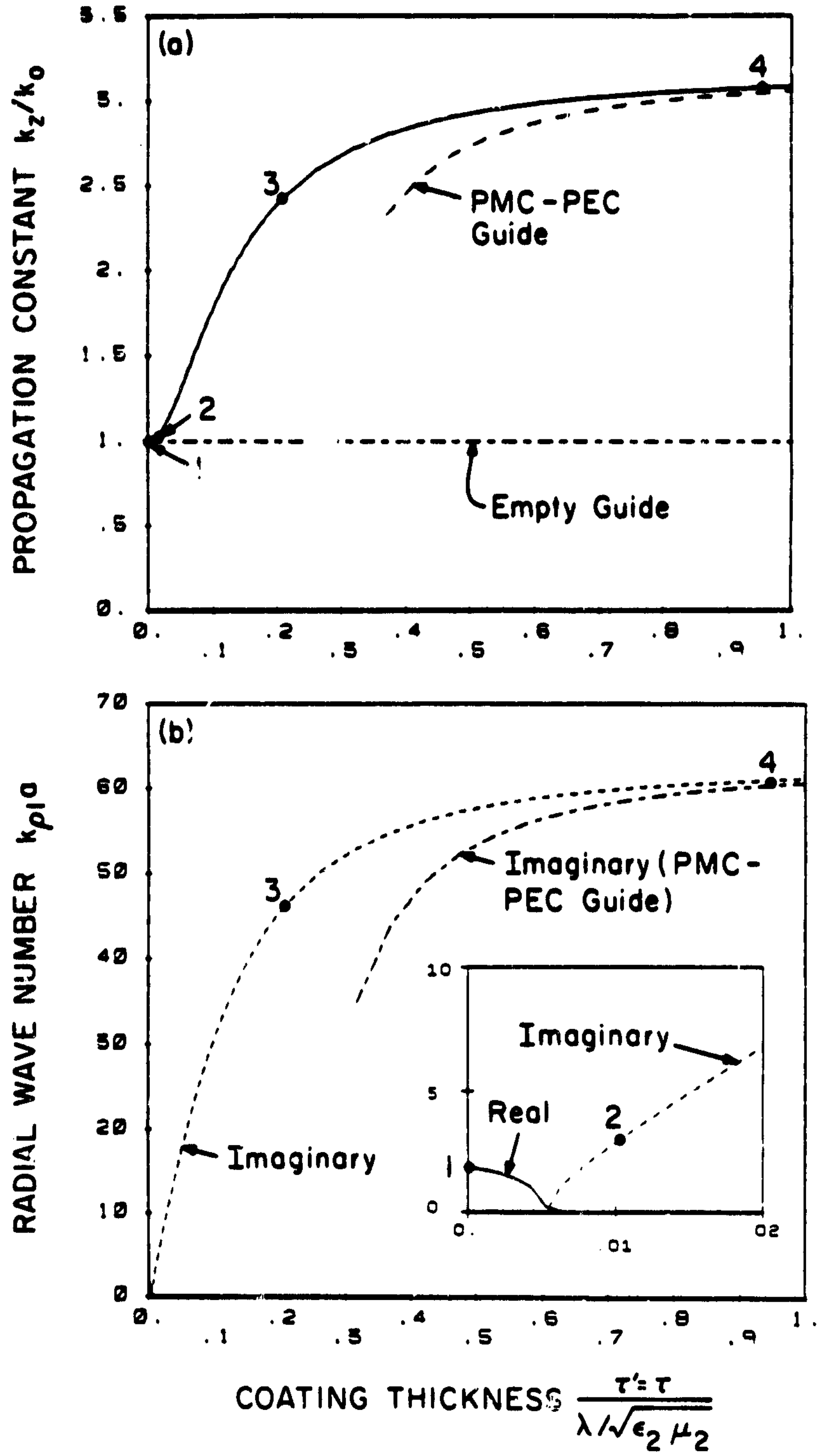

Figure 7. a) Normalized propagation constant and b) radial wave number ($k_{\rho 1}a$) of the HE_{11} mode in a magnetic-coated waveguide ($\mu_2 = 10, \epsilon_2 = 1$) as a function of the lining thickness in "effective" wavelength ($\tau' = \tau\sqrt{\epsilon_2 \mu_2}/\lambda$). The power distributions of the four marked points are shown in Figure 8. The approximate solution of the surface mode using the two-slab model is also shown (see Section III).

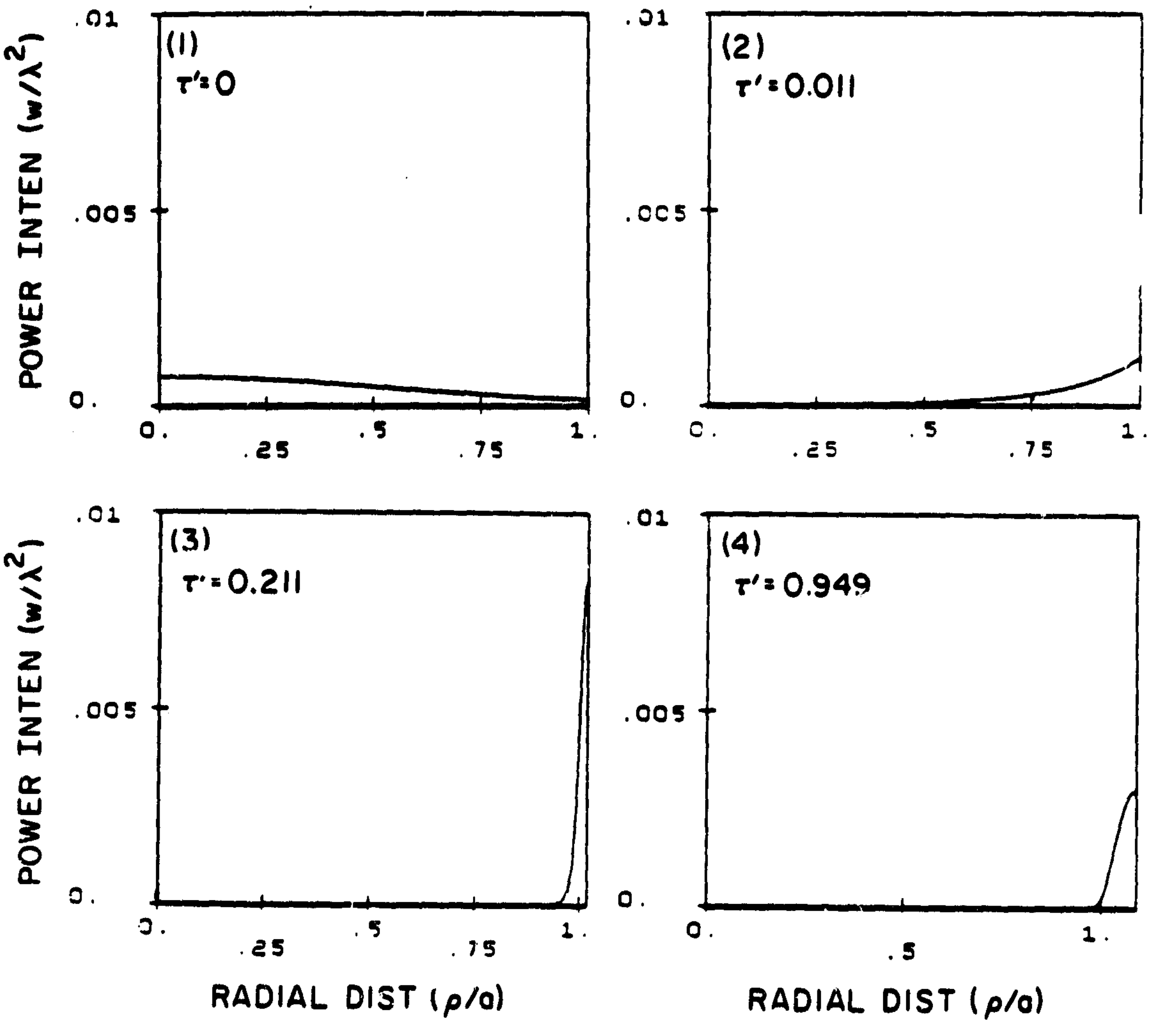

Figure 8. Normalized angle-averaged power distribution in watts/λ^2 as a function of radial distance in a magnetic-coated waveguide ($\mu_2 = 10$, $\varepsilon_2 = 1$) with four different coating thicknesses. The corresponding points for these diagrams are marked in Figure 7 ($\tau' = \tau\sqrt{\varepsilon_2\mu_2}/\lambda$).

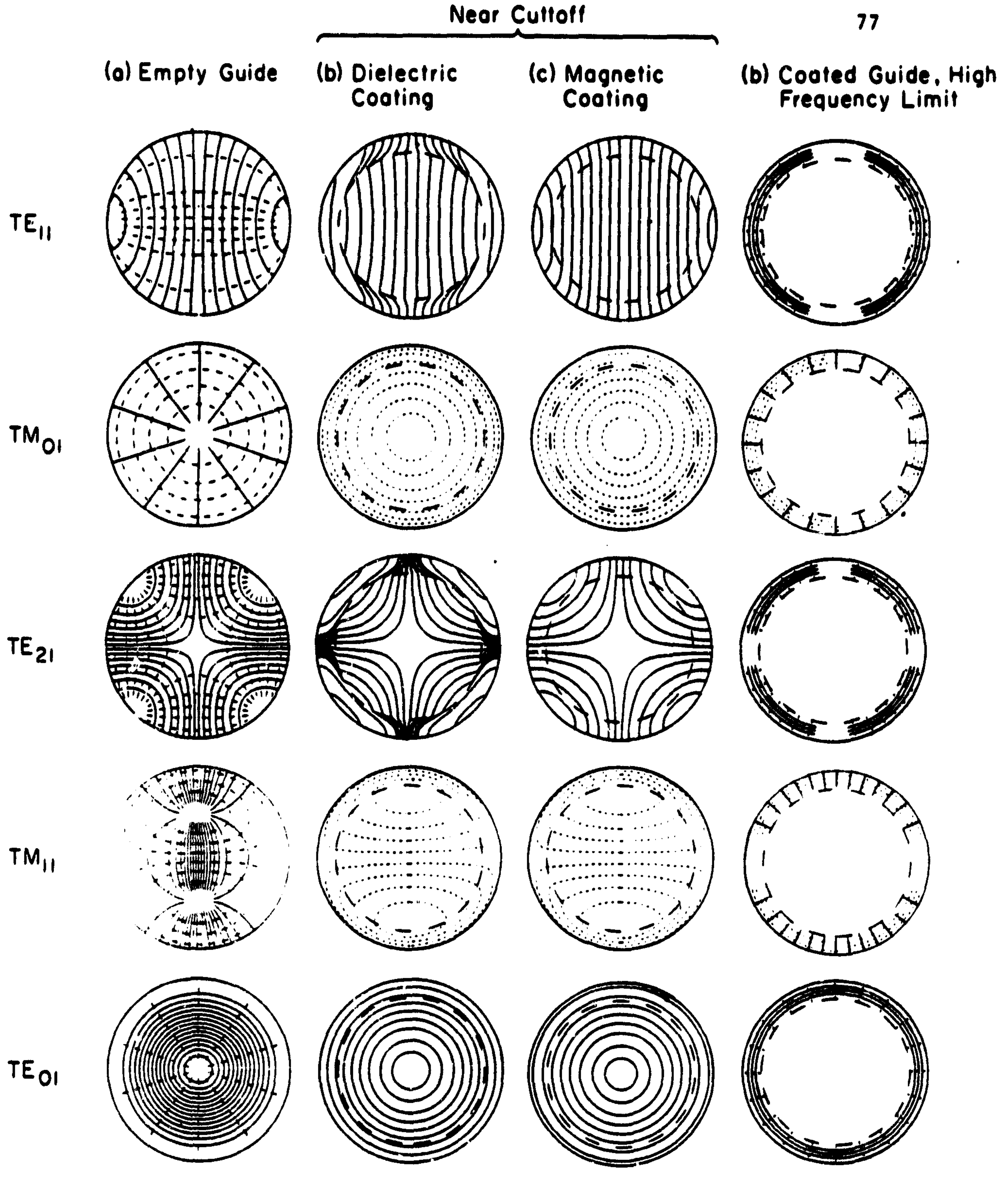

Figure 9. Transverse field distributions of the normal modes in a) empty guide, b) dielectric-coated guide at cutoff frequencies, c) magnetic-coated guide at cutoff frequencies and d) coated guide at the high-frequency limit.

region, as shown in the diagrams where the blank space indicates that the fields are negligible.

III. MODAL CHARACTERISTIC EQUATIONS, FIELDS AND CLASSIFICATION

The general problem is shown in Figure 1. Here both the permittivity $\epsilon_2\epsilon_0$ and permeability $\mu_2\mu_0$ of the coating material are allowed to be complex. The characteristic equation for the propagation constant k_z of a normal mode is well known [10], [11], and we list the final expression, which is solved numerically using Müller's method (available in International Mathematical Statistical Libraries subroutines):

$$k_{\rho 1}^2\left[F_1'(a) - \epsilon_2 \frac{F_1(a)F_3'(a)}{F_3(a)} \frac{k_{\rho 1}}{k_{\rho 2}}\right]\left[F_1'(a) - \mu_2 \frac{F_1(a)F_4'(a)}{F_4(a)} \frac{k_{\rho 1}}{k_{\rho 2}}\right]$$

$$- [k_z m/(k_0 a)]^2 \, F_1^2(a) \, [1 - (k_{\rho 1}/k_{\rho 2})^2]^2 = 0 \tag{1a}$$

where

$$k_{\rho 1}^2 + k_z^2 = k_0^2 \tag{1b}$$

$$k_{\rho 2}^2 + k_z^2 = \epsilon_2 \mu_2 k_0^2 \tag{1c}$$

$$F_1(\rho) = J_m(k_{\rho 1}\rho) \;, \quad F_1'(\rho) = J_m'(k_{\rho 1}\rho) \tag{1d}$$

$$F_3(\rho) = J_m(k_{\rho 2}\rho)\, N_m(k_{\rho 2}b) - N_m(k_{\rho 2}\rho)\, J_m(k_{\rho 2}b) \tag{1e}$$

$$F_3'(\rho) = J_m'(k_{\rho 2}\rho)\, N_m(k_{\rho 2}b) - N_m'(k_{\rho 2}\rho)\, J_m(k_{\rho 2}b) \tag{1f}$$

$$F_4(\rho) = J_m(k_{\rho 2}\rho)\, N_m'(k_{\rho 2}b) - N_m(k_{\rho 2}\rho)\, J_m'(k_{\rho 2}b) \tag{1g}$$

$$F_4'(\rho) = J_m'(k_{\rho 2}\rho)\, N_m'(k_{\rho 2}b) - N_m'(k_{\rho 2}\rho)\, J_m'(k_{\rho 2}b) \tag{1h}$$

Here $k_{\rho 1}$ and $k_{\rho 2}$ are the radial wave vectors of regions I and II, respectively; ω is the angular frequency; $k_0 = 2\pi/\lambda$; and a and b are the radii of the air region and the conducting cylinder, respectively. J_m is the Bessel function and N_m is the Neumann function of order ~. The prime indicates differentiation with respect to argument. The modal fields are given by

$$E_\rho^I = -[(Ak_z/k_0)\ F_1'(\rho) + (Bm/k_{\rho 1}\rho)\ F_1(\rho)]\ \cos m\phi \tag{2a}$$

$$E_\rho^{II} = -[(Ck_z/k_2)\ F_3'(\rho) + (Dm/k_{\rho 2}\rho)\ F_4(\rho)]\ \cos m\phi \tag{2b}$$

$$E_\phi^I = [\{Ak_z m/(k_0 k_{\rho 1}\rho)\}\ F_1(\rho) + BF_1'(\rho)]\ \sin m\phi \tag{2c}$$

$$E_\phi^{II} = [\{Ck_z m/(k_2 k_{\rho 2}\rho)\}\ F_3(\rho) + DF_4'(\rho)]\ \sin m\phi \tag{2d}$$

$$E_z^I = -j(Ak_{\rho 1}/k_0)\ F_1(\rho)\ \cos m\phi \tag{2e}$$

$$E_z^{II} = -j(Ck_{\rho 2}/k_2)\ F_3(\rho)\ \cos m\phi \tag{2f}$$

$$H_\rho^I = -Y_0[(Am/k_{\rho 1}\rho)\ F_1(\rho) + (Bk_z/k_0)\ F_1'(\rho)]\ \sin m\phi \tag{2g}$$

$$H_\rho^{II} = -Y_2[(Cm/k_{\rho 2}\rho)\ F_3(\rho) + (Dk_z/k_2)\ F_4'(\rho)]\ \sin m\phi \tag{2h}$$

$$H_\phi^I = -Y_0[F_1'(\rho) + \{Bk_z m/(k_0 k_{\rho 1}\rho)\}\ F_1(\rho)]\ \cos m\phi \tag{2i}$$

$$H_\phi^{II} = -Y_2[CF_3'(\rho) + \{Dk_z m/(k_2 k_{\rho 2}\rho)\}\ F_4(\rho)]\ \cos m\phi \tag{2j}$$

$$H_z^I = -jY_0(Bk_{\rho 1}/k_0)\ F_1(\rho)\ \sin m\phi \tag{2k}$$

$$H_z^{II} = -jY_2(Dk_{\rho 2}/k_2)\ F_4(\rho)\ \sin m\phi \tag{2l}$$

The convention of $\exp[j(\omega t - k_z z)]$ is understood and omitted; superscripts I and II indicate Regions I and II (Figure 1), and subscripts ρ, ϕ and z indicate the radial, angular and propagation-directional components of the fields, respectively; $k_2 = \sqrt{\epsilon_2\mu_2}\, k_0$; and Y_0 is the free-space admittance, $\sqrt{\epsilon_0/\mu_0}$ and $Y_2 = Y_0\sqrt{\epsilon_2/\mu_2}$. A, B, C and D are the constants, which are determined by the boundary conditions and the normalization requirement. Those constants are related by

$$C = A\sqrt{\epsilon_2\mu_2}\, k_{\rho 1}F_1(a)/[k_{\rho 2}F_3(a)] \tag{3}$$

$$D = B\mu_2 k_{\rho 1}F_1(a)/[k_{\rho 2}F_4(a)] \tag{4}$$

$$\frac{B}{A} = -\frac{k_0 k_{\rho 1} a[F_1'(a)/F_1(a) - \epsilon_2 k_{\rho 1}F_3'(a)/\{k_{\rho 2}F_3(a)\}]}{k_z m[1 - (k_{\rho 1}/k_{\rho 2})^2]} \quad (m \neq 0) \tag{5}$$

$\left(\left|\frac{B}{A}\right| << 1 \quad \text{for "quaci" TM modes}\right)$

Equation (5) can also be written as

$$\frac{A}{B} = -\frac{k_0 k_{\rho 1} a[F_1'(a)/F_1(a) - \mu_2 k_{\rho 1}F_4'(a)/\{k_{\rho 2}F_4(a)\}]}{k_z m[1 - (k_{\rho 1}/k_{\rho 2})^2]} \quad (m \neq 0) \tag{6}$$

$\left(\left|\frac{A}{B}\right| << 1 \quad \text{for "quasi" TE modes}\right)$

and the elimination of A and B from Eqs. (5) and (6) gives the characteristic equation (Eq. (1)). There is no mode coupling between the TE and TM modes for $m = 0$. Thus, $A = 0$ and $B = 1$ for the TM_{0n} modes, and $A = 1$ and $B = 0$ for the TE_{0n} modes. We note that there are two degenerate modes for each angular mode index m except $m = 0$. In the above expression of the fields, we have arbitrarily chosen one of those two modes.

There are three types of normal modes in an overmoded waveguide coated with a lossy material. The properties of these modes are explained below along with the approximate propagation constants and field distributions.

A. Inner Mode

When the coating material is sufficiently lossy and a/λ is large, most of the low-order modes become inner modes. The field distributions of these modes are mostly confined in the air region. In the limit as a/λ becomes infinite, the characteristic equation is simplified to

$$[F_1'(a)/F_1(a)]^2 - (m/x)^2 = 0 \tag{7}$$

where

$$x = k_{\rho 1} a$$

The solutions of this equation are

$$J_{m-1}(x_0^+) = 0 \quad \text{for} \quad EH_{mn}^{MS} \tag{8}$$

$$J_{m-1}(x_0^-) = 0 \quad \text{for} \quad EH_{-mn}^{MS} \tag{9}$$

Superscript MS indicates the notation by Marcatili and Schmeltzer. This superscript is used to distinguish this notation from the conventional notation. In this case, the field distributions are also simplified. Equations (6) (or equivalently Eq. (5)) in this limit becomes

$$A/B = +1 \quad \text{for} \quad EH_{mn}^{MS} \tag{10}$$

$$A/B = -1 \quad \text{for} \quad EH_{-mn}^{MS} \tag{11}$$

and the modal fields in the air region are given by

$$E_\rho = -BJ_{m-1}(k_{\rho 0}^+ \rho) \cos m\phi \,, \quad H_\rho = -Y_0 E_\phi \tag{12a}$$

$$E_\phi = BJ_{m-1}(k_{\rho 0}^+ \rho) \sin m\phi \,, \quad H_\phi = Y_0 E_\rho \tag{12b}$$

$$E_z = H_z = 0 \qquad \text{for} \quad EH^{MS}_{mn} \tag{12c}$$

$$E_\rho = -BJ_{m+1}(k^-_{\rho 0}\rho)\cos m\phi\,, \quad H_\rho = -Y_0 E_\phi \tag{13a}$$

$$E_\phi = -BJ_{m+1}(k^-_{\rho 0}\rho)\sin m\phi\,, \quad H_\phi = Y_0 E_\rho \tag{13b}$$

$$E_z = H_z = 0 \qquad \text{for} \quad EH^{MS}_{-mn} \tag{13c}$$

where

$$k^+_{\rho 0} = x^+_0/a\,, \quad k^-_{\rho 0} = x^-_0/a$$

Here x^+_0 and x^-_0 are given in Eqs. (8) and (9), respectively, and B is a constant. The fields in the lossy region are vanishingly small. The field diagrams of the EH^{MS}_{mn} and EH^{MS}_{-mn} modes in the air region are shown in Figure 2 in Reference [2].

When a/λ is large but finite, the attenuation constants of the normal modes are small and the fields decay very rapidly from the interface to the lossy layer. In this case, the asymptotic forms of the Bessel functions can be used for the field functions in the lossy region. The characteristic function of Eq. (1) in this approximation is then simplified to

$$[xF_1'(a)/F_1(a)]^2 + jx[xF_1'(a)/F_1(a)](k_{\rho 1}/k_{\rho 2})(\varepsilon_2 + \mu_2)$$
$$- m^2 - x^2\varepsilon_2\mu_2(k_{\rho 1}/k_{\rho 2})^2 = 0 \tag{14}$$

where $x = k_{\rho 1}a$

Suppose $x = x_0 + \Delta x$ where x_0 is the solution as a/λ becomes infinite. Taking the first-order terms in $k_{\rho 1}/k_{\rho 2}$ of the above equation, the attenuation constant is given by

$$\alpha_{mn} \approx \left(\frac{\xi_{mn}}{2\pi}\right)^2 \frac{\lambda^2}{a^3} \mathrm{Re}(\nu_n) \tag{15a}$$

where

$$\nu_n = \begin{cases} \epsilon_2/\sqrt{\epsilon_2\mu_2 - 1} & \text{for } TM_{0n} \text{ modes } (m = 0) & (15b) \\ \mu_2/\sqrt{\epsilon_2\mu_2 - 1} & \text{for } TE_{0n} \text{ modes } (m = 0) & (15c) \\ \frac{1}{2}(\epsilon_2 + \mu_2)/\sqrt{\epsilon_2\mu_2 - 1} & \text{for } EH^{MS}_{mn} \text{ and } EH^{MS}_{-mn}\ (m \neq 0) & (15d) \end{cases}$$

Here ξ_{mn} is the solution of

$$J_0'(\xi_{0n}) = 0 \quad \text{for} \quad TM_{0n} \text{ and } TE_{0n} \text{ modes } (m = 0) \tag{15e}$$

$$J_{m-1}(\xi_{mn}) = 0 \quad \text{for} \quad EH^{MS}_{mn} \text{ modes } (m \neq 0) \tag{15f}$$

$$J_{m+1}(\xi_{mn}) = 0 \quad \text{for} \quad EH^{MS}_{-mn} \text{ modes } (m \neq 0) \tag{15g}$$

This is almost the same as the result of Marcatili and Schmeltzer except that the coating material is not restricted to a dielectric but can be magnetic as well.

For the first-order approximation of the attenuation constant with $m \neq 0$, we neglected the last term of Eq. (14). Even though this term is of the second order in $k_{\rho 1}/k_{\rho 2}$, the coefficient $|x^2\epsilon_2\mu_2|$ can be a large number for the higher-order modes. Thus we expect that the agreement between our exact solution and the first-order solution requires a larger value of a/λ for a higher-order mode (more discussion is given in Section IV).

B. Surface Mode

When the coating material is not lossy enough, some of the normal modes become surface modes. The fields of those modes are confined within the thin layer of the coating and the propagation constants are nearly independent of the inner radius a. When a/λ is sufficiently large, the characteristic equation is approximated to

$$\left[1 + \epsilon_2 \frac{jk_{\rho 1}}{k_{\rho 2}} \cot(k_{\rho 2}\tau)\right]\left[1 - \mu_2 \frac{jk_{\rho 1}}{k_{\rho 2}} \tan(k_{\rho 2}\tau)\right] = 0 \tag{16}$$

where τ is the layer thickness, b - a. Assuming $|k_{\rho 1}| >> k_0$, we obtain

$$k_z = \begin{cases} \left[\epsilon_2\mu_2k_0^2 - \left\{\left(n - \frac{1}{2}\right) \pi/\tau\right\}^2\right]^{1/2} & \text{for} \quad TM_{mn}^{su} \quad (17) \\ \left[\epsilon_2\mu_2k_0^2 - (n\pi/\tau)^2\right]^{1/2} & \text{for} \quad TE_{mn}^{su} \quad (18) \end{cases}$$

where n = 1, 2, 3, ...

Superscript su indicates the surface mode. The fields in Region II in this limit can be approximately shown to be

$$E_\rho = C_1 \cos k_{\rho 2}(b - \rho) \tag{19a}$$

$$E_z = -jC_1(k_{\rho 2}/k_z) \sin k_{\rho 2}(b - \rho) \tag{19b}$$

$$H_\phi = C_1Y_2(k_2/k_z) \cos k_{\rho 2}(b - \rho) \tag{19c}$$

$$E_\phi = H_\rho = H_z = 0 \qquad \text{for} \quad TM_{mn}^{su} \tag{19d}$$

$$E_\phi = D_1 \sin k_{\rho 2}(b - \rho) \tag{20a}$$

$$H_\rho = -D_1Y_2 (k_z/k_2) \sin k_{\rho_2} (b - \rho) \tag{20b}$$

$$H_z = -jD_1Y_2(k_{\rho 2}/k_2) \cos k_{\rho 2}(b - \rho) \tag{20c}$$

$$E_\rho = E_z = H_\phi = 0 \qquad \text{for} \quad TE_{mn}^{su} \tag{20d}$$

where C_1 and D_1 are constants. Thus the TE^{su}_{mn} mode can be approximated by a normal mode between two PEC slabs and the TM^{su}_{mn} mode by a normal mode between PMC and PEC slabs. The correspondence between the normal modes in a thinly coated waveguide and the surface modes is not unique but depends on the type of coating material. When the coating material is lossless, the $HE_{mn}(EH_{mn})$ modes become $TM^{su}_{mn}(TE^{su}_{mn})$ (except m = 0) as the layer thickness increases. The normal modes with m = 0 are pure TE or TM as indicated in Section II.

C. Interface Mode

There exists an "interface" mode, which is unique to the waveguide coated with a lossy material. The interface mode has large fields near the interface between the air and lossy regions, and the fields decay exponentially to both sides of the interface. Since the fields are limited to the interface region, the attenuation constant is independent of the radius of the waveguide. As a/λ is sufficiently large and the coating material is sufficiently lossy, the characteristic equation for the interface mode is well-approximated to

$$(1 + \epsilon_2 k_{\rho 1}/k_{\rho 2})(1 + \mu_2 k_{\rho 1}/k_{\rho 2}) = 0 \tag{21}$$

The propagation constants are then evaluated to be

$$k_z = \begin{cases} k_0[(\epsilon_2^2 - \epsilon_2\mu_2)/(\epsilon_2^2 - 1)]^{1/2} & \text{for} \quad TM^{in} \qquad (22) \\ k_0[(\mu_2^2 - \epsilon_2\mu_2)/(\mu_2^2 - 1)]^{1/2} & \text{for} \quad TE^{in} \qquad (23) \end{cases}$$

The modal fields are given by

$$E^I_\rho = C_2 \exp[jk_{\rho 1}(a - \rho)] \; , \quad E^{II}_\rho = (C_2/\epsilon_2) \exp[-jk_{\rho 2}(\rho - a)] \tag{24a}$$

$$E^I_z = -(k_{\rho 1}/k_z)\, E^I_\rho \; , \quad E^{II}_z = -(k_{\rho 2}/k_z)\, E^{II}_\rho \tag{24b}$$

$$H_\phi^I = (Y_0 k_0/k_z)\, E_\rho^I \quad , \quad H_\phi^{II} = (Y_2 k_2/k_z)\, E_\rho^{II} \tag{24c}$$

for TM^{in}

$$E_\phi^I = D_2 \exp[jk_{\rho 1}(a - \rho)] \quad , \quad E_\phi^{II} = D_2 \exp[-jk_{\rho 2}(\rho - a)] \tag{25a}$$

$$H_\rho^I = -(Y_0 k_z/k_0)\, E_\phi^I \quad , \quad H_\rho^{II} = -(Y_2 k_z/k_2)\, E_\phi^{II} \tag{25b}$$

$$H_z^I = (Y_0 k_{\rho 1}/k_0)\, E_\phi^I \quad , \quad H_z^{II} = (Y_2 k_{\rho 2}/k_2) E_\phi^{II} \tag{25c}$$

for TE^{in}

where all other field components vanish and C_2 and D_2 are constants. Here superscript in indicates the interface mode. From the above results, we can see that the interface mode is well-approximated to the normal mode on the surface of a semi-infinite lossy material.

There exist two interface modes at most. The fields of the interface mode decay rapidly to both sides of the interface. The conditions for the interface mode to exist are easily recognized from Eqs. (24) and (25) to be

$$\mathrm{Im}(k_{\rho 1} a) >> 1 \tag{26}$$

and

$$-\mathrm{Im}(k_{\rho 2} \tau) >> 1 \tag{27a}$$

Using the boundary conditions at the interface, Eq. (27a) can be rewritten equivalently either

$$-\mathrm{Im}(k_{\rho 1} \varepsilon_2 \tau) >> 1 \qquad \text{for } TM^{in} \tag{27b}$$

or

$$-\mathrm{Im}(k'_{\rho 1} \mu_2 \tau) >> 1 \qquad \text{for } TE^{in} \tag{27c}$$

Thus for dielectric coating, only TM^{in} of the two modes can exist, and only the TE^{in} mode can be excited in a waveguide coated with a magnetic material.

IV. NUMERICAL RESULTS AND DISCUSSION

A. Lossless Coating

When the coating material is lossless, the normal modes in the overmoded coated waveguide become surface waves as the layer thickness increases, in the order of HE_{m1}, EH_{m1}, HE_{m2}, EH_{m2}, ... ($m \neq 0$) and EH_{01}, HE_{01}, EH_{02}, HE_{02}, ... ($m = 0$) [4]. These features of the normal modes are shown in Figure 10 (Figure 11) for a dielectric (magnetic) coating, where the radial wave numbers are plotted as a function of the layer thickness. The large imaginary part of a complex radial number indicates that the modal field shifts to the waveguide wall and the mode behaves as a surface mode. Note that the HE_{11} in the magnetic-coated guide becomes a surface mode with a much thinner coating layer than that in the dielectric-coated guide. Otherwise, the onset of a new surface mode occurs around every quarter-wavelength thickness as the layer thickness increases.

B. Slightly Lossy Coating

Figure 12 (Figure 13) shows the radial wave numbers of the normal modes in a circular guide coated with a slightly lossy dielectric (magnetic) material. The general trend of the normal mode with variation of the layer thickness remains similar to that for the waveguide coated with a lossless material (Figures 10 and 11). As shown in Figures 14 and 15, the mode with a large imaginary part of the complex radial number of a surface-wave type has a large attenuation constant. This is due to the fact that the surface mode has a large

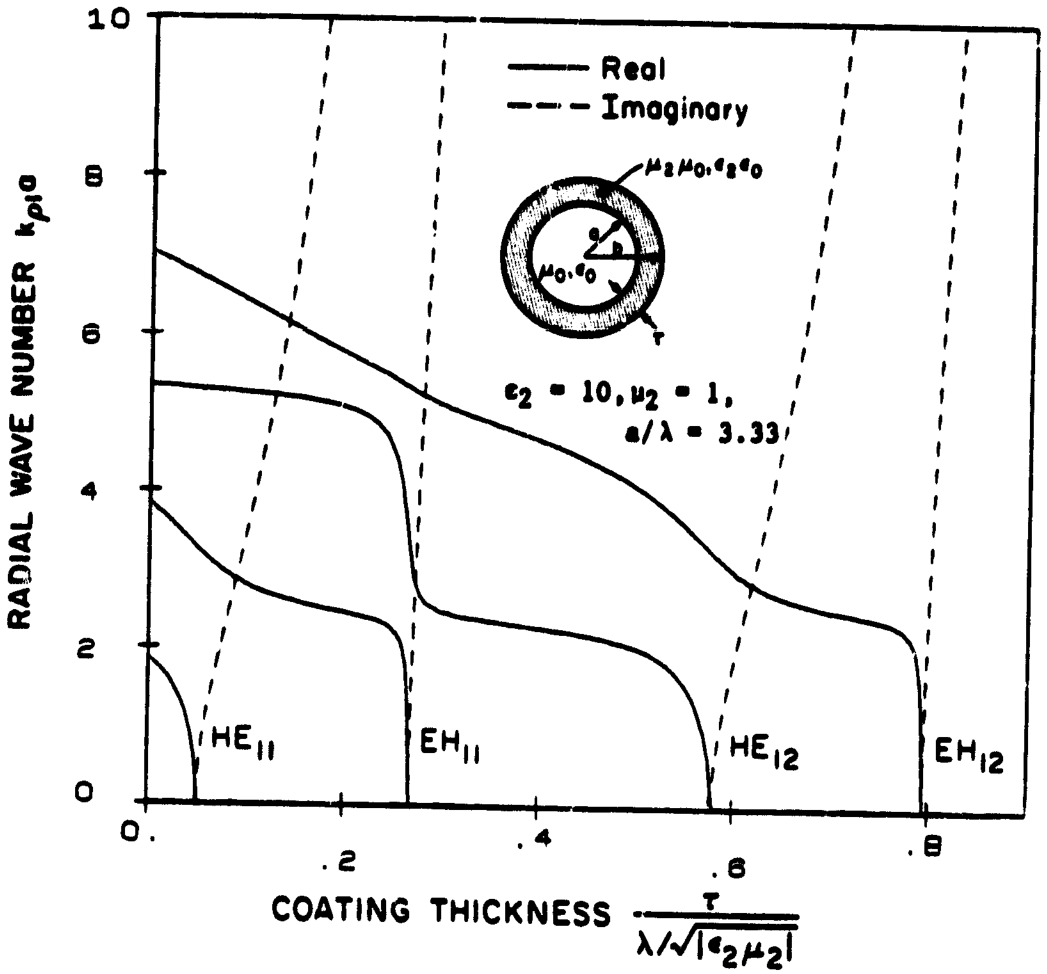

Figure 10. Radial wave numbers of the normal modes in a waveguide coated with lossless dielectric material ($\epsilon_2 = 10, \mu_2 = 1, a/\lambda = 3.33$).

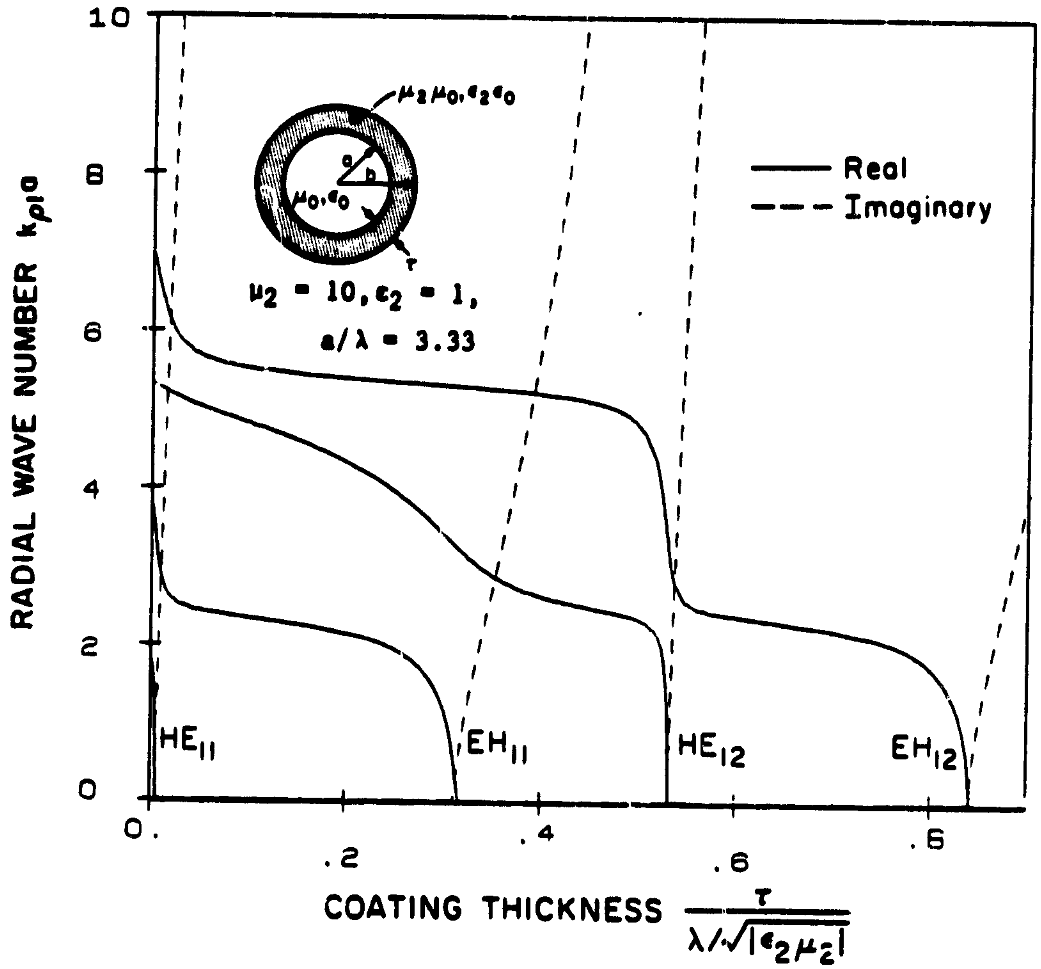

Figure 11. Radial wave numbers of the normal modes in a waveguide coated with a lossless magnetic material ($\mu_2 = 10, \epsilon_2 = 1$, $a/\lambda = 3.33$).

C-2

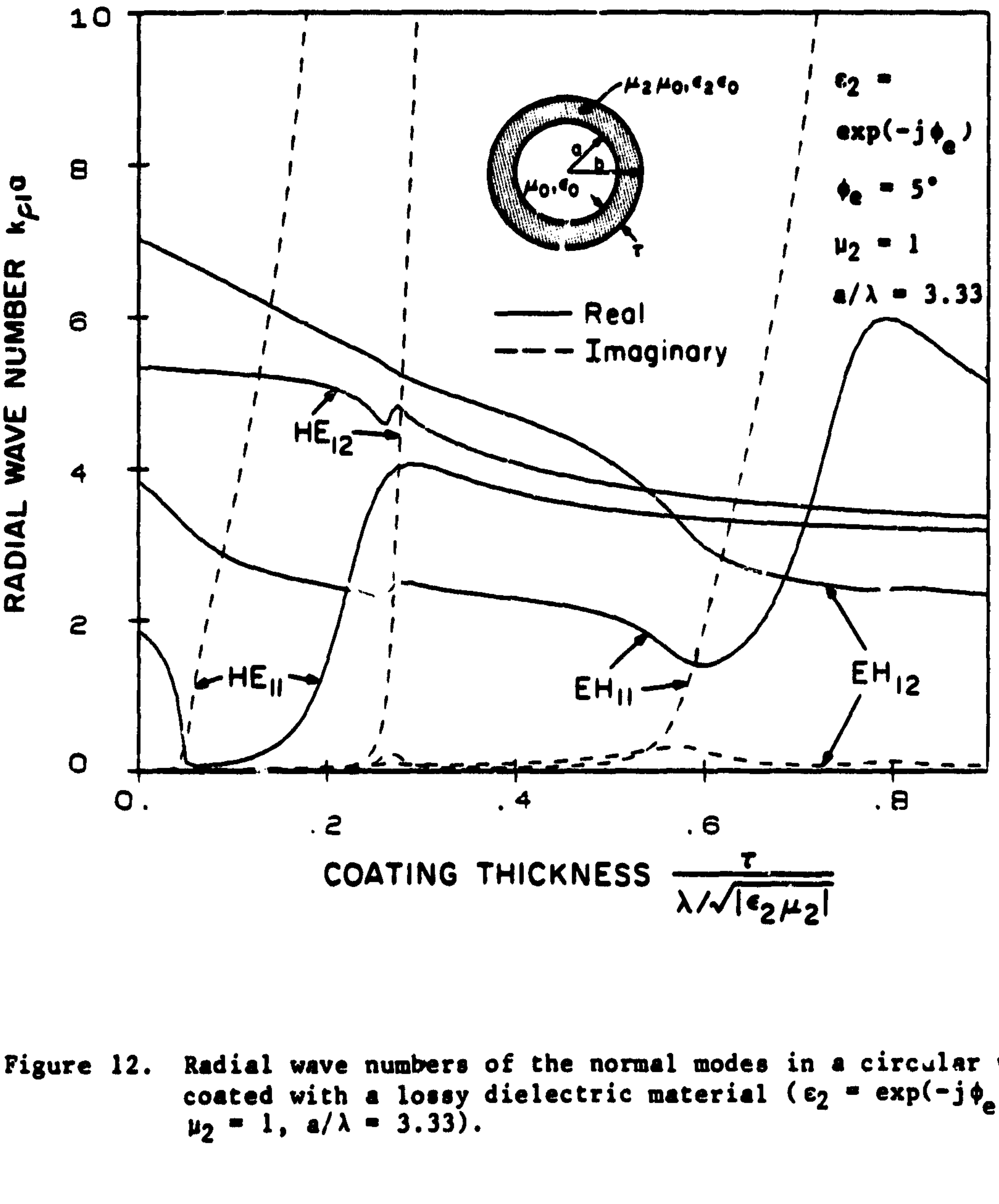

Figure 12. Radial wave numbers of the normal modes in a circular waveguide coated with a lossy dielectric material ($\epsilon_2 = \exp(-j\phi_e)$, $\phi_e = 5°$, $\mu_2 = 1$, $a/\lambda = 3.33$).

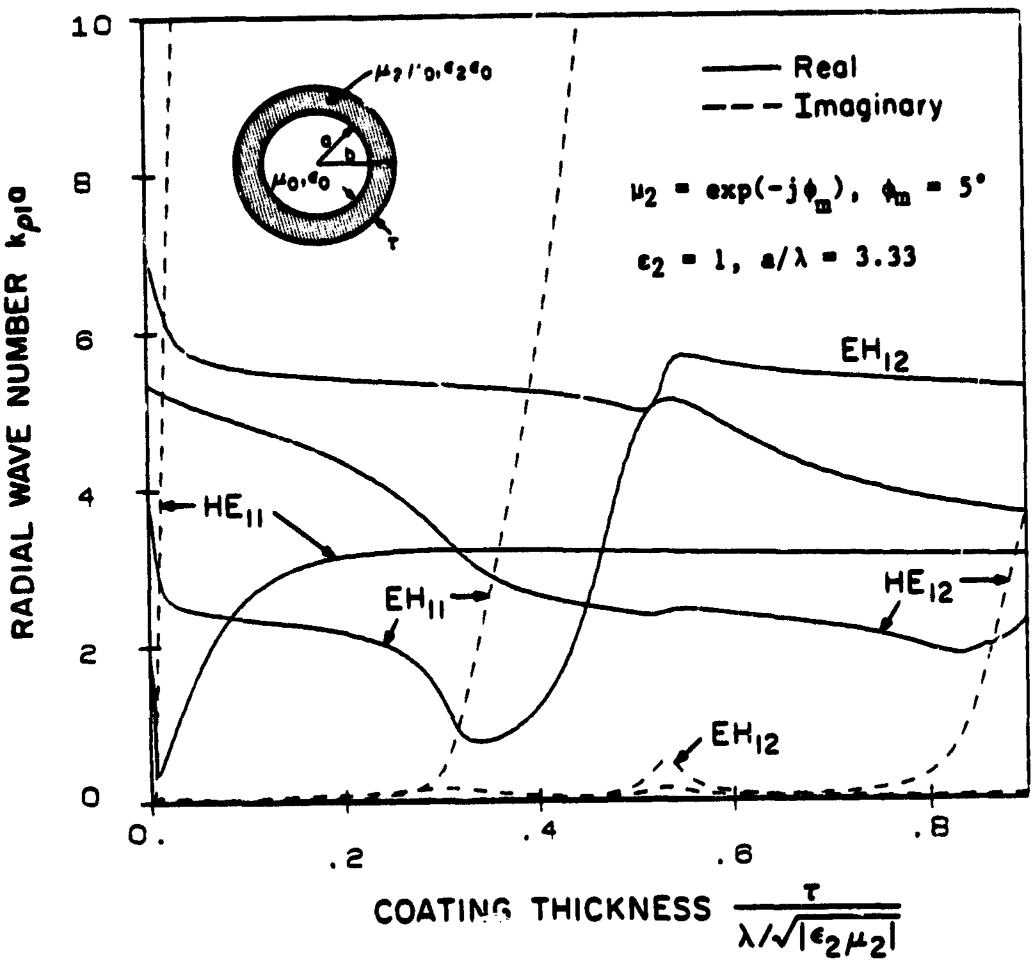

Figure 13. Radial wave numbers of the normal modes in a circular waveguide coated with a lossy magnetic material ($\mu_2 = \exp(-j\phi_m)$, $\phi_m = 5°$, $\varepsilon_2 = 1$, $a/\lambda = 3.33$).

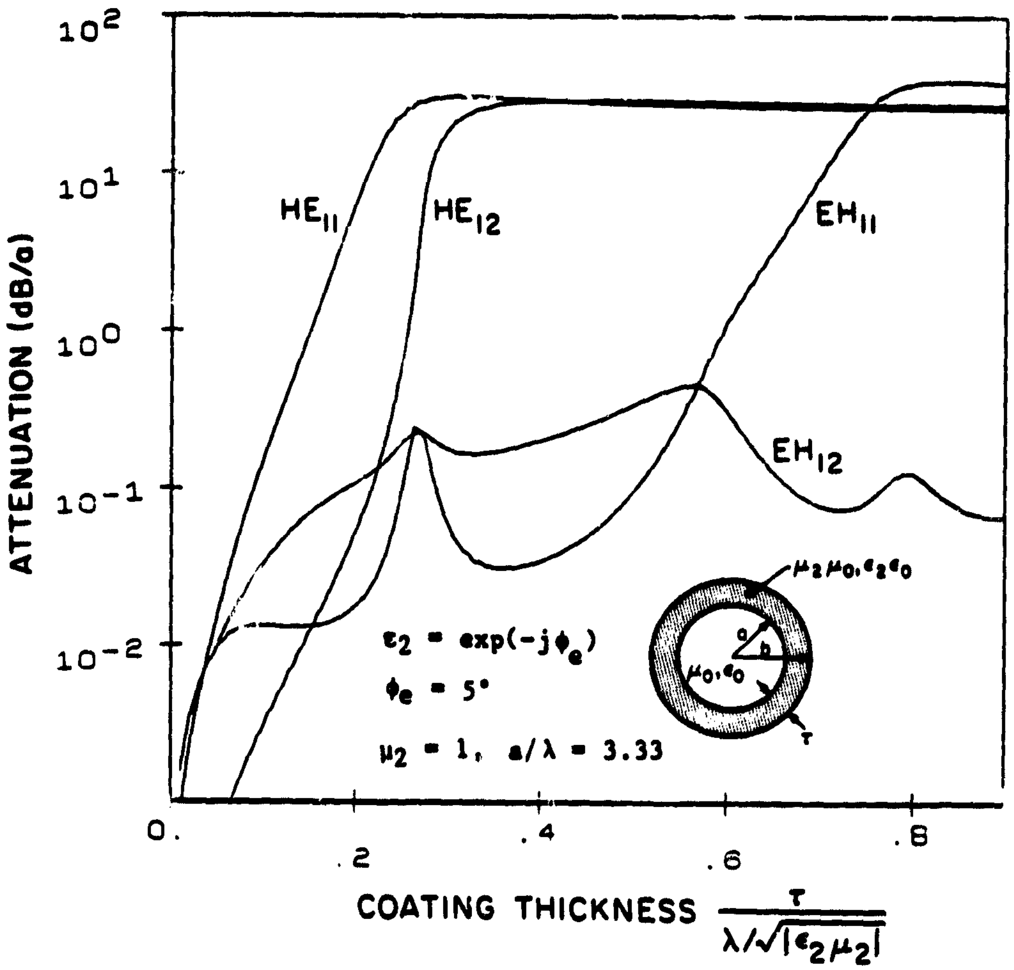

Figure 14. Attenuation constants of the normal modes in a circular waveguide coated with a lossy dielectric material ($\varepsilon_2 = \exp(-j\phi_e)$, $\phi_e = 5°$, $\mu_2 = 1$, $a/\lambda = 3.33$).

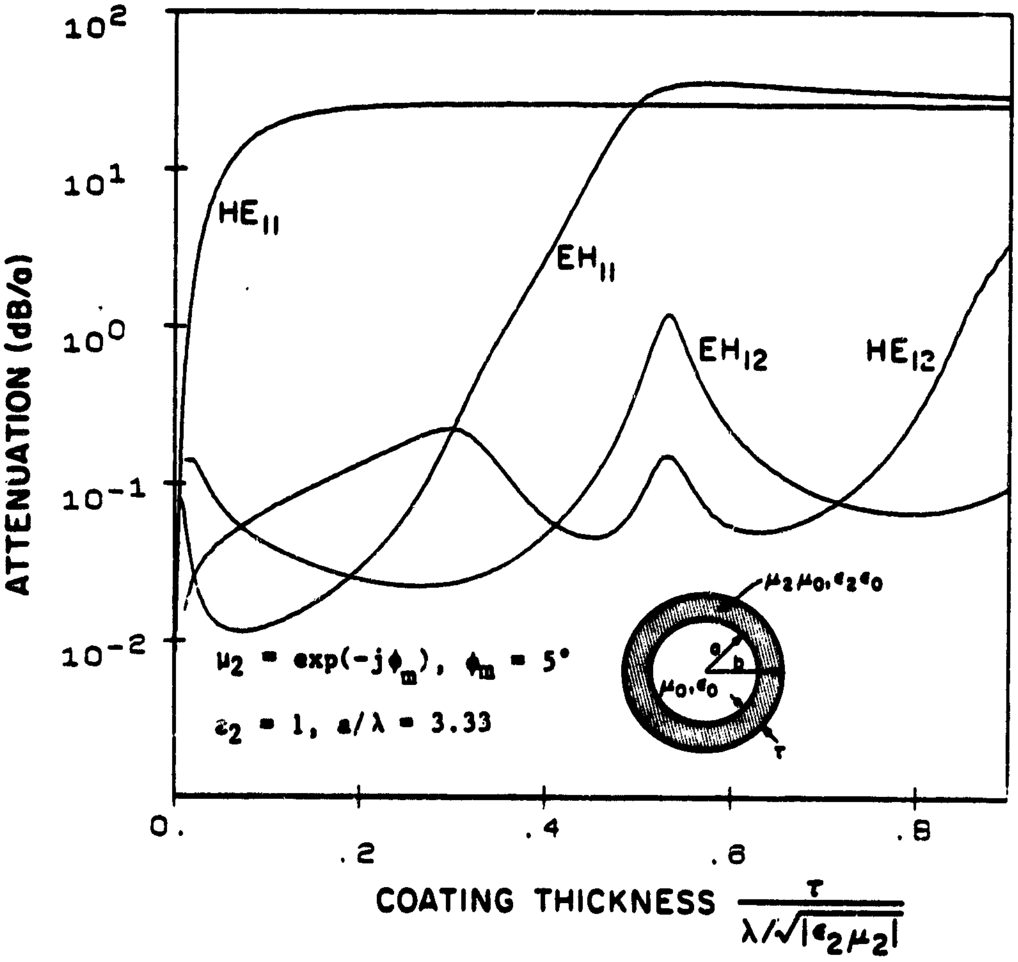

Figure 15. Attenuation constants of the normal modes in a circular waveguide coated with a lossy magnetic material ($\mu_2 = \exp(-j\phi_m)$, $\phi_m = 5°$, $\epsilon_2 = 1$, $a/\lambda = 3.33$).

field concentration within the lossy region near the waveguide wall. It is interesting to note that the HE_{11} in the magnetic-coated guide acquires a very large attenuation constant with a much thinner coating layer than that in the dielectric-coated guide. The higher-order modes also become surface modes and acquire large attenuation constants only at a much thicker coating layer.

C. Very Lossy Coating

When the coating material becomes very lossy, those features of the normal modes in the waveguide coated with a lossless material disappear. In fact, the propagation constant of the normal mode is independent of the layer thickness if the lossy layer is thicker than the skin depth of the normal mode (Figures 16 and 17). There is a mode separation between highly attenuated and lowly attenuated low-order modes. The highly attenuated modes in a dielectric-coated guide are usually lowly attenuated modes in magnetic-coated guide and vice versa (Figures 18 and 19). In general, the mode separation is less distinctive for higher-order modes.

When a/λ is large and the coating material is lossy enough, most of the low-order modes are inner modes which are mainly confined in the air region and the attenuation constants are small. Marcatili and Schmeltzer [5] evaluated the attenuation constants using the perturbation theory under the assumption that a/λ is large and the fields within the lossy region are small (see Section III). Figure 20 shows the comparison of the exact solutions with the approximate solutions by Marcatili and Schmeltzer for the attenuation constants of the normal modes in a dielectric-coated guide. Here the coating thickness τ is fixed while a/λ is varied. We note that the exact and approximate solutions are in better agreement at a larger value of a/λ. The high-order modes usually require a large value of a/λ for good agreement between the exact and approximate solutions (see Section IIIA). This result indicates that the low-order modes become

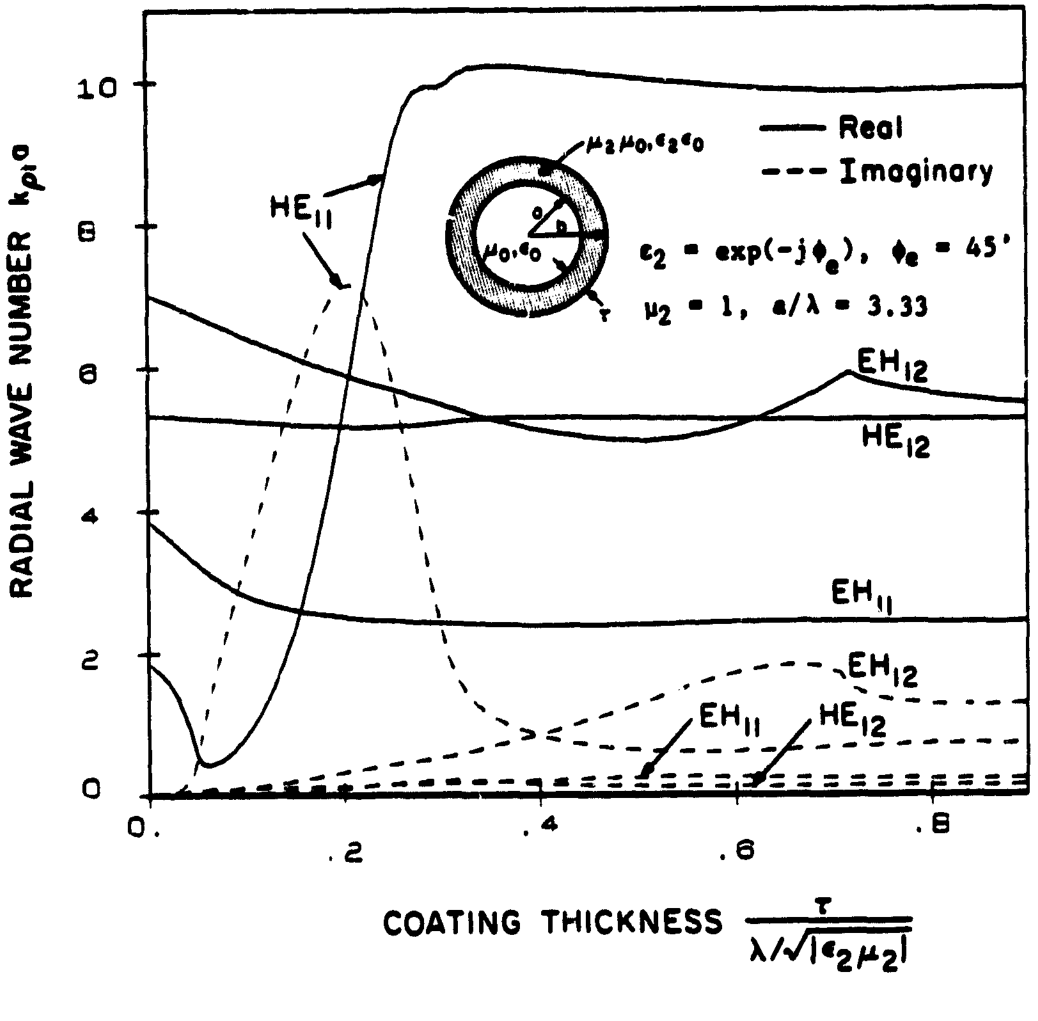

Figure 16. Radial wave numbers of the normal modes in a circular waveguide coated with a lossy dielectric material ($\varepsilon_2 = \exp(-j\phi_e)$, $\phi_e = 45°$, $\mu_2 = 1$, $a/\lambda = 3.33$).

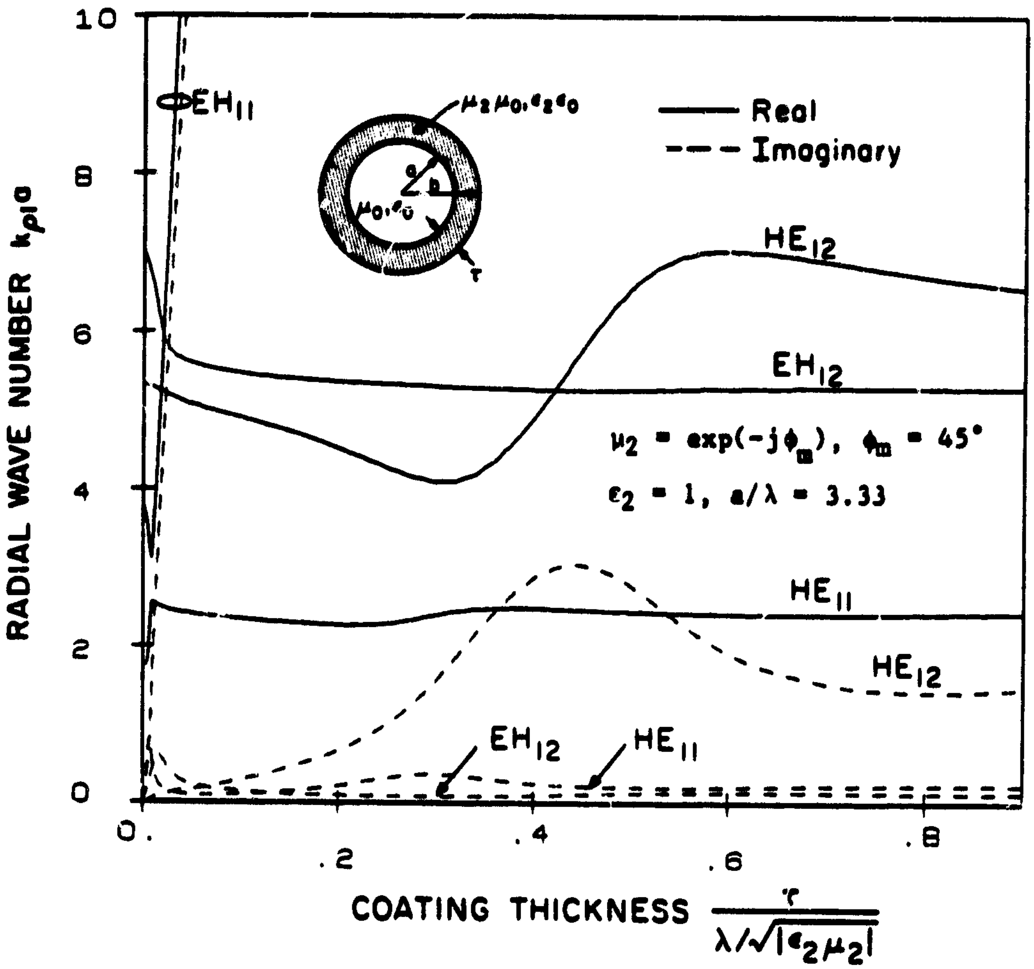

Figure 17. Radial wave numbers of the normal modes in a circular waveguide coated with a lossy magnetic material ($\mu_2 = \exp(-j\phi_m)$, $\phi_m = 45°$, $\epsilon_2 = 1$, $a/\lambda = 3.33$).

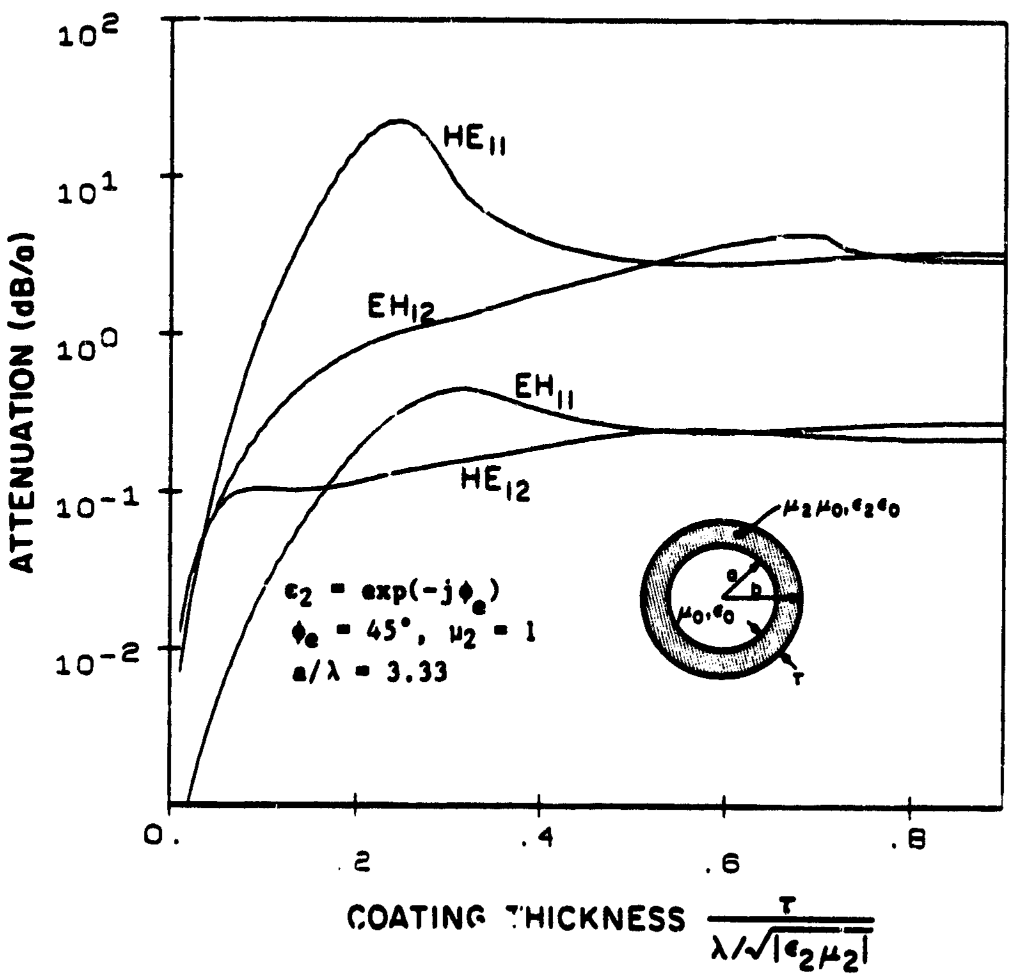

Figure 18. Attenuation constants of the normal modes in a circular waveguide coated with a lossy dielectric material ($\varepsilon_2 = \exp(-j\phi_e)$), $\phi_e = 45°$, $\mu_2 = 1$, $a/\lambda = 3.33$).

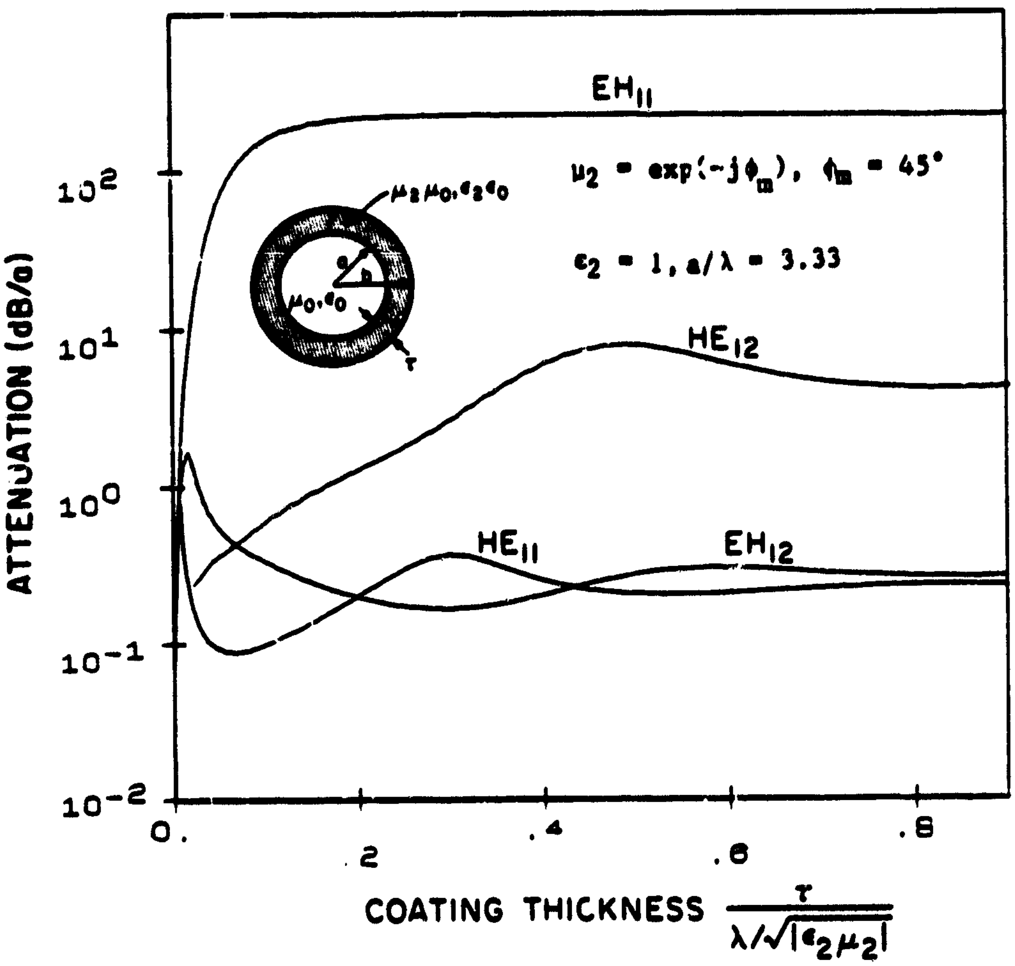

Figure 19. Attenuation constants of the normal modes in a circular waveguide coated with a lossy magnetic material ($\mu_2 = \exp(-j\phi_m)$, $\phi_m = 45°$, $\epsilon_2 = 1$, $a/\lambda = 3.33$).

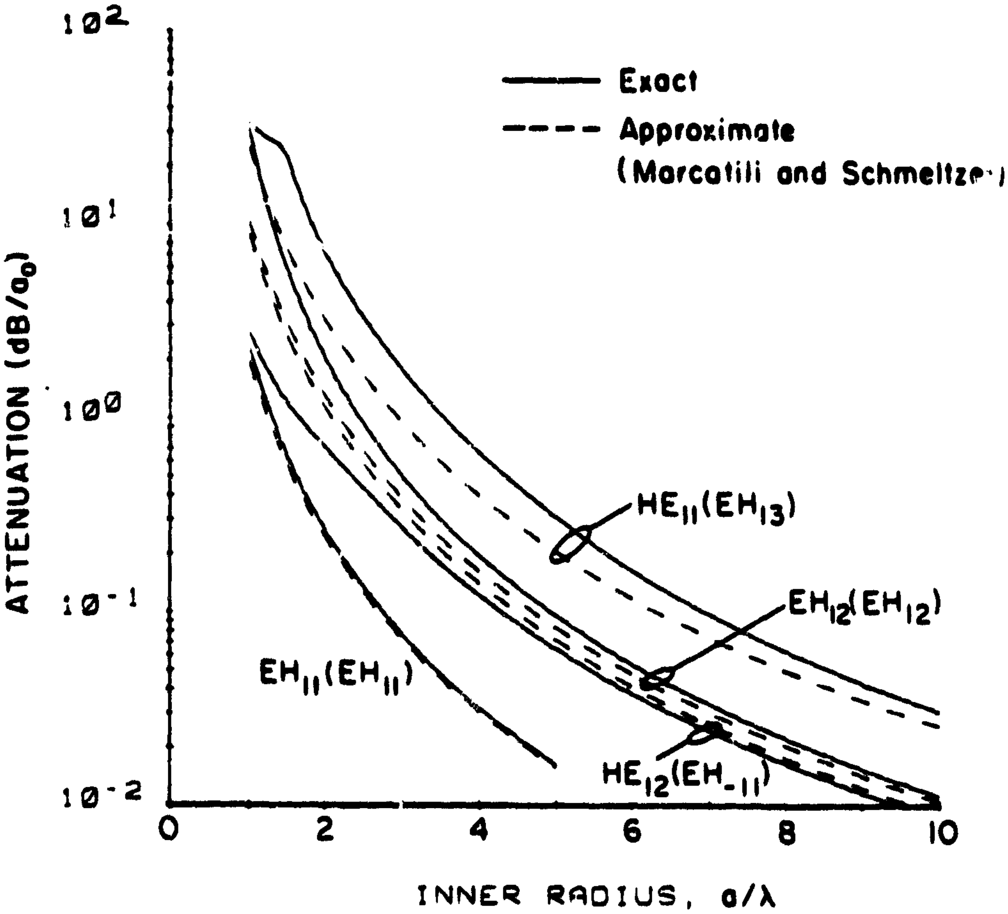

Figure 20. Attenuation constants of the normal modes as a function of the inner radius, a, with a fixed layer thickness ($\tau = 0.949\ \lambda/\sqrt{|\epsilon_2\mu_2|}$) in a circular waveguide coated with a lossy dielectric material ($\epsilon_2 = \exp(-j\phi_e)$, $\phi_e = 45°$, $\mu_2 = 1$, $a_0/\lambda = 3.33$). The mode names in the parentheses correspond to those in Marcatili and Schmeltzer's paper [5].

excluded from the lossy layer near the wall at a smaller value of a/λ than do the high-order modes.

Figure 21 shows the comparison of the exact and various approximate solutions for the attenuation constants of the normal modes in a magnetic-coated circular guide. Most of the low-order modes become inner modes at a large value of a/λ as in the case of the dielectric coating (Figure 20). However, certain modes are confined near the wall. The EH_{11} mode at a large a/λ becomes a surface mode (Section IIIB), whose fields are mainly confined within the lossy region and have a large attenuation constant. The exact solution of the attenuation constant is well-approximated by the solution for the surface mode given in Eq. (17). The existence of the surface mode in a waveguide coated with a lossy material depends on whether the characteristic equation (Eq. (16)) has a solution close to the value for a surface mode (Eq. (17) or (18)). Also note that the HE_{12} mode becomes an interface mode (Section IIIC) whose fields are limited to the region near the interface between the air and lossy material. The attenuation constant of the interface mode is well-approximated by that of the mode on the surface of a semi-infinite lossy material. The criteria for the existence of the interface modes in a coated guide are given in Eqs. (26) and (27). Thus the attenuation constant of the interface mode is not as large as that of the surface mode but much larger than that of the inner mode (Figure 21).

In Figures 20 and 21, the mode names in the parentheses for the inner modes correspond to the mode names by Marcatili and Schmeltzer [5], where the field diagrams of those modes are also shown. The surface mode does not exist when the lossy layer becomes infinitely extended. However, the interface mode should exist in a hollow lossy circular guide if the conditions in Eq. (26) and (27) are satisfied.

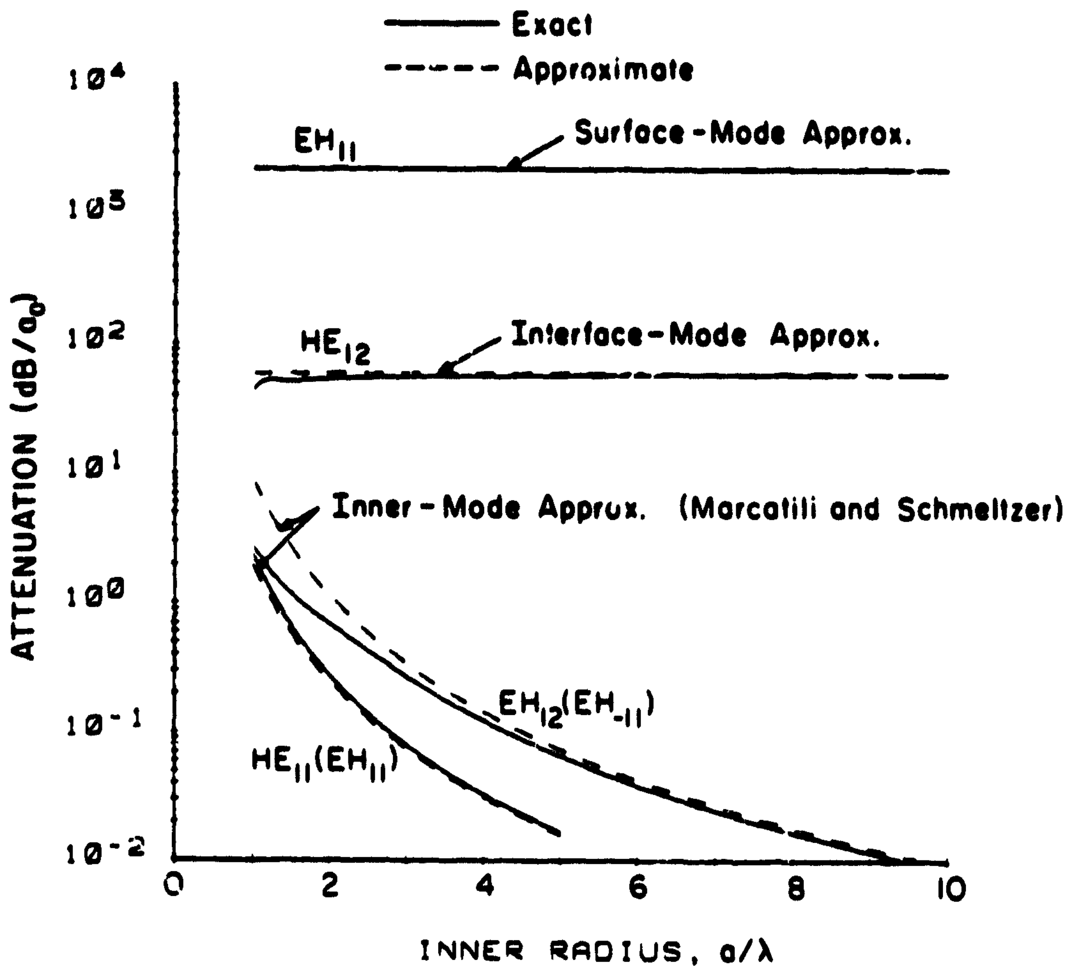

Figure 21. Attenuation constants of the normal modes as a function of the inner radius, a, with a fixed layer thickness ($\tau = 0.949\ \lambda/\sqrt{|\epsilon_2\mu_2|}$) in a circular waveguide coated with a lossy magnetic material ($\mu_2 = \exp(-j\phi_m)$, $\phi_m = 45°$, $\epsilon_2 = 1$, $a_0/\lambda = 3.33$). The mode names in the parentheses correspond to those in Marcatili and Schmeltzer's paper [5].

D. Mode Suppressor

So far, we have seen that the attenuation properties of the normal modes in a coated waveguide depend on the coating material, layer thickness and frequency. When the coating material is not very lossy, the attenuation constants of the normal modes strongly vary with the layer thickness. Since each mode has its own region where the mode is significantly attenuated, the coated guide can be used as a simple mode suppressor [12]. The device will be especially useful for eliminating low-order modes. Since low-order modes are mainly responsible for the radar cross section (RCS) at a small incident angle from a cavity-type structure, coating the cavity wall with a lossy material will be effective in reducing the RCS due to the undesirable interior irradiation from the normal modes in a cavity [13], [14]. In a practical design, the transition region between the uncoated and coated sections of the waveguide must be long enough to prevent any mode conversion [15].

E. CP Antenna

When the coating material is sufficiently lossy and a/λ is large, most of the normal modes become inner modes if the coating layer is thick enough, i.e., thicker than the skin depths of the modal fields. Both the magnetic and electric fields of the inner mode are small near the waveguide wall. The HE_{11} mode in the waveguide coated with a lossy magnetic material becomes an inner mode at a much smaller value of a/λ than that with a lossy dielectric material. The boundary conditions of the HE_{11} mode in this case are similar to those of a corrugated waveguide [16] - [19]; hence, this waveguide can be used as an alternate to the corrugated waveguide to produce circularly polarized radiation or reduce the side-lobe level. Even though the loss of the HE_{11} mode in the coated waveguide may be higher than that of a well-designed corrugated waveguide, the coated waveguide is cheaper to build and lighter in weight than the corrugated waveguide, as explained in [20].

V. CONCLUSION

The normal modes in a circular guide coated with a lossy material are classified and analyzed, emphasizing the attenuation properties of the normal modes. It is shown that the coating material should not be too lossy for the low-order modes to be significantly attenuated. A much thinner coating layer is required for the attenuation of the HE_{11} mode when the coating material is magnetic rather than dielectric. The coating technique is especially useful in reducing the radar cross section from a jet engine inlet, a subject that will be reported by us in a future communication.

When a/λ is large and the coating material is very lossy, most of the low-order modes become inner modes, which have small fields within the lossy region and small attenuation constants. An interesting application of the HE_{11} mode in an open-ended waveguide coated with a very lossy magnetic material is that it can be used for circularly polarized radiation [20].

REFERENCES

[1] M. Miyagi, A. Hongo, and S. Kawakami, "Transmission characteristics of dielectric-coated metallic waveguide for infrared transmission: slab waveguide model," IEEE J. Quantum Electron., vol. QE-19, pp. 136-145, February 1983.

[2] H. G. Unger, "Lined waveguide," Bell System Tech. J., vol. 41, pp. 745-768, March 1962.

[3] J. W. Carlin and P. D'Agostino, "Low-loss modes in dielectric lined waveguide," Bell System Tech. J., vol. 50, pp. 1631-1638, May-June 1971.

[4] J. W. Carlin and P. D'Agostino, "Normal modes in overmoded dielectric-lines circular waveguide," Bell System Tech. J., vol. 52, pp. 453-486, April 1973.

[5] E. A. J. Marcatili and R. A. Schmeltzer, "Hollow metallic and dielectric waveguides for long distance optical transmission and lasers," Bell System Tech. J., pp. 1783-1809, July 1964.

[6] C. Dragone, "High-frequency behavior of waveguides with finite surface impedances," Bell System Tech. J., vol. 60, pp. 89-116, January 1981.

[7] P. J. B. Clarricoats, "Propagation along unbounded and bounded dielectric rods," Part 1 and Part 2, Proc. IEE, Mon. 409E and 410E, pp. 170-186, October 1960.

[8] G. N. Tsandoulas and W. J. Ince, "Modal inversion in circular waveguides-part 1: theory and phenomenology," IEEE Trans. Microwave Theory Tech., vol. MTT-19, pp. 386-392, April 1971.

[9] G. N. Tsandoulas, "Bandwidth enhancement in dielectric-lined circular waveguides," IEEE Trans. Microwave Theory Tech., vol. MTT-21, pp. 651-654, October 1973.

[10] C. S. Lee, S. L. Chuang, S. W. Lee, and Y. T. Lo, "Wave attenuation and mode dispersion in a waveguide coated with lossy dielectric material," Univ. of Illinois Electromagnetics Laboratory, Urbana, IL, Technical Report, No. 84-13, July 1984.

[11] R. F. Harrington, Time Harmonic Electromagnetic Fields. New York: McGraw-Hill Book Co., 1961.

[12] T. N. Anderson, "Low loss transmission using overmoded waveguide, a practical 1981 review of the state of the art," presented at the IEEE AP/MTT-S, Philadelphia Section, Benjamin Franklin 1981 Symposium on Advances in Antenna and Microwave Technology, May 1981.

[13] S. W. Lee, Y. T. Lo, S. L. Chuang, and C. S. Lee, "Numerical methods for analyzing electromagnetic scattering," Semiannual Report to NASA Lewis Research Center, Cleveland, Ohio, March 1985.

[14] H. R. Witt and E. L. Price, "Scattering from hollow conducting cylinders," Proc. IEE, vol. 115, pp. 94-99, January 1968.

[15] H. Unger, "Circular waveguide taper of improved design," Bell System Tech. J., vol. 37, pp. 899-912, July 1958.

[16] M. J. Al-Hakkak and Y. T. Lo, "Circular waveguide and horns with anisotropic and corrugated boundaries," Antenna Laboratory Report No. 73-3, University of Illinois, Urbana, Illinois, 1973.

[17] P. J. B. Clarricoats, A. D. Olver, and S. L. Chong, "Attenuation in corrugated ciruclar waveguide, Part 1, Theory," Proc. IEE, vol. 122, pp. 1173-1179, 1975.

[18] C. Dragone, "Reflection and mode conversion in a corrugated feed," Bell System Tech. J., vol. 56, pp. 835-867, 1977.

[19] C. Dragone, "Attenuation and radiation characteristics of the HE mode," IEEE Trans. Microwave Theory Tech., vol. MTT-28, pp. 704-710, 1980.

[20] C. S. Lee, S. L. Chuang, and S. W. Lee, "A simple version of corrugated waveguide: smooth-walled circular waveguide coated with lossy magnetic material," AP-S International Symposium Digest, vol. 1, pp. 303-306, 1985.

[21] M. Abramowitz and I. A. Stegun, Handbook of Mathematical Functions. New York: Dover, 1972.

APPENDIX 1.

DEGENERACY BETWEEN THE CUTOFF FREQUENCIES OF THE TM_{11} AND TE_{01} MODES IN A DIELECTRIC-COATED CIRCULAR WAVEGUIDE

At the cutoff frequency ($k_z = 0$), the characteristic equation in Eq. (1) becomes

$$J_1'(k_{CM}a)[J_1(k_{CM2}a)\, N_1(k_{CM2}b) - N_1(k_{CM2}a)\, J_1(k_{CM2}b)]$$
$$- \sqrt{\epsilon_2/\mu_2}\, J_1(k_{CM}a)[J_1(k_{CM2}a)\, N_1(k_{CM2}b) - N_1'(k_{CM2}a)\, J_1(k_{CM2}b)] = 0$$
$$\text{for } TM_{11} \qquad (A1.1)$$

or

$$J_0'(k_{CE}a)[J_0(k_{CE2}a)\, N_0'(k_{CE2}b) - N_0(k_{CE2}a)\, J_0'(k_{CE2}b)]$$
$$- \sqrt{\mu_2/\epsilon_2}\, J_0(k_{CE}a)[J_0'(k_{CE2}a)\, N_0'(k_{CE2}b) - N_0'(k_{CE2}a)\, J_0'(k_{CE2}b)] = 0$$
$$\text{for } TE_{01} \qquad (A1.2)$$

where

$$k_{CM} = \frac{2\pi}{c} f_{CM} \quad , \qquad k_{CM2} = k_{CM}\sqrt{\epsilon_2\mu_2}$$

$$k_{CE} = \frac{2\pi}{c} f_{CE} \quad , \qquad k_{CE2} = k_{CE}\sqrt{\epsilon_2\mu_2}$$

Here f_{CM} and f_{CE} are the cutoff frequencies for the TM_{11} and TE_{01} modes, respectively.

Using the recurrence relations of Bessel functions [21], the derivative expressions in Eqs. (A1.1) and (A1.2) can be eliminated, and we obtain

$$\begin{aligned} &J_1(k_{CM}a)[J_0(k_{CM2}a)\,N_1(k_{CM2}b) - N_0(k_{CM2}a)\,J_1(k_{CM2}b)] \\ &\quad - [\sqrt{\mu_2/\epsilon_2}\,J_0(k_{CM}a) - (1/\sqrt{\epsilon_2\mu_2} - \sqrt{\mu_2/\epsilon_2})/k_{CM}a][J_1(k_{CM2}a)\,N_1(k_{CM2}b) \\ &\quad - N_1(k_{CM2}a)\,J_1(k_{CM2}b)] = 0 \end{aligned} \qquad \text{(A1.3)}$$

$$\text{for } TM_{11}$$

and

$$\begin{aligned} &J_1(k_{CE}a)[J_0(k_{CE2}a)\,N_1(k_{CE2}b) - N_0(k_{CE2}a)\,J_1(k_{CE2}b) \\ &\quad - \sqrt{\mu_2/\epsilon_2}\,J_0(k_{CE}a)[J_1(k_{CE2}a)\,N_1(k_{CE2}b) - N_1(k_{CE2}a)\,J_1(k_{CE2}b)] = 0 \end{aligned}$$

$$\text{for } TE_{01} \qquad \text{(A1.4)}$$

When $\mu_2 = 1$, the two characteristic equations are identical, and the cutoff frequencies of the TM_{11} and TE_{01} modes are the same. On the other hand, when the coating material is magnetic ($\mu_2 \neq 1$), the degeneracy of these two modes at their cutoff frequencies is not present.

APPENDIX 2

FIELDS OF THE NORMAL MODES IN A COATED CIRCULAR GUIDE WHEN $k_{\rho 1} = 0$ (DIRECT METHOD).

From Maxwell's equations, we obtain four equations for the normal modes in a circular guide,

$$\nabla \times \nabla \times \vec{E} - k_0^2 \vec{E} = 0 \tag{A2.1a}$$

$$\nabla \cdot \vec{E} = 0 \tag{A2.1b}$$

First consider the case for $m \neq 0$. Due to the symmetry of the problem, we can assume that

$$E_\rho = R_\rho(\rho) \cos m\phi\, e^{-jk_z z} \tag{A2.2a}$$

$$E_\phi = R_\phi(\rho) \sin m\phi\, e^{-jk_z z} \tag{A2.2b}$$

$$E_z = R_z(\rho) \cos m\phi\, e^{-jk_z z} \tag{A2.2c}$$

Since $k_{\rho 1} = 0$, from the dispersion relation

$$k_z = k_0 \tag{A2.3}$$

Substituting Eq. (A2.2) in Eq. (A2.1), three linearly independent equations are obtained:

$$\rho \frac{d}{d\rho} [\rho(\frac{dR_\rho(\rho)}{d\rho})] - m^2 R_z(\rho) = 0 \tag{A2.4a}$$

$$m\rho \frac{d}{d\rho} [\rho R_\phi(\rho)] + m^2 R_\rho(\rho) - jk_0\rho^2 \frac{dR_z(\rho)}{d\rho} = 0 \tag{A2.4b}$$

$$\frac{d}{d\rho} [\rho R_\rho(\rho)] + mR_\phi(\rho) - jk_0\rho R_z(z) = 0 \tag{A2.4c}$$

Solving these coupled equations, the fields in Region I ($m \neq 0$) are given by

$$E_\rho^I = (C_1\rho^{m+1} + C_2\rho^{m-1}) \cos m\phi \tag{A2.5a}$$

$$E_\phi^I = (C_1\rho^{m+1} - C_2\rho^{m-1}) \sin m\phi \tag{A2.5b}$$

$$E_z^I = \frac{2(m+1)\,C_1}{jk_0}\,\rho^m \cos m\phi \tag{A2.5c}$$

$$H_\rho^I = -Y_0\left[C_1\rho^{m+1} + \left(\frac{2m(m+1)\,C_1}{k_0^2} - C_2\right)\rho^{m-1}\right] \sin m\phi \tag{A2.5d}$$

$$H_\phi^I = Y_0\left[C_1\rho^{m+1} - \left(\frac{2m(m+1)\,C_1}{k_0^2} - C_2\right)\rho^{m-1}\right] \cos m\phi \tag{A2.5e}$$

$$H_z^I = -Y_0\,\frac{2(m+1)\,C_1}{jk_0}\,\rho^m \sin m\phi \tag{A2.5f}$$

Using Eq. (A2.3), the fields in Region II ($m \neq 0$) are obtained from Eq. (2):

$$E_\rho^{II} = -\left[\frac{D_1}{\sqrt{\epsilon_2\mu_2}}\,G_3'(\rho) + \frac{D_2 m}{k_{\rho 2}\rho}\,G_4(\rho)\right] \cos m\phi \tag{A2.6a}$$

$$E_\phi^{II} = \left[\frac{D_1 m}{\sqrt{\epsilon_2\mu_2}\;k_{\rho 2}\rho}\,G_3(\rho) + D_2 G_4'(\rho)\right] \sin m\phi \tag{A2.6b}$$

$$E_z^{II} = \frac{D_1 k_{\rho 2}}{jk_2}\,G_3(\rho) \cos m\phi \tag{A2.6c}$$

$$H_\rho^{II} = -\,Y_2\left[\frac{D_1 m}{k_{\rho 2}\rho}\,G_3(\rho) + \frac{D_2}{\sqrt{\epsilon_2\mu_2}}\,G_4'(\rho)\right] \sin m\phi \tag{A2.6d}$$

$$H_\phi^{II} = -\left[Y_2\,D_1 G_3'(\rho) + \frac{D_2 m}{\sqrt{\epsilon_2\mu_2}\;k_{\rho 2}\rho}\,G_4(\rho)\right] \cos m\phi \tag{A2.6e}$$

$$H_z^{II} = Y_2 \frac{D_2 k_{\rho 2}}{jk_2} G_4(\rho) \sin m\phi \tag{A2.6f}$$

where

$$G_3(\rho) = J_m(k_{\rho 2}\rho)\, N_m(k_{\rho 2}b) - N_m(k_{\rho 2}\rho)\, J_m(k_{\rho 2}b) \tag{A2.6g}$$

$$G_3'(\rho) = J_m'(k_{\rho 2}\rho)\, N_m(k_{\rho 2}b) - N_m'(k_{\rho 2}\rho)\, J_m(k_{\rho 2}b) \tag{A2.6h}$$

$$G_4(\rho) = J_m(k_{\rho 2}\rho)\, N_m'(k_{\rho 2}b) - N_m(k_{\rho 2}\rho)\, J_m'(k_{\rho 2}b) \tag{A2.6i}$$

$$G_4'(\rho) = J_m'(k_{\rho 2}\rho)\, N_m'(k_{\rho 2}b) - N_m'(k_{\rho 2}\rho)\, J_m'(k_{\rho 2}b) \tag{A2.6j}$$

Note that the convention of $e^{j(\omega t - k_0 z)}$ is understood and omitted. Here $k_{\rho 2} = \sqrt{\epsilon_2\mu_2 - 1}\, k_0$, and C_1, C_2, D_1 and D_2 are constants to be determined by imposing the boundary conditions at the interface between the air and material regions. These constants are related by

$$C_1 = \frac{G_3(a)\; k_{\rho 2} D_1}{\sqrt{\epsilon_2\mu_2}\; 2(m+1)\; a^m} \tag{A2.7a}$$

$$D_2 = -\sqrt{\mu_2/\epsilon_2}\; \frac{G_3(a)}{G_4(a)}\, D_1 \tag{A2.7b}$$

$$C_2 = a^2 C_1 - \left[\frac{D_1 m\, G_3(a)}{\sqrt{\epsilon_2\mu_2}\; k_{\rho 2} a} + D_2 G_4'(a)\right] / a^{m-1} \tag{A2.7c}$$

The coating thickness is determined by the characteristic equation,

$$\frac{(k_{\rho 2}a)^2}{m+1} + (k_{\rho 2}a)\left[\frac{G_3'(a)}{G_3(a)}\,\epsilon_2 + \frac{G_4'(a)}{G_4(a)}\,\mu_2\right] - m(\epsilon_2\mu_2 + 1) = 0 \tag{A2.8}$$

Note that the fields are neither TE nor TM and the fields in Region I do not show a Bessel-function dependence of radial distance.

The fields for $m = 0$ can be similarly shown to be

$$E_\rho^I = \frac{jk_0C_{10}}{2}\rho \quad , \quad E_\rho^{II} = -\frac{j\,C_{20}}{\sqrt{\epsilon_2\mu_2 - 1}}G_{30}'(\rho) \tag{A2.9a}$$

$$H_\phi^I = Y_0E_\rho^I \quad , \quad H_\phi^{II} = Y_0\epsilon_2E_\rho^{II} \tag{A2.9b}$$

$$E_z^I = C_{10} \quad , \quad E_z^{II} = C_{20}G_{30}(\rho) \qquad \text{for } TM_{0n} \tag{A2.9c}$$

and

$$H_\rho^I = \frac{jk_0D_{10}}{2}\rho \quad , \quad H_\rho^{II} = -\frac{j\,D_{20}}{\sqrt{\epsilon_2\mu_2 - 1}}G_{40}'(\rho) \tag{A2.10a}$$

$$E_\phi^I = -H_\rho/Y_0 \quad , \quad E_\phi^{II} = -\mu_2H_\rho^{II}/Y_0 \tag{A2.10b}$$

$$H_z^I = D_{10} \quad , \quad H_z^{II} = D_{20}G_{40}(\rho) \qquad \text{for } TE_{0n} \tag{A2.10c}$$

where $G_{30}(\rho)$, $G_{30}'(\rho)$, $G_{40}(\rho)$ and $G_{40}'(\rho)$ are $G_3(\rho)$, $G_3'(\rho)$, $G_4(\rho)$ and $G_4'(\rho)$ with $m = 0$, respectively. All other field components vanish, and C_{10}, C_{20}, D_{10} and D_{20} are constants which are related by

$$C_{10} = C_{20}G_{30}(a) \tag{A2.11a}$$

$$D_{10} = D_{20}G_{40}(a) \tag{A2.11b}$$

The coating thickness for $m = 0$ is determined by the following characteristic equation,

$$G_{30}(a) + \frac{2\epsilon_2}{k_0a\sqrt{\epsilon_2\mu_2 - 1}}G_{30}'(a) = 0 \qquad \text{for } TM_{0n} \tag{A2.12a}$$

or

$$G_{40}(a) + \frac{2\mu_2}{k_0 a\sqrt{\epsilon_2\mu_2 - 1}}\, G_{40}'(a) = 0 \qquad \text{for } TE_{0n} \qquad (A2.12b)$$

The fields are either TE or TM and the fields in the air region show a linear dependence of radial distance instead of the usual Bessel-function dependence in the case of an uncoated guide.

APPENDIX B

LECTURE NOTES IN RCS: VOLUME I

This set of lecture note was presented by professor S. W. Lee at NASA-Lewis Research Center on August 16, 1985.

LECTURE NOTES ON RCS: VOLUME I

S. W. LEE

DEPARTMENT OF ELECTRICAL AND COMPUTER ENGINEERING
UNIVERSITY OF ILLINOIS
URBANA, ILLINOIS 61801

(217)333-0278

AUGUST 1985

Lecture on RCS No. 1

9:00-10:15 (75 min)	30 min	10:45-11:45 (60)
Overview One-minute formulas	coffee	RCS by PO Calculation

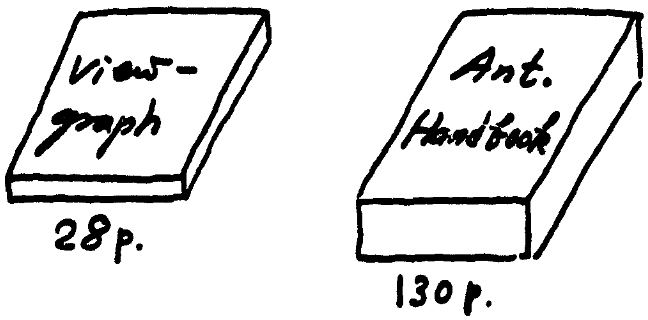

$\boxed{\text{Evalution Sheet}} \Longrightarrow$ future lectures

LECTURE NOTES ON RCS VOLUME I

Part A: Overview and One-minute Formulas

Part B: RCS Computation by Physical Optics

Mono-static & Bi-static Radars

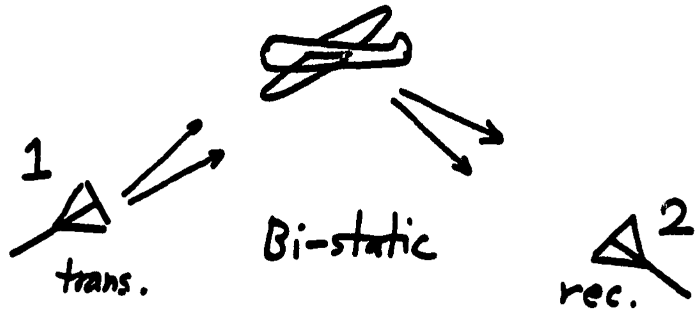

RCS in $(\text{meter})^2$

$10 \log_{10} \text{RCS}$ in dBSM

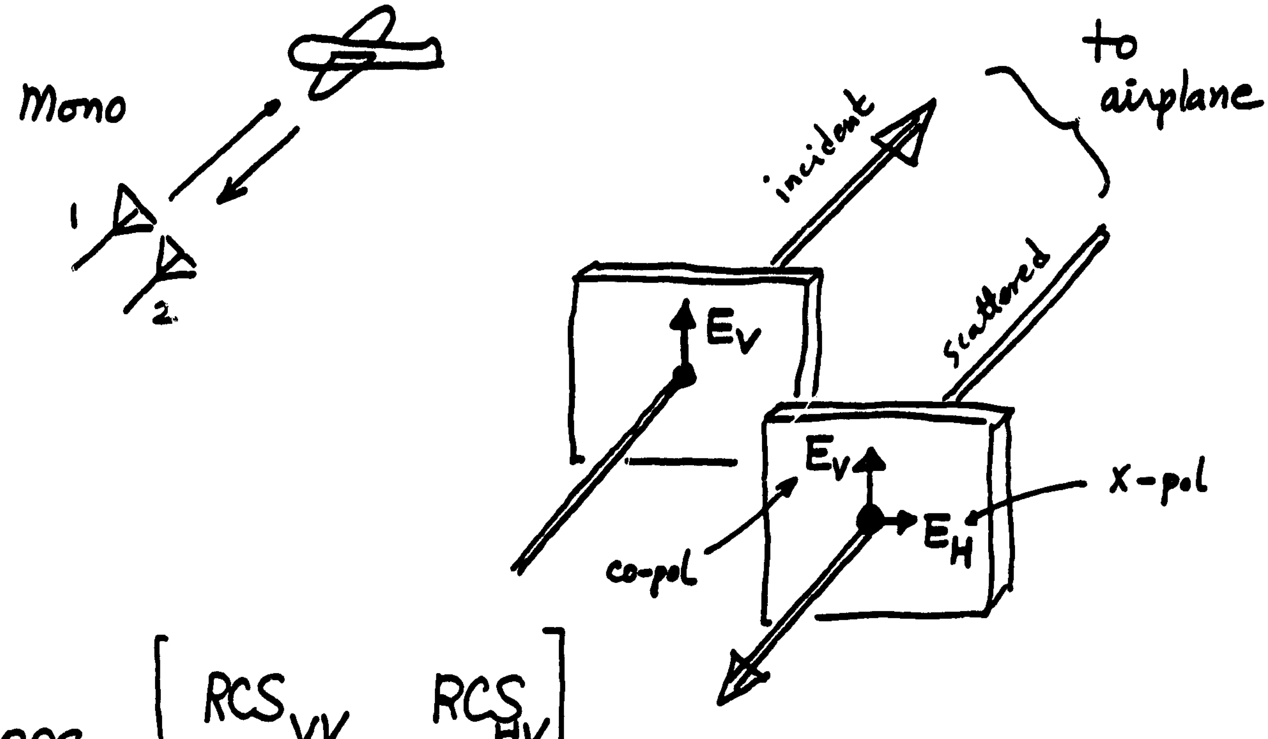

$$\text{RCS} = \begin{bmatrix} \text{RCS}_{VV} & \text{RCS}_{HV} \\ \text{RCS}_{VH} & \text{RCS}_{HH} \end{bmatrix}$$

$\left.\begin{matrix} V \\ H \end{matrix}\right\}$ Related to $\left\{\begin{matrix} TE\,(E_\perp) \\ TM\,(E_\parallel) \end{matrix}\right.$

TE and TM

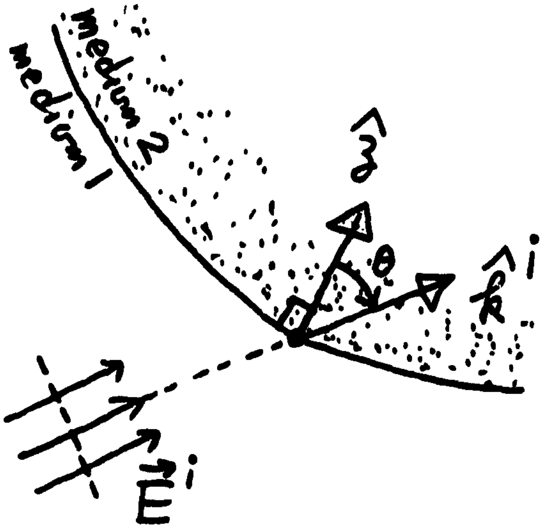

$\hat{z}$ = a ref. direction such as the normal of the interface

$\hat{k}^i$ = direction of incidence

$\boxed{(\hat{z}, \hat{k}^i) \text{ define "plane of incidence"}}$

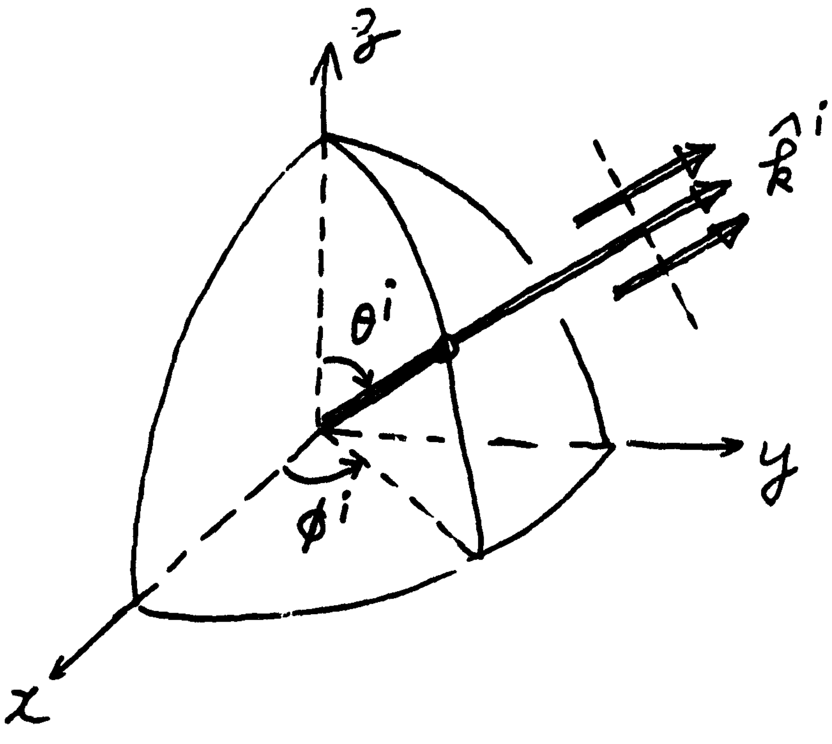

TE : E_ϕ or $E_\perp$

TM : E_θ or $E_{\parallel}$

Eq (102) ch. 1

Meaning of RCS

(1) A hypothetical isotropic scatterer

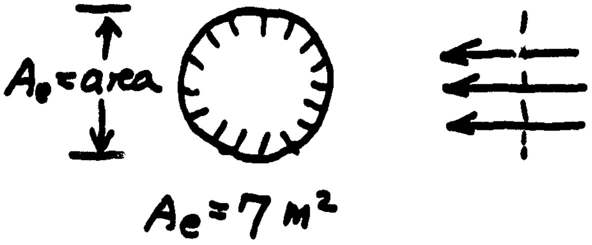

* Power of incident wave:

$$p^i = 5\ \text{watts}/m^2$$

* Power interapted by isotropic scatterer is

$$p^{int} = 7\ m^2 \times 5\ \frac{W}{m^2} = 35\ W$$

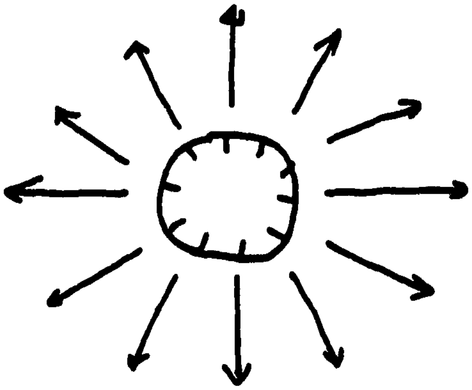

* p^{int} is irradiated isotropically

$$\text{irradiation} = \frac{35\ W}{4\pi\ \text{steradian}}$$

(2) $\boxed{\text{Airplane's RCS} = 7\ m^2}$ means

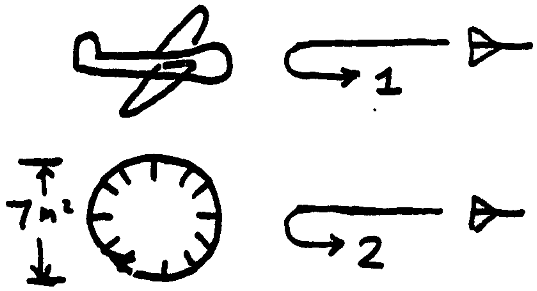

Return 1 = Return 2

(3) $\text{RCS} = \text{function of} \begin{bmatrix} \theta \\ \phi \end{bmatrix}, f, \text{polarization}$

$\boxed{\text{Order of Fields Relative to } \vec{E}^{\,i}}$

High Freq : $k = \frac{2\pi f}{c} = \frac{2\pi}{\lambda}$ = wave number $\Longrightarrow \infty$

$$\boxed{\text{Total field } \vec{E} \sim e^{iks}\left\{ \frac{1}{k^0}\Box + \frac{1}{k^{1/2}}\Box + \frac{1}{k}\Box + \cdots \right\}}$$

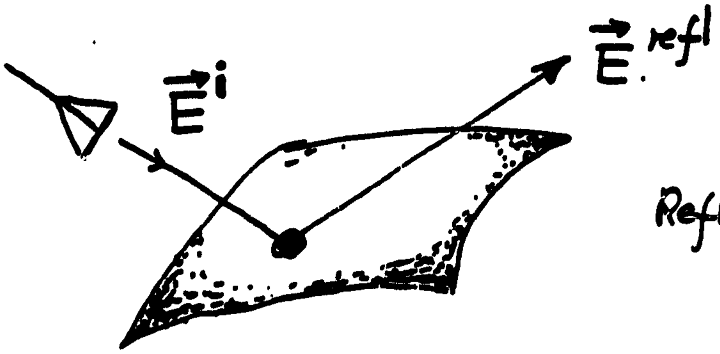

Reflected $\vec{E}^{refl} = O\left(\frac{1}{k^0}\right)$

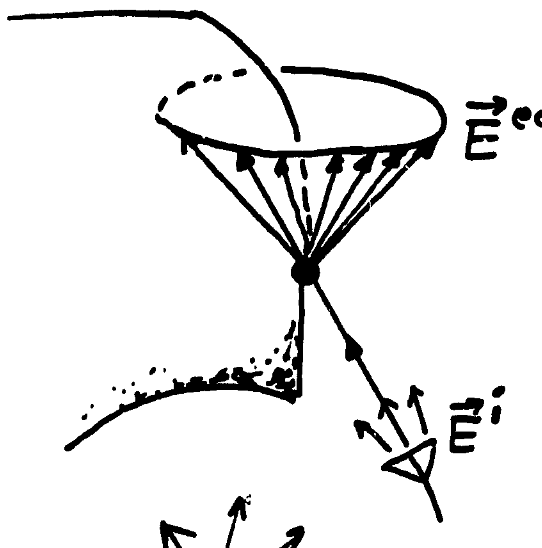

$\vec{E}^{edge} = O\left(\frac{1}{k^{1/2}}\right)$

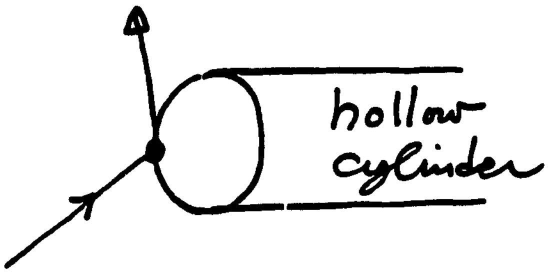

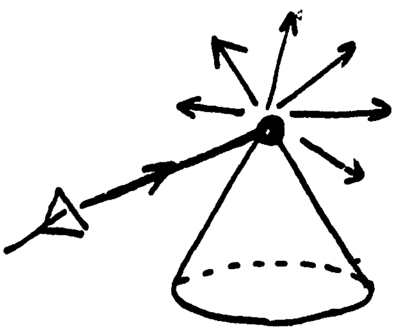

$\vec{E}^{tip} = O\left(\frac{1}{k}\right)$

RCS From Specular

conductor surface near O

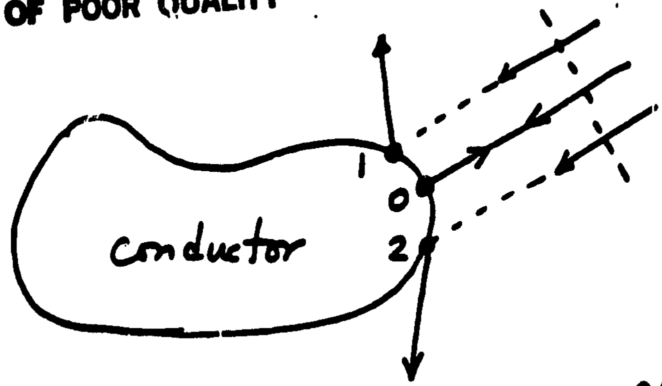

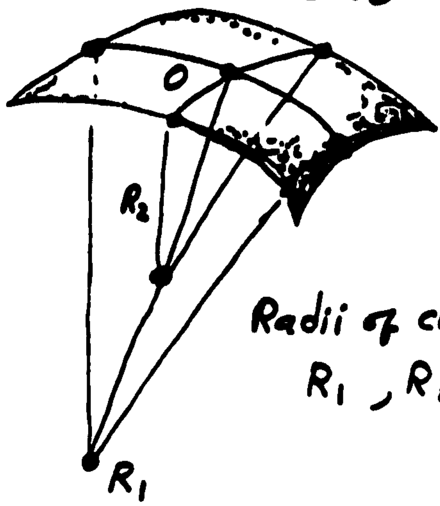

Radii of curvature R_1, R_2

$O(k^0)$

$$\boxed{RCS \approx \pi |R_1 R_2|}$$

Same result for convex or concave

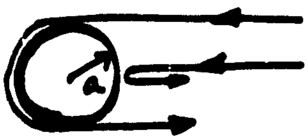

Creeping ← oscillation

GO ← πa^2

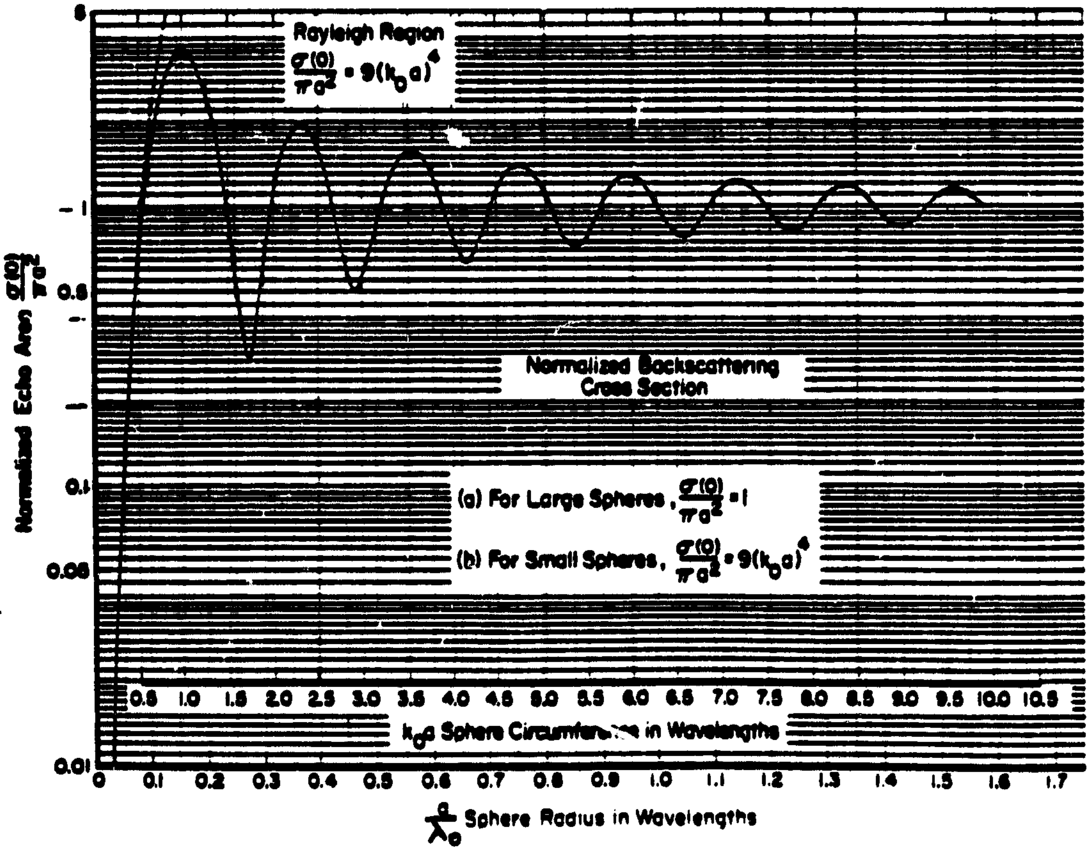

① For small $\frac{a}{\lambda} \to 0$ scattering $\propto k^4$ which explains blue sky.

②

a/λ	Creeping wave
0.5	±3dB
1	0.8dB
1.5	±0.5dB

RCS from Continuous Specular Points

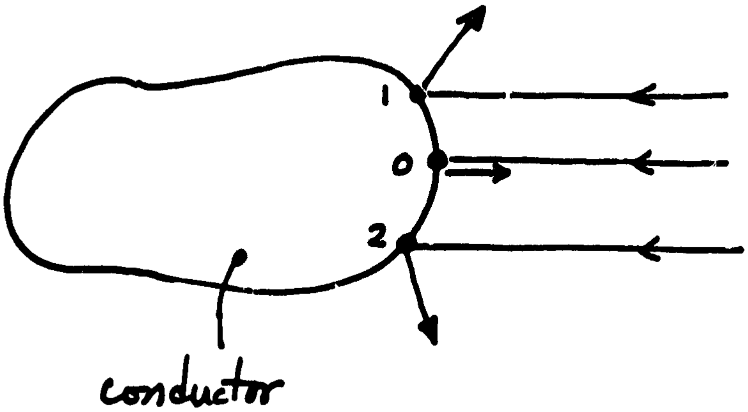

$$\boxed{RCS = \pi\,|R_1 R_2| \propto k^0}$$

Indep. of f

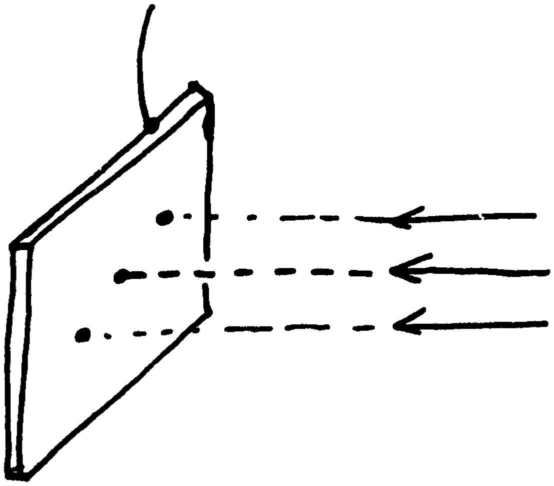

$$\boxed{RCS = \left(\frac{4\pi \cdot Area}{\lambda^2}\right)\cdot Area \propto k^2}$$

proportional to f^2

Gain factor of an aperture

RCS From Edge

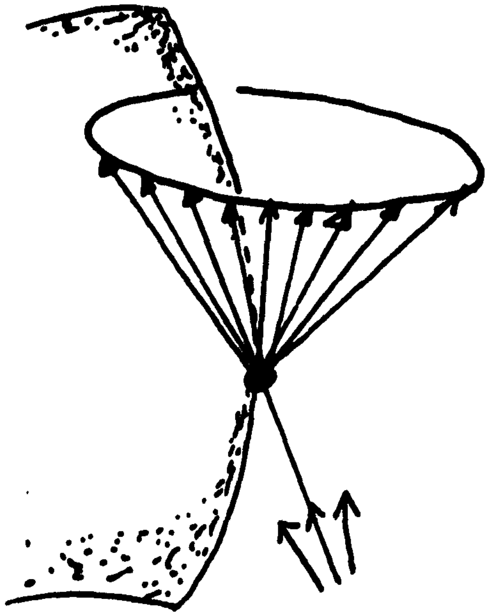

oblique incidence

$$RCS \approx 0$$

Vertical metal plate

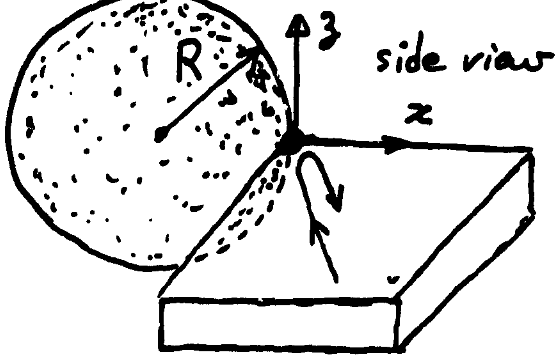

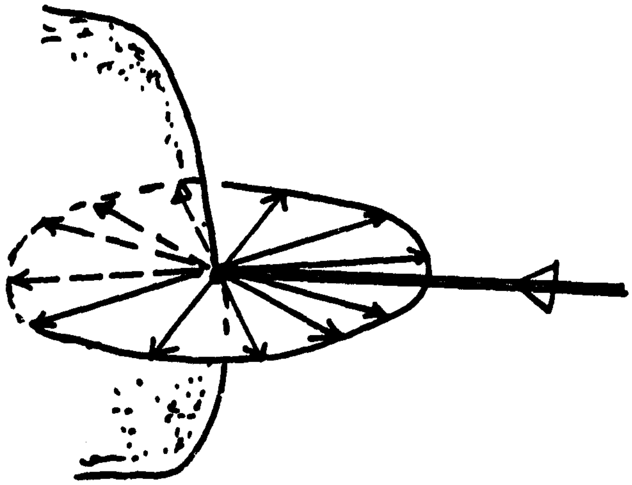

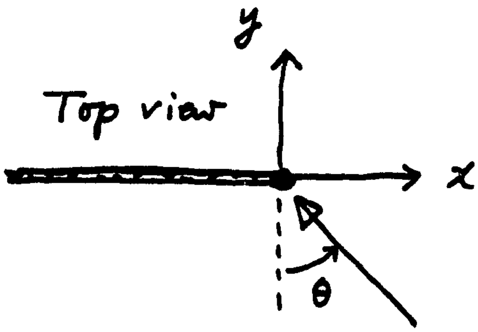

$$\boxed{RCS \approx \frac{R}{4k}\,\frac{\left(1 \pm \frac{1}{\sin\theta}\right)^2}{\sin\theta}}$$

decrease as f^{-1}
concave or convex, $\pm$ sign for different polarizations

RCS from Continuous Edge Points

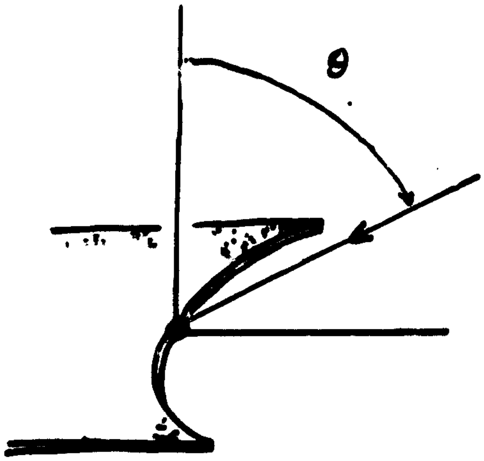

curved edge

$$\boxed{RCS \approx \frac{R}{4k}\left[\frac{\left(1 \pm \frac{1}{\sin\theta}\right)^2}{\sin\theta}\right]}$$

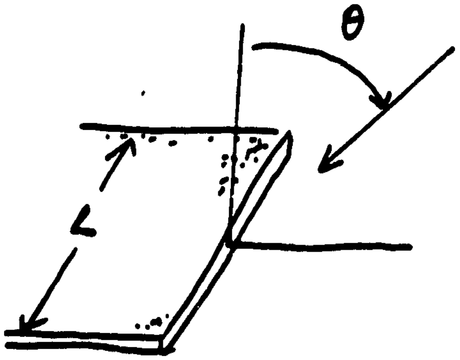

straight edge

$$\boxed{RCS \approx \frac{L^2}{4\pi}\left(1 \pm \frac{1}{\sin\theta_0}\right)^2}$$ indep of f

2 parallel edges

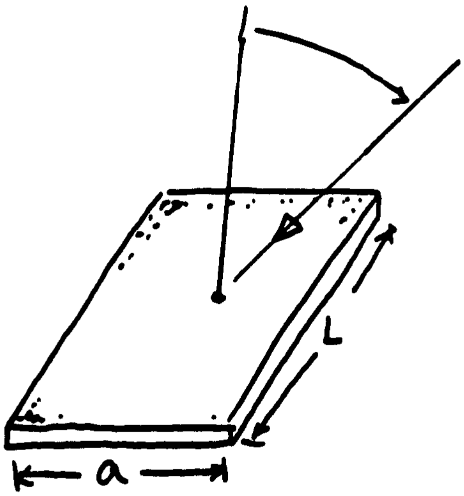

$$\boxed{RCS \approx \frac{L^2}{\pi}\left(\text{Array factor of spacing } a\right)^2}$$

, for $\theta \neq 0$

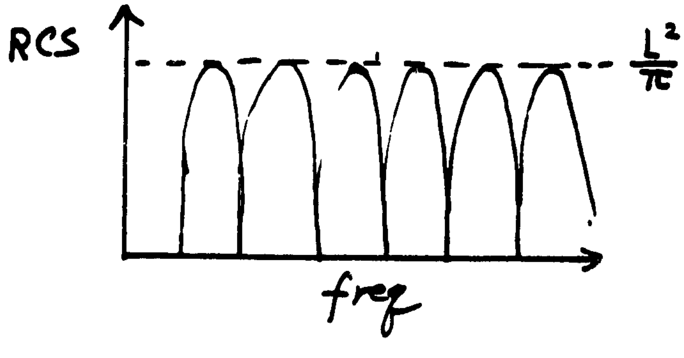

RCS of Open-ended Cylinder

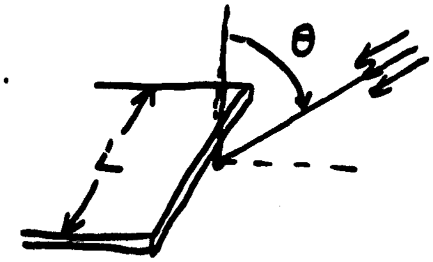

$$RCS \approx \frac{L^2}{4\pi}\left(1 \pm \frac{1}{\sin\theta}\right)^2$$

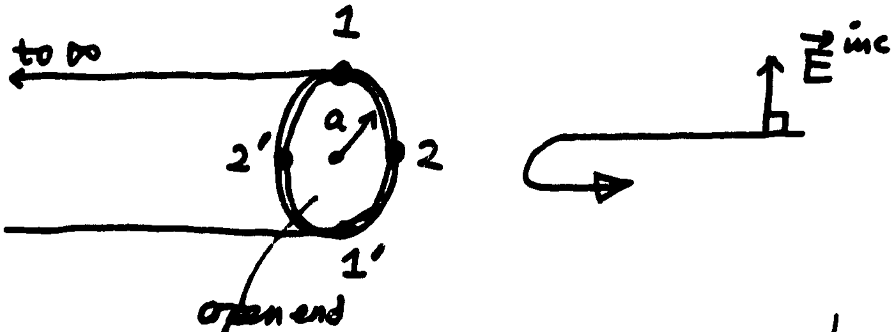

* At pts 1 and 1' : $\left(1 - \frac{1}{\sin 90^\circ}\right) = 0$ ($E_\perp$ edge)

At pts 2 and 2' : $\left(1 + \frac{1}{\sin 90^\circ}\right) = 2$ ($E_\parallel$ edge)

Average = 1

* $L = 2\pi a$

$$\text{RCS of cylinder} = \frac{(2\pi a)^2}{4\pi} \cdot 1^2 = \pi a^2$$

RCS From tip

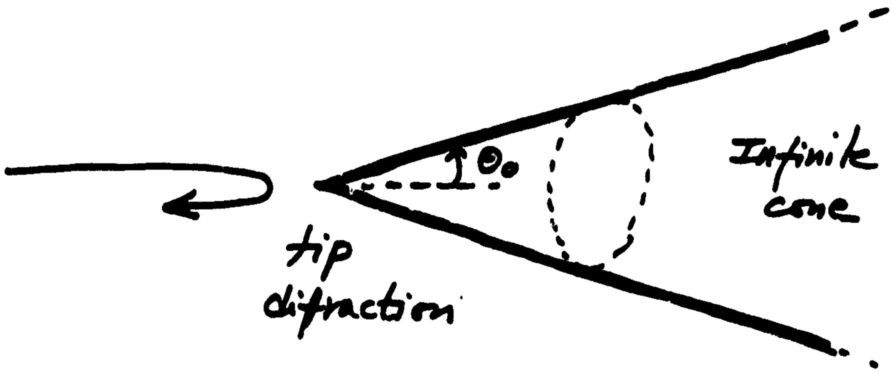

$$RCS \approx \frac{1}{k^2}\left(\frac{\pi}{4}\tan^4\theta_0\right)$$

Freq dependance

object	RCS
smooth 	k^0
edge	k^{-1}
tip	k^{-2}

Creeping Wave

Ray creeps on surface
for a distance t

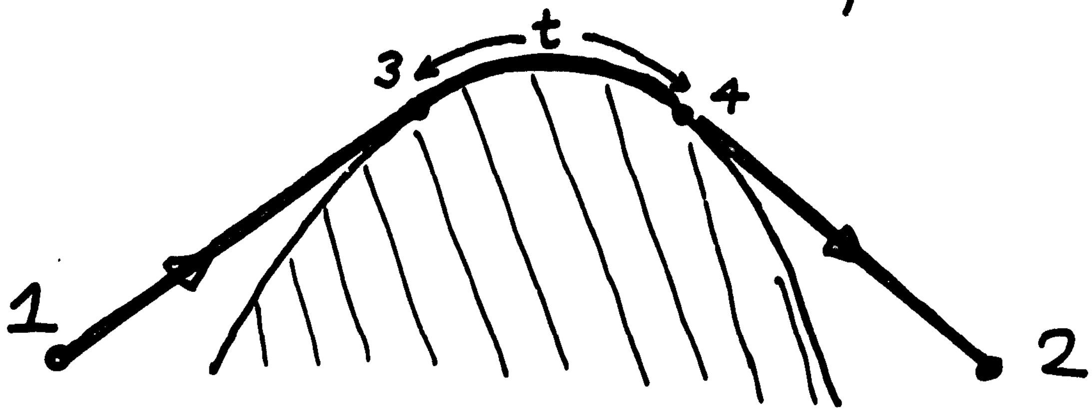

Creeping rays follow geodesics

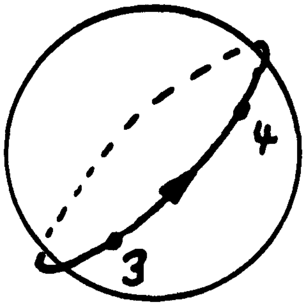

sphere: great circle

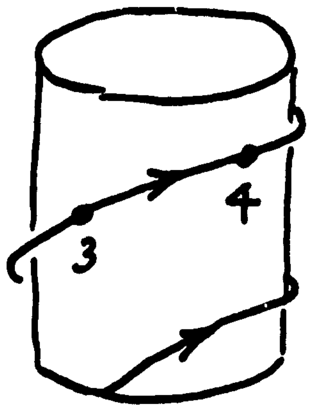

cylinder
helix

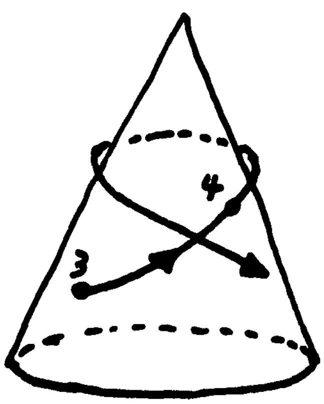

cone: straight line
on a developable surface

Difficulty with Geodesic

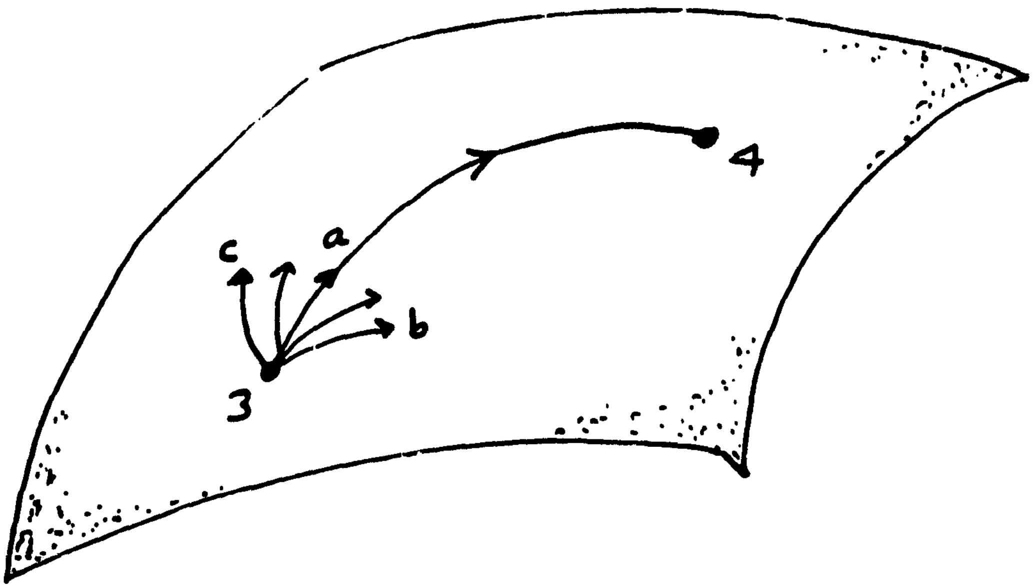

Given: Pts 3 & 4 on a general surface

No analytical way to determine the geodesic.
Must trail-and-error

Exponential Decay while creeping

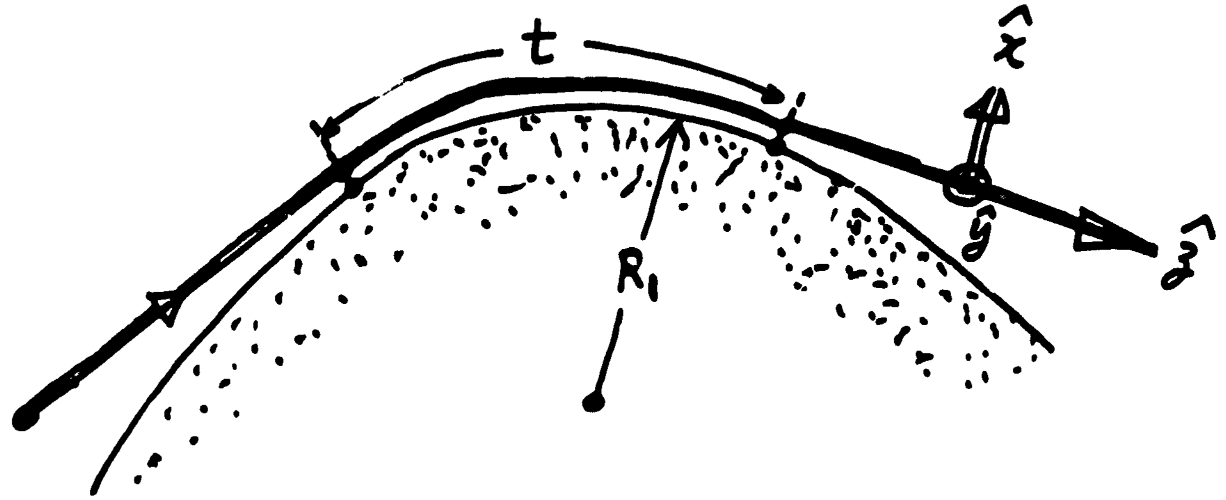

Hard polarization ($E_\perp = E_x$)

$$\boxed{\text{Field Decay} = e^{-1.29\left(\frac{R_1}{\lambda}\right)^{1/3}\left(\frac{t}{R_1}\right)}}$$

or $\boxed{11.2\left(\frac{R_1}{\lambda}\right)^{1/3}\left(\frac{t}{R_1}\right) \text{ dB}}$

Soft polarization ($E_\parallel = E_y$)

$$\boxed{\text{Field Decay} = e^{-2.97\left(\frac{R_1}{\lambda}\right)^{1/3}\left(\frac{t}{R_1}\right)}}$$

or $\boxed{25.8\left(\frac{R_1}{\lambda}\right)^{1/3}\left(\frac{t}{R_1}\right) \text{ dB}}$

Specular vs. Creeping

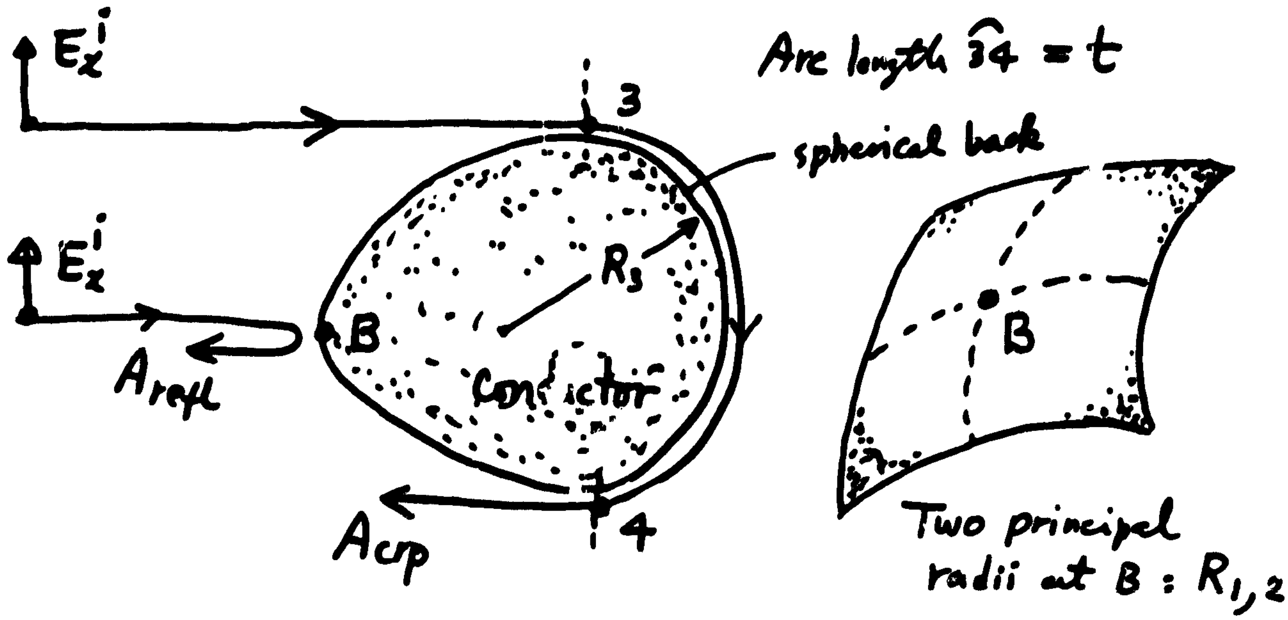

Incident $\vec{E}^i = \hat{x}\, e^{-jkz}$

Backscattered $\vec{E}^{bs} \approx \hat{x}\, \dfrac{e^{+jkz}}{x}\, [\, A_{refl} + A_{crp} \,]$

$$\left| A_{refl} \right| = \sqrt{\left(\frac{R_1}{2}\right)\left(\frac{R_2}{2}\right)}$$

$$\left| A_{crp} \right| = \left| \frac{R_3}{2} \right| \left(\frac{R_3}{\lambda} \right)^{1/3} 5 \cdot \left(\begin{matrix} \text{Hard Field} \\ \text{Decay P.9c} \end{matrix} \right)$$

Example next page

Sphere : Creeping Wave

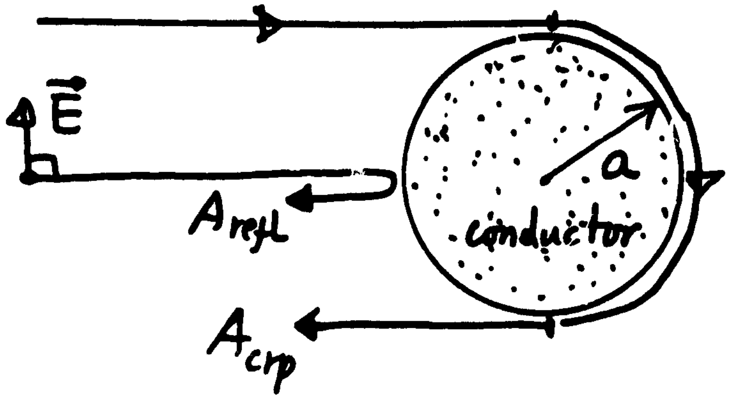

Assume $\frac{a}{\lambda} = 1$

$$\left|\frac{A_{crp}}{A_{refl}}\right| = 5 \cdot 1^{1/3} \cdot e^{-1.29 \cdot 1^{1/3} \cdot \pi} = 0.09 \;, -21\,dB$$

$$\text{RCS ripple} = \left(1 + \left|\frac{A_{crp}}{A_{reft}}\right|\right)^2 = (1.09)^2, \quad 0.7\,dB$$

Assume $\frac{a}{\lambda} = 5$

$$\left|\frac{A_{crp}}{A_{refl}}\right| = 0.008 \;, -42\,dB$$

$$\text{RCS ripple} = 0.07\,dB$$

RCS of Resonant structure

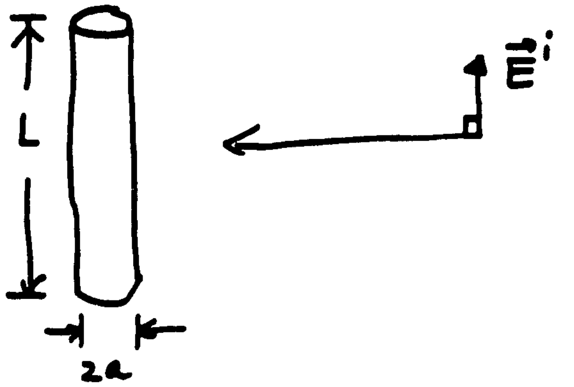

RCS has spikes when

$$L = n\frac{\lambda}{2}$$

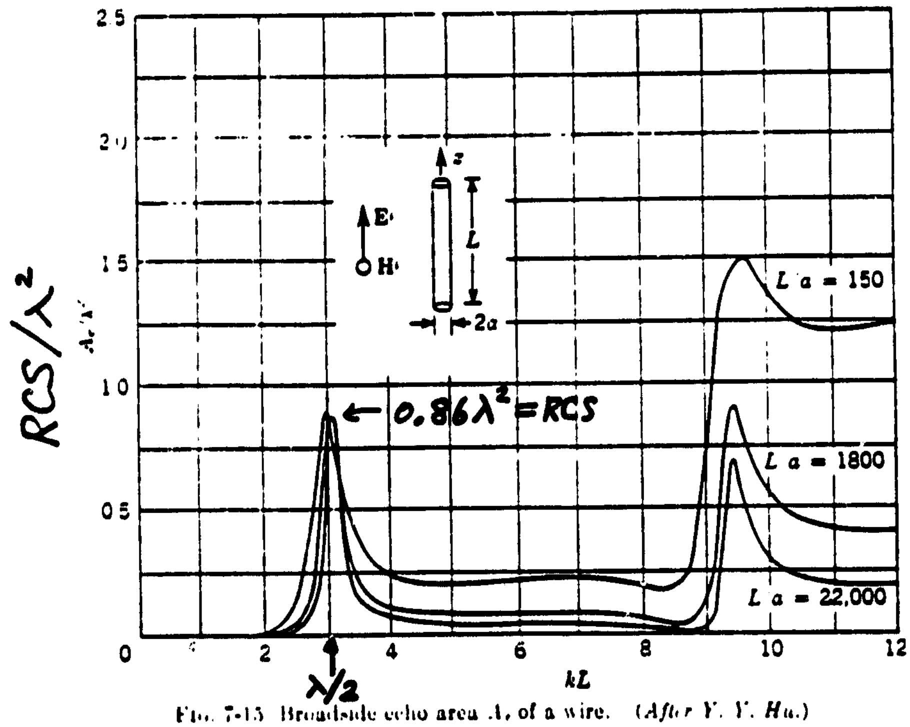

FIG. 7-13 Broadside echo area A_e of a wire. (*After Y. Y. Hu.*)

Multiple Diffraction

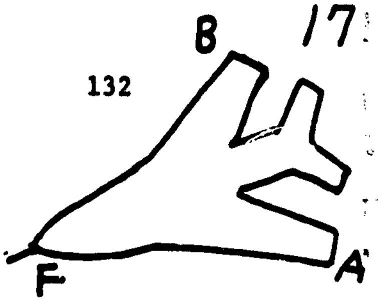

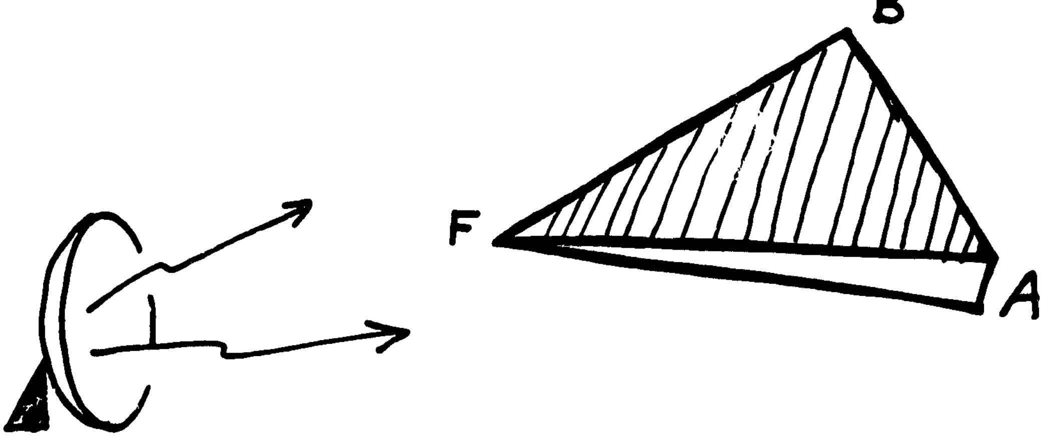

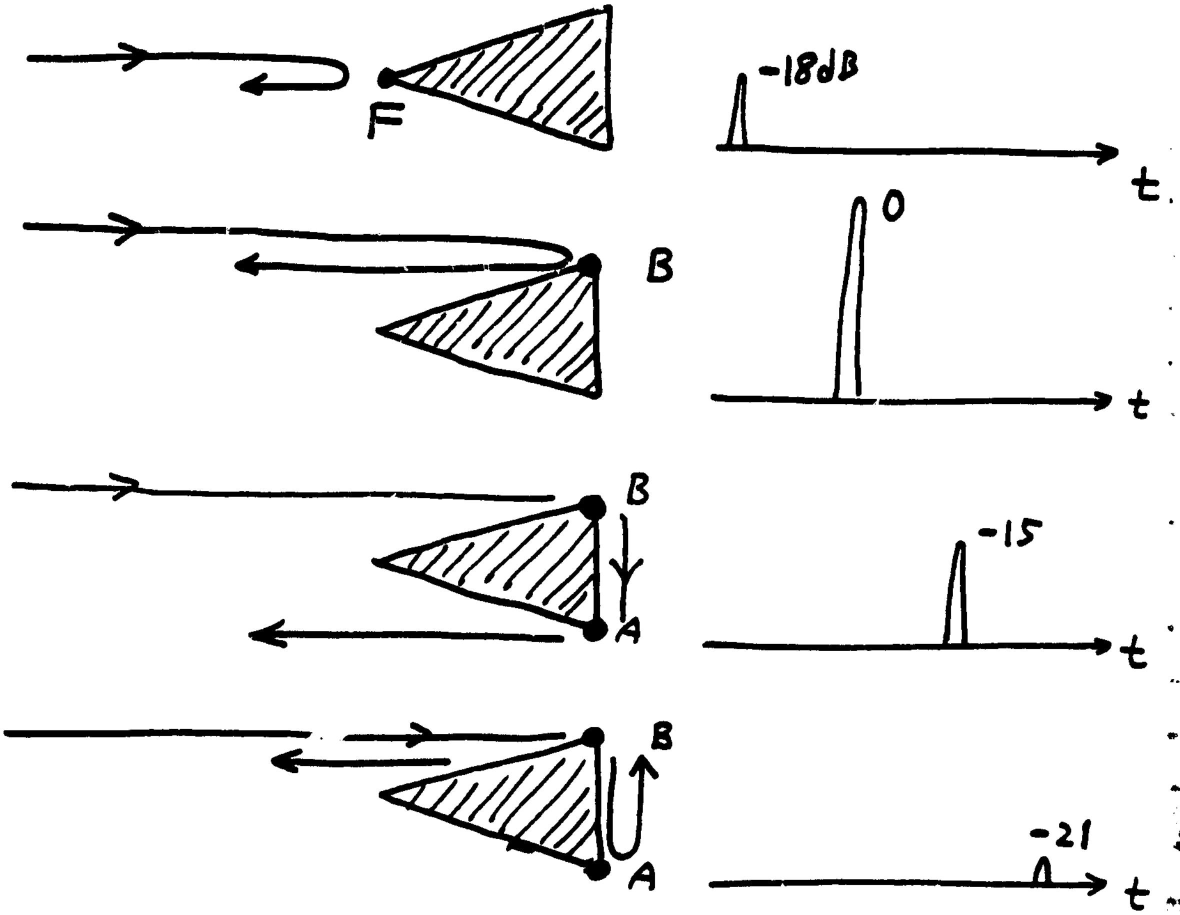

TARGET RCS CONTOURS

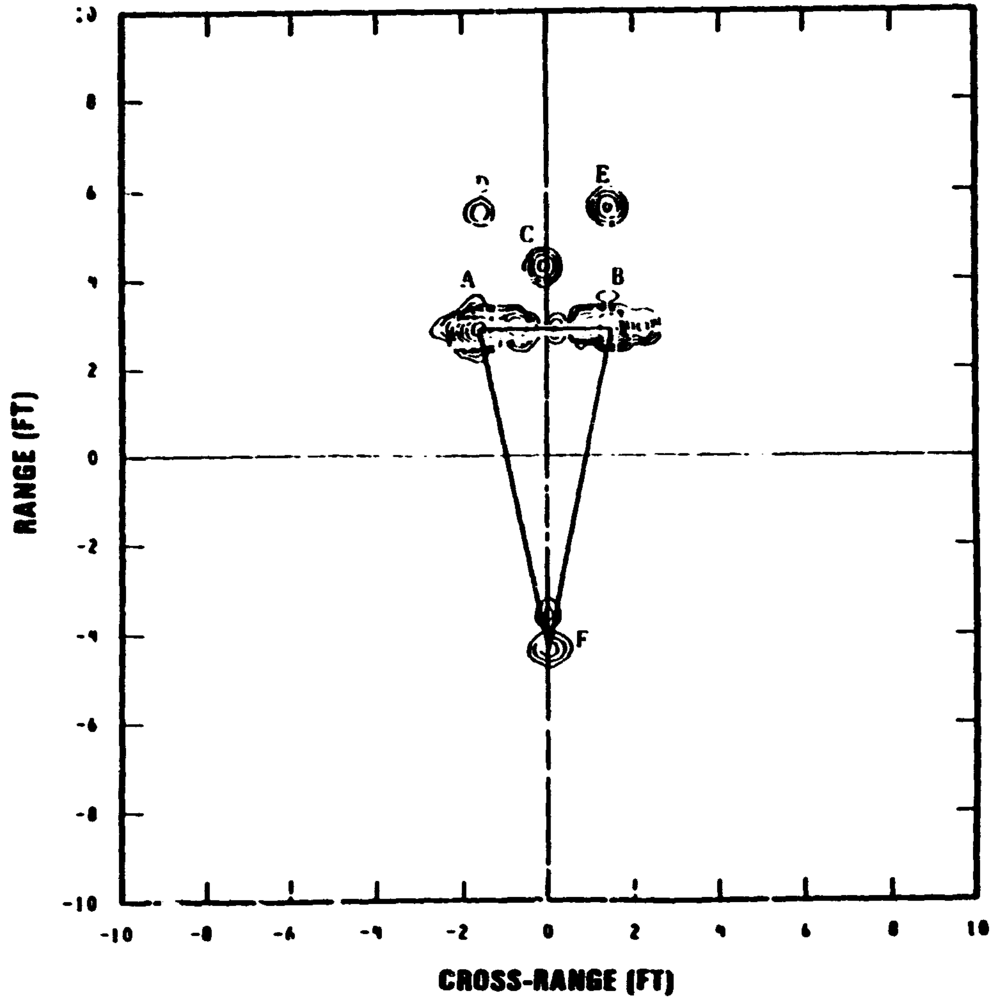

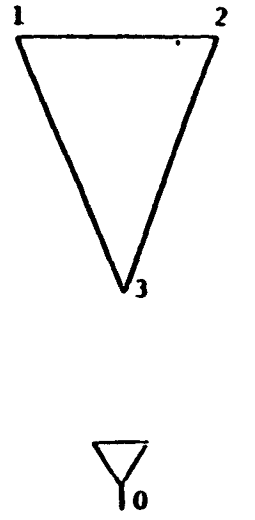

A = 0-1-0 (0 dB)
B = 0-2-0 (0 dB)
C = 0-1-2-0 (-15 dB)
D = 0-1-2-1-0 (-20 dB)
E = 0-2-1-2-0 (-15 dB)
F = 0-3-0 (-18 dB)

Dr. L. Yu

Complex Vector

134

Time convention $e^{j\omega t}$

$\vec{E}(t) = Re\{\vec{E}\, e^{j\omega t}\}$

phasor is a complex vector

(1) Examples :

- Far-field amplitude vector

$$\vec{A} = \hat{x}\,(1+j) + \hat{y}\; 2e^{j40^\circ}$$

- Unit LHCP

$$\vec{L} = \frac{1}{\sqrt{2}}\,(\hat{x}\, e^{j90^\circ} + \hat{y})$$

(2) Magnitude of complex vector:

$$|\vec{A}|^2 = \vec{A}\cdot\vec{A}^* = 2 + 4 = 6$$

$$|\vec{L}|^2 = \left(\frac{1}{\sqrt{2}}\right)^2 (1+1) = 1 \quad \leftarrow \text{unitary vector}$$

(3) Projection of $\vec{A}$ onto $\vec{L}$:

conjugate

$$\text{Component of } \vec{A} \text{ in the direction of } \vec{L} = \vec{A}\cdot\frac{\vec{L}^*}{|\vec{L}|}$$

$$= \frac{1}{\sqrt{2}}\left((1+j)(j)^* + 2e^{j40^\circ}(1)^* \right)$$

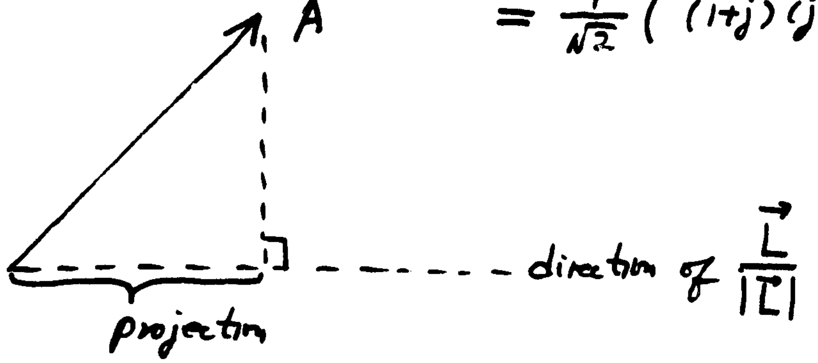

Plane Wave

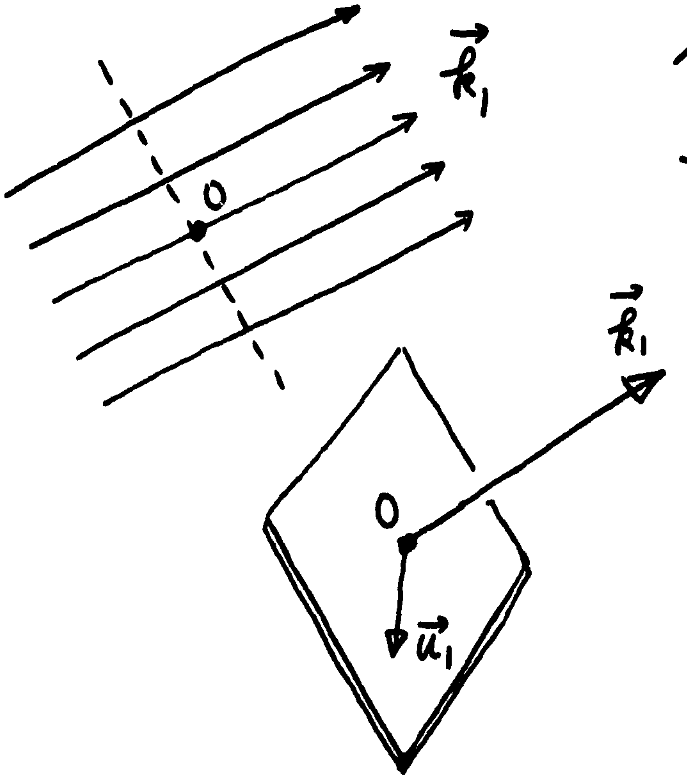

Amplitude : C

State : $(\vec{k}_1, \vec{u}_1)$

direction polarization

$$\begin{bmatrix} \vec{E}(\vec{r}) \\ \vec{H}(r) \end{bmatrix} = C \begin{bmatrix} \sqrt{Z}\,\vec{u}_1 \\ \sqrt{Y}\,\hat{k}_1 \times \vec{u}_1 \end{bmatrix} e^{-j\vec{k}_1 \cdot \vec{r}} \tag{52}$$

where

$\vec{k}_1$ = wave vector with magnitude $k = \omega\sqrt{\mu\varepsilon}$ and pointing in the direction of propagation of F^i

$Z = Y^{-1} = \sqrt{\mu/\varepsilon} \doteq 120\pi$ ohm

$\vec{u}_1$ = a unitary vector which describes the polarization of F^i and is orthogonal to $\vec{k}_1$.

C = amplitude of F^i in $(\text{watt})^{1/2}\ m^{-1}$

We say that F^i is in state $(\vec{k}_1, \vec{u}_1)$.

Plane Wave Example

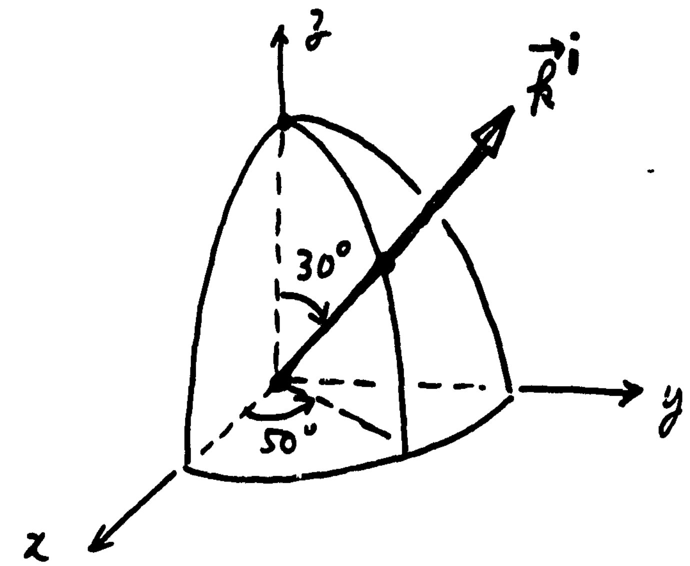

plane wave propagating into

$(\theta = 30°,\ \phi = 50°)$

$$\vec{E}^i(\vec{r}) = [\hat{\theta}^i A + \hat{\phi}^i B]\sqrt{Z}\, e^{-j\vec{k}^i\cdot\vec{r}}$$

$$\vec{k}^i = \left(\frac{\omega}{c}\right)\left[\hat{x}\sin 30°\cos 50° + \hat{y}\sin 30°\sin 50° + \hat{z}\cos 50°\right]$$

$$\hat{\theta}^i = (\hat{x}\cos 50° + \hat{y}\sin 50°)\cos 30° - \hat{z}\sin 30° = \hat{\phi}^i \times \hat{k}^i$$

$$\hat{\phi}^i = -\hat{x}\sin 50° + \hat{y}\cos 50°$$

If $\begin{cases} A \equiv 0 \\ B \equiv 0 \end{cases}$, then the field is $\begin{matrix} TE\ (E_\perp) \\ TM\ (E_\parallel) \end{matrix}$

$\boxed{\text{Polarization}}$

Antenna Handbook
ch. 1 Sec 5

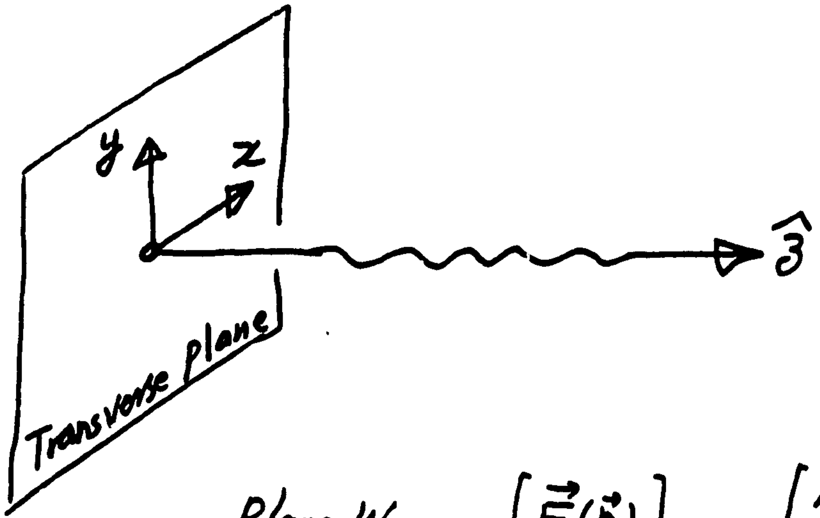

Plane Wave $\begin{bmatrix} \vec{E}(\vec{r}) \\ \vec{H}(\vec{r}) \end{bmatrix} = c \begin{bmatrix} \sqrt{Z}\ \vec{u} \\ \sqrt{Y}\ \hat{z} \times \vec{u} \end{bmatrix} e^{-jkz}$

polarization vector $\boxed{\vec{u} = \hat{x}\, a_x + \hat{y}\, a_y}$

complex

(1) $\boxed{\text{Linar pol}}$ a_x and a_y are in phase

$a_x = 2e^{j35°}$, $a_y = 3e^{j35°}$

(2) $\boxed{\text{Circular pol}}$ $|a_x| = |a_y|$ and 90° out of phase

$a_x = 2e^{j35°}$, $a_y = 2e^{j(35° \pm 90°)}$

(3) $\boxed{\text{Elliptical pol.}}$ None of the above

$\vec{E}$ vector of different polarizations

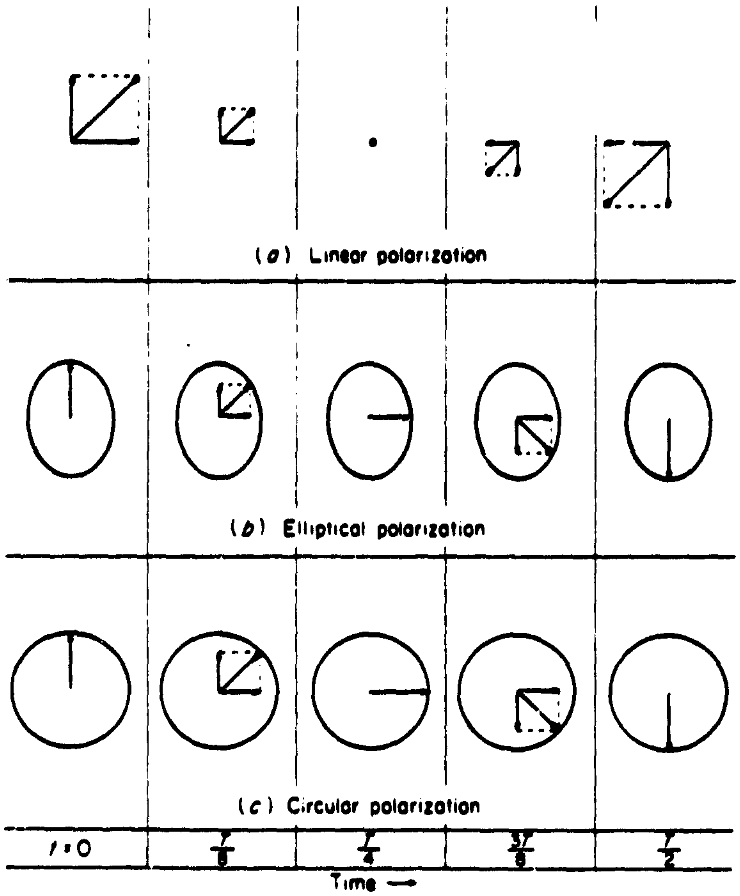

Figure 5-4. Linear, elliptical and circular polarization. (Jordan + Balmain)

$$T = \frac{1}{f} = \text{period}$$

Far Field

Antenna Handbook
Ch. 1 Sec 6 + 7 139

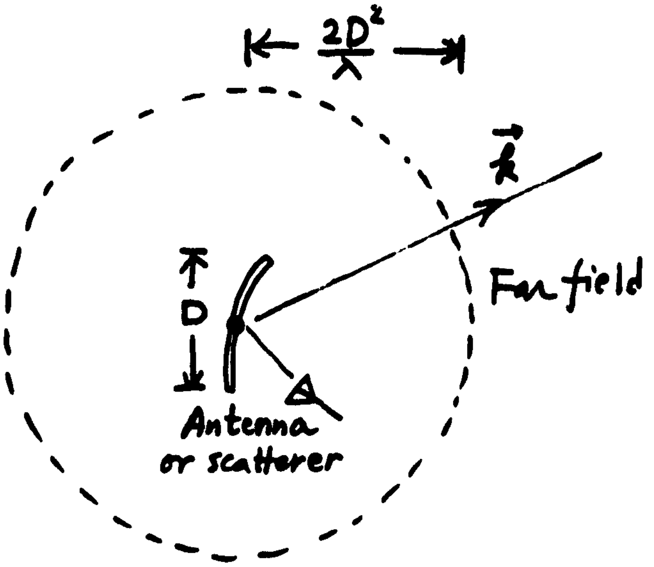

$$\begin{bmatrix} \vec{E}(\vec{r}) \\ \vec{H}(\vec{r}) \end{bmatrix} = \begin{bmatrix} \sqrt{Z}\,\vec{A}(\vec{k}) \\ \sqrt{Y}\,\hat{k}\times\vec{A}(\vec{k}) \end{bmatrix} \frac{e^{-jkr}}{r}$$

where : $Z = Y^{-1} = 120\pi$ ohm = free space impedance $= \sqrt{\mu_0/\epsilon_0}$

$\vec{r} = (r, \theta, \phi)$ = far-field observation point (in meter)

$\vec{k} = (k, \theta, \phi)$ = wave vector (in m^{-1})

$\vec{A}(\vec{k})$ = amplitude vector (in watt$^{1/2}$), a complex vector

Characterisics of Far Field

(1) spherical wave

(2) Impedance relation $|\vec{E}|/|\vec{H}| = 120\pi$ ohm

(3) Triplet : $\vec{E} \perp \vec{H} \perp \vec{k}$

} locally plane wave

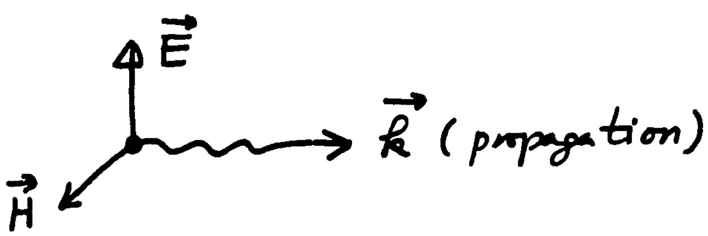

Far Field Amplitude Vector

* $\vec{A}(\vec{k})$ in watt$^{1/2}$

* Radiation intensity (in all pol)

$$= |\vec{A}(\vec{k})|^2 \quad \text{watts/steradian}$$

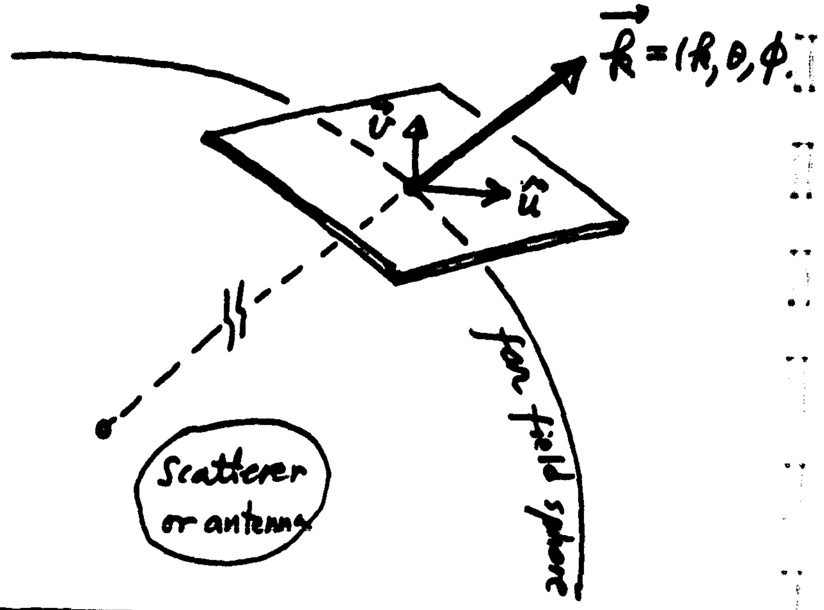

Decomposition of $\vec{A}(\vec{k})$

(1) General
$$\boxed{\vec{A}(\vec{k}) = A(\vec{k}, \vec{u})\, \vec{u} + A(k, \vec{v})\, \vec{v}}$$

where: $A(k, \vec{u}) = \vec{A}(\vec{k}) \cdot \vec{u}^*$

$(\vec{u}, \vec{v})$ = two unitary vectors

(2) Spherical:
$$\boxed{\vec{A}(\vec{k}) = A_\theta(\vec{k})\, \hat{\theta} + A_\phi(\vec{k})\, \hat{\phi}}$$

(3) Ref-pol and X-pol:
$$\boxed{\vec{A}(\vec{k}) = A(\vec{k}, \vec{R})\, \vec{R} + A(\vec{k}, \vec{C})\, \vec{C}}$$

see section 9 for $\vec{R}$ and $\vec{C}$ definition

RCS Definition

P.18 and P.21
Chapter 2, Ant Handbook

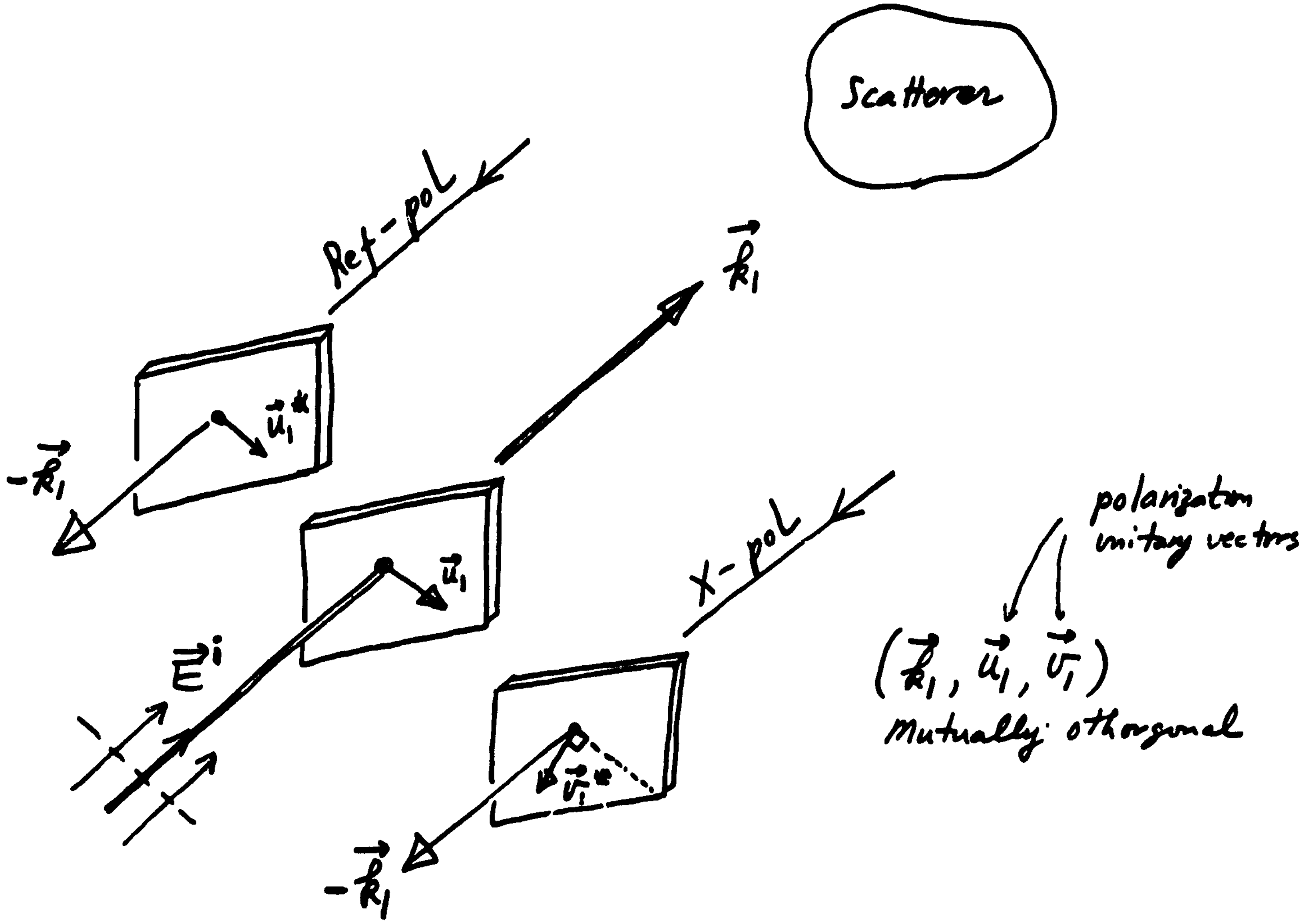

Incident $\vec{E}^i = \sqrt{Z}\, \vec{u}_1 e^{-j\vec{k}_1 \cdot \vec{r}}$, $Z = 120\pi$ ohm

Backscattered $\vec{E}^{bs} \sim \sqrt{Z}\, \vec{A}(-\vec{k}_1) \dfrac{e^{-jkr}}{r}$, $r \to \infty$

RCS of Ref pol $= 4\pi \left| \vec{A}(-\vec{k}_1) \cdot \vec{u}_1 \right|^2$ (A)

RCS of x-pol $= 4\pi \left| \vec{A}(-\vec{k}_1) \cdot \vec{v}_1 \right|^2$

no conjugate because $(\vec{u}_1^*)^*$

Physical Optics Scattering

$$\vec{J}_{po} = \begin{cases} 2\hat{N}\times\vec{H}^i, & \text{lit} \\ 0, & \text{shadow} \end{cases}$$

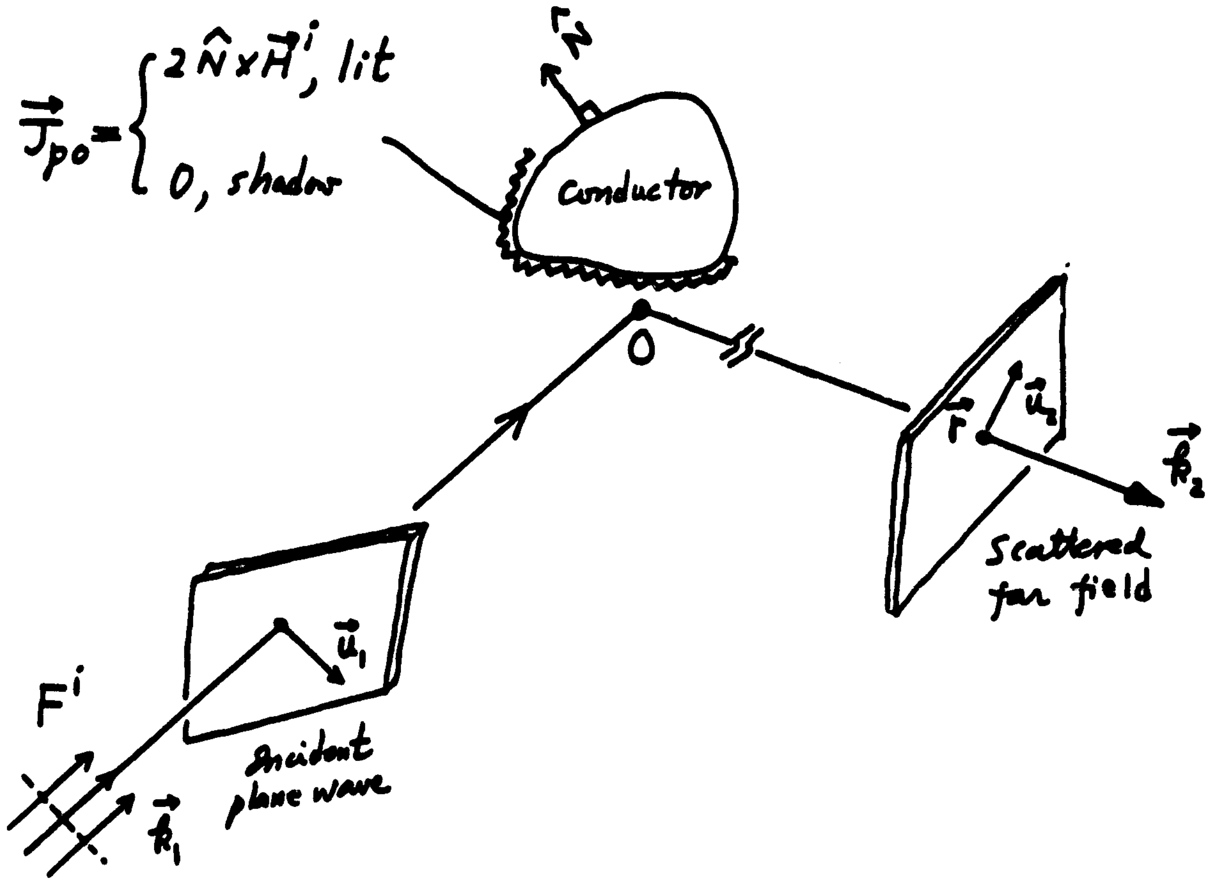

Incident $\vec{E}^i = \sqrt{Z}\,\vec{u}_1\, e^{-j\vec{k}_1\cdot\vec{r}}$, $Z = 120\pi$, $\vec{u}_1$ = unitary vector

Scattered far field :

$$\vec{E}^s \sim \sqrt{Z}\,\vec{A}(\vec{k}_2)\,\frac{e^{-jkr}}{r}$$

where

$$\vec{A}(\vec{k}_2)\cdot\vec{u}_2^{\,*} = \frac{jk}{2\pi}\left[\vec{u}_2^{\,*}\times(\hat{k}_1\times\vec{u}_1)\right]\cdot\iint_{lit}\hat{N}\,e^{j(\vec{k}_2-\vec{k}_1)\cdot\vec{r}\,'}\,ds' \qquad (B)$$

Example 1 of RCS by PO

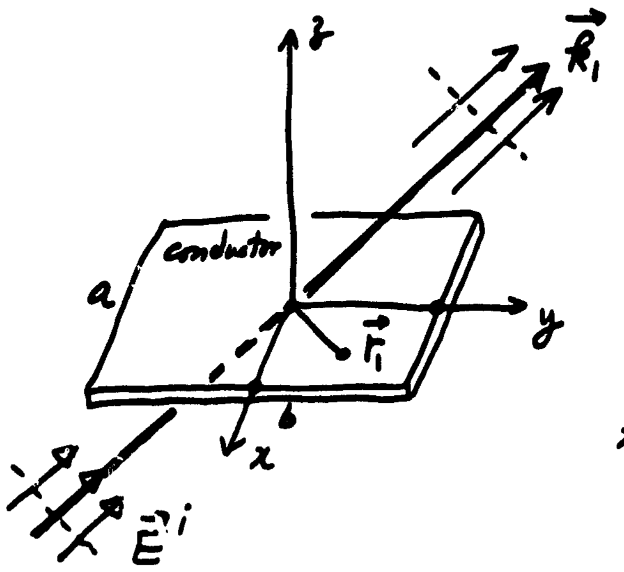

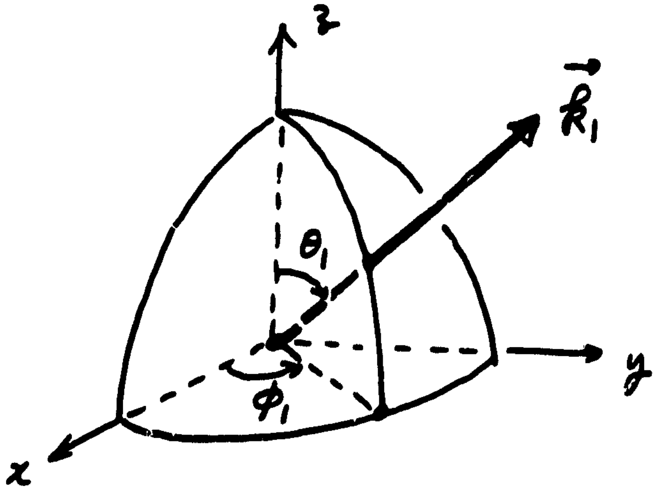

TE : $\vec{E}^i = \sqrt{2}\,\hat{\phi}_1 e^{-j\vec{k}_1\cdot\vec{r}}$

Eq. (B), p.27

$$\hat{u}_1 = \hat{\phi}_1 = -\sin\phi_1\,\hat{x} + \cos\phi_1\,\hat{y}$$

$$\hat{u}_2 = (\hat{u}_1)^*$$

$$\hat{k}_1 = \hat{r} = \sin\theta_1(\hat{x}\cos\phi_1 + \hat{y}\sin\phi_1) + \hat{z}\cos\theta_1$$

$$\hat{k}_2 = -\hat{k}_1 \quad , \quad \hat{N} = -\hat{z}$$

$$\vec{A}(-\hat{k}_1)\cdot\hat{\phi}_1 = \frac{jk}{2\pi}(-\cos\theta_1)\int_{-a/2}^{a/2}dx'\int_{-b/2}^{b/2}dy'\; e^{-j2k\sin\theta_1(x'\cos\phi_1 + y'\sin\phi_1)}$$

Eq (A), p. 26

$$RCS = \frac{1}{\pi}\left[kab\cos\theta_1 \frac{\sin\alpha}{\alpha}\frac{\sin\beta}{\beta}\right]^2$$

$$\alpha = ka\sin\theta_1\cos\phi_1 \quad , \quad \beta = kb\sin\theta_1\sin\phi_1$$

Example 2 RCS by PO

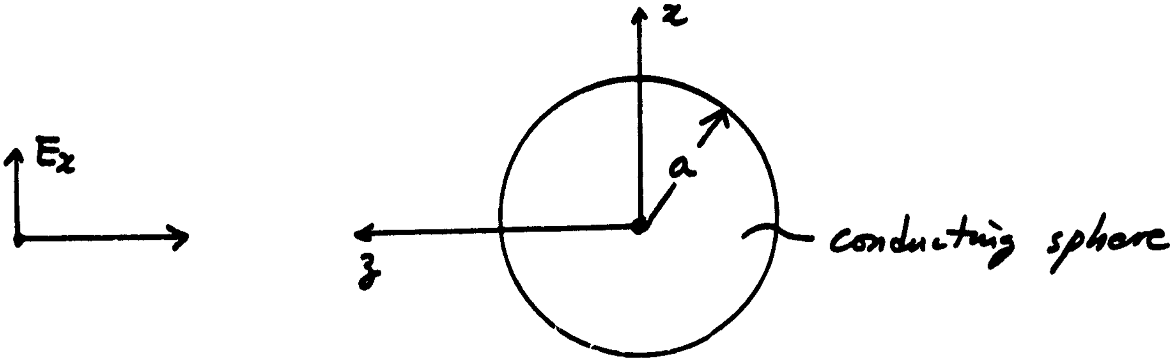

$$\vec{E}^i = \sqrt{Z}\, \hat{x}\, e^{jkz}$$

Eq (B), P.27

$$\hat{u}_1 = \hat{u}_2^* = \hat{x}$$
$$\hat{k}_1 = -\hat{k}_2 = -\hat{z}$$
$$\hat{N} = \hat{n}' = \sin\theta' (\hat{x}\cos\phi' + \hat{y}\sin\phi') + \hat{z}\cos\theta'$$
$$ds' = a^2 \sin\theta'\, d\theta'\, d\phi'$$
$$\int_0^{j2ka} \alpha e^{\alpha} d\alpha = [\, 1 - e^{j2ka}(1 - j2ka)]$$
$$\approx j2ka\, e^{j2ka}, \quad \text{for } ka \gg 1$$

Eq (A), P.26

$$RCS \approx \pi a^2$$

EVALUATION SHEET FOR RCS LECTURE NO. 1

(1) Lecture level:

☐ too elementary ☐ too high ☐ about right

(2) Topics that I like in today's lecture:

☐ overview ☐ physical optics ☐ both

(3) For future lectures, I'd like to see the following topics:

☐ Modes in waveguides.

☐ Scattering by open-ended cylinder: UI approach.

☐ Scattering by open-ended cylinder: OSU approach.

☐ Introduction to GTD.

☐ Usage of UI and OSU computer codes developed under current grants.

☐ Others (specify).

(4) Comments:

APPENDIX C

SIMPLE VERSION OF CORRUGATED GUIDE: CIRCULAR GUIDE COATED WITH LOSSY MAGNETIC MATERIAL

This set of viewgraphs was presented at the AP meeting in Vancouver, B.C., in June 1985.

SIMPLE VERSION OF CORRUGATED GUIDE: CIRCULAR GUIDE COATED WITH LOSSY MAGNETIC MATERIAL

C.S. Lee, S.L. Chuang, and S.W. Lee

University of Illinois

1. Objective

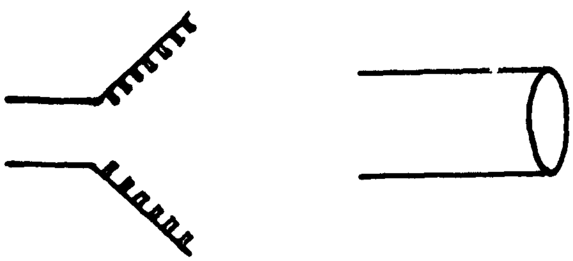

2. Numerical Results

3. Summary

To produce a ***CIRCULARLY POLARIZED*** (CP) Radiation

Corrugated waveguide:

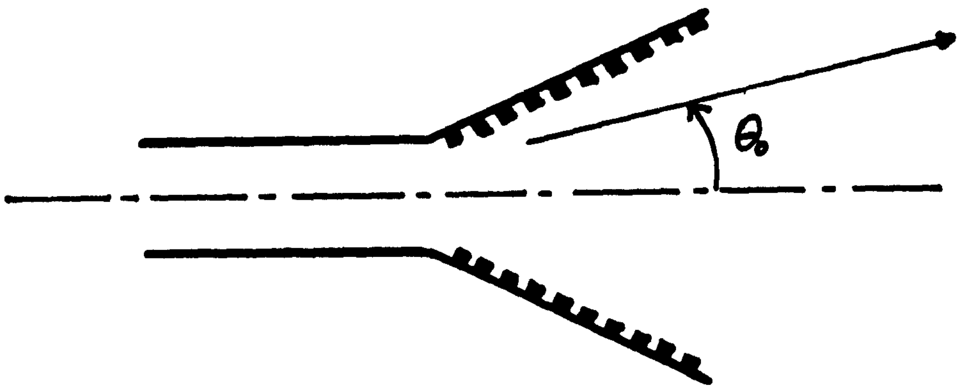

- Good CP for $\theta_o \lesssim 60^\circ$
- But expensive and heavy.

An *ALTERNATIVE* to the Corrugated Waveguide

Boundary conditions for CP radiation:

$$E_\phi = 0 \; ; \qquad H_\phi = 0 \,\Big|_{\text{at boundary}}$$

* Approximately satisfied by the corrugated waveguide.

* Can be satisfied by a ***COATED CIRCULAR GUIDE***

if

1) The coating material is sufficiently ***Lossy,***

2) The material is ***Magnetic.***

E_ϕ, H_ϕ (HE_{11}) at the *INTERFACE* in the guide coated with a *LOSSLESS DIELECTRIC*

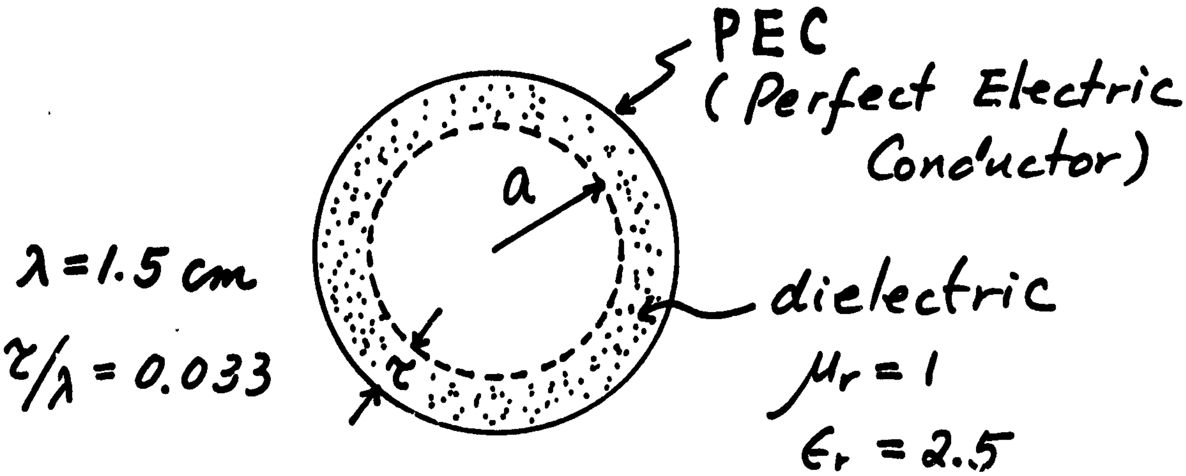

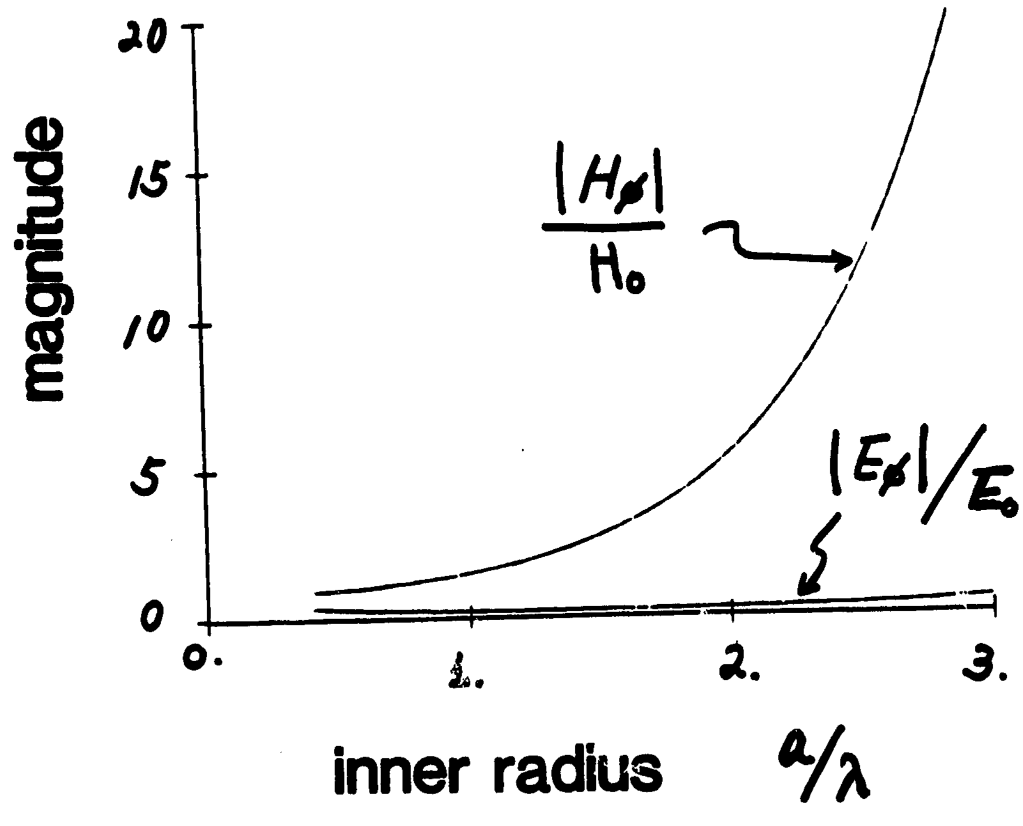

E_ϕ, H_ϕ (HE_{11}) at the ***INTERFACE*** in the guide coated with a ***LOSSY MAGNETIC MATERIAL***

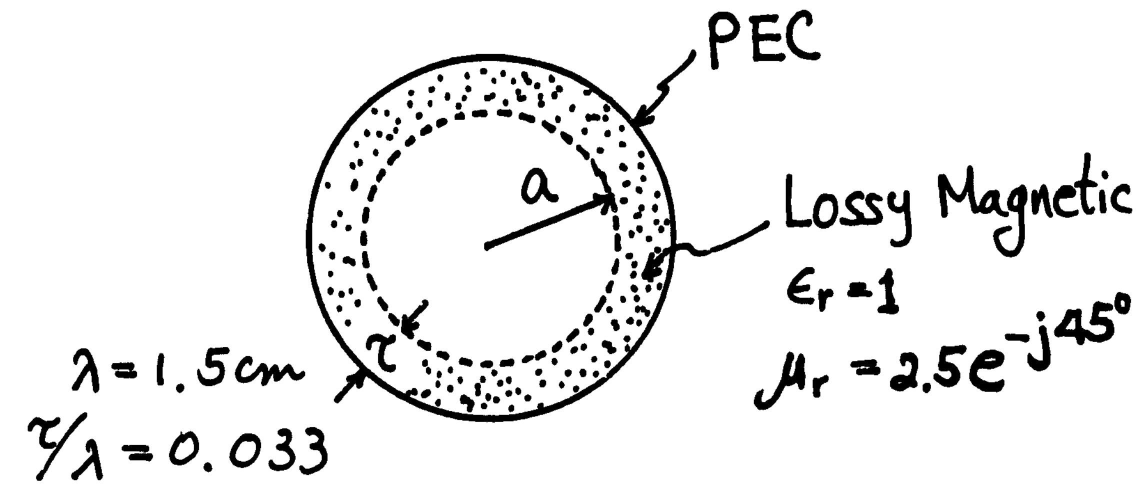

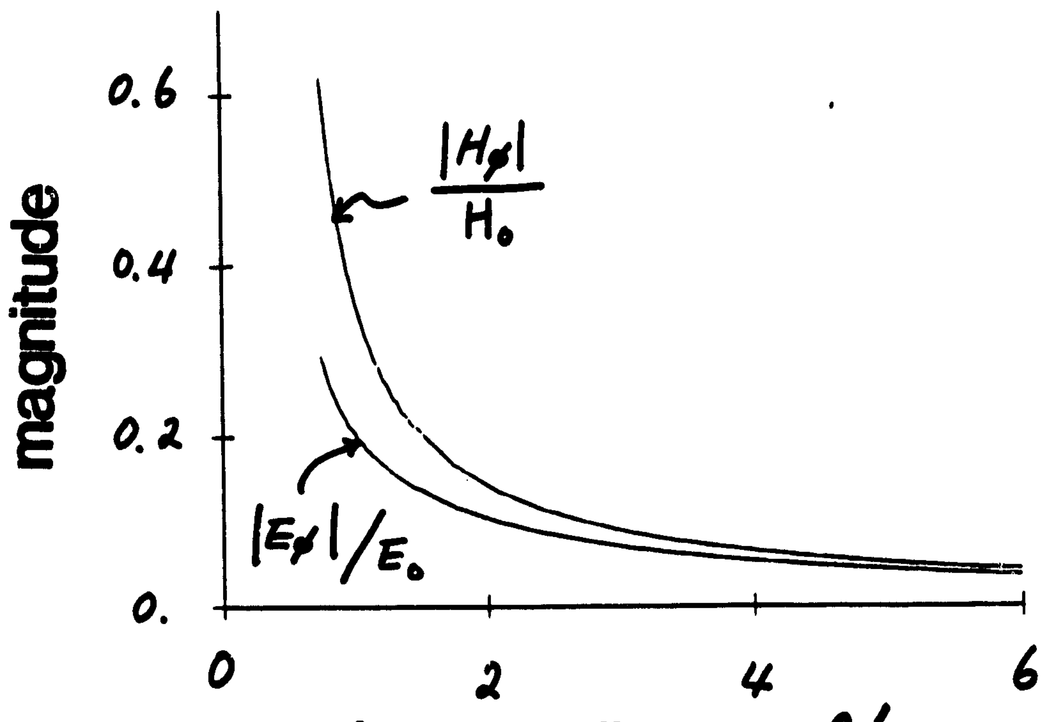

FIELD DISTRIBUTION

Empty guide

$E_\phi = 0$

$H_\phi \neq 0$

at boundary

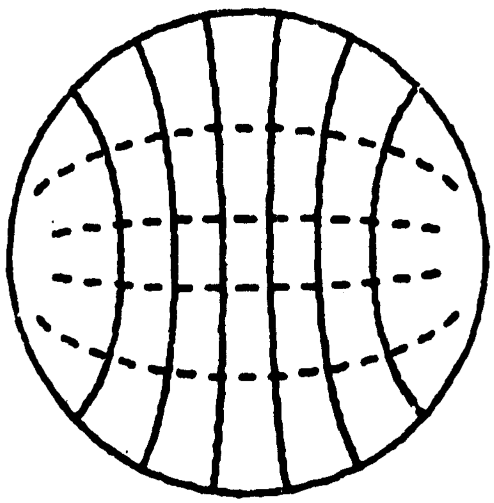

TE_{11}

Coated guide

$E_\phi = 0$

$H_\phi = 0$

at boundary

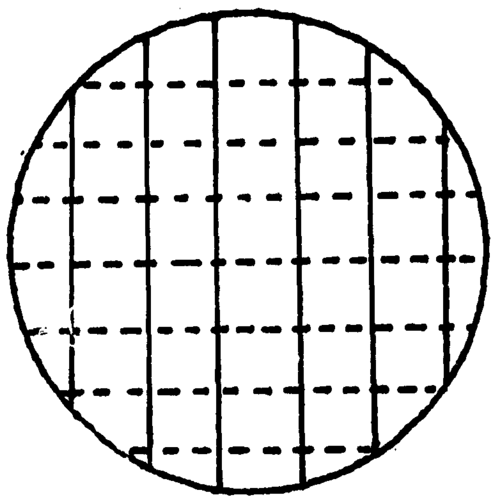

HE_{11}

RADIATION PATTERN

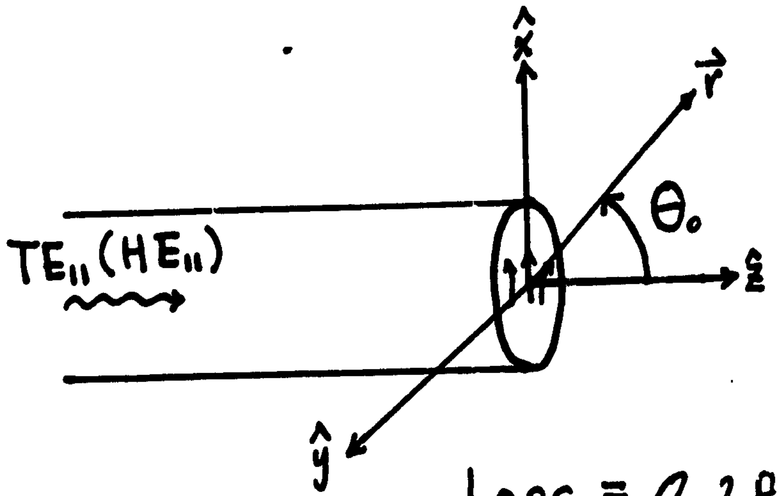

—— E plane (x–z plane)

- - - - - H plane (y–z plane)

Loss = 0.284 dB/m

$a/\lambda = 6.7$

$\tau/\lambda = 0.033$

$\epsilon_r = 1$

$\mu_r = 2.5e^{-j45}$

$\lambda = 1.5$ cm

Coated

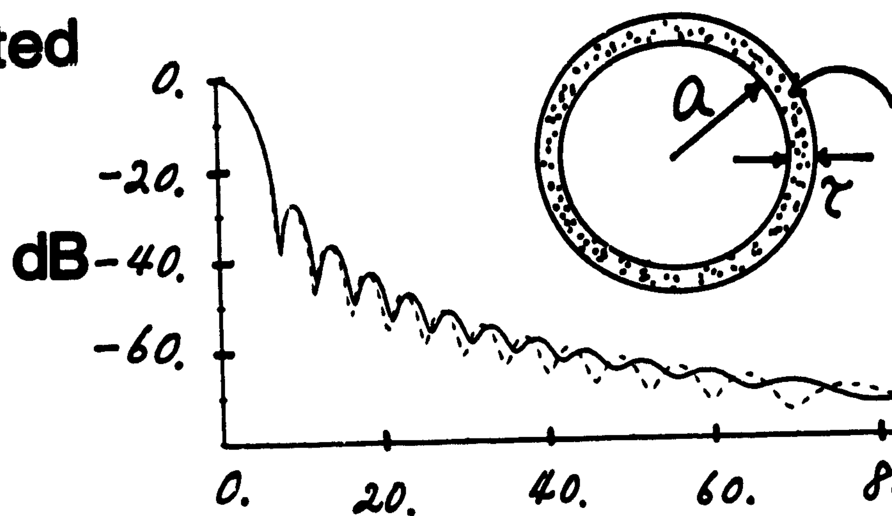

Empty

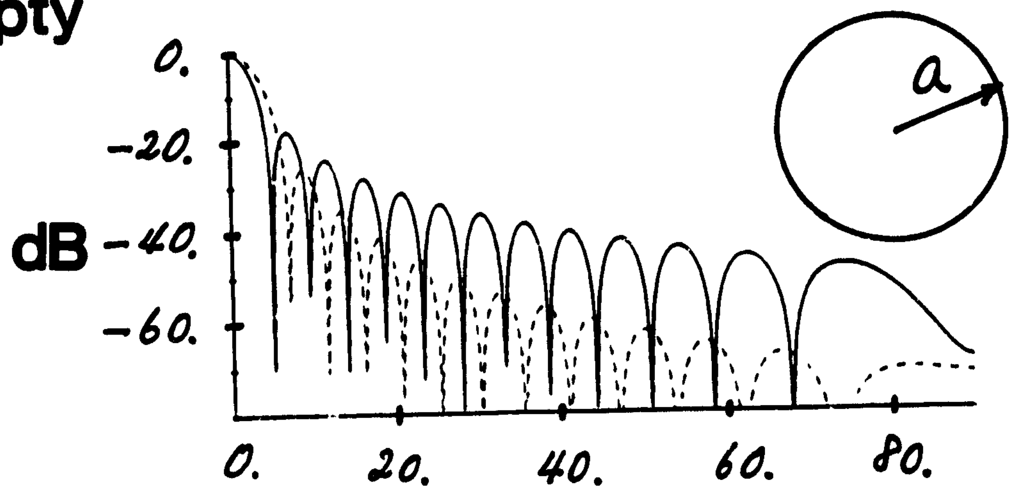

$a/\lambda = 6.7$

θ_o, angle (°)

RADIATION PATTERN

· *With Smaller value of* a/λ

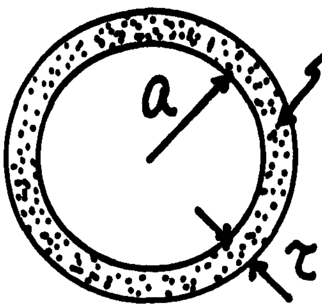

$\begin{cases} \epsilon_r = 1 \\ \mu_r = 2.5\, e^{-j45^\circ} \end{cases}$

$\tau/\lambda = 0.033$, $\lambda = 1.5$ cm

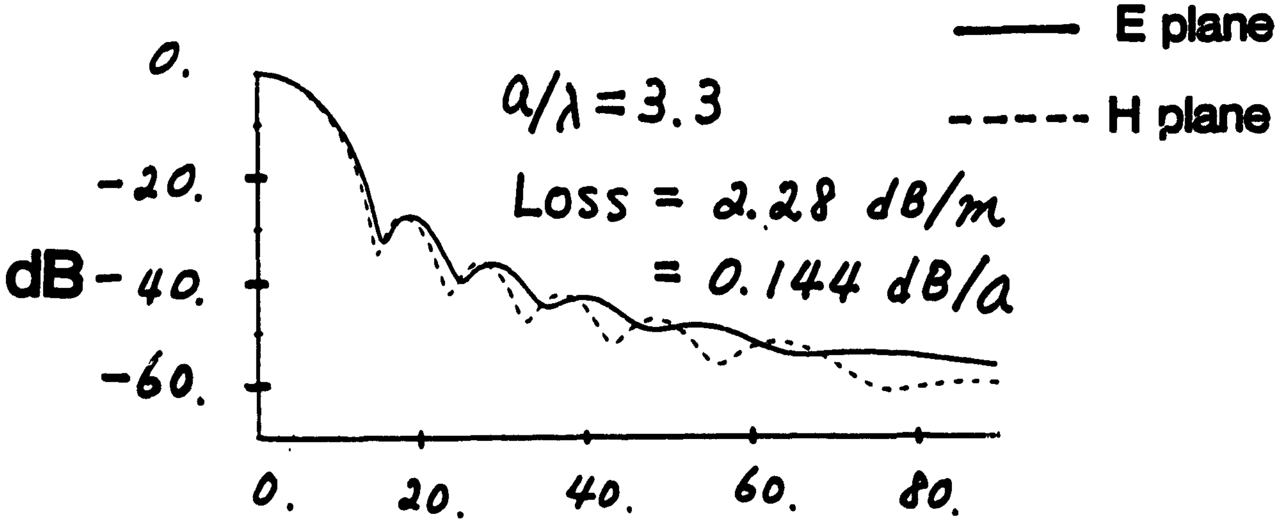

$a/\lambda = 3.3$

Loss = 2.28 dB/m
= 0.144 dB/a

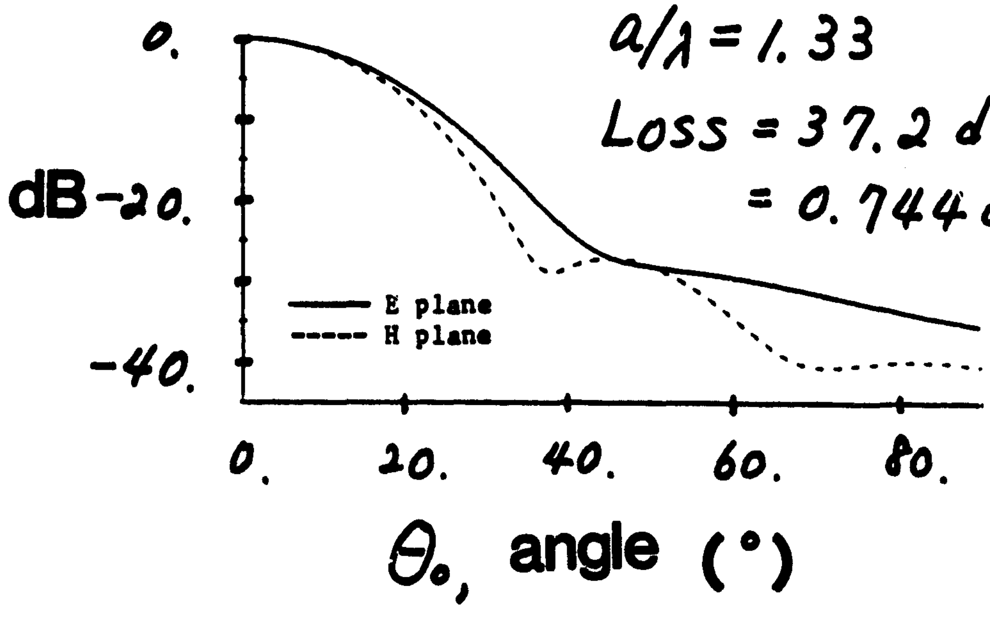

$a/\lambda = 1.33$

Loss = 37.2 dB/m
= 0.744 dB/a

ATTENUATION vs a/λ

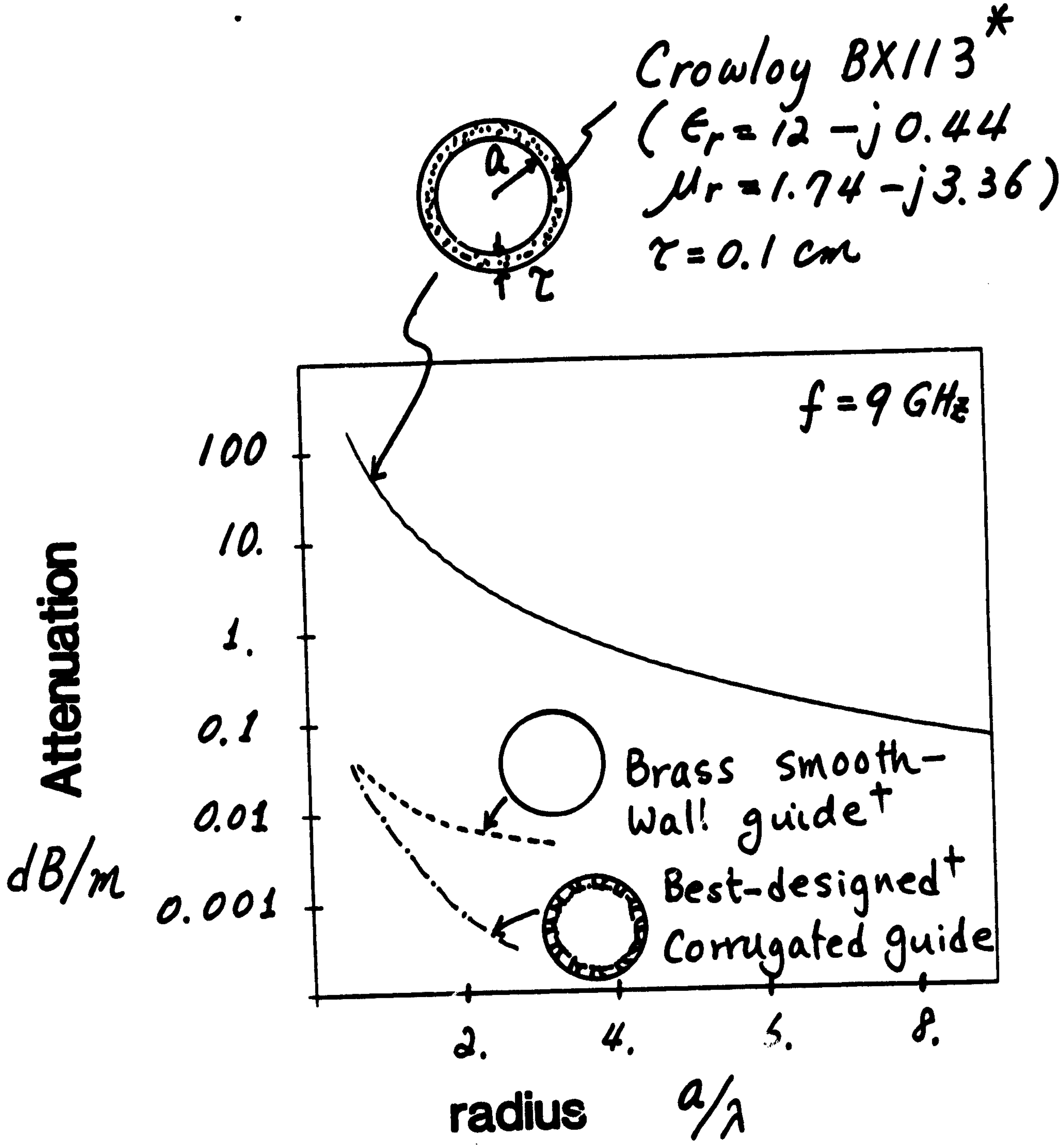

* A. Von Hippel, 1954

† P. Clarricoats, 1975

SUMMARY

Advantages **of the coated guide over the corrugated guide:**

* Less expensive to build
* Lighter in weight
* Wider operating–frequency range

Disadvantage:

* Attenuation may be higher than the well designed corrugated guide.

APPENDIX D

A PROPOSAL FOR CONTINUATION OF NASA NAG 3-475, "NUMERIACL METHODS FOR ANALYZING ELECTROMAGNETIC SCATTERING"

A Proposal for Continuation

of NASA NAG 3-475

NUMERICAL METHODS FOR ANALYZING ELECTROMAGNETIC SCATTERING

Period: November 24, 1985 through November 23, 1986

Amount: $ 80,000

Prepared for

Mr. Boyd M. Bane
Contracting Officer
National Aeronautics and Space Administration
Lewis Research Center
Mail Stop 500-302
Cleveland, OH 44113

Prepared by

S. W. Lee, Y. T. Lo, and S. L. Chuang
Department of Electrical and Computer Engineering
College of Engineering
University of Illinois
Urbana-Champaign Campus
1406 W. Green St.
Urbana, Illinois 61801

August 1985

Co-Principal Investigator	S W Lee S. W. Lee
Co-Principal Investigator	Y. T. Lo Y. T. Lo
Co-Principal Investigator	S L Chuang S. L. Chuang
Department of Electrical and Computer Engineering	
College of Engineering	
Secretary, Research Board	
Director, Contract and Grant Administration	

I. INTRODUCTION

The research grant No. NAG 3-475 entitled "Numerical methods for analyzing electromagnetic scattering" was first awarded to the University of Illinois by NASA-Lewis Research Center on September 28, 1983. Dr. Y. C. Cho (Sept. '83 - June '84) and Mr. Edward J. Rice (June '84 - Present) of NASA Lewis Research Center are the technical officers. The past and proposed fundings are as follows:

PHASE	PERIOD	FUNDING
I	Sept. 28, 1983 - Nov. 23, 1984	$74,985.00
II	Nov. 24, 1984 - Nov. 23, 1985	$80,009.00
III	Nov. 24, 1985 - Nov. 23, 1986	$80,000.00

The present continuation proposal is for Phase III.

II. TECHNICAL DISCUSSION

In the past two years, we have made significant progress toward the RCS reduction of a jet engine inlet. We modeled the inlet by an open-ended cylindrical waveguide, and have developed a set of computer codes for calculating the RCS from the rim diffraction [1], [2] and the interior irradiation [2], [3]. Our calculated results are in excellent agreement with experimental data [4] (Figures 1 and 2). To reduce the interior irradiation, a single layer of lossy magnetic material is employed to coat the interior wall of the circular guide. With proper material, even a very thin layer of coating can be effective in reducing the RCS drastically for the low-frequency case. (The radius a of the guide is about one wavelength or less. See Figure 3.) In the coming year (Nov. '85 to Nov. '86), we propose to continue our present study by carrying out the following tasks:

Task A. Waveguide Transition Study: At high frequency ($a >> \lambda$), the modes in a coated waveguide are divided into two distinctive groups:

- Highly attenuated surface-wave modes
- Nearly unattenuated inner modes.

The key in reducing RCS is to be able to direct most incoming electromagnetic energy from the radar into the highly attenuated surface-wave modes. Therefore, the study of the proper waveguide transition (Figure 4) becomes a most crucial problem. We shall investigate this problem both theoretically and experimentally.

Task B. Multilayered Coating: At high frequency ($a > 3\lambda$), when the thickness of coating layer is less than $\lambda/4$, a significant RCS reduction is achievable only for nearly normal incidence, or more precisely, for

$$\theta_o < \sin^{-1}(0.3\lambda/a) \;, \quad \text{for } a > 3\lambda$$

where θ_o is the incident polar angle measured from the axis of the cylinder (Figure 5). For $a = 3.3\lambda$, for example, θ_o is less than 5°. Thus, to achieve RCS reduction over a broad incident angle at high frequencies, a multilayered coating is necessary. In the next grant year, we will study carefully the multilayered structure in Figure 5. The inner layer is a lossless dielectric layer, which is used to "attract" the incident electromagnetic energy to the waveguide wall. The outer layer is made of a lossy magnetic material for producing large attenuation.

Task C. Waveguide with Non-circular Cross Section: The use of the finite-element method to analyze the modal field with non-circular cross section (Figure 6) was initiated in the current grant period. Based on a variational technique, the determination of the modal propagation constant is reduced to that of an eigenvalue. This method is applicable to a waveguide with an arbitrary cross section with nonuniform or multilayered coatings. This effort will be continued.

REFERENCES

[1] C. A. Chuang, C. S. Liang, and S. W. Lee, "High frequency scattering from an open-ended semi-infinite cylinder," IEEE Trans. Antennas Propagat., vol. AP-23, pp. 770-776, November 1975.

[2] R. Mittra, S. W. Lee, and C. A. Chuang, "Analytic modeling of the radar scattering characteristics of aircraft," Univ. of Illinois Electromagnetics Laboratory, Urbana, Illinois, Scientific Report No. 74-1, January 1974.

[3] S. W. Lee, Y. T. Lo, S. L. Chuang, and C. S. Lee, "Numerical methods for analyzing electromagnetic scattering," Semiannual Report to NASA Lewis Research Center, Cleveland, Ohio, March 1985.

[4] H. A. Brooks and J. W. Crispin, Jr., "Comments on the RCS characteristics of cylinders, hollow pipes, and cylindrical cavities," Conductor Corporation Report No. 1801-2-T(0043-147), Ann Arbor, Michigan, August 1966.

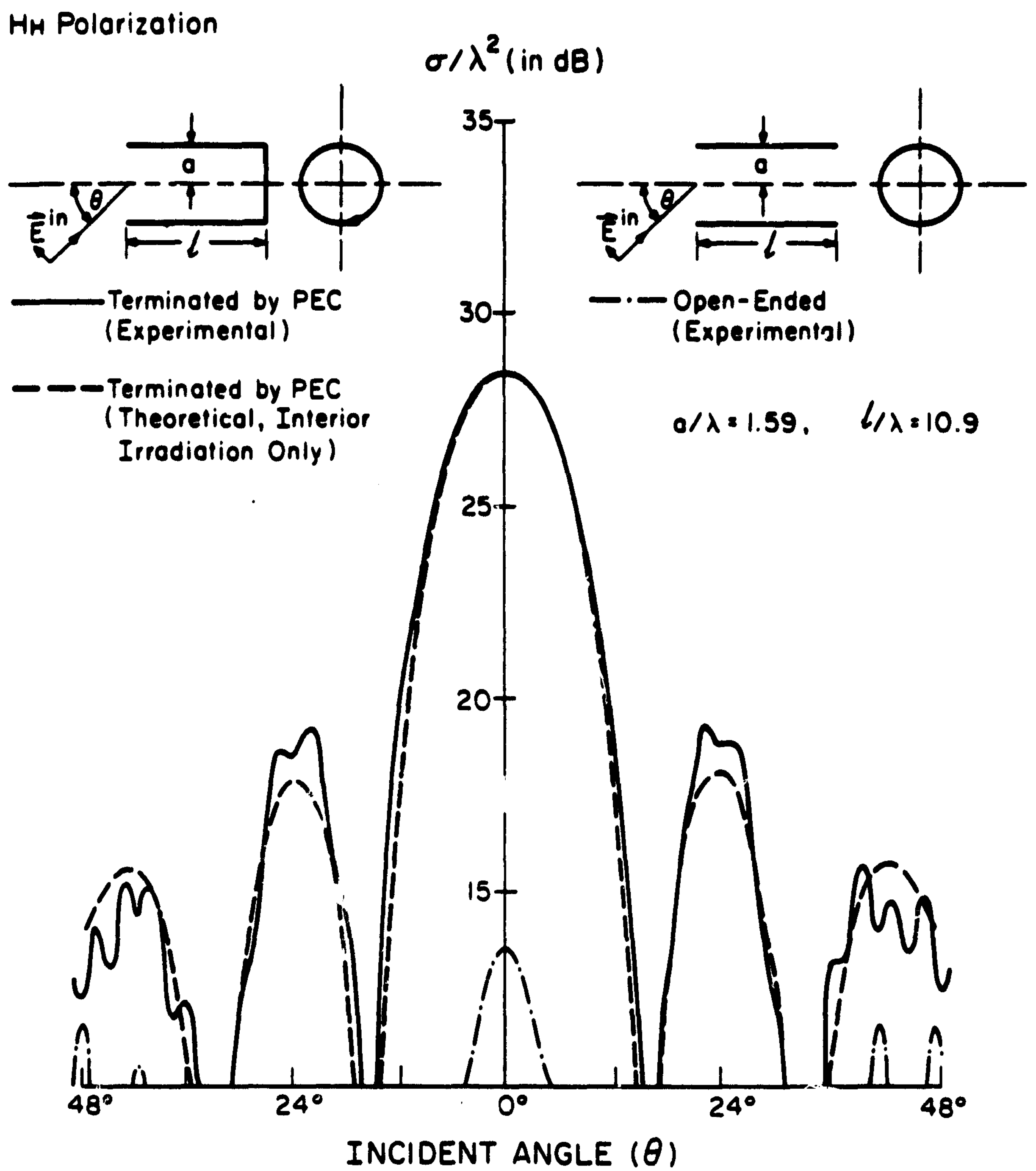

Figure 1. The RCS's from a PEC-terminated waveguide (——— experimental, — — — theoretical, interior irradiation only) and from an open-ended waveguide (— · — experimental) as a function of the incident angle (HH polarization, a = 3.137 cm, f = 15.20 GHz, a/λ = 1.589, l = 21.59 cm).

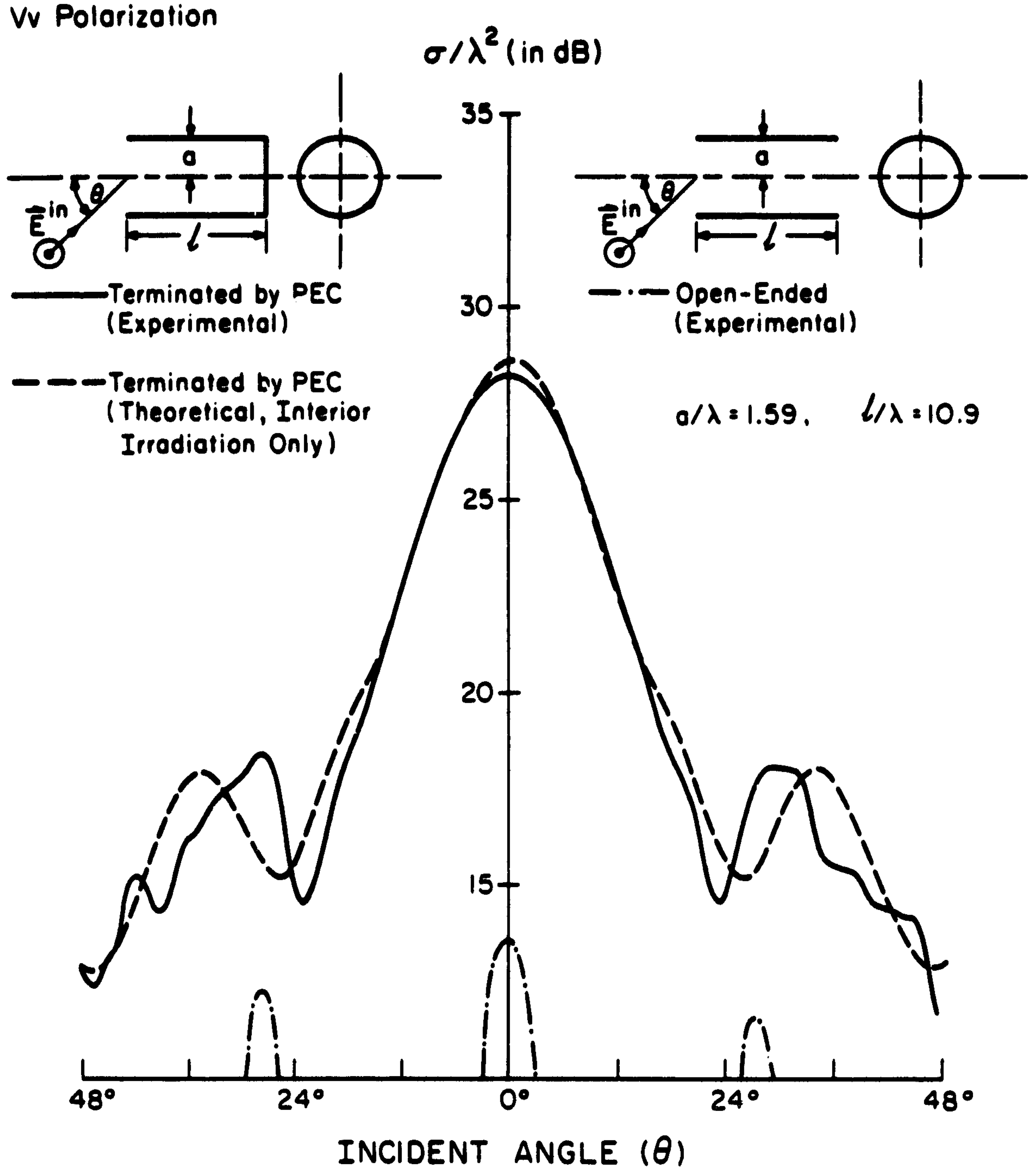

Figure 2. The RCS's from a PEC-terminated waveguide (——— experimental, — — — theoretical, interior irradiation only) and from an open-ended waveguide (— · — experimental) as a function of the incident angle (VV polarization, a = 3.137 cm, f = 15.20 GHz, a/λ = 1.589, l = 21.59 cm).

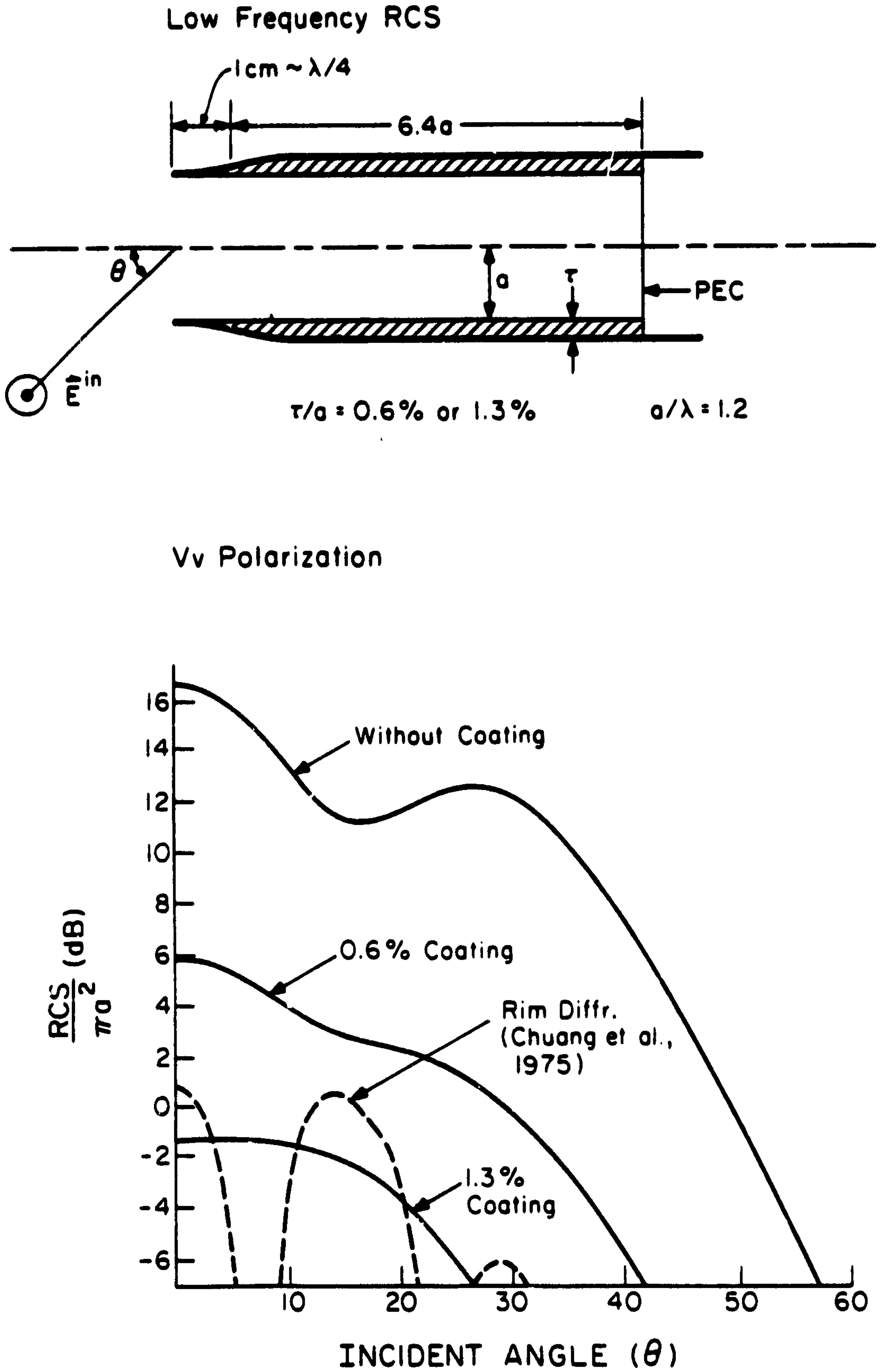

Figure 3. The RCS's (theoretical) as a function of the incident angle from a circular waveguide coated with a lossy material (Crowloy BX113, $\epsilon_r = 12 - j0.144$, $\mu_r = 1.74 - j3.306$) and terminated by a PEC for layer thicknesses of $\tau = 0$, 0.025 cm (0.6% coating) and 0.05 cm (1.3% coating) ($a = 3.95$ cm, $f = 9.2$ GHz, $a/\lambda = 1.2$, length = 26.46 cm, vertical polarization).

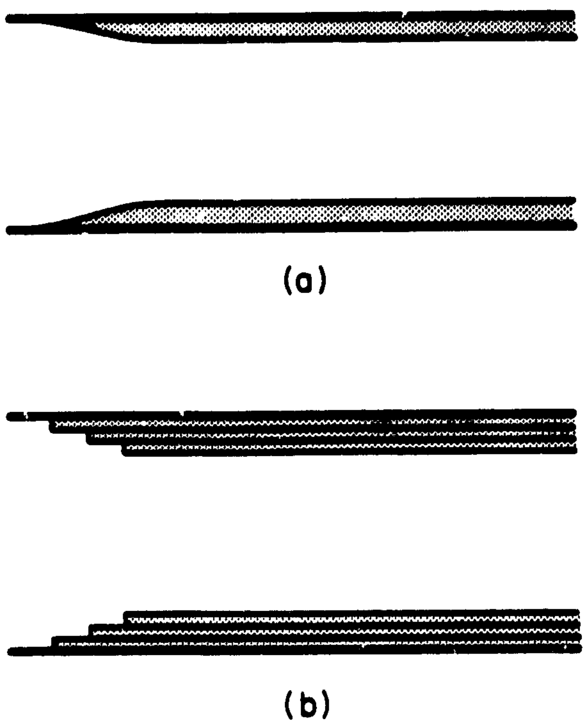

Figure 4. (a) The coated guide with a smooth transition of the layer thickness. (b) Step transition, the simplified version of (a).

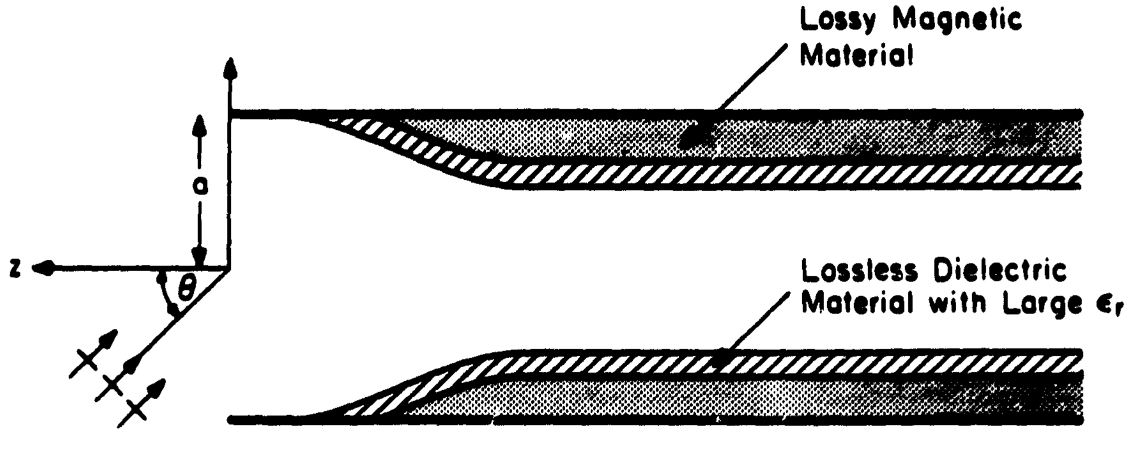

Figure 5. A waveguide coated with double layers.

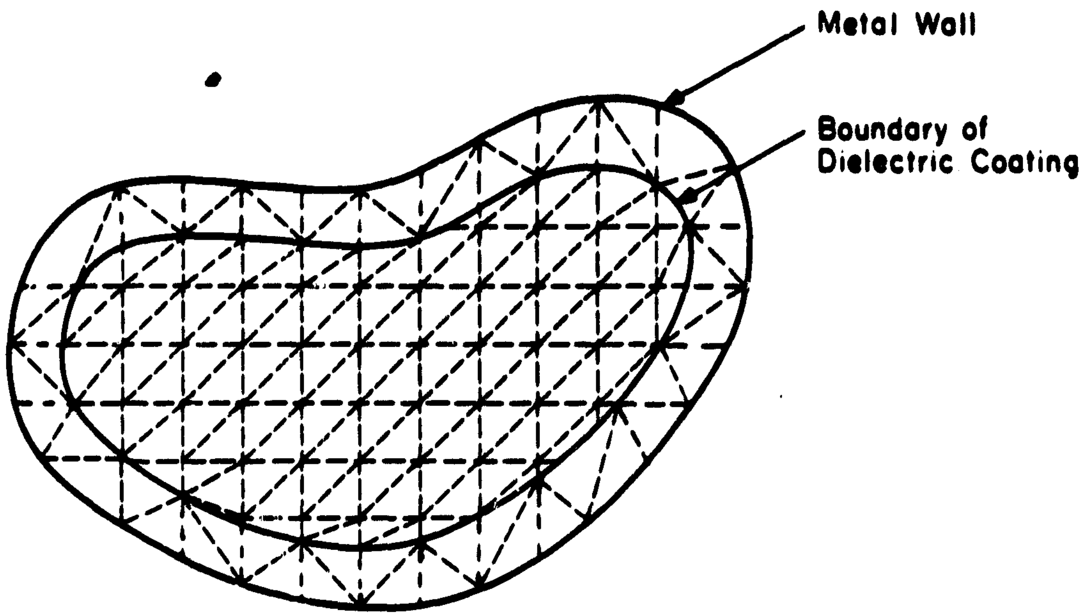

Figure 6. A waveguide with an arbitrary cross-section is divided into triangular elements for the use of the finite-element method.